GEOLOGICA ULTRAIECTINA

Mededelingen van het
Instituut voor Aardwetenschappen der
Rijksuniversiteit te Utrecht

No. 51

SOME ROCKMAGNETIC PARAMETERS FOR NATURAL GOETHITE, PYRRHOTITE AND FINE-GRAINED HEMATITE

MARINUS JACOBUS DEKKERS

GEOLOGICA ULTRAIECTINA

Mededelingen van het
Instituut voor Aardwetenschappen der
Rijksuniversiteit te Utrecht

No. 51

SOME ROCKMAGNETIC PARAMETERS FOR NATURAL GOETHITE, PYRRHOTITE AND FINE-GRAINED HEMATITE

SOME ROCKMAGNETIC PARAMETERS FOR NATURAL GOETHITE, PYRRHOTITE AND FINE-GRAINED HEMATITE

GESTEENTE-MAGNETISCHE PARAMETERS VOOR NATUURLIJKE GOETHIET, PYRRHOTIEN EN FIJNKORRELIGE HEMATIET

MET EEN SAMENVATTING IN HET NEDERLANDS

PROEFSCHRIFT

TER VERKRIJGING VAN DE GRAAD VAN DOCTOR AAN
DE RIJKSUNIVERSITEIT TE UTRECHT, OP GEZAG VAN
DE RECTOR MAGNIFICUS, PROF. DR. J.A. VAN GINKEL,
INGEVOLGE HET BESLUIT VAN HET COLLEGE VAN DEKANEN
IN HET OPENBAAR TE VERDEDIGEN OP 27 JANUARI 1988
DES NAMIDDAGS TE 2.30 UUR

DOOR

MARINUS JACOBUS DEKKERS

GEBOREN OP 3 DECEMBER 1956 TE WILLEMSTAD (CURAÇAO)

1988
OFFSETDRUKKERIJ KANTERS B.V., ALBLASSERDAM

PROMOTORES: PROF. DR. J.D.A. ZIJDERVELD
PROF. DR. R.D. SCHUILING

aan mijn grootouders

SUMMARY

The increasing importance of sediments for paleomagnetic research prompted a study of rockmagnetic parameters of natural goethite, pyrrhotite and hematite. Grain-size dependent behaviour of such parameters is poorly known for goethite and pyrrhotite as well as for fine-grained hematite. Data of hematite indicate a complex rockmagnetic behaviour. Existing data seem to be contradictory in many aspects. The rockmagnetic parameters reported in the present thesis for the natural goethite and pyrrhotite samples comprise twelve grain-size fractions from 250 micrometer down to <5 micrometer. For the natural hematite sample, which has a low-temperature origin, the <5 micrometer fraction was divided into six grain-size fractions down to <0.25 micrometer.

Goethite literature data are reviewed in Chapter 1. In order to keep close to the paleomagnetic reality, natural goethites from different supergene geologic origin were selected for investigation: two marine sedimentary goethites, a fluviatile replacement goethite, a goethite from a gossan and a caprock goethite from a siderite ore. Their chemical and X-ray characteristics as well as the preparation method of the artificial samples are described in Chapter 2.

In Chapter 3 the grain-size dependence of room temperature hysteresis parameters in magnetic fields up to $16*10^6$ Am^{-1} (20 Tesla) is described. The relation between the goethite rockmagnetic parameters and its chemical composition is discussed. The magnetic properties of the microcrystalline goethites are best understood when crystallite size and crystallite exchange interaction are taken into account.

The behaviour of a thermoremanent magnetization during continuous and stepwise thermal demagnetization, alternating field demagnetization and low-temperature treatment is discussed in Chapter 4. The maximum blocking temperature of goethite appears to be gouverned by the amount of isomorphously substituted cations in the goethite lattice. The goethites are extremely hard with respect to alternating field demagnetization. Only in extremely fine-crystalline goethite (with crystallite sizes close to the superparamagnetic threshold size) alternating field demagnetization results in a noticeable remanence decay. During low-temperature treatment, a goethite remanence continuously increases with decreasing temperature with a rate depending on the goethite chemical composition. Goethite is unique in showing such behaviour. Low-temperature treatment is an useful technique for the determination of goethite without the need to heat a sample.

Goethite dehydrates to hematite in a temperature range 250-350 °C (differential scanning calorimetry). The magnetic impact of the goethite dehydration reaction during stepwise thermal demagnetization is discussed in Chapter 5. The initial susceptibility slightly decreases during the dehydration reaction. As a consequence of the goethite dehydration A flux of water vapour is released within the goethite grain. This promotes recrystallization of traces hematite already present in the original goethite concentrates, resulting in a bending point in the thermal decay curves. This bending point is thus not related to the maximum blocking temperature of another magnetic mineral phase. At temperatures above 400 °C the initial susceptibility increases considerably due to the creation of small quantities of a magnetite(-like) phase. The rockmagnetic characteristics of hematite and magnetite, originating from goethite, strongly depend on their thermal history. A self-reversal can be observed during stepwise thermal demagnetization above 600 °C.

Pyrrhotite literature data are reviewed in chapter 6. Pyrrhotite samples from various ore-parageneses were selected for rockmagnetic experiments: one from an orthomagmatic Fe-Ni-Cu-ore, two from magnetite-pyrrhotite skarns and one from a chalcopyrite-bearing pyrometasomatic ore. Their chemical composition and XRD-features as well as the preparation techniques for the artificial samples are discussed in chapter 7.

Pyrrhotite room temperature hysteresis parameters are discussed in chapter 8. Compositional differences hardly show up in the remanent coercive force versus grain size trend. Hysteresis parameters of pyrrhotite are compared with those of magnetite. The ratio of the saturation isothermal remanent magnetization and the initial susceptibility appears to be larger than the remanent coercive force for pyrrhotite, whereas the opposite applies for magnetite.

The behaviour of the thermoremanence and isothermal remanent saturation magnetization during stepwise and continuous thermal demagnetization and low-temperature treatment is dealt with in chapter 9. Continuous thermal demagnetization reveals virtually identical decay curves for all fractions. The saturation isothermal remanence differs before and after thermal treatment due to partial preservation of high-temperature pyrrhotite phases during cooling. Decay curves of the saturation isothermal remanent magnetization have a slightly less steep approach to the maximum blocking temperature than decay curves of the thermoremanence. The specific thermoremanence decreases with grain size. Stepwise thermal demagnetization of the thermoremanence shows that the remanence is for its major part removed between 300 and 325 °C. Stepwise thermal demagnetization of the saturation isothermal remanent magnetization reveals a different behaviour for coarse- and fine-grained fractions of the same sample. The former decrease monotonously up to the maximum blocking temperature; the latter show a larger decay at moderate temperatures followed by a partial remanence recovery before complete removal at the maximum blocking temperature. The remanence behaviour during low temperature treatment is related to the strong temperature dependence of the pyrrhotite anisotropy constants.

Some rockmagnetic parameters for extremely fine grain-size fractions (10 micrometer down to <0.25 micrometer) of a natural hematite of low-temperature origin are discussed in chapter 10. The magnetic properties appear to be strongly dependent on the thermal history of the hematite. Prior to thermal treatment, the hematite shows no Morin transition, indicating that the remanence is carried by the "defect moment". The remanent hysteresis parameters reveal a maximum in the 1.0-0.5 micrometer fraction. After thermal treatment, the hematite does show a Morin transition and it has become considerably harder; the maximum in remanent hysteresis parameters have shifted to 2.1-1.0 micrometer fraction. Rockmagnetic parameters obtained from hematites synthesized at high temperatures are thus not representative for natural low-temperature hematite. The observed differences in magnetic behaviour prior to and after thermal treatment might provide a basis for the discrimination of DRM and CRM in hematite-bearing sediments.

SAMENVATTING

Het toenemende belang van sedimentaire gesteenten voor paleomagnetisch onderzoek maakt een studie naar de gesteentemagnetische parameters van natuurlijke goethiet, pyrrhotien en hematiet noodzakelijk. Voor goethiet en pyrrhotien is de korrelgrootte-afhankelijkheid van deze parameters is slechts zeer ten dele bekend. De hematietgegevens wijzen op een gecompliceerd gesteentemagnetisch gedrag en bestaande gegevens lijken elkaar op vele gebieden tegen te spreken. De gesteentemagnetische parameters in dit proefschrift zijn bepaald voor twaalf korrelgrootte fracties van natuurlijke goethiet en pyrrhotien monsters variërend van 250 micrometer tot <5 micrometer. Voor het natuurlijke hematiet monster dat een laag-temperatuur oorsprong heeft, is de <5 micrometer fractie opgedeeld in zes fracties tot <0.25 micrometer.

In Hoofdstuk 1 wordt een literatuuroverzicht van goethiet gegeven. Om zo dicht mogelijk bij de paleomagnetische realiteit te blijven, zijn natuurlijke goethiet monsters van supergeen geologische oorsprong uitgezocht voor het onderzoek: twee marien sedimentaire goethieten, een fluviatiele "replacement" goethiet, een goethiet uit een gossan en een goethiet uit de oxidatiezone boven een sideriet erts. Hun chemische en röntgenografische karakteristieken worden in Hoofdstuk 2 beschreven, evenals de gevolgde methode voor het vervaardigen van kunstmatige monsters.

In Hoofdstuk 3 wordt de korrelgrootte-afhankelijkheid van de hysterese parameters in magnetische velden tot $16*10^6$ Am^{-1} (20 Tesla) en gemeten bij kamertemperatuur, beschreven. De relatie tussen de gesteentemagnetische parameters van de goethieten en hun chemische samenstelling wordt besproken. De magnetische eigenschappen van de microkristallijne goethieten kunnen het best beschreven worden, indien de kristallietgrootte en "exchange" interactie in mede beschouwing worden genomen.

Het gedrag van een thermoremanente magnetisatie gedurende continue en stapsgewijze thermische demagnetisatie, wisselvelddemagnetisatie en laag-temperatuur behandeling wordt beschreven in Hoofdstuk 4. De maximum "blocking" temperatuur van goethiet blijkt bepaald te worden door de hoeveelheid isomorfe substitutie in het goethiet rooster. De goethiet magnetisaties vertonen een extreme hardheid ten opzichte van wisselvelddemagnetisatie. Slechts extreem fijn-kristallijne goethiet (met een kristallietgrootte zeer dicht bij de grens waaronder superparamagnetisch gedrag optreedt) vertoont een afname bij wisselvelddemagnetisatie. Bij afkoeling vanaf kamertemperatuur in een veldvrije ruimte neemt de remanentie van goethiet geleidelijk toe. De toename hangt af van de chemische compositie van de goethiet. Dit gedrag kenmerkend voor goethiet. Laag-temperatuur behandeling is een goede manier om de aanwezigheid van goethiet vast te stellen zonder een monster te moeten verhitten.

Goethiet dehydrateert naar hematiet in een temperatuur traject van 250 tot 350 °C ("differential scanning calorimetry"). De invloed van deze dehydratie op het magnetische gedrag van de monsters gedurende stapsgewijze thermische demagnetisatie wordt behandeld in Hoofdstuk 5. De initiële susceptibiliteit neemt in geringe mate af tijdens de dehydratiereactie. De dehydratie resulteert in een flux van waterdamp in de goethiet korrel. Deze flux bevordert de rekristallisatie van sporen hematiet die reeds aanwezig waren in het oorspronkelijke goethietconcentraat. Dit resulteert in een knikpunt in afnamecurves dat niet gerelateerd is aan de maximum "blocking" temperatuur van nog een magnetisch mineraal. Vanaf 400 °C neemt de initiële susceptibiliteit aanzienlijk toe ten gevolge van de vorming van kleine hoeveelheden van een magne-

tiet-achtige fase. De gesteentemagnetische eigenschappen van de gevormde hematiet en magnetiet hangen sterk samen met hun thermische geschiedenis. Een "zelf-omkering" van de remanentie kan worden waargenomen tijdens de stapsgewijze thermische demagnetisatie in het temperatuurbereik boven 600 °C.

Een overzicht van de literatuurgegevens van pyrrhotien wordt gegeven in Hoofdstuk 6. Pyrrhotien monsters afkomstig uit diverse erts-paragenesen zijn geselecteerd voor het onderzoek: één uit een orthomagmatisch Fe-Ni- Cu erts, twee uit magnetiet-pyrrhotien skarnen één uit een pyrometasomatisch chalcopyriet erts. Hun chemische compositie en kristallografische eigenschappen worden beschreven in Hoofdstuk 7, evenals de gevolgde methodiek voor het vervaardigen van de kunstmatige monsters.

De korrelgrootte-afhankelijkheid van de hysterese parameters, gemeten bij kamertemperatuur, wordt beschreven in Hoofdstuk 8. Verschillen in chemische samenstelling van de pyrrhotien monsters komen nauwelijks tot uiting in de korrelgrootte-trend van de remanente coërcitiefkracht. De pyrrhotien hysterese parameters worden vergeleken met die van magnetiet. Voor pyrrhotien blijkt de verhouding van de isothermale remanente verzadigingsmagnetisatie en de initiële susceptibiliteit groter te zijn dan de remanente coërcitiefkracht, terwijl voor magnetiet het omgekeerde geldt.

Het gedrag van de thermoremanente magnetisatie en de isothermale remanente verzadigingsmagnetisatie tijdens stapgewijze en continue thermische demagnetisatie en laag-temperatuur behandeling wordt beschreven in Hoofdstuk 9. Continue thermische demagnetisatie resulteert in nagenoeg dezelfde afnamecurves voor iedere fractie. Doordat bij afkoeling hoog-temperatuur modificaties van pyrrhotien gedeeltelijk behouden blijven, verschilt de isothermale remanente verzadigingsmagnetisatie voor thermische behandeling met die van erna. Afnamecurves van de isothermale remanente verzadigings magnetisatie vertonen een iets minder steile nadering tot de maximum "blocking" temperatuur dan die van de thermoremanente magnetisatie. De "specifieke" thermoremanente magnetisatie neemt af met de korrelgrootte. Stapsgewijze thermische demagnetisatie van de thermoremanente magnetisatie laat zien dat de het grootste deel van de remanentie wordt afgebroken bij temperaturen boven 300 °C. Stapgewijze thermische demagnetisatie van de isothermale remanente verzadigings magnetisatie toont verschillen in gedrag tussen grove en fijne fracties. De eerstgenoemde vertonen een constante afname tot de maximum "blocking" temperatuur; de laatstgenoemde nemen sterker af bij matige verhitting waarna een gedeeltelijk herstel van de remanentie waargenomen wordt, voordat deze geheel wordt afgebroken bij de maximum "blocking" temperatuur. Het gedrag van de remanentie tijdens laag-temperatuur behandeling kan aannemelijk gemaakt worden door de sterke temperatuursafhankelijkheid van de anisotropieconstanten van pyrrhotien.

Enige gesteentemagnetische parameters voor extreem fijne korrelgrootte-fracties (van 10 micrometer tot <0.25 micrometer) van een natuurlijke hematiet van laag-temperatuur origine worden behandeld in Hoofdstuk 10. De magnetische eigenschappen blijken sterk van de thermische geschiedenis van de hematiet af te hangen. Vóór thermische behandeling vertoont de hematiet geen Morin transitie. De remanentie in deze hematiet wordt gedragen door het "defect moment". De remanente hysterese parameters vertonen een maximum in de 1.0-0.5 micrometer fractie. Ná thermische behandeling vertoont de hematiet wel een Morin transitie. De remanentie van de hematiet is aanzienlijk harder geworden; het maximum

in de hysterese parameters is opgschoven naar de 2.1-1.0 micrometer fractie. De gesteentemagnetische parameters van hematiet, gesynthetiseerd bij hoge temperaturen, zijn derhalve niet representatief voor natuurlijke hematiet van laag-temperatuur oorsprong. De waargenomen verschillen in magnetische eigenschappen voor en na thermische behandeling zouden een basis kunnen verschaffen voor het onderscheid tussen depositionele remanente magnetisatie en chemisch remanente magnetisatie in hematiet-dragende sedimenten.

DANKBETUIGING

Allen die hebben bijgedragen aan de totstandkoming van dit proefschrift, wil ik hartelijk bedanken.

Mijn bijzondere erkentelijkheid gaat uit naar Prof. Dr. J.D.A. Zijderveld, wiens niet aflatende kritiek resulterend in "zwart geschreven" manuscripten, voor mij van zeer groot nut is geweest. Prof. Dr. R.D. Schuiling wil ik danken voor zijn steun aan het onderzoek.

Aan de verzamelreis samen met drs. Maarten Pieters bewaar ik prettige herinneringen.

Jan de Groot en zijn collega's vervaardigden de dunne doorsneden en polijstvlakken. Röntgendiffractie analyses zijn uitgevoerd door Charles Laman. Peter van Krieken voerde de "differential scanning calorimetry" en de "thermogravimetric analyses" uit. Nat-chemische analyses zijn gedaan in het Service Laboratorium door Ir. Berta Djie Kwee, Theo van Zessen en Chiel Eussen. Drs. Joyce Wevers adviseerde bij de infrarood spectrometrische analyses en Dr. Rob Kreulen bij het quenchen van de pyrrhotienen voor Röntgenanalyse. Microprobe analyses zijn uitgevoerd onder supervisie van Dr. Manfred van Bergen. Electronenmicroscoop werk is gedaan onder supervisie van Dr. Herman van Roermund.

Drs. Simon Vriend ben ik erkentelijk voor zijn adviezen aangaande de chemische aspecten van dit onderzoek.

Henk Meijer en Piet Jan Verplak dank ik voor hun bijdrage aan de magnetische metingen en Dr. Cor Langereis voor zijn paleomagnetische adviezen. Tom Mullender ben ik erkentelijk voor zijn bijzondere bijdrage bij het in "top running condition" houden van de HALT spinner en de vele vruchtbare discussies.

Een niet onbelangrijk deel van de magnetische metingen is uitgevoerd aan de faculteit der Natuurkunde van de Katholieke Universiteit te Nijmegen. Ik ben Cees Beers en de medewerkers van het Laboratorium voor Hoge Magneetvelden Dr. Harald Myron, Ir. Klaas van Hulst, Jos Rook, Hung van Luong en in het bijzonder Dr. Jos Perenboom veel dank verschuldigd voor hun gastvrijheid en hulpvaardigheid.

Het onderzoek naar het magnetische gedrag van zeer fijnkorrelige hematiet is uitgevoerd in samenwerking met Drs. Jan Linssen.

Ir. R.G.W.J. Nelissen van het Centraal Laboratorium van de N.V. Koninklijke Sphinx te Maastricht ben ik zeer erkentelijk voor het ter beschikking stellen van de pipetcentrifuge en ondersteunende laboratorium faciliteiten. Ik wil de medewerkers van dit laboratorium hartelijk danken voor hun steun en interesse in de korrelgrootteschеidings problematiek.

Jaco Bergenhenegouwen vervaardigde de figuren en droeg zorg voor verfraaiing van computergetekende figuren. De fotokamer onder leiding van Hans Schiet maakte in zeer kort tijdsbestek een groot aantal "copy proofs".

Hoogovens N.V. te IJmuiden ben ik erkentelijk voor het ter beschikking stellen van een aantal goethiet monsters.

Shell Nederland B.V. maakte het mij door middel van een reisdonatie mogelijk een deel van de resultaten van dit proefschrift te presenteren op de XIX General Assembly van de International Union of Geodesy and Geophysics, gehouden van 9 tot 22 augustus 1987 te Vancouver, Canada.

Het onderzoek beschreven in dit proefschrift is gesteund door de Stichting Aardwetenschappelijk Onderzoek Nederland (AWON) met financiële steun van de Nederlandse Organisatie voor Zuiver-Wetenschappelijk Onderzoek (Z.W.O., subsidienummer 751-354-006)

CONTENTS

Chapter 8, "Magnetic properties of natural pyrrhotite part I: Behaviour of initial susceptibility and saturation-magnetization related rock-magnetic parameters in a grain-size dependent framework" is currently in press in Physics of the Earth and Planetary Interiors

Chapters 3, 4, 5, 9 and 10 have been or will be submitted for publication in international journals.

LIST OF FIGURES

Chapter 1

Chapter 2

Chapter 3

Chapter 4

Chapter 5

Chapter 6

Chapter 8

Chapter 9

Chapter 10

LIST OF TABLES

Chapter 1

Chapter 2

Chapter 3

Chapter 4

Chapter 5

Chapter 7

Chapter 8

Chapter 9

Chapter 10

GENERAL INTRODUCTION

The natural remanent magnetization (NRM) of rocks resides in titaniferous iron-oxides (titanomagnetite, titanomaghemite, hematite), iron-hydroxides (goethite) or iron sulfides (pyrrhotite). These minerals constitute only a very small part of the rock volume, usually far below one percent. (Titano-)magnetite and hematite are the most important magnetic minerals. (Titano-)maghemite, goethite and pyrrhotite are the so-called minor magnetic minerals.

The part of the NRM acquired by rocks during or shortly after their formation is referred to as the primary remanence. The direction and intensity of this remanence are related to the local geomagnetic field at the time of formation. Geologic processes (e.g. burial, diagenesis, metamorphism, intrusive activity or weathering), which may have occurred any time during the geologic history of the rock, often add secondary remanence components to the primary component. A secondary remanence component may also originate from viscous remanence acquisition of the magnetic particles without being related to one of the geologic processes listed above. A secondary component may partly overprint as well as replace the primary component.

The main object of paleomagnetic research is to isolate the primary remanence component for geotectonic, magnetostratigraphic or geomagnetic interpretations. This can be achieved by so-called progressive demagnetization. A rock specimen is subjected to increasing alternating fields or it is stepwise heated to increasing temperatures. After each step, the alternating field is removed or the specimens are cooled to room temperature. Both procedures are carried out in a field-free space and the remanence of the rock specimens is measured after each step. This procedure yields a string of remanence vectors representing the various NRM components in the rock specimen. A single-component remanence shows a linear decay and multi-component remanences usually show up by linear segments connected by curved parts, because of the partial overlap of the coercive force or blocking temperature spectra of the different components. Although progressive demagnetization is rather simple and straightforward from the experimental point of view, the geological interpretation of its results is often difficult. In quite a number of cases it appears to be hardly possible to label a specific remanence component as primary remanence.

These difficulties arise from the complex magnetic properties of the remanence carriers in natural rocks, which determine the behaviour of the natural remanent magnetization during progressive demagnetization. Apart from being obviously dependent on the type of magnetic mineral, the magnetic properties of each individual mineral type are strongly dependent on their mode of formation, particle size, amount of isomorphous substitution, amount of defects in the crystal lattice and exsolution phenomena. The magnetic mineral content of natural rocks usually is a composite of different magnetic minerals with for each magnetic mineral a specific grain-size range. Although the number of natural magnetic minerals is fairly limited, combination of the factors mentioned above may lead to very complex magnetic properties for natural rocks.

The results of rockmagnetic studies of magnetic mineral properties as function of grain size, chemical composition etc., allows a more reliable determination of the magnetic minerals in natural rocks. This enhances the insight in the timing and stability of the various NRM components.

Most rockmagnetic studies are devoted to (titano-)magnetite (e.g. Parry, 1965; Day et al., 1977; Hartstra, 1982; O'Reilly, 1984; Dunlop, 1986; Worm and Markert, 1987; Heider et al., 1987) and (titano-)maghemite (e.g. Özdemir and O'Reilly, 1982; Nishitani and Kono, 1983; Özdemir and Banerjee, 1984; Moskowitz, 1987). (Titano-)magnetite is the most common terrestrial natural magnetic mineral, so the relevance of knowledge of its magnetic properties is beyond discussion. Titano-maghemite widely occurs in oceanic basalts. However, rockmagnetic data on the other magnetic minerals (hematite, goethite and pyrrhotite) are scarce, despite their relevance especially for sedimentary rocks.

The present thesis intends to contribute to the knowledge of the rockmagnetic properties of natural goethite, natural pyrrhotite and fine-grained natural hematite.

The magnetic properties of hematite (with obvious relevance to red beds) are complex (e.g. Haigh, 1957; Smith and Fuller, 1967; Dunlop, 1971; Dankers, 1978, 1981; Hartstra, 1982; O'Reilly, 1984) and data are contradictory (e.g. Dunlop, 1971; O'Reilly, 1984; Vincenz, 1987). For a correct understanding of the understanding of the hematite rockmagnetic properties, more data are needed. Particularly studies of the behaviour of extremely fine-grained low-temperature hematite are of importance for paleomagnetic research on sediments.

Pyrrhotite is regarded as a minor magnetic mineral because of its assigned limited occurrence in direct spatial relation with sulphidic ores. It is, however, nowadays apparent that its occurrence is not restricted to such ores: pyrrhotite may occur in igneous rocks (e.g. Soffel, 1977), metamorphic rocks (e.g. Carpenter, 1974; Rochette, 1987) and also sediments (e.g. Kligfield and Channell, 1981; Freeman, 1986). Hence, pyrrhotite is a much more common magnetic mineral than previously assumed. Although much study was devoted to its intrinsic properties (cf. reviews by Ward, 1970; Schwarz, 1975), grain-size dependence of its hysteresis properties is up to now only recently reported by Clark (1984).

Goethite is usually regarded as a minor magnetic mineral carrying only secondary remanences related to weathering. However, one should realize that the goethite occurrence is not restricted to a specific rock type: goethite can be an accessory constituent of virtually all rocks, especially sediments. Besides being related to weathering it can also be precipitated from circulating ground water giving rise to a secondary remanence of much older age. Goethite often occurs intimately intergrown with hematite. Grain-size dependence of goethite rockmagnetic parameters was unknown before the present study was started.

Knowledge of goethite magnetic properties contributes to the understanding of the magnetic behaviour of finely crystalline goethite-hematite intergrowths.

Secondary remanence components with directions different from the present geomagnetic field, i.e. not related to present day weathering, may also yield useful paleomagnetic information.

Goethite dehydrates to hematite at 250-400 C. The goethite dehydration reaction may influence the magnetic properties of other magnetic minerals present in the sample. Study of this dehydration reaction is therefore highly relevant for the interpretation of thermal demagnetization diagrams of especially sediments. For a good evaluation of the impact of the goethite dehydration reaction, the rockmagnetic properties of goethite have to be known.

References

Carpenter R.H., 1974, Pyrrhotite isograde in SE Tenessee and SW North Carolina, Geol. Soc. Amer. Bull. 85, 451-6.

Clark D.A., 1984, Hysteresis properties of sized dispersed monoclinic pyrrhotite grains, Geophys. Res. Lett. 11, 173-6.

Dankers P.H.M., 1978, Magnetic properties of dispersed natural iron-oxides of known grain size, Ph.D. thesis University of Utrecht, 142pp.

Dankers P.H.M., 1981, Relationship between median destructive field and remanent coercive forces for dispersed natural magnetite, titanomagnetite and hematite, Geophys. J. R. astr. Soc. 64, 447-461.

Day R., Fuller M., Schmidt V.A., 1977, Hysteresis properties of titanomagnetites: grain size and compositional dependence, Phys. Earth Plan. Inter. 13, 260-7.

Dunlop D.J., 1971, Magnetic properties of fine particle hematite, Ann. Geophys. 27, 269-93.

Dunlop D.J., 1986, Hysteresis properties of magnetite and their dependence on particle size: a test of pseudo-single-domain remanence models, J. Geophys. Res. B 91, 9569-84.

Freeman R., 1986, Magnetic mineralogy of pelagic limestones, Geophys. J. R. astr. Soc. 85, 433-52.

Haigh G., 1957, Observations on the magnetic transition in hematite at -15 °C, Phil. Mag. 2, 877-90.

Hartstra R.L., 1982, Some rockmagnetic parameters for natural iron-titanium oxides, Ph.D. thesis University of Utrecht, 145pp.

Hedley I.G., 1971, The weak ferromagnetism of goethite (α-FeOOH), Zeitschrift Geoph. 37, 409-20.

Heider F., Dunlop D.J., Sugiura N., 1987, Magnetic properties of hydrothermally recrystallized magnetite crystals, Science 236, 1287-90.

Kligfield R., Channell J.E.T., 1981, Widespread remagnetization of Helvitic limestones, J. Geophys. Res. B 86, 1888-1900.

Moskowitz B.M., 1987, Towards resolving the inconsistencies in characteristic physical properties of synthetic titanomaghemites, Phys. Earth Plan. Inter. 46, 173-83.

Nishitani T., Kono M., 1983, Curie temperature and lattice constant of oxidized titanomagnetite, Geophys. J. R. astr. Soc. 74, 585-600.

O'Reilly W., 1984, Rock and mineral magnetism, Blackie Glasgow and London, 220pp.

Özdemir Ö., Banerjee S.K., 1984, High temperature stability of maghemite (γ-Fe_2O_3), Geophys. Res. Lett. 11, 161-4.

Özdemir Ö., O'Reilly W., 1982, Magnetic hysteresis properties of synthetic monodomain titanomaghemites, Earth Plan. Sci. Letters 57, 141-54.

Parry L.G., 1965, Magnetic properties of dispersed magnetite powders, Philos. Mag. 11, 303-12.

Rochette P., 1987, Metamorphic control of the magnetic susceptibility of black shales in the Swiss Alps: toward the use of "Magnetic Isograde", Earth Plan. Sci. Letters 84, 446-56.

Schwarz E.J., 1975, Magnetic properties of pyrrhotite and their use in applied geology and geophysics, Geol. Surv. Can. Paper 74-59, 24pp.

Smith R.W., Fuller M., 1967, Alpha-hematite: stable remanence and memory, Science 156, 1130-3.

Soffel H.C., 1977, Pseudo-Single-Domain effects and Single-Domain Multidomain transition in natural pyrrhotite deduced from domain structure observations, J. Geophys. 42, 351-9.

Vincenz S.A., 1987, Discrepancies between experimental observations in natural and synthetic samples, Phys. Earth Plan. Inter. 46, 164-72.

Ward J.C., 1970, The structure and properties of some iron sulphides, Rev. Pure Appl. Chem. 20, 175-206.

Worm H.-U., Markert H., 1987, Magnetic hysteresis properties of fine particle titanomagnetites precipitated in a silicate matrix, Phys. Earth Plan. Inter. 46, 84-92.

CHAPTER 1

GOETHITE: SYNOPSIS OF SOME RELEVANT LITERATURE

1 INTRODUCTION

1.1 The α to δ-FeOOH series

Goethite, which is the natural magnetic mineral to be investigated in the first part of this thesis, is one of the four known polymorphs of iron-oxyhydroxide (FeOOH). Three of those: goethite, akaganeite and lepidocrocite (resp. α, β and γ-FeOOH) are naturally occurring minerals. The fourth, δ-FeOOH, is only known as synthesized at low temperatures in the laboratory. It is a rather poorly characterized phase, considered as metastable.

The goethite structure is based on hexagonal close-packed oxygen layers. Fe^{3+} occupies octahedrally coordinated sites between the layers. The (slightly distorted) octahedra form strips of two-octahedra wide, running parallel to the c-axis (cf. Fig. 1A; Ewing, 1935; Deer et al., 1962). A projection onto the a-b plane is shown in Fig. 1B. Each unit cell contains four iron ions. Goethite and lepidocrocite are orthorhombic. The difference between the two polymorphs lies in the packing of the oxygen atoms: goethite has a hexagonal close-packed and lepidocrocite a cubic close-packed structure. Akaganeite is tetragonal and δ-FeOOH is hexagonal. The crystal structures of the four polymorphs are compiled in Table I. Cell constants are listed in Table II.

Table I: Crystal structures of FeOOH polymorphs

Polymorph	Mineral name	Crystal structure		Néel point 1)
α-FeOOH	goethite	orthorhombic	Pbnm	127 °C
β-FeOOH	akaganeite	tetragonal	I4/m	17 °C
γ-FeOOH	lepidocrocite	orthorhombic	Cmcm	-200 °C
δ-FeOOH	--	hexagonal	P312?	--

1) after Johnson (1969)

Table II: Cell constants of FeOOH polymorphs

Polymorph	Crystal axes			reference
α-FeOOH	a= 4.602	b= 9.952	c= 3.021	1, 2, 3
β-FeOOH	a= 10.48	b= 10.48	c= 3.02	4
γ-FeOOH	a= 3.88	b= 12.54	c= 3.07	5, 6
δ-FeOOH	a= 2.94	b= 4.49	c= 4.49	7
diaspore	a= 4.40	b= 9.42	c= 2.84	8

References: 1) Goldstaub (1935), 2) Sampson (1969), 3) Harrison et al. (1975), 4) Mackay (1960), 5) Rooksby (1951), 6) Peacock (1942), 7) Bernal et al. (1959), 8) Ewing (1935).

The lattice parameters refer to ideal mineral compositions. In all minerals the octahedra are known to be slightly distorted and there can be isomorphous substitution. Diaspore (α-AlOOH) has the same lattice structure as goethite. This allows for considerable isomorphous substitution of aluminum in goethite leading to smaller lattice constants,

proportionally with the aluminum content (e.g. Norrish and Taylor, 1961; Thiel, 1963).

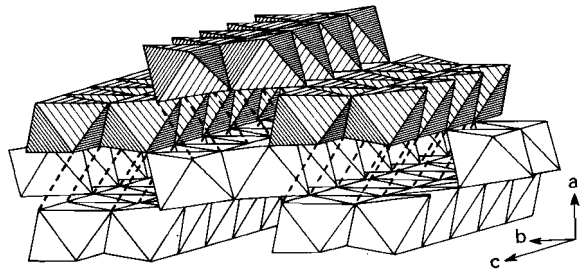

Fig. 1A. Pictorial representation of the goethite structure (after Ewing, 1935). Fe^{3+}-centered (slightly distorted) octahedra form chains of two octahedra wide along the c-axis.

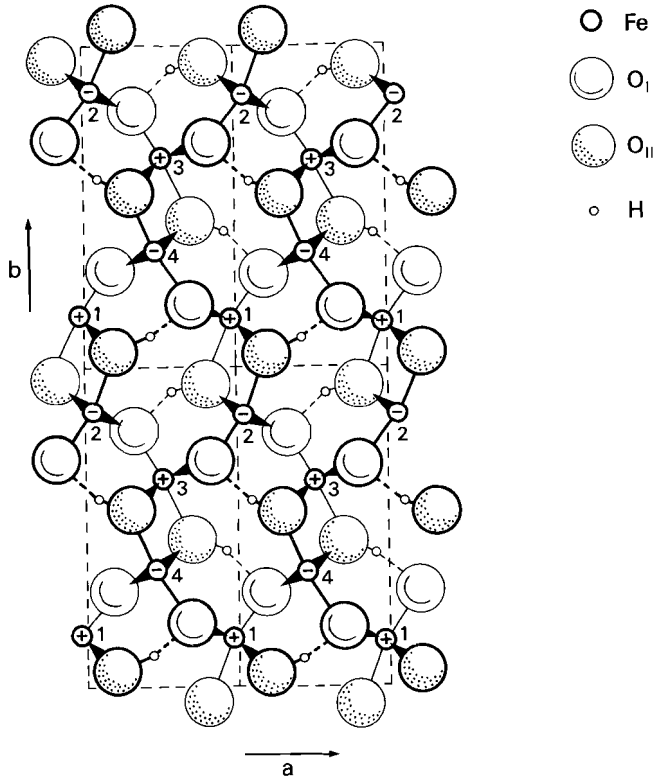

Fig. 1B. The goethite structure projected on 001. The c-axis is perpendicular to the plane of the page. The iron atoms are numbered; the signs denote their antiferromagnetic coupling (cf. Fig. 7). Oxygen atoms with heavy and light lines are on the mirror planes with c= +1/4 and c= -1/4 respectively.

1.2 Geological modes of occurrence of goethite

Goethite is a typical low-temperature mineral. At temperatures above 80 to 140 °C (the former at 1 bar, the latter at 4 kbar) it is thermodynamically calculated to convert to hematite (e.g. Langmuir, 1971, 1972; Wefers, 1966). Goethite usually coexists in nature with hematite (α-Fe_2O_3), lepidocrocite, and (iron-rich) clay minerals. Intimate intergrowths may occur.

Paleomagnetic interest for goethite-bearing rocks had been raised already a few decades ago since goethite may be a constituent of the hematite-rich red beds which are important for paleomagnetic research. In a later stage, when the sensitive cryogenic magnetometers became in vogue, it appeared that the weakly magnetic goethite could be present in trace amounts in virtually all sediments. Predominantly four types of goethite can be distinguished genetically:

1) sedimentary deposited
2) originated through replacement processes
3) as a soil constituent, formed during weathering
4) in low-temperature hydrothermal (telethermal) veins.

1) The sedimentary goethite type is found predominantly in the oolithic iron ores, which have been an important source of iron in the past. The ore layers are iron-enriched strata up to a few meters thickness in calcareous rocks. The exact mode of formation as well as the source of the iron are not known in detail, but all evidence points to a synsedimentary deposition or iron-enrichment (and oolith formation) shortly after deposition. Generally, the ores are low grade iron ores. Besides goethite, hematite and chamosite are important constituents. In Mesozoic ores goethite is predominant over hematite whereas in Paleozoic ores the reverse is true (e.g. James, 1966).
2) Goethite-rich ores may also be formed long after the formation of the host rock as so called replacement ores (e.g. Robe River, Western Australia, Harms and Morgan, 1964). These ores have oolithic and pisolithic zones. Solution of iron from iron-rich silicates is thought to be the source of iron for the goethite in the replacement ores.
   Epigenetic goethite is related to replacement goethite. It is precipitated in small quantities from circulating groundwater in the pores of sedimentary (e.g. calcareous) rocks without actual replacement of the host-rock minerals.
3) Perhaps the most important mode of occurrence of goethite is that of the weathering zone. Goethite can be formed through weathering of Fe-bearing silicates, but also by oxidation of magnetite, Fe-bearing sulfides and carbonates and hydration of hematite. As such, goethite may be a constituent of soils, but it is also known to be an important mineral in numerous gossans above sulphidic and carbonaceous ores (e.g. Zitzmann, 1978).
4) Goethite can be a constituent of low-temperature (telethermal) hydrothermal veins. Localities are known in the Harz (West Germany) and Cornwall (England). This goethite type is usually well-crystallized (e.g. Govaert et al., 1976A).

2 PREPARATION OF GOETHITE

Natural goethite is, despite its simple ideal formula, a complex mineral phase. Various elements can be isomorphically substituted in the

goethite lattice and sorption onto the goethite surface may amply occur. Knowledge of goethite growth mechanisms and of the influence of isomorphous substitution and sorption on the characteristics of the formed goethite can be obtained by studying simple well-defined experimental systems. These experimental data can be extended to existing natural goethite and, as such, form a framework for the understanding of the properties of the sampled natural goethite.

Synthetic goethite is prepared by aging of amorphous ferri-hydroxide ($Fe(OH)_3$) solutions, also referred to as ferrihydrite. Generally, aging takes place at high pH. However, examples of aging in acid solutions are known (van der Woude and de Bruyn, 1983; van der Woude et al., 1983, 1984).

Aluminous goethite may be obtained by aging aluminous ferri-hydroxide solutions - formed by coprecipitating iron(III)nitrate and aluminum nitrate bearing solutions in an alkaline environment - under hydrothermal conditions (Thiel, 1963; Goodman and Lewis, 1981) or under atmospheric conditions (Lewis and Schwertmann, 1979A). Aluminous goethite can also be obtained by aging freshly prepared ferri-hydroxide in an aluminate solution (Atkinson et al., 1968; Lewis and Schwertmann, 1979B).

Alternatively, (aluminous) goethite can be obtained by oxidation starting from iron(II)-bearing solutions (Derie et al., 1975; Goodman and Lewis, 1981). The oxidation may take place in acid or alkaline environments. The acid process is generally slow, it involves oxidation (mostly by air) of $Fe(OH)_2$ in the presence of Fe^{2+} in solution. In the alkaline processes an iron(II)hydroxide suspension is oxidized by air in (considerable) excess alkali; these processes are much faster. Depending on the starting material the reaction rate in both groups is different and sometimes besides goethite, lepidocrocite or maghemite (γ-Fe_2O_3) are obtained.

Goethite forms through dissolution of ferrihydrite and crystallization of goethite from solution; hematite has its precursor in ferrihydrite aggregates with nucleation taking place within these aggregates (Fischer and Schwertmann, 1975; Lewis and Schwertmann, 1979B). The conversion rate of ferrihydrite to goethite decreases as the aluminum concentration increases (Lewis and Schwertmann, 1979A). The goethite crystallites are increasingly smaller when more aluminum is incorporated in the goethite lattice (e.g. Landa and Gast, 1973). Aluminum substitution in goethite is proportional with log [Al] in solution (Lewis and Schwertmann, 1979A, 1979B). The degree of Al-substitution in goethite appears not to be influenced by the presence of salts in the initial solution. The degree of Al-substitution is not affected whether one starts with an Al-ferrihydrite or with ferrihydrite in an aluminate solution (Lewis and Schwertmann, 1979A).

The solubility of ferrihydrite increases with increasing [OH]. Therefore goethite formation is favoured by increasing [OH]. Hematite formation is promoted by increasing [Al] (aluminum in solution retards goethite nucleation) and temperature (Lewis and Schwertmann, 1979B). In general hematite formation is promoted by low pH, Mg^{2+}, Ca^{2+} and Al^{3+}; high pH, CO_3^{2-}, SO_4^{2-} and Fe^{2+} favour goethite crystallization. Crystallization is retarded or inhibited by silicate (Schwertmann and Taylor, 1972), phosphate, oxalate (Fischer and Schwertmann, 1975) and other organic compounds (Landa and Gast, 1973 and references therein). Retardation can be overcome by seeding with goethite crystals.

All experimental results indicate that goethite formation and characteristics are extremely sensitive to the experimental conditions. The presence of species in solution promoting or retarding crystallization is of major importance in obtaining (aluminous) goethite in model systems. Besides goethite, hematite, lepidocrocite or maghemite may form simultaneously even in well-characterized experimental systems. α- to γ-FeOOH and Fe_2O_3 have amorphous precursors in ferrihydrite systems. The aging process is dependent on local conditions within the amorphous aggregates, which can result in intimately intergrown goethite and hematite. Natural systems, which obviously are more complex than experimental ones, will be (considerably) more difficult to characterize in detail. It is apparent that (minor) changes in physical and chemical conditions during goethite growth process have impact on the kinetics of this process and may result in widely different goethites with respect to their chemical composition and crystallite size.

3 THERMODYNAMIC STABILITY OF GOETHITE

The relative thermodynamic stabilities of goethite and hematite represented in the reaction goethite = hematite + water have been the subject of considerable study (e.g. Schmalz, 1959; Wefers, 1966; Berner, 1969; Langmuir, 1971, 1972). Langmuir's work is the only study which takes into account the effects of particle size on the equilibrium. The pH_2O vs. temperature stability regions of goethite and hematite in Fig. 2 are from Langmuir (1971).

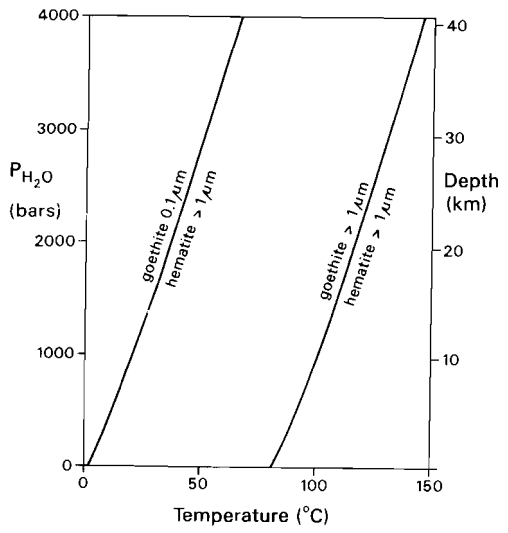

Fig. 2. pH_2O-T diagram illustrating the grain size influence on the goethite = hematite + H_2O equilibrium (after Langmuir, 1971). Equilibrium curves for goethite grains of 0.1 micrometer and hematite grains > 1 micrometer and for both phases > 1 micrometer are shown. The position of the curve for hematite with small grain size (0.1 micrometer) and goethite > 1 micrometer is in between the two curves, close to the left curve.

He concludes that fine-grained goethite (< 0.1 micrometer) is thermodynamically unstable with respect to coarse-grained hematite (> 1 mi-

crometer) under geologic conditions. Coarse-grained goethite (> 1 micrometer) would be stable up to about 80 °C at 1 bar. This conclusion refers to the pure goethite/hematite system.

In natural samples, goethite coexists often with hematite, chamosite and sometimes with lepidocrocite. In the presence of organic matter it may react to maghemite instead of hematite (Van der Marel, 1951; Schwertmann, 1959).

Langmuir (1971) pointed out that, because of sluggish kinetics, the goethite dehydration reaction may in fact take place at much higher temperatures as one would expect on thermodynamical grounds. The goethite stability field is enlarged with a metastable region for kinetic reasons. When heating goethite in DTA runs the transformation to hematite takes place at some 300 - 400 °C depending on its particle size, indeed a higher temperature than one would expect on thermodynamical grounds.

Apart from kinetic reasons, a straightforward application of thermodynamic data of the pure 'goethite = hematite + water' system to natural systems, is hindered by the chemical composition and the adsorbing capacity of goethite under natural conditions. Considerable substitution of Al and also some Si is observed in natural goethite (e.g. Norrish and Taylor, 1961; Norrish, 1975). In synthetic goethite up to 33 mol% Al can be isomorphically incorporated in the structure (Thiel, 1963; Franz, 1978). Experiments referring to the Si content contained in goethite have not been found by the present author. Goethite can adsorb for instance PO_4, CO_2 and organic compounds. This is also expected to have some influence on the goethite stability field, since the goethite surface structure is altered by sorption.

Regarding the influence of isomorphous substitution, Yapp (1983) calculated the stability of aluminous goethite with respect to hematite (with and without Al-substitution) according to the same reaction as in the pure system. He treated the goethite-diaspore solid solution as ideal. Though this is certainly an oversimplification (since solid solution only exists up to 33 mol% diaspore), trends found in the calculations are applicable. He concluded that fine-grained aluminous goethite is considerably more stable with respect to hematite than in the pure system and that it could well be stable under geologic conditions.

4 DETERMINATION OF GOETHITE

Apart from standard microscopical observation (transmittent and reflected light) and chemical analysis (obtained by microprobe or with classical wet chemical methods), goethite may be determined by means of X-ray diffraction analysis (XRD), infrared absorption spectroscopy (IRS), electron microscope observations, differential thermal analysis (DTA) and Mössbauer spectroscopy.

4.1 X-ray diffraction analysis

Goethite is easily determined with X-ray diffraction (XRD) analysis; its strongest reflection 110 has a d-value of 4.18 Å. A diffractogram of well-crystallized goethite is depicted in Fig. 3. Wolska (1977) mentioned that 3% goethite in a hematite matrix could be determined in X-ray diffractograms. Due to similar lattice spacings - the positions of some strong hematite reflections coincide with goethite reflections - the determination of traces hematite in a goethite-rich matrix is less easy. Tests carried out for the present research showed that 5% hematite in a goethite matrix was well detectable in Debye- Scherrer films

(standard addition, Debye-Scherrer camera; Fe K_α-rays). The determination of 2% hematite was tentative.

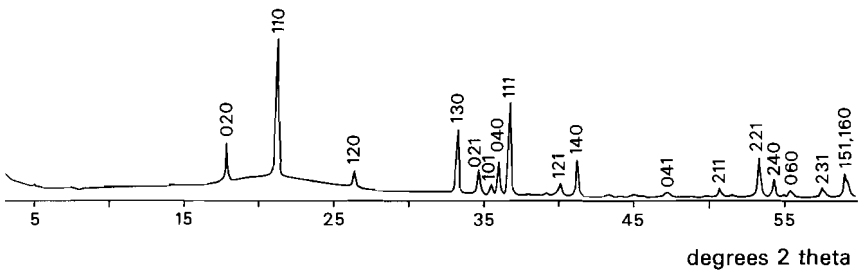

Fig. 3. Diffractogram of a well crystallized goethite (Cornwall, England). The hkl indices for each reflection are indicated. The vertical scale is arbitrary.

The position of the goethite 111 reflection appears to be dependent on the amount of Al-substitution. This is observed in natural (e.g. Norrish and Taylor, 1961) and in synthetic goethites (e.g. Thiel, 1963). It has become common practice to determine the aluminum content in goethite by the position of the 111 reflection (e.g. Schellman, 1964; Jonas and Solymar, 1970; Murad, 1979; Lewis and Schwertmann, 1979A, 1979B; Golden et al., 1979; Goodman and Lewis, 1981; Fysh and Clark, 1982). In synthetic systems this method is simple and straightforward. However, in the more complex natural systems, several isomorphous substitutions may act together and their combined influence on the lattice spacing is not exactly known. Isomorphous substitution of Si^{4+} is known to occur in goethites (Norrish, 1975). The effect of the small Si^{4+} (0.42 Å) ion on the goethite lattice is similar to that of Al^{3+} (0.51 Å) when replacing Fe^{3+} (0.64 Å). The larger difference in ionic radius between Si^{4+} and Fe^{3+} than between Al^{3+} and Fe^{3+} probably limits possible substitution far more than the better known Al-substitution (Schwertmann and Taylor, 1977).

Goethite grains (both synthetic and natural) may consist of aggregates of small crystallites, usually much smaller than the grain size. The fine crystallites show broad reflections in an X-ray diffractogram. The average size of these (goethite) crystallites may be calculated from the line width at half peak height in X-ray diffractograms. This procedure is referred to as crystallite size determination derived from X-ray line broadening. A correction for the instrumental line width has to be applied (Klug and Alexander, 1974). When dealing with goethite, the latter is usually approximated by the line width of a well-crystallized goethite specimen. The correction for the observed line width for the instrumental line width has to be done for each reflection separately. The size of the crystallites (usually in Å) in the direction corresponding to the d-value of each reflection can be calculated from the corrected line widths. Despite sometimes rather large uncertainties in the instrumental line width estimation, this procedure leads to reasonable estimates for the average crystallite size: Mørup et al. (1983) claim that the crystallite size determinations of their goethite with electron microscope observation was consistent with their crystallite size determinations derived from XRD line broadening.

Because absolute values of crystallite sizes are influenced by approximations for the instrumental line width, sometimes the line width

in degrees 2θ is given as a measure for the average crystallite size (e.g. Lewis and Schwertmann, 1979A, 1979B; Murad, 1982). Also the peak area is sometimes used for an estimate of the crystallite size (large peak areas indicate a small crystallite size; e.g. Lewis and Schwertmann, 1979A).

Natural goethite can have excess water in its structure. Then it is referred to as hydrogoethite. The difference between goethite and hydrogoethite can not be established by means of XRD.

4.2 Infrared absorption spectrometry

The presence of goethite can easily be established by infrared absorption spectrometry (IRS). Typical spectra of goethite and hematite are in Fig. 4 (after van der Marel and Beutelspacher, 1976).

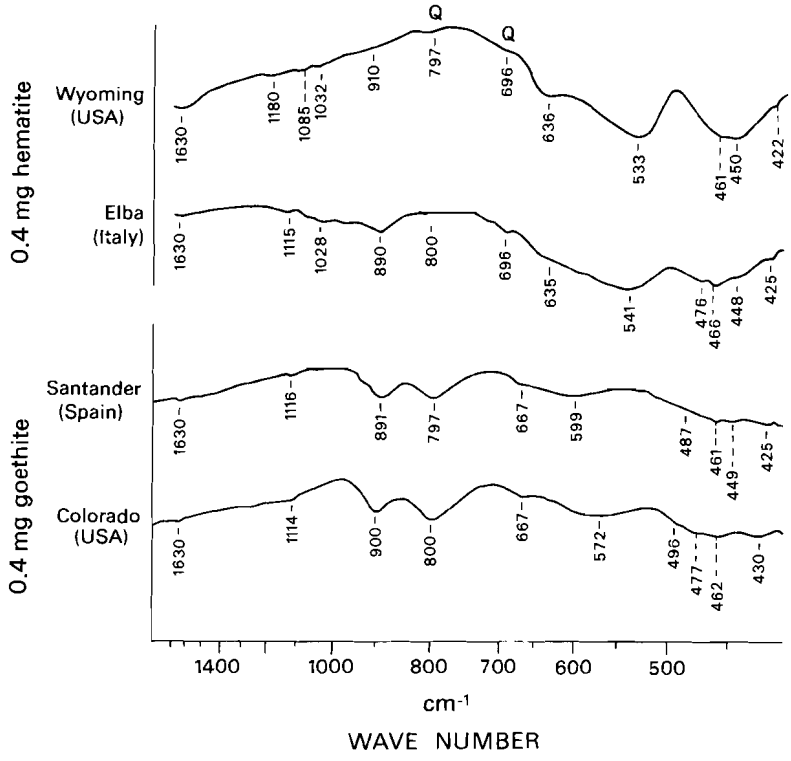

Fig. 4. Infrared spectrograms of natural hematite and goethite (after van der Marel and Beutelspacher, 1976). Q denotes a quartz absorption peak. The vertical scale is arbitrary.

The absorption bands at approximately 800 and 890 cm^{-1} are characteristic for goethite (Marshall and Rutherford, 1971; absorption bands are observed for akaganeite at 680 and 805 cm^{-1} and for lepidocrocite at 730 and 1025 cm^{-1}). Hematite shows absorption peaks at approximately 485, 550 and 585 cm^{-1} (e.g. Bentley et al., 1968). These absorption lines are bulk absorption lines related to bending and

stretching of bonding in the molecules under influence of the infrared light.

Traces hematite in a goethite matrix are difficult to detect. With the standard addition method it turned out that 5% hematite can be detected if absorption spectra are recorded (instead of the more routinely obtained transmission spectra).

Adsorption onto the goethite surface (which is not extraordinary) may be revealed by infrared studies. Suchlike studies focus on the high wave numbers (roughly 4000 cm^{-1} to 2000 cm^{-1}) where these absorption peaks are observed. Studied are for instance adsorption of phosphate (Atkinson et al., 1974; Parfitt et al., 1976), sulphate (Parfitt et al., 1977) and carbondioxide (Russell et al., 1975). Two types of surface hydroxyl groups are reported (Russell et al., 1974; Parfitt et al., 1976). Their interaction with D_2O is studied by Rochester and Topham (1979). The goethite surface structure is of importance for growth and aging mechanisms. The adsorbed species may influence the goethite stability field.

4.3 Electron microscope observations

Goethite crystals, either synthetic or natural, are reported as acicular, lath-shaped, star-shaped or irregular (e.g. Mackenzie et al., 1971; Sudo and Takahashi, 1971).

Natural goethite often occurs in ooliths. Oolithic goethite may have a considerable variation in their habitus. Vernet and Ferrari (1969) describe them as stocky prisms with diameters between 0.02 - 0.05 micrometer and heights between 0.03 and 0.08 micrometer, whereas goethite as flakes of 0.01 - 0.03 micrometer thickness with hexagonal outline is known in German (Dogger) and Turkish ooliths (Radszewski and Scheiderhöhn, 1962; Izgiz et al., 1972). Also goethite flakes with sizes of 1 - 2 micrometer and approximately 0.1 micrometer thickness occur; they are polycrystalline aggregates (Rohrlich, 1975).

Synthetic goethites, obtained by aging ferric hydroxide solutions, are needles of about 1 micrometer long and 0.04 micrometer wide with no evidence of granular material which was present in the freshly prepared amorphous gel (Landa and Gast, 1973). Sometimes a platy habitus is observed. Lewis and Schwertmann (1979A) prepared aluminous goethites at room temperature consisting of thin elongated plates of approximately 0.1 micrometer length with serrated edges and reduced growth in the direction of the crystallographic a-axis. They produce the usual acicular needles at higher temperatures. The substitution of aluminum in goethite leads to more defects and lowers the crystal ordering.

Composite goethite crystals consist of highly coherent intergrown crystallites as was revealed by high resolution electron microscopy and electron diffraction patterns (Cornell et al., 1983). Small crystals up to 0.03 * 0.1 micrometer are perfect single crystals; larger crystals (0.1 * 1 micrometer) often show striations, extinction contours and a stepped appearance in the [001] direction. Their composite nature can best be visualized through the development of fissures on the (100) face in acid media (Cornell et al., 1974). The perfect monocrystalline crystallites may be misoriented to each other by a few degrees; a narrow disorderded region may exist between them.

4.4 Differential thermal analysis

Pure, well-crystallized goethite has an endothermic peak at about 400 °C in differential thermal analysis (DTA) runs (e.g. Kulp and

Trites, 1951; Smykatz-Kloss, 1974), when it reacts to hematite. However, natural and synthetic goethites may dehydrate at considerably lower temperatures, down to 270 °C (e.g. Banerjee, 1970; Singh et al., 1977; Murad, 1979; Maeda et al., 1974; Lewis and Schwertmann, 1979A). Examples of goethite DTA profiles are presented in Fig. 5. Occasionally a double peak is observed (Fig. 5B).

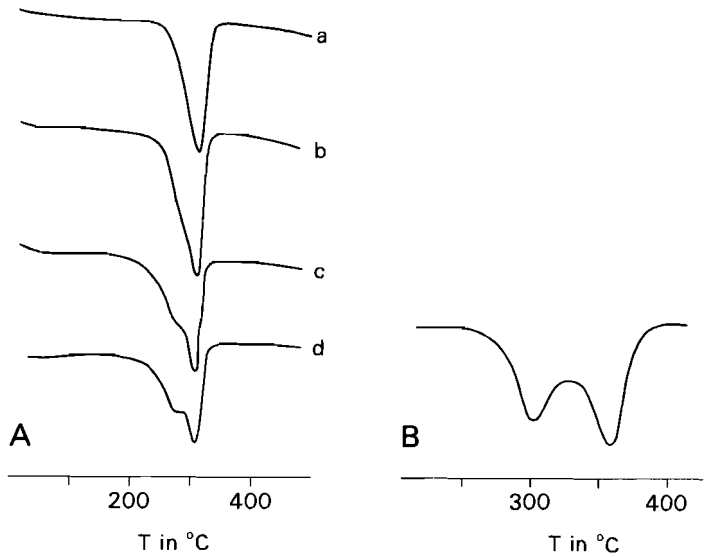

Fig. 5A. DTA profiles of a natural goethite showing the influence of sample treatment (after Murad, 1979). Curve a: unground sample; curve b: same sample broken, but not ground; curve c: same sample ground; curve d: same sample ground and corroded with HCl. The scale of the ordinate is arbitrary.

Fig. 5B. DTA profile of a synthetic goethite; the dehydration reaction takes place in two steps resulting in two peaks (after Maeda et al., 1974). The scale of the ordinate is arbitrary.

The lowering of the dehydration temperature is generally attributed to impurity content and/or particle size effects. Relatively broad peaks indicate a relatively large crystallite size spectrum. Murad (1979) points towards inhibition of the dehydration reaction in unground samples. If a sample is thoroughly ground, dehydration may take place at lower temperatures due to the presence of more escape conduits for the liberated water.

A goethite with a double peak DTA curve was studied by Maeda et al. (1974). They showed that both hematite and goethite exist during the temperature interval of the intermediate region between the two peaks. The dehydration process, which depends on the goethite structure, takes place in two steps.

Alternative explanations for small shoulders on the goethite DTA peak are advocated by Banerjee (1970) and Lewis and Schwertmann (1979A). Banerjee attributed the shoulder to excess water in the goethite and Lewis and Schwertmann to a sharp exothermic peak of ferrihydrite superimposed on the endothermic goethite peak.

Thermogravimetric analyses (TGA) indicate also that the water loss takes place during a temperature interval rather than at a specific

temperature (e.g. Forsyth et al., 1968; Bagin et al., 1976; Govaert et al., 1976A). The temperature interval of the dehydration reaction is small if well-crystalline goethite is dehydrating. Moreover, TGA curves point generally to an excess water in the goethite structure. Bagin et al. (1976) term this goethite type hydrogoethite. When the goethite is well-crystalline, its excess water is minimal. Such a goethite contains approximately 10.1 weight percent water (recalculated to an equivalent molar amount hematite this is 11.2 weight percent).

4.5 Mössbauer spectroscopy

Goethite, which usually exhibits typical asymmetrically broadened Mössbauer spectra (cf. Fig. 6A), has been investigated by many researchers (e.g. Forsyth et al., 1968; Govaert et al., 1976A; Murad, 1979; Golden et al., 1979; Goodman and Lewis, 1981; Fysh and Clark, 1982; Mørup et al., 1983). Well-crystalline goethite shows, below its Néel point, a well resolved spectrum of six (almost) completely symmetric peaks (cf. Harz and Loswithiel goethite in Fig. 6A).

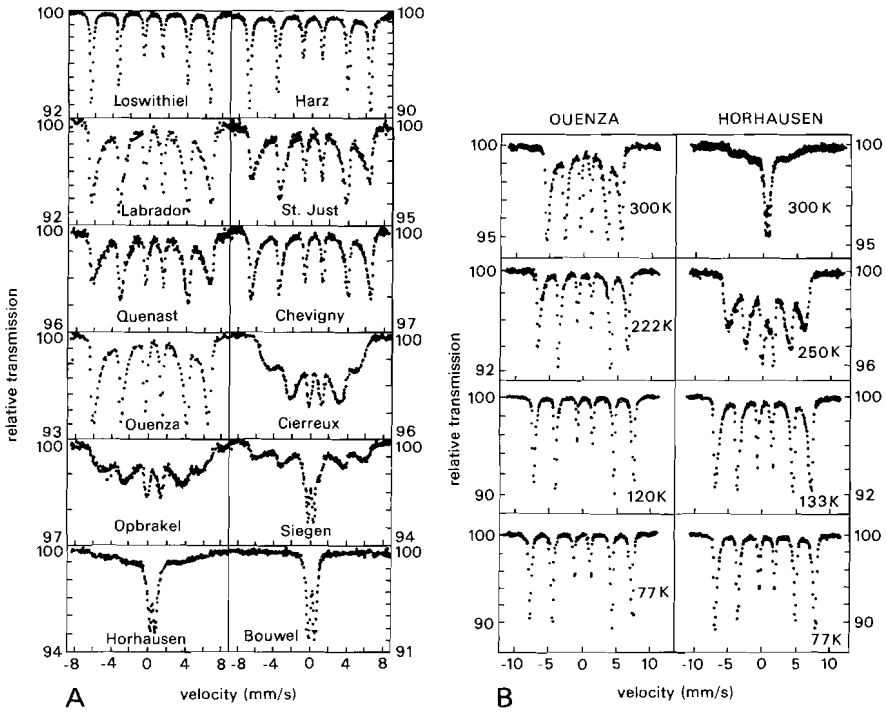

Fig. 6A. Mössbauer spectra at room temperature of some natural goethites (cf. Govaert et al., 1976A). Differences in crystallite size and substitution between the goethites give rise to differences in the asymmetrically broadened spectra. Well crystallized goethites (Harz, Loswithiel) show well defined spectra with narrow lines, whereas soil goethites (Horhausen, Opbrakel) show a paramagnetic doublet due to extremely small crystallite size and/or considerable substitution.

Fig. 6B. Influence of temperature (K) lowering on Mössbauer spectra, demonstrated on two samples of Fig. 6A. When the temperature is lowered the amount of asymmetric broadening decreases (cf. Govaert et al., 1976B).

With decreasing crystallite size the peaks in the Mössbauer spectrum become increasingly asymmetrically broadened and with extremely fine crystallite size the spectrum evolves into a paramagnetic doublet. A paramagnetic doublet is also observed when the temperature at which the Mössbauer spectrum is recorded, is above the (goethite) Néel point. When the temperature at which the spectrum is recorded, is lowered, the asymmetry of the peaks of a given goethite decreases (Fig. 6B).

The existence of a paramagnetic doublet in ultra-fine goethite crystallites is due to the extremely small relaxation time of their magnetic structure, which is then smaller than the time needed for the γ-rays to decay from a nuclear excited state to the ground state (approximately 10^{-8} sec.). Isomorphous substitution lowers the goethite Néel point and, at a given temperature below the Néel point, will lower the relaxation time of the magnetic structure. Thus, both a small crystallite size and an increase of isomorphous substitution contribute to increasingly asymmetrically broadened Mössbauer spectra of goethite. The asymmetry of a Mössbauer spectrum of a goethite sample is thus the result of its crystallite size distribution and isomorphous substitution (Murad, 1979, 1982; Johnston and Norrish, 1981). Explanations which take only crystallite size effects into account (Govaert et al., 1976A, 1976B, 1977) are an oversimplification of the real situation.

Mørup et al. (1983) report theoretical calculations on Mössbauer spectra of microcrystalline goethite and conclude that they are best described when magnetic exchange interaction between crystallites is taken into account. Hence, Mössbauer results do not only indicate that the goethite crystallite size and the amount isomorphous substitution are of importance for the understanding of its magnetic properties, but also that exchange interaction between crystallites can be important.

5 MAGNETIC PROPERTIES OF GOETHITE

Goethite has an uniaxial antiferromagnetic structure with collinear c-axis parallel spins (cf. Fig. 7). The iron atoms related by the 'b' glide planes are coupled ferromagnetically (resp. numbers 1 and 3; numbers 2 and 4). Antiferromagnetic coupling exists between neighbour atoms (resp. numbers 1 and 2; numbers 3 and 4). The chemical and magnetic unit cells are the same as was retrieved from single crystal Mössbauer and neutron diffraction studies (Forsyth et al., 1968).

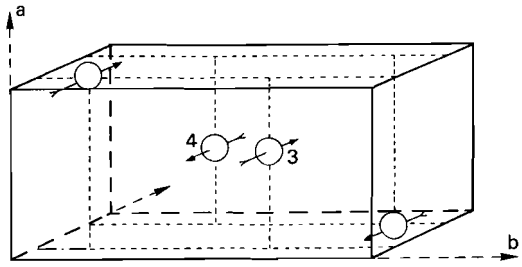

Fig. 7. Magnetic structure of goethite (after Forsyth et al., 1968). Only the iron atoms are shown for clarity. Their numbering corresponds to that in Fig. 1. The arrows indicate the orientation of the spins (c-axis directed). Atom 1 is coupled antiferromagnetically with atom 2; atom 3 with atom 4.

This structure poses some problems concerning the capability of goethite in carrying remanent magnetizations, since ideal antiferromagnetic materials cannot carry any remanence. Creer (1962) assumed initially that goethite has no spontaneous magnetization, but reported nonetheless that fine-grained goethite particles had high susceptibilities. Indeed, it turned out that goethite had a spontaneous magnetization, as Strangway et al. (1967, 1968) showed that goethite may carry a stable thermoremanent magnetization (TRM) when cooled through its Néel point in the geomagnetic field. This TRM was extremely weak and in some cases larger inducing fields than the geomagnetic field were necessary to produce any measurable remanence. The authors attributed the remanences to unbalanced spins in the goethite structure. Banerjee (1970) showed that in a single crystal the TRM was along the c-axis, the axis of antiferromagnetic alignment. In polycrystalline material the TRM would be due to "alignment of moment-carrying links" which is easy to achieve just below the Néel point. Hedley (1971) showed that with increasing Al^{3+} substitution the saturation magnetization increases, giving rise to higher remanences than in non-substituted material. The weak net-ferromagnetic moment could be correlated with the Al-substitution.

Well-crystalline goethite has a Néel point of approximately 120 °C (e.g. Hedley, 1971). The Néel points of natural goethites, however, vary with substitution, crystallinity and excess water in the crystal structure. This makes the wide variety of Néel points reported plausible. More substitution, lower crystallinity and higher excess water give rise to lower Néel points. Hedley (1971) reports an interval between 80 °C and 117 °C. Szytula et al. (1966) showed that a synthetic goethite has a Néel point as low as 60 °C; their fibrous mineral sample has a Néel point of 70 °C. Banerjee (1970) mentions 100 °C and 115 °C depending on the crystallinity. Strangway et al. (1968) report natural goethites with Néel points varying from 63 to 97 °C. Bagin et al. (1976) showed that the Néel point of goethite decreased from 110 to 58 °C with increasing excess water. Heller (1978) demonstrated that the maximum temperatures in a goethite IRM blocking spectrum during continuous thermal demagnetization were approximately 90 °C. A remanence carried by goethite can be removed by heating up to above the maximum Néel point (approximately 120 °C) in a field free space.

A goethite remanence shows considerable hardness with respect to alternating field (AF) demagnetization (Strangway et al., 1968; Banerjee, 1970; Hedley, 1971; Ryabushkin et al., 1976) due to its antiferromagnetic character with high exchange energies of the sublattices. The hardness is demonstrated as well by acquisition curves of the isothermal remanent magnetization (IRM acquisition curves or remanent acquisition (RA) curves). Goethite shows widely different RA curves. Occasionally, goethite RA curves are very similar to hematite RA curves, but in other cases saturation of the IRM is sometimes not reached in applied fields of 5 Tesla (Heller, 1978; Lowrie and Heller, 1982). The contribution of goethite to the IRM is small in fields lower than 1.5 Tesla. Thompson (1986) shows that IRM saturation is not achieved in a 20 Tesla field for a well-crystallized goethite.

The coercive force (H_c) of synthetic goethite is reported by Banerjee (1970) to be depending upon the goethite structure (H_c values of $<0.4*10^4$ Am^{-1} for an antiferromagnetic goethite of high purity and approximately $2*10^4$ Am^{-1} for a less well-crystalline goethite).

The goethite saturation magnetization (J_s) is one to three orders of magnitude smaller than reported J_s values for hematite. Bagin et al. (1976) measured values of 0.025 to 0.15 Am^2kg^{-1} increasing with more excess water in the structure. Pastrana and Hopstock (1977) give values

of 0.014 and 0.026 Am^2kg^{-1}. Morris et al. (1985) report J_s values of 0.06 and 0.10 Am^2kg^{-1} for commercial goethite powders. Hedley (1971) reports values increasing from practically zero to 1 Am^2kg^{-1} with rising aluminum content in the goethite. His upper limit of J_s is the most extreme reported.

Goethite initial susceptibilities are approximately $0.4*10^{-6}$ m^3kg^{-1} (Creer, 1962; Strangway et al., 1968; Forsyth et al., 1968). Banerjee (1970) reports figures of some $1.0*10^{-6}$ m^3kg^{-1}.

Goethite low-temperature behaviour is investigated by Heller (1978) and Lowrie and Heller (1982). J_{rs} curves showed a continuous increase with lowering temperature. Heller (1978) studied the rockmagnetic features of goethite-bearing limestone during thermal treatment at progressively higher temperatures. He concluded that hematite was formed at the expense of goethite at approximately 300 °C and that traces magnetite were created above 550 °C.

6 IMPLICATIONS FOR THE PRESENT STUDY

From the foregoing it is apparent that many magnetic parameters of natural goethite are rather poorly known, such as the coercive force (H_c), remanent coercive force (H_{cr}) and isothermal remanent magnetization (J_{rs}). There is a great variety in reported values for the saturation magnetization (J_s), so that a similar variety in the other parameters may exist as well. About the behaviour of goethite rockmagnetic parameters in a grain-size dependent framework, hardly anything is known at all. Knowledge of grain size dependence of magneto-mineralogical parameters may contribute to a better understanding of the mechanism by which goethite exhibits a magnetic remanence. Chemical differences in goethite may also result in differences in magneto-mineralogical parameters (e.g. the J_s dependence on Al-substitution).

The goethite of which the magnetic behaviour during low- and high-temperature treatment is reported in Heller's (1978) and Lowrie and Heller's (1982) papers, is rather poorly defined with respect to its chemistry and grain size. Thermal experiments with well defined goethite samples are desired as an extension of Heller's experiments to achieve a better interpretation of thermal demagnetization curves of goethite-bearing rock samples. This is especially important because goethite is known to decompose to hematite at temperatures of 200 to 350 °C. It produces new magnetic grains in the sample which may carry a spurious remanence.

To study the processes involved, artificial samples containing natural goethites were prepared according to the procedure described by Dankers (1978) and Hartstra (1982). Details on the chemical and mineralogical characterization of the goethites and on the preparation of the artificial samples are presented in chapter 2, variations in isothermal (remanent) magnetization properties are treated in chapter 3, low- and high-temperature features in chapter 4 and the decomposition behaviour of goethite during annealing up to 700 °C in chapter 5.

7 REFERENCES

Atkinson R.J., Parfitt R.L., Smart R.S.C., 1974, Infrared study of phosphate adsorption on goethite, J.C.S. Faraday I 70, 1472-9.

Atkinson R.J., Posner A.M., Quirk J.P., 1968, Crystal nucleation in Fe(III) solutions and hydroxide gels, J. Inorg. Nucl. Chem. 30, 2371-81.

Bagin V.I., Gendler T.S., Kuz'min R.N., Rybak R.S., Urazayeva T.K., 1976, The weak ferromagnetism of natural hydrogoethites, Izv. Acad. Sci. USSR, Phys. Solid Earth 12, 328-33 (eng. ed.).

Banerjee S.K., 1970, Origin of thermoremanence in goethite, Earth Plan. Science Letters 8, 197-201.
Bentley F.F., Smithson C.D., Rozek A.L., 1968, Infrared spectra and characteristic frequencies 700 - 300 cm-1, Interscience, New York.
Bernal J.D., Dasgupta D.R., Mackay A.L., 1959, The oxides and hydroxides of iron and their structural inter-relationships, Clay minerals Bull. 4, 15-30.
Berner R.A., 1969, Goethite stability and the origin of red beds, Geochim. Cosmochim. Acta 33, 267-73.
Cornell R.M., Mann S., Skarnulis A.J., 1983, A high resolution electron microscopy examination of domain boundaries in crystals of synthetic goethite, J.C.S. Faraday I 79, 2679-84.
Cornell R.M., Posner A.M., Quirk J.P., 1974, Crystal morphology and the dissolution of goethite, J. Inorg. Nucl. Chem. 36, 1937-46.
Creer K.M., 1962, On the origin of the magnetization of red beds, J. Geomagn. Geoelectr. 13, 86-100.
Dankers P.H.M., 1978, Magnetic properties of dispersed natural iron-oxides of known grain-size, Ph.D. thesis University of Utrecht, 143pp.
Deer W.A., Howie R.A., Zussman J., 1962, Rock forming minerals Vol 5, Non silicates, Longmans London.
Derie R., Ghodsi M., Hourez R.J., 1975, A new method for the preparation of acicular goethite crystals, J. appl. Chem. Biotechnol. 25, 509-13.
Ewing F.J., 1935, The crystal structure of diaspore, J. Chem. Phys. 3, 203-7.
Fischer W.R., Schwertmann U., 1975, The formation of hematite from amorphous Fe(III)hydroxide, Clays Clay Minerals 23, 33-7.
Forsyth J.B., Hedley I.G., Johnson C.E., 1968, The magnetic structure and hyperfine field of goethite (α-FeOOH), J. Phys. C2 1, 179-88.
Franz E.D., 1978, Synthetic solid solutions between goethite and diaspore, Min. Mag. 42, 159.
Fysh S.A., Clark P.E., 1982, Aluminous goethite: A Mössbauer study, Phys. Chem. Minerals 8, 180-7.
Golden D.G., Bowen L.H., Weed S.B., Bigham J.M., 1979, Mössbauer studies of synthetic and soil-occurring aluminum substituted goethites, Soil Sci. Soc. Am. J. 43,802-8.
Goldstaub S., 1935, Structure de la goethite, Soc. France Min. Bull. 58, 25-43.
Goodman B.A., Lewis D.G., 1981, Mössbauer spectra of aluminous goethites (α-FeOOH), J. Soil Sci. 32, 351-63.
Govaert A., Dauwe C., De Sitter J., De Grave E., 1976B, On the surface contribution to the line profile of small particles of goethite, J. Phys. Coll. C6 37, 291-2.
Govaert A., Dauwe C., De Sitter J., De Grave E., Robbrecht G., 1977, On the bulk and surface contributions to the magnetic hyperfine field of small particles of goethite (α-FeOOH), Physica B & C 86-88B, 1427-8.
Govaert A., Dauwe C., Plinke P., De Grave E., De Sitter J., 1976A, A classification of goethite minerals based on the Mössbauer behaviour, J. Phys. Coll. C6 37, 825-7.
Harms J.E., Morgan B.D., 1964, Pisolithic limonite deposits in North-West Australia, Proc. Australas. Inst. Min. Metall. 212, 91-124.
Harrison R.K., Aitkenhead N., Young B.R., Dagger P.F., 1975, Goethite from Hindlow, Derbyshire, Bull. Geol. Surv. Great Britain 52, 51-4.
Hartstra R.L., 1982, Some rockmagnetic parameters for natural iron-titanium oxides, Ph.D. thesis University of Utrecht, 145pp.
Hedley I.G., 1971, The weak ferromagnetism of goethite (α-FeOOH), Zeitschrift Geoph. 37, 409- 20.
Heller F., 1978, Rockmagnetic studies of Upper Jurassic limestones from Southern Germany, J. Geophys. 44, 525-43.
Izgiz S., Burchard W.G., Butenuth E., Fraenzele O., 1972, Elektronenmikroskopische Untersuchungen zur Morphologie des Goethites am Beispiel türkischer Eisenerze, Tscherm. Min. Petr. Mitt. 17, 250-62.
James H.L., 1966, Chemistry of the Iron-rich Sedimentary Rocks, Geol. Surv. Prof. Paper 440-W., U.S. Gov. Printing Office, Washington, 61pp.
Johnson C.E., 1969, Antiferromagnetism of γ-FeOOH: a Mössbauer study, J. Phys. C (solid state physics) series 2, 1996-2001.
Johnston J.H., Norrish K., 1981, A ^{57}Fe Mössbauer spectroscopic study of a selection of Australian and other goethites, Aust. J. Soil Res. 19, 231-7.
Jónás K., Solymàr K., 1970, Preparation, X-ray, derivatographic and infrared study of aluminum-substituted goethites, Acta Chim. Acad. Sci. Hung. 66, 383-94.
Klug H.P., Alexander L.E., 1974, X-ray diffraction procedures, J. Wiley & sons New York, Chapman and Hall, London, second edition.

Kulp J.L., Trites A.F., 1951, Differential thermal analysis of natural hydrous ferric oxides, Am. Min. 36, 23-44.

Landa E.R., Gast R.G., 1973, Evaluation of crystallinity in hydrated ferric oxides, Clays Clay Minerals 21, 121-30.

Langmuir D., 1971, Particle size effect on the reaction goethite = hematite + water, Am. J. Sci. 271, 147-56.

Langmuir D., 1972, Correction particle size effect on the reaction goethite = hematite + water, Am. J. Sci. 272, 972.

Lewis D.G., Schwertmann U., 1979A, The influence of Al on iron oxides. part III: preparation of Al-goethites in M KOH, Clay Minerals 14, 115-26.

Lewis D.G., Schwertmann U., 1979B, The influence of aluminum on the formation of iron oxides IV: The influence of [Al], [OH] and temperatura, Cleys Clay Minerals 27, 195-200.

Loseva G.V., Murashko N.V., Petukhov E.P., Novitskiy V.A., Teplyakova N.V., 1976, Transformation of δ-FeOOH into goethite and hematite, Phys. Solid Earth 11, 548-52 (eng. ed.).

Lowrie W., Heller F., 1982, Magnetic properties of marine limestones, Rev. Geoph. Space Phys. 20, 171-92.

Mackay A.L., 1960, β-ferric oxyhydroxide, Min. Mag. 32, 545-57.

Mackenzie R.C., Fouett E.A.C., Meldau R., 1971, The oxides iron, aluminum and manganese, in: the electron optical investigation of Clays (ed. Gard J.A.), Mineral. Soc. London, 315-44.

Maeda Y., Igarashi M., Terada A., Yoshimura F., 1974, On the intermediate state of dehydration of synthetic goethite, Japan. J. Appl. Phys. 13, 381-2.

Marshall P.R., Rutherford D., 1971, Physical investigations on colloidal iron-dextran complexes, J. Colloid Interface Sci. 37, 390-402.

Morris R.V., Lauer H.V., Lawson C.A., Gibson E.K., Nace G.A., Stewart C., 1985, Spectral and other physico-chemical properties of submicron powders of hematite (α-Fe_2O_3), maghemite (γ-Fe_2O_3), magnetite (Fe_3O_4), goethite (α-FeOOH) and lepidocrocite (γ-FeOOH), J. Geophys. Res. B90, 3126-44.

Mørup S., Madsen M.B., Franck J., Villedsen J., Koch C.J.W., 1983, A new interpretation of Mössbauer spectra of microcrystalline goethite: "superferromagnetism" or "super-spin-glass" behaviour?, J. Magn. Magn. Mat. 40, 163-74.

Murad E., 1979, Mössbauer spectra of goethite: evidence for structural imperfections, Min. Mag. 43, 355-61.

Murad E., 1982, The characterization of goethite by Mössbauer spectroscopy, Am. Min. 67, 1007-11.

Norrish K., 1975, Geochemistry and mineralogy of trace elements, in Nicholas D.J.D., Egan A.R. (eds.) Trace elements in Soil-Plant-Animal systems, Acad. Press New York, 55-81.

Norrish K., Taylor R.M., 1961, The isomorphous replacement of iron by aluminum in soil goethites, J. Soil Sci. 12, 294-306.

Parfitt R.L., Russell J.D., Farmer V.C., 1976, Confirmation of the surface structures of goethite (α-FeOOH) and phosphated goethite by infrared spectroscopy, J.C.S. Fareday I 72, 1082-7.

Parfitt R.L., Smart R.St.C., 1977, Infrared spectra from binuclear bridging complexes of sulfate adsorbed on goethite, J.C.S. Faraday I 73, 796-802.

Pastrana J.M., Hopstock D.M., 1977, Magnetic properties of natural hematite and goethite, AIME Trans. 262, 1-5.

Peacock M.A., 1942, Goethite and lepidocrocite, Trans. R. Soc. Canada IV 36, 107-18.

Radszewski D.E., Scheiderhöhn P., 1962, Elektronenmikroskopische Untersuchungen von Nadeleisenerz-ooiden in Pulverpräparaten und Dünnschliffen, Beitr. Mineral. Petr. 8, 349-53.

Rochester C.H., Topham S.A., 1979, Infrared study of surface hydroxyl groups on goethite, J.C.S. Faraday I 75, 591-602.

Rohrlich V., 1975, Microstructure and microchemistry of iron ooliths, Mineralium Oeposita 9, 133-42.

Rooksby L., 1951, X-ray diffraction and crystal structures of clay minerals, London, (page 264).

Russell J.D., Parfitt R.L., Fraser A.R., Farmer V.C., 1974, Surface structures of gibbsite, goethite and phosphated goethite, Nature 248, 220-1.

Russell J.D., Paterson E., Fraser A.R., Farmer V.C., 1975, Adsorption of carbon dioxide on goethite (iron oxide hydroxide) surfaces and its implications for anion adsorption, J.C.S. Faraday I 71, 1623-30.

Ryabushkin P.K., 1976, Variability of magneto-mineralogical properties of iron hydroxides, Izv. Acad. Sci. USSR, Phys. Solid Earth 12, 723-6 (eng. ed.).

Sampson C.F., 1969, The lattice parameters of natural single crystal and synthetically produced goethite (α-FeOOH), Acta Cryst. B25, 1683-5.

Schellmann W., 1964, Zur Rolle des Aluminiums in Nadeleisenerz Oolden, N. Jhrb. Min. Monatsh. 1964, 49-56.

Schmalz R.F., 1959, A note on the system Fe2O3-H2O, J. Geophys. Res. 64, 575-9.

Schwertmann U., 1959, Synthesis of definite iron oxides under various conditions, Zeitschr. Anorg. Allg. Chem. 298, 337-48.

Schwertmann U., Taylor R.M., 1972, The influence of silicate on the transformation of lepidocrocite to goethite, Clays Clay Minerals 20, 159-64.

Schwertmann U., Taylor R.M., 1977, Iron oxides (in soils), in Dixon J.B., Weed S.B. (eds.), Minerals in Soil Environments, Soil Sci. Soc. Am. Madison Wisconsin, 145-80.

Singh A.K., Jain B.K., Chandra K., 1977, Mössbauer studies of natural goethite and bog iron ore, Phys. Stat. Sol. A 44, 443-7.

Smykatz-Kloss W., 1974, Differential thermal analysis, minerals and rocks Vol 11, Springer Verlag, Berlin-Heidelberg-New York, 185pp.

Strangway D.W., Honea R.M., McMahon B.E., Larson E.E., 1968, The magnetic properties of naturally occurring goethite, Geophys. J. R. Astr. Soc. 15, 345-59.

Strangway D.W., McMahon B.E., Honea R.M., 1967, Stable magnetic remanence in antiferromagnetic goethite, Science 158, 785-7.

Sudo T., Takahashi H., 1971, The chlorites and intrastratified minerals, in: Gard J.A. (ed.), The electronoptical investigation of Clays, Mineral. Soc. London, 277-300.

Szytula A., Burewicz A., Dyrek K., Hrynkiewicz A. Kulgawczuk D., Obuszko Z., Rzany H., Wanic A., 1966, Susceptibility measurements of the antiferromagnetic A-goethite, Phys. Stat. Sol. 17, K195-7.

Thiel R., 1963, Zum System α-FeOOH - α-AlOOH, Z. Anorg. Allg. Chemie 326, 70-8.

Thompson R., 1986, Modelling magnetization data using SIMPLEX, Phys. Earth Plan. Int. 42, 113-27.

Ven der Marel H.W., 1951, γ ferric oxide in sediments, J. Sed. Petrol. 21, 12-21.

Van der Marel H.W., Beutelspacher H., 1976, Atlas of infrared spectroscopy of clay minerals and their admixtures, Elsevier Sci. Publ. Comp. Amsterdam-Oxford-New York, 396pp.

Van der Woude J.H.A., De Bruyn P.L., 1983, Formation of colloidal dispersions from supersaturated iron(III)nitrate solutions. I Preparation of amorphous iron hydroxide, Colloids Surf. 8, 55-78.

Van der Woude J.H.A., Verhees P., De Bruyn P.L., 1983, Formation of colloidal dispersions from supersaturated iron(III)nitrate solutions. II Kinetics of growth at elevated temperatures, Colloids Surf. 8, 79-92.

Van der Woude J.H.A., Rijnbout J.B., De Bruyn P.L., 1984, Formation of colloidal dispersions from supersaturated iron(III)nitrate solutions, Colloids and Surfaces 11, 391-400.

Van Oosterhout G.W., 1965, The structure of goethite, Proc. Int. Conf. Magn. Nottingham, Inst. Phys. London, 529-32.

Vernet J.P., Ferrari J.M., 1969, Ultrastructure des oolithes ferrugineuses du Callovien du Jura méridional, C.R. séance SPHN, Genève NS4, 38-41.

Vlasow A.Y., Gornushkina N.A., 1973, Chemical remanent magnetization during the lepidocrocite-maghemite-hematite temperature transformation, Izv. Acad. Sci. USSR, Phys. Solid Earth 2, 110-5 (eng. ed.).

Wefers K., 1966, Zum System Fe2O3 - H2O, Ber. Dtsch. Keram. Ges. 43, 703.

Wolska E., 1977, Die Bedeutung von Aluminiumspuren im Alterungsvorgang von amorphem Eisen(III)Hydroxid für die Eliminierung der Goethitphase, Monatsh. Chem. 108, 819-28.

Yapp C.J., 1983, Effects of AlOOH-FeOOH solid solution on goathite-hematite equilibrium, Clays Clay Minerals 31, 239-40.

Zitzmann A. (ed.), 1977, The iron ore deposits of Europe and adjacent areas volume I, Bund. Geowiss. Rohst. Hannover (Schweizerbart), 418pp.

Zitzmann A. (ed.), 1978, The iron ore deposits of Europe and adjacent areas volume II, Bund. Geowiss. Rohst. Hannover (Schweizerbart), 386pp.

CHAPTER 2

GOETHITE: SEPARATION PROCEDURE, CHARACTERISTICS AND PREPARATION OF THE ARTIFICIAL SAMPLES

1 INTRODUCTION

The magnetic experiments, discussed in the next three chapters, were carried out with natural goethites, to enhance the interpretative value of their results for paleomagnetic applications. Goethites of non-hydrothermal origin were selected for the present investigation, because the predominant occurrence of goethite is in sedimentary rocks. The importance of sediments for paleomagnetic research is evident: sediments offer the most detailed record of the geomagnetic field for magnetostratigraphic and geomagnetic studies. Soil-goethite was not sampled, the other non-hydrothermal goethite types (section 1.2 of chapter 1) are represented in the five natural goethites studied. Investigated are two oolithic marine sedimentary goethites (from Kahlenberg and Blumberg, both in Western Germany), a pisolithic fluviatile replacement goethite (from the Robe River mining district, Western Australia), a caprock goethite (from the Menera mining district, Spain) and a gossan goethite (from Sain Bel, France).

Goethite-rich rocks from Kahlenberg, Blumberg and Sain Bel were collected in October-November 1983 during the sampling campaign for this study. The Robe River and Menera samples were commercial iron ore concentrates put kindly at our disposal by Hoogovens Ltd. IJmuiden (The Netherlands). The Kahlenberg, Blumberg, Sain Bel, Menera and Robe River samples are labelled respectively: MKB, MBL, FSB, MEN and RR.

A concise description of the goethite concentrates, which have been mixed with a non-magnetic matrix in order to obtain artificial samples, is given in chapter 3. The reader is referred to appendix 1 for general information concerning sampling sites, their geology and mining history (the samples are all 'ore-grade' goethite-rich rocks). The goethite separation procedure with purity controls of its products, some chemical and mineralogical characteristics of the goethite concentrates and the preparation methods of the artificial samples are discussed in the present chapter.

2 SEPARATION PROCEDURE

The raw samples were not monomineralic and goethite had to be separated from these raw samples. Preliminary optical investigation (transmittent and reflected light) combined with XRD examination showed that goethite was indeed a major constituent of the sampled material. Besides goethite, varying amounts of hematite, calcite, quartz and clay minerals were present. These minerals were frequently intimately intergrown as shown by microscopical observations. Literature study (cf. chapter 1 sections 1.2 and 3) indicated that goethite usually occurs in this way.

This implies that one has to take special care to remove as much as possible these intergrowths from the goethite concentrate. The prevalence of goethite to occur intimately intergrown made it very difficult to remove all other minerals completely. Consequently, small amounts of hematite, quartz and clay minerals in the goethite concentrates cannot be avoided.

The goethite was upgraded from the raw samples after establishing whether its amount in the raw sample was sufficient for the desired

rockmagnetic experiments. The procedure applied by Dankers (1978) and Hartstra (1982) to achieve high purity mineral concentrates of a well-defined grain size was for the greater part retained. This procedure consisted of five steps, schematically outlined below.

Crushing
Sieving step one
Heavy liquid separation
Magnetic separation
Micro-precision sieving (sieving step two)

2.1 Crushing

The samples were crushed by hand in a copper mortar to prevent magnetic contamination. This is important because goethite has only a very weak magnetic moment.

2.2 Sieving step one

Since the results of heavy liquid and magnetic separation considerably improve if the grain-size interval to be processed is not too large, the crushed samples were sieved before subsequent separation steps. A.S.T.M. specified sieves with pore sizes of 250 micrometer, 149 micrometer, 105 micrometer, 75 micrometer, 53 micrometer and 37 micrometer were used. Wet sieving was performed to make the amount of adhering small particles as small as possible. Acetone was used as flushing fluid.

2.3 Heavy liquid separation

Heavy liquid separation was carried out only on the MKB and MBL fractions, since in the other samples the content of light minerals was negligible. The separation was executed by the mineral separation laboratory at the Institute of Earth Sciences of the State University of Utrecht. A laboratory overflow centrifuge according to the design of IJlst (1973) was used. To remove intergrowths with a large quartz or calcite content the density of the separating bromoform-diiodoethane mixture was set at 3.15 g/cm^3 (natural goethite is reported with a density interval of 3.2 g/cm^3 to 4.2 g/cm^3). The smallest fraction (<37 micrometer) yielded unsatisfactory results in trial runs, so on this fractions no heavy liquid separation has been performed.

2.4 Magnetic separation

Magnetic separation was carried out by means of a Frantz isodynamic separator (Hess, 1956) adapted for separation in a liquid medium (modified after Greene and Cornitius, 1971). The iron block is set at an angle of 45 degrees to the horizontal plane with the slit between the pole shoes in vertical position facing down (cf. Fig. 1). A glass tube with three stopcocks (the so called separation tube, ST) is filled with alcohol and attached to the device between the pole shoes. The upper side of the ST consists of an opening through which the sample grains can be introduced. Grain supply for the separation of the coarse fractions (the grain size fractions of 250-149, 149-105, 105-75, 75-53 and 53-37 micrometer) was achieved with the standard automatic feeder. Grain supply for the separation of < 37 micrometer fractions was

achieved in a different way, because application of the standard feeder did not result anymore in a regular supply for these fine fractions. Therefore, a sample supply was created in suspended form in alcohol. The developed system (Fig. 1; see also Dekkers et al., in prep.) consists of a storage vessel where the suspension is vigorously stirred. A tube leads to the ST, which is actually a bypass in a closed pumping system. A widening just before the ST slows down the stream velocity of the incoming suspension. A small part of the incoming suspension settles down in the ST for magnetic separation, a much larger part is directly pumped back into the storage vessel by a nitrogen gas driven airlift. A closed system is created in this way. A regular supply of sample material is guaranteed, which leads to a considerable improvement of separation results. A small flow in the ST considerably enhances the separation capacity without damaging the quality of its results.

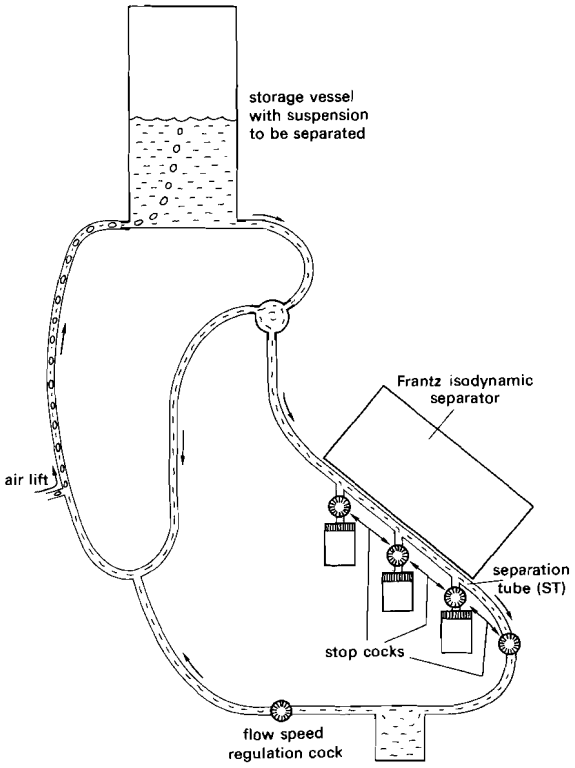

Fig. 1. Schematic picture of the device for the magnetic separation of fine-grained (<37 micrometer) particles (after Dekkers et al., in prep.).

2.5 Micro-precision sieving (sieving step two)

Micro-precision sieving was the final step in the separation procedure. The applied sieves are photo-etched sieves manufactured by Huikeshoven Ltd. (The Netherlands) with pore sizes of 250, 150, 100, 75, 55, 40, 30, 25, 20, 15, 10 and 5 micrometer. The procedure consisted of two steps:

1) Wet sieving with the aid of a Fritsch Analysette vibrating device. Acetone is used as flushing fluid; one sieve is used at a time.
2) Ultrasonic sieving to remove the last adhering particles from the material. This is carried out by placing the sieves one by one in an ultrasonic bath (Fig. 2); acetone is used as flushing fluid. When sieving batches for the first time, the acetone colours immediately brown. It is replaced by fresh acetone and the same batch is treated again. The procedure is repeated until the acetone stays clear after some 30 seconds ultrasonic treatment (requires sometimes up to five times acetone replacement). Since the acetone ultimately stays transparent, the ultrasonic damage to the goethite grains is apparently minor and a finite process. The grain-size intervals are optically controlled (transmitted light).

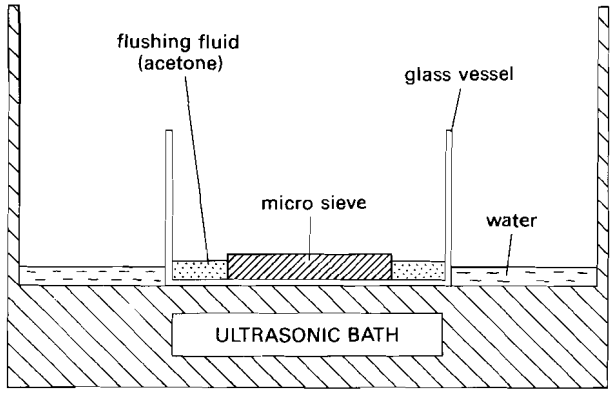

Fig. 2. Schematic representation of the micro-precision sieving device.

3 PURITY CONTROLS

3.1 Heavy liquid separation

The results of the heavy liquid separation were checked with a binocular. The amount of intergrowths of goethite with light minerals was low in the heavy mineral fraction ($d > 3.15$ g/cm^3).

3.2 Magnetic separation

The results of the magnetic separation cannot be checked by simple optical examination since goethite and hematite look similar under a microscope. Separation results were checked predominantly with XRD analysis. Also IRS analysis was applied.

Before magnetic separation was carried out, each sample was examined with XRD analysis and IRS analysis. By comparing XRD films and IRS spectra before and after a magnetic separation step, the separation results can be checked. When necessary, the current in the Frantz device can be adapted or a run can be repeated. XRD analysis was done by means of a Debye-Scherrer camera (diameter 114.6 mm,. Fe K_α-rays); IRS measurements were performed on a Perkin-Elmer 580 Infrared Spectrophotometer. Prior to magnetic separation, besides goethite, minor quartz is present in all samples. Hematite is a minor constituent of the MKB, MEN, FSB and RR samples; in the MBL sample no hematite could be detected with

XRD or IRS analysis. Minor calcite is present in the MKB fractions (IRS analysis). Magnetite or maghemite were never detected in any sample with XRD or IRS analysis.

The magnetic separation was performed in two steps: in the first step hematite (which has a slightly higher magnetic susceptibility than goethite) was removed from the raw sample. Goethite and the non-magnetic minerals stayed together in the remaining batch. The non-magnetic minerals (quartz, calcite) were extracted in the second step. In the RR fractions an extremely magnetic impurity appeared to be present in trace amounts. It was removed from the sample in an extra run in the Frantz device before removing the hematite from the goethite. The magnetic impurity and hematite could not be removed in a single run, because of clogging of the ST due to the magnetic impurity.

The appropriate currents in the Franz isodynamic separator for each step were determined in trial runs. After each trial run the result was checked with XRD and IRS analysis. The detection limit for hematite in a goethite-rich matrix was estimated by standard addition at approximately 4-5%; quartz and calcite are detectable down to approximately 2%. In the ultimately obtained grain-size fractions small amounts of hematite and quartz remain present due to intergrowths.

4 SOME CHARACTERISTICS OF THE GOETHITE CONCENTRATES

4.1 Chemical characteristics

Wet-chemical (WC) and microprobe (MP) analyses of the goethite concentrates are presented in Table I. Because optically homogeneous parts of goethite grains were selected for the microprobe analyses, the difference between wet-chemical and probe analyses is due to the presence of intergrown quartz, calcite and clay minerals. The microprobe analyses are averages based on some 25 spot analyses of different goethite grains. From the chemical variation in the spot analyses it is concluded that the FSB, RR and MEN goethites are more homogeneous than the oolithic MKB and especially MBL goethite. The grains of the MBL goethite were difficult to polish and gave a large scatter in the microprobe analyses. The hematite content cannot be estimated from the differences between wet-chemical and microprobe analyses, because iron is trivalent in both goethite and hematite.

The pure goethite composition is best approximated by the MP analysis (the goethite crystallite size is smaller than the spot size of the microprobe, cf. section 4.2.3). In the MP analysis contents below 0.5 percent can be regarded as insignificant. Besides Fe, Si is present in all goethites (SiO_2 between some 2.5 and 5 weight percent). The Al content is varying from insignificant amounts (FSB) up to some 7 weight percent Al_2O_3 (MBL). Goethite is known to show isomorphous substitution and for its adsorbing capacities (cf. chapter 1). The aluminum is isomorphously substituted in the goethite lattice. The silica is at least for its majority sorbed or dispersed between the goethite crystallites for reasons pointed out later.

RR goethite contains besides Fe, Al and Si, no other elements in significant amounts. FSB goethite (with the smallest crystallite size cf. 4.2.3) contains 4 weight percent SO_3, as sulphate sorbed onto the goethite or due to jarosite intergrowths. MEN goethite contains approximately one weight percent MnO and MgO. Mn can form a large number of Mn-bearing minerals in a supergene environment. Mn-oxyhydroxides have similar structures as corresponding Fe-oxyhydroxides (the manganese α-form has the mineral name groutite; the γ-form is termed manganite). Hence,

isomorphous substitution of trivalent Mn may well occur in goethite. Substitution of Mg in goethite is never described, so one may safely assume that, whenever it occurs, the substituted amount will be low. Mg has to be considered as a constituent of minerals intergrown on a microscale with goethite and/or is sorbed onto the goethite in the MEN, MBL and MKB goethite samples. The P_2O_5 in MKB and MBL goethite is as phosphate probably sorbed onto the goethite.

Table I: Wet-chemical (WC) and microprobe (MP) analyses of the goethite concentrates.

	MKB		MBL		MEN		FSB		RR	
	WC	MP	WC	MP	WC	MP	WC	MP	WC	MP
SiO_2	7.20	2.51	6.72	4.89	7.68	3.05	6.88	3.27	5.44	2.80
TiO_2	0.33	0.02	0.54	0.44	0.09	0.02	0.11	0.01	0.23	0.02
Al_2O_3	7.77	2.86	9.32	7.16	4.61	0.84	2.06	0.34	3.81	2.15
V_2O_3	nd	0.10	nd	nd	nd	0.04	nd	0.03	nd	0.04
Fe_2O_3	61.82	76.32	66.19	68.44	67.62	79.55	71.95	80.58	77.58	79.33
FeO	0.31	nd	0.53	nd	<dl	nd	0.26	nd	0.12	nd
MnO	0.20	0.24	0.13	0.06	2.88	0.93	<dl	0.02	0.12	0.05
MgO	1.13	0.92	0.85	0.86	0.98	0.95	0.09	0.10	0.12	0.09
CaO	5.45	0.27	0.57	0.26	0.24	0.17	0.07	0.08	0.14	0.07
Na_2O	0.08	0.13	0.04	nd	0.02	0.09	0.01	0.03	0.02	0.02
K_2O	0.53	0.07	0.47	nd	0.60	0.01	0.25	0.02	0.02	0.02
P_2O_5	1.31	1.79	0.74	0.84	0.23	0.28	0.17	0.07	0.12	0.07
H_2O	13.17	nd	13.43	nd	14.09	nd	17.68	nd	11.79	nd
SO_3	nd	0.81	nd	0.36	nd	0.31	nd	4.20	nd	0.33
total	99.30	86.10	99.53	83.34	99.04	86.29	99.53	88.77	99.89	85.16
Cu	60		10		58		885		28	
Zn	280		395		110		460		142	
Co	65		70		58		<dl		20	
Ni	177		235		180		40		52	
Pb	90		90		52		690		40	

Contents above the dashed line in weight percentages; below the dashed line in ppm; nd = not determined; <dl = below detection limit. Iron in the microprobe analyses is calculated as Fe_2O_3. Wet-chemical analytical methods are for total iron (as Fe_2O_3), SiO_2, TiO_2, P_2O_5 and Al_2O_3 colorimetry, for FeO titrimetry (titration with $K_2Cr_2O_7$; Fe_2O_3 in Table IV = total iron - FeO*1.11), for MnO, MgO, CaO, K_2O and Na_2O atomic absorption (air-acetylene flame), for H_2O the Penfield method and for trace elements atomic absorption (air-acetylene flame; Pb flameless). Wet-chemical analyses were done by the Service Laboratory of the Institute of Earth Sciences at the State University of Utrecht. Microprobe analyses were carried out on a TPD (Technisch Physische Dienst) microprobe fitted with a TRACOR Northern Energy Dispersive (ED) system. Operating conditions were 15 keV and 2 - 3 nA. ZAF matrix correction was applied.

The isomorphous substituted amount of tetravalent Si will be low in these goethites, because, apart from the rather deviating Si^{4+} ionic radius (only 0.42 Å; that of Fe^{3+} is 0.66 Å), one would expect a similar molar amount of divalent ions also substituted in the goethites in order to maintain electric neutrality. Inspecting the analyses, an amount of divalent ions to compensate for tetravalent Si is never present. Also the presence of ferrous iron for this compensation can be ruled out, because wet-chemical analyses show that the amount ferrous iron is insignificant (even for the total sample). One has to conclude that at least the majority of Si will be sorbed onto or dispersed between the goethite crystallites.

The marine sedimentary goethites (MKB, MBL) have the highest amount of isomorphous substitution - approximated by the total Al plus Mn amount (only MEN goethite has a significant Mn-content) - followed by RR and MEN goethite and finally by FSB in which hardly any isomorphous substitution occurs. RR and MEN goethite have the least sorbed or dispersed impurities - approximated by the quantities of the remaining non-Fe elements - followed by MKB, MBL and finally FSB goethite.

Trace-element contents are low, only the FSB goethite concentrate contains more Cu, Zn and Pb than the others indicating its origin from chalcopyrite-bearing pyritic ores.

The wet-chemical analyses show more Si and Al than corresponding average MP analyses. Intergrowths with goethite are predominantly quartz-rich, because the SiO_2 difference is the largest. This agrees with the presence of quartz in the goethite concentrates (XRD determination). The high CaO content of MKB goethite is due to carbonate because IRS analysis indicate CO_3-bonding absorption peaks. The high water content of FSB goethite is in fact a combined water + sulphur content, since SO_2 condenses with water when cooling the hot gases liberated from the samples (annealed at 900 °C, Penfield method).

The RR goethite seems to be the most homogeneous goethite concentrate because the difference between the MP and WC analysis is minimal. Also its water content approaches most closely that of 'ideal' goethite (10.1 weight percent). The higher Mn-content of MEN goethite in the WC analysis than in MP analysis indicates that, besides substituted Mn, also intergrown Mn-bearing minerals occur.

4.2 XRD characteristics

4.2.1 Unit cell calculations

The goethite unit cell parameters are calculated for each sample from the position of the goethite peaks in a Debye-Scherrer film (Fe K_α-rays) with the help of an interactive computer program (Strom, 1976). The reflections used in the calculation are listed in Table II.

Table II: Goethite reflections selected for unit cell calculation.

MKB		MBL		MEN		FSB		RR	
hkl	4θ	hkl	4θ	hkl	4θ	hkl	4θ	hkl	4θ
020	45.63	020	45.36	020	45.22	020	45.12	020	45.21
110	54.14	110	53.97	110	53.73	110	53.74	110	54.21
		120	66.89						
130	84.66	130	84.72	130	84.44	130	84.26	130	84.82
021	88.76	021	88.72	021	88.55	021	88.26	021	88.62
101	90.96					101	90.66	101	91.02
111	94.06	111	93.93	111	93.35	111	93.36	111	93.92
		121	102.54	121	102.05			121	102.42
		140	105.85	140	105.26			140	105.52
		211	130.98						
221	138.20	221	137.99	221	137.37	221	137.29	221	137.63
240	140.60			240	139.97	240	139.59	240	140.23
231	149.40								
160	154.21								

The 4θ values for each reflection were corrected for shrinkage of the film. Uncertainty in each reflection is estimated at 0.05 degrees; each reflection was given the same weight in the computation. The program computes the optimal unit cell by least square fitting. The unit cell parameters in Table III.

Table III: unit cell parameters of the natural goethites

axis	MKB	MBL	MEN	FSB	RR
a	4.585±0.003	4.586±0.004	4.612±0.004	4.611±0.004	4.596±0.004
b	9.908±0.007	9.884±0.008	9.920±0.008	9.962±0.009	9.909±0.008
c	2.995±0.002	3.000±0.002	3.011±0.002	3.008±0.003	2.998±0.002
Vol.	136.06	136.00	137.76	138.17	136.53

Lengths of the crystal axes in Å; volume (Vol.) in $Å^3$.

The FSB goethite approaches best the 'ideal' goethite cell parameters (e.g. Sampson, 1969; Harrison et al., 1975). This is a further indication that Si^{4+} will be for the majority dispersed between the goethite crystallites. The other goethites have smaller unit cells proportionally with the amount of other elements substituted in the lattice (predominantly Al^{3+}).

4.2.2 Aluminum content from the position of the 111 reflection

The d-value of the 111 reflection for each goethite sample is listed in Table IV.

Table IV: Comparison of the aluminum content of goethite derived from the position of the (111) reflection with that determined by microprobe analyses.

	2θ	d_{111}	mol% AlOOH XRD[1]	mol% AlOOH XRD[2]	mol% AlOOH + MnOOH MP		Cell volume
MKB	47.032	2.428	19.5	24	5.8	(5.5 0.3)	136.06
MBL	46.965	2.431	17.5	19	14.2	(14.1 0.1)	136.00
MEN	46.674	2.445	6.5	5	2.9	(1.6 1.3)	137.76
FSB	46.681	2.445	6.5	5	0.7	(0.7 0.0)	138.17
RR	46.959	2.431	17.5	19	4.1	(4.1 0.0)	136.53

Debye-Scherrer camera, Fe K_α-rays. XRD = X-ray diffraction; MP = microprobe; the first column between parentheses refers to the percentage AlOOH, the second to the percentage MnOOH. Cell volumes are in $Å^3$. The first column molar percentages AlOOH (XRD[1]) is based on the calibration curve of Thiel (1963); the second column (XRD[2]) on that of Norrish and Taylor (1961). The calibration curve of Norrish and Taylor is based on natural goethite; that of Thiel on synthesized goethite.

Comparison of the molar percentages AlOOH according to the different methods in Table IV leads to the conclusion that there is only moderate agreement between the two methods. The general trend (smaller d-values with higher aluminum contents) is reflected, but there are clear differences between the aluminum contents determined by XRD and microprobe. This is partly due to isomorphous substitution of other ions than Al^{3+} (predominantly Mn^{3+} and a very limited amount of Si^{4+}, which can not be totally excluded) in the goethite lattice. The effect of combined substitution on the lattice parameters is not known. A second cause for the moderate agreement is the unknown impact of the dispersed and/or

sorbed ions, which may lead to (a slight?) distortion of the goethite lattice itself, when it occurs in a goethite with isomorphous substitution. It is an oversimplification to attribute the smaller unit cell sizes in natural goethite solely to increasing aluminum contents.

4.2.3 Crystallite-size determination

The impurity contents and the presence of intergrowths implies that the crystallite size of the goethite samples is smaller than the grain size. To get an impression of the crystallite size and to determine the crystallite-size order of the samples, the line width at half peak height ($B_{1/2}$) of selected goethite peaks was measured in diffractograms (Cu K_{α}-rays, recording velocity one degree 2θ per minute). Correction for the instrumental line ($b_{1/2}$) width was made by subtracting the line width of corresponding reflections of a well-crystalline goethite. The average line widths of two well-crystalline goethites (from Loswithiel, Cornwall and from Pikes Peak, USA) were used. The two goethites revealed (nearly) identical line widths for corresponding reflections. The assumption is made that these goethites are single crystals, so that the line width of their reflections is only caused by instrumental broadening. This assumption may be not quite correct, but can surely be regarded as a good approximation (the calculated goethite crystallite sizes will be slightly too small). The relative crystallite- size order of the goethites will not be influenced by this procedure. The correction for the line width of the sample goethite is:

$\beta_{1/2} = B_{1/2} - b_{1/2}$ (Klug and Alexander, 1974)

which is generally valid for low angle and back reflections. The crystallite sizes (d-values of reflections) are computed with

$d_{hkl} = K*\lambda*(\beta_{1/2})^{-1}*\cos(\theta)^{-1}$ (Klug and Alexander, 1974)

K is a constant with an empirical value of 0.9 for line widths at half peak heights. λ is the wavelength of the X-rays in Å, consequently d_{hkl} is also in Å. Crystallite sizes perpendicular to 020, 110, 021, 111, 121 and 221 are computed. The results are listed in Table V. Because of the estimated instrumental line broadening, the presented crystallite sizes have to be regarded as somewhat approximate.

Table V: Crystallite sizes of selected d_{hkl} spacings of some natural goethites

hkl	MKB	MBL	MEN	FSB	RR
020	250	170	200	135	230
110	425	290	290	160	280
021	440	360	640	310	695
111	525	335	465	225	495
121	845	425	*	385	445
221	405	370	260	220	255
aver.	480	325	370	240	400

Crystallite sizes in Å; "aver." refers to the average crystallite size in each goethite sample. The * indicates that due to peak-overlap a proper measurement was impossible.

The crystallite sizes are considerably smaller than the grain sizes, so each goethite grain consists of many crystallites. It appears from

Table V that reflections with a non-zero "l" index generally have larger crystallite sizes than others, implying some elongation of the crystals in the direction of the crystallographical c-axis in agreement with numerous EM-observations of goethite crystallites. Sample ranking results in the following crystallite size order:

FSB < MBL < MEN < RR < MKB

4.3 DTA-characteristics

Differential scanning calorimetry (DSC) runs (Dupont 1090 DSC cell) for each goethite sample are given in Fig. 3.

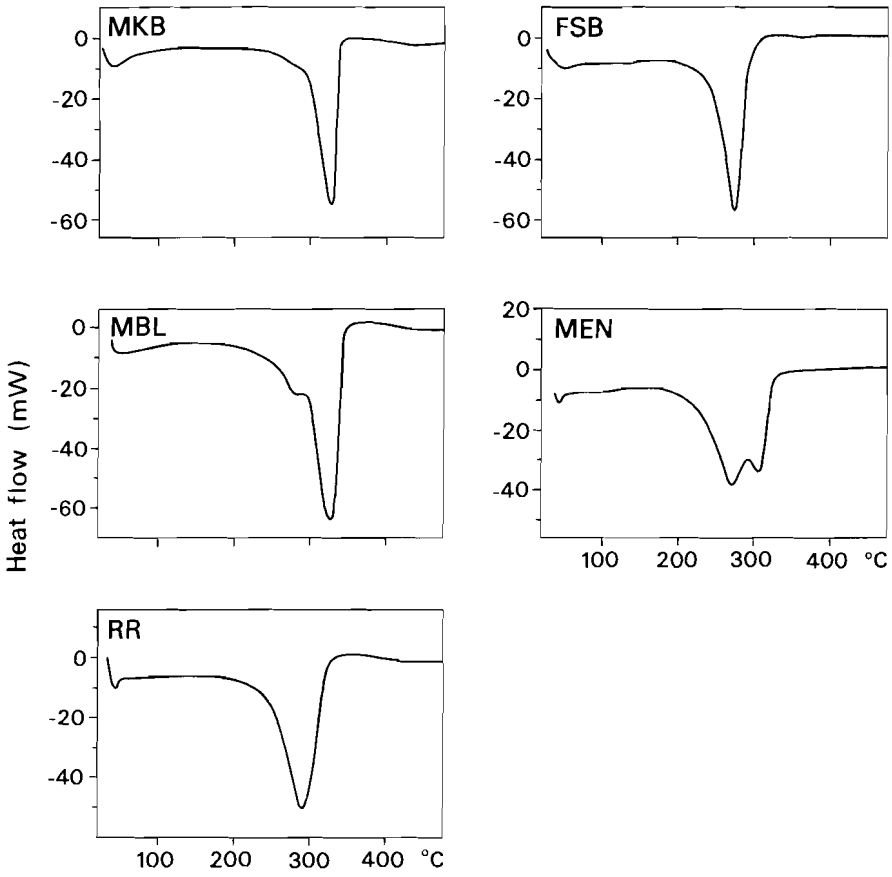

Fig. 3. Differential scanning calorimetry (DSC) runs of the natural goethites investigated. Heating rate of the goethite is 10 °Cmin^{-1} (in air).

There are distinct differences between the goethites. Relatively sharp singular peaks occur (MKB and FSB goethite), a broader singular peak (RR goethite), a peak with a small shoulder developed on its low temperature side (MBL goethite) and a curve with two maxima (double peak, MEN goethite). Despite large differences in the shape of the DSC

curves, the first signs of the onset of the endothermic goethite dehydration reaction already shows up at approximately 200 °C in all samples. The shape of DTA curves (and curves obtained with similar thermal techniques, as DSC) is dependent on sample preparation (e.g. Murad, 1979). The differences in the present DSC curves are due to different properties of the goethites themselves, since all samples underwent exactly the same preparation procedure.

The temperature at which the relative sharp peaks of MKB and FSB goethite occurs, is lower in the FSB sample. The relatively sharp peaks indicate that in both samples the crystallite-size spectrum is relatively small. The average crystallite size of the FSB would be smaller than that of MKB. This is indeed the case (cf. section 4.2.3), but the higher decomposition temperature of the MKB goethite can also be due to its higher Al-content. This will be pointed out later.

RR goethite, with a broader peak than the aforementioned two goethites, has a larger crystallite-size spectrum. Its average crystallite size is close to that of MKB goethite (cf. section 4.2.3). The shoulder on the MBL curve and the two-peak MEN curve indicate that the dehydration reaction in those samples occurs in two stages; in the intermediate region both hematite and goethite will be present (e.g. Maeda et al., 1974). It could be that in MBL and especially in MEN goethite two crystallite types exist; one is dehydrating at a distinctly lower temperature than the other, resulting in a shoulder or in a two-peak curve depending on the sample abundances of each type. The presence of two goethite crystallite types did not show up in the XRD determination.

Regarding the high temperature of the MKB goethite DSC peak, it is remarkable that MBL goethite also displays its peak in an identical temperature interval, despite its smaller crystallite size (cf. section 4.2.3). In fact, the crystallite size of MBL goethite approaches that of FSB goethite most of all samples. The MBL goethite has also a high amount of substituted Al. Yapp's (1983) thermodynamic calculations indicate that Al-goethite is considerably more stable with respect to hematite plus water than Al-free goethite (in agreement with the fact that diaspore has a much larger thermal stability than goethite). This is in excellent agreement with the observed DSC curves. The general observation that Al-bearing goethite should dehydrate at lower temperatures than Al-free goethite (e.g. Smykatz-Kloss, 1974) is thus not due to the Al content of the goethite but to its smaller crystallite size (generally Al-goethite has a small crystallite size).

Thermogravimetric analysis (TGA) showed that water-loss starts even below 100 °C; the temperature interval of the dehydration reaction itself closely corresponds with that determined by DSC. The TGA curves are indicative for a rather low crystallite size which is in agreement with XRD-broadening determinations.

4.4 Determination of the hematite content

The hematite content of each microprecision-sieved fraction was estimated magnetically. Acquisition curves of the isothermal remanent magnetization (RA curves) for each fraction were determined in applied fields up to $16*10^6$ Am^{-1} (20 Tesla). All magnetic minerals (goethite, hematite and maghemite) were saturated in this field (in some RR fractions the goethite was not entirely saturated, however, since it was close to saturation, the magnetic percentage of the non-goethite minerals is only slightly biased). The fractions were subsequently thermally demagnetized at 150 °C. The goethite remanence is completely removed and the remaining magnetic moment is attributed to hematite (multiplied by 1.11 to

correct for the part of the hematite which is also thermally demagnetized; the correction factor is derived from thermal decay curves of hematite saturation remanences, cf. Dankers, 1978). Taking a saturation remanence of 0.2 Am^2kg^{-1} for hematite (e.g. Dankers, 1978, 1981; Hartstra, 1982) the measured hematite-moment is recalculated to a corresponding hematite weight. Results are compiled in Table VI.

Table VI: Magnetically determined hematite percentages

	MKB	MBL	MEN	FSB	RR
250 - 150	6	<2	4	6	3
150 - 100	4	<2	4	6	4
100 - 75	6	<2	4	7	2
75 - 55	6	<2	4	7	3
55 - 40	5	<2	5	11	4
40 - 30	5	<2	4	13	4
30 - 25	5	<2	5	15	5
25 - 20	4	<2	5	14	6
20 - 15	3	<2	5	14	6
15 - 10	2	2	6	16	8
10 - 5	<2	2	9	17	7*
< 5	3	2	7	14	7*

In the RR fractions maghemite appears to be present in trace amounts; comparison of RA curves of the RR fractions with fractions of the other samples revealed that the maghemite magnetic percentage is reasonably estimated by half of the non-goethite remanence. Because of its high saturation remanence compared to that of hematite, the maghemite weight content can be ignored compared to that of hematite. The smallest two fractions (10 - 5 and < 5 micrometer, indicated with an asterisk) contain a higher (trace) amount of maghemite. Therefore the magnetically estimated hematite content has unfortunately a larger error.

5 PREPARATION OF THE ARTIFICIAL SAMPLES

5.1 Samples for high-temperature measurements

The non-magnetic matrix should meet the following characteristics (after Dankers, 1978):

1) A low magnetic signal.
2) It has to withstand temperatures from -200 °C to +700 °C.
3) Homogeneous dispersion of the magnetic grains in the matrix has to be achieved.
4) The magnetic grains should remain fixed in the matrix during the experiments in order to retain the random orientation.
5) No reaction of the magnetic material should take place with the matrix, at least at room temperature.

Because goethite has a very low magnetization, the non-magnetic matrix has to be extremely pure to obtain interpretable results. It turned out that the original Al_2O_3 matrix applied by Dankers (1978) and Hartstra (1982) produced too much magnetic noise. After some trial runs it was decided to take a calcareous matrix for two reasons:

1) Its extremely low magnetic noise level (saturation remanence approximately $7*10^{-6}$ Am^2kg^{-1}, some 200 times lower than the Al_2O_3 matrix used before).
2) The possibility to simulate processes in calcareous rocks during

thermal demagnetization. Calcareous rocks form a large part of the sediments suitable for paleomagnetic research.

As a rule, approximately 400 mg goethite powder was put in each specimen to ensure reliably measurable magnetic signals. The manufacture of the artificial samples was carried out as follows. Sample moulds of 25 mm height and one inch inner diameter were prepared of a perspex tube. The bottom consisted of a piece of PVC which was glued to the perspex cylinders. Analytical grade $CaCO_3$ (Merck, Fe < 0.001%) was mixed with some 10% analytical grade Al_2O_3 (Baker, Fe < 0.01%). Before waterglass was added the $CaCO_3$-Al_2O_3 mixture was stirred in the sample mould with the magnetic grains to a homogeneous mixture. The sample mould was filled to the desired level by adding appropriate amounts of $CaCO_3$ and waterglass while stirring. Waterglass was added in small amounts because the mixture had to remain extremely viscous during the hardening to prevent settling of the magnetic grains. Hardening was done in a field-free space to prevent the acquisition of a post-depositional remanent magnetization (PDRM) in the specimens. After two weeks the bottom was removed and the samples were hardened further upside down for another two weeks.

Al_2O_3 was added because it is rather coarse-grained. During trial runs it appeared that the $CaCO_3$ was too fine-grained to obtain hardening within a reasonable time. The hardened part of the sample formed a fleece enclosing the rest from the air thus preventing its hardening. By adding coarse-grained Al_2O_3 the fleece was not formed and hardening of the specimen was achieved in four weeks.

The hardening of waterglass (Na-silicate.nH_2O) may be compared with the aggregation of silica from a supersaturated solution. The precipitation of silica occurs by neutralizing the sodium silicate solution with an acid. Colloidal particles will form, which are flocculated by the sodium ions in solution. The aggregation and flocculation rates are determined by kinetical factors (Iler, 1976). At approximately pH 6 rapid coagulation occurs. CO_2 is a weak acid which lowers the pH of the waterglass - a base substance - at the reaction zone, so that coagulation i.c. hardening occurs. Test runs carried out in a CO_2 atmosphere showed indeed that hardening was achieved in two days instead of four weeks. However, the specimens were too friable to withstand magnetic measurements in routine equipment.

The sample moulds are greased with vaseline to prevent water absorption by the perspex. The first series specimens with non-greased perspex holders was hardened concentrically from the edge which resulted in considerably more shrinkage in their inner parts.

5.2 Samples for room temperature high-field measurements

The size of samples for high-field measurements was dictated by the sample-holder size of the magnetometers available at the High Field Magnet Laboratory, Faculty of Physics, University of Nijmegen (The Netherlands). Maximum sample sizes are cylinders with a diameter of 4.5 mm and a height of 5 mm. Because no thermal experiments had to be carried out on these samples (only moderate heating to 150 °C) an epoxy resin (Araldit D with hardener HY 956, Cyba-Geigi) was selected as non-magnetic matrix. Its magnetic noise level is an order of magnitude lower than the calcareous waterglass matrix described in the previous section. The araldit-hardener mixture was already hardened for 60 to 75 minutes in a sample mould to an extremely viscous paste before adding the goethite grains. Settling of the grains was thus prevented. 20-30 mg goethite was

put in each sample. Grains with low remanences such as goethite, have such a low magnetic interaction that the packing density has no detectable influence on the magnetic signal as Dunlop (1971) showed in experiments with hematite.

6 REFERENCES

Dankers P.H.M., 1978, Magnetic properties of dispersed natural iron-oxides of known grain-size, Ph.D. thesis University of Utrecht, 143pp.

Dekkers M.J., Hartstra R.L., Mullender T.A.T., in prep., A device for the magnetic separation of fine-grained particles.

Dunlop D.J., 1971, Magnetic properties of fine particle hematite, Ann. Geophys. 27, 269-93.

Greena G.M., Cornitius L.E., 1971, A technique for magnetically separating minerals in a liquid mode, J. Sed. Petrol. 41, 310-2.

Hartstra R.L., 1982, Some rockmagnetic parameters for natural iron-titanium oxides, Ph.D. thesis University of Utrecht, 145pp.

Hess H.H., 1956, Notes on the operation of the Frantz isodynamic separator: instruction booklet, S.G. Frantz Company, Trenton New Yersey, USA.

Iler R.K., 1976, The chemistry of silica, John Wiley & Sons, 866pp.

Klug H.P., Alexander L.E., 1974, X-ray diffraction procedures, John Wiley & Sons New York, Chapman and Hall, London, 2nd edition, 966pp.

Maeda Y., Igarashi M., Terada A., Yoshimura F., 1974, On the intermediate state of dehydration of synthetic goethite, Japan. J. Appl. Phys. 13, 381-2.

Murad E., 1979, Mössbauer spectra of goethite: evidence for structural imperfections, Min. Mag. 43, 355-61.

Smykatz-Kloss W., 1974, Differential thermal analysis, minerals and rocks Vol 11, Springer Verlag Berlin-Heidelberg-New York, 185pp.

Strom C., 1976, UNITCELLD, an interactive APL program for computing cell constants, unpubl. Leiden.

Yapp C.J., 1983, Effects of AlOOH-FeOOH solid solution on goethite-hematite equilibrium, Clays Clay Minerals 31, 239-40.

Ujist L., 1973, A laboratory overflow-centrifuge for heavy liquid mineral separation, Am. Min. 58, 1088-93.

CHAPTER 3

MAGNETIC PROPERTIES OF NATURAL GOETHITE

PART I

GRAIN-SIZE DEPENDENCE OF SOME LOW- AND HIGH-FIELD RELATED ROCKMAGNETIC PARAMETERS MEASURED AT ROOM TEMPERATURE

Abstract

Five goethite concentrates, separated from natural samples of different supergene geological origin, are sieved in twelve well-defined grain-size fractions ranging from 250 micrometer down to <5 micrometer. The goethites show differences in their isomorphous substitution and in their contents of dispersed non-Fe elements. The crystallite size ranges from 240 Å to 480 Å, which is considerably smaller than the grain size of even the smallest fraction. Nevertheless grain-size dependent trends are present in the derived rockmagnetic parameters. Grain-size dependence is reported for the initial susceptibility (X_{in}), the high field susceptibility (X_{hf}), the saturation magnetization (J_s), the saturation remanence (J_{rs}; acquired in fields of $16*10^6$ Am^{-1} or 20 Tesla), the coercive force (H_c), ferromagnetic coercive force ($H_{c\ ferr.}$), remanent coercive force (H_{cr}) and the remanent acquisition coercive force ($H_{cr'}$). X_{hf}, H_c and H_{cr} decrease with grain size for each sample. A tendency to decrease with grain size is observed for J_{rs}. X_{in} shows a weak maximum in the intermediate grain-size range. $H_{c\ ferr.}$ is approximately constant in the coarse grain-size fractions; it falls in the same grain-size range as X_{in} rises. No grain-size dependence of J_s is observed. $H_{cr'}$ does not show a straightforward grain size dependence: in three samples it is grain-size independent and the other two it decreases with grain size.

There is a great variety between the samples in the absolute figures of J_s (30-450*10^{-3} Am^2kg^{-1}), J_{rs} (15-115*10^{-3} Am^2kg^{-1}), H_c (2-20*10^4 Am^{-1}), $H_{c\ ferr.}$ (2-70*10^4 Am^{-1}), H_{cr} (40-320*10^4 Am^{-1}) and $H_{cr'}$ (100-550*10^4 Am^{-1}). X_{in} shows smaller differences (0.50-1.50*10^{-6} m^3kg^{-1}) and X_{hf} is approximately equal for all samples (varying from 0.40*10^{-6} m^3kg^{-1} down to 0.20*10^{-6} m^3kg^{-1} with decreasing grain size). Sample differences and some ratios of these parameters are discussed in terms of different goethite chemical composition, crystallite size and the presence of intergrowths. The magnetic properties of microcrystalline goethite are best understood by taking into account crystallite size and exchange interaction amongst crystallites.

1 INTRODUCTION

The increasing importance of sedimentary rocks for paleomagnetic research requires a better knowledge of rockmagnetic parameters of goethite (α-FeOOH), which is generally thought to be the source of disturbing secondary magnetizations in sediments. The interest of paleomagnetists for goethite has already been raised since the early sixties, because goethite can be a constituent of red beds. Goethite is certainly not specifically associated with red beds: it may occur in trace amounts in virtually all sediments. Goethite may in principle carry a thermoremanent magnetization (TRM) as was first established by Strangway et al. (1967, 1968), but most goethite remanences carried in natural rocks are

considered to have been acquired below its Néel point by growth of goethite through its blocking volume, which makes it a chemical remanent magnetization (CRM) (e.g. O'Reilly, 1984). Goethite Néel points are reported to vary from 55 to 130 °C (e.g. Strangway et al., 1968; Hedley, 1971; Bagin et al., 1976), depending on crystallinity, isomorphous substitution and content of excess water. Well-crystalline goethite has a Néel point between 120 and 130 °C.

Goethite is an uniaxial antiferromagnetic mineral; spin-coupling is collinear and parallel to the c-axis (Forsyth et al., 1968). Since an ideal antiferromagnetic mineral can not carry a magnetic moment, the observed goethite remanence is due to deviations from the perfect antiferromagnetic structure, which result in a weak ferromagnetism. Various explanations for the weak ferromagnetism have been advocated: it would be caused by imperfect coupled spins, vacancies, impurities, crystal defects or an odd number of spins in very small goethite grains. A definitive explanation has yet to be given. It could well be possible that the weak ferromagnetism observed is caused by a combination of the above mentioned factors.

Goethite rockmagnetic parameters are sensitive to defects and isomorphous substitution in the crystal lattice. Hedley (1971) showed that the weak ferromagnetic moment increases when the aluminum content of the goethite increases. There is a great variety in reported figures for the saturation magnetization (J_s) of natural goethite as well as commercial goethite powders, from practically zero to 1 Am^2kg^{-1} (e.g. Hedley, 1971; Pastrana and Hopstock, 1977; Morris et al., 1985). Saturation remanence (J_{rs}) is only a slight fraction of the observed J_s figures. Initial susceptibility is reported to be some $0.4*10^{-6}$ m^3kg^{-1} (Creer, 1962; Strangway et al., 1968; Forsyth et al., 1968). Other rockmagnetic parameters are rather poorly known, e.g. Banerjee (1970) mentions coercive forces of $2*10^4$ Am^{-1} and $< 0.4*10^4$ Am^{-1}.

Goethite shows an extreme hardness with respect to alternating field (AF) demagnetization due to its antiferromagnetic character with high exchange energies of the magnetic sublattices (Strangway et al., 1968; Hedley, 1971; Banerjee, 1970; Ryabushkin et al., 1976). The hardness is also demonstrated in acquisition curves of the isothermal remanent magnetization (IRM); these curves are referred to as remanent acquisition (RA) curves. The isothermal remanence acquired in fields up to $1.2*10^6$ Am^{-1} (1.5 Tesla) is generally small compared to that acquired in stronger fields. Heller (1978), Lowrie and Heller (1982) and Thompson (1986) present distinctly different RA curves for natural goethite: some curves are indistinguishable from hematite RA curves (some goethite-bearing specimens investigated by Lowrie and Heller), but the IRM of other goethites does not saturate in fields up to $16*10^6$ Am^{-1} (20 Tesla, cf. Thompson, 1986).

The behaviour of goethite rockmagnetic parameters in a grain-size dependent framework is at present poorly documented. This paper describes the grain-size dependence of some rockmagnetic parameters of five natural goethites of different geologic origin. Goethite concentrates are sieved in well-defined grain-size fractions following the procedure of Dankers (1978, 1981) and Hartstra (1982). In order to study the rockmagnetic parameters the goethite fractions are homogeneously dispersed in a non-magnetic matrix.

1.1 Sample preparation

Goethite concentrates were obtained by subsequent crushing, sieving, heavy liquid separation, magnetic separation and micro-precision sieving

of the raw samples. In this way twelve grain-size fractions, ranging from 250 micrometer down to < 5 micrometer were obtained. Details are given in Dekkers (1988A) and Dekkers et al. (in prep.). Samples for measurements of the initial susceptibility were standard sized paleomagnetic samples containing approximately 400 mg goethite dispersed in a calciumcarbonate/waterglass matrix (analytical grade chemicals). Samples for high field measurements were cylinders of 4.5 mm diameter and 5 mm height with 20-30 mg goethite dispersed in an epoxy resin (araldite D-hardener HY 956, Ciba Geigi).

1.2 Sample description

Goethite-rich concentrates are separated from samples of supergene environmental origin. Three samples were collected by the author (MKB: Kahlenberg, Western Germany; MBL: Blumberg, Western Germany; FSB: Sain Bel, France); two others (MEN; Menera mining district, Spain; RR: Robe River mining district, Western Australia) were kindly provided by Hoogovens Ltd. (Beverwijk, The Netherlands). The samples comprise two marine oolithic iron ores (MKB, MBL), a fluviatile pisolitic replacement ore (RR), a caprock ore above sideritic iron ore (MEN) and a goethite-rich gossan above a pyritic body (FSB). A concise description is given hereafter; for a more detailed overview the reader is referred to Dekkers (1988B).

1.2.1 Kahlenberg (MKB)

MKB is a goethite concentrate from a marine sedimentary oolithic iron ore of Dogger-β age (Sauer and Simon, 1975A) from Kahlenberg (Western Germany). Ooliths have diameters from 0.2 - 0.5 mm; they show concentric layering. The larger grain-size fractions consist of broken ooliths. The small grain-size fractions contain approximately equidimensional grains; the ooliths have broken up into small fragments obscuring their oolithic origin. Traces of quartz (X-ray diffraction, XRD; infrared spectroscopy, IRS), calcite (IRS) and hematite (XRD, IRS) due to intergrowths are present.

1.2.2 Blumberg (MBL)

The MBL goethite concentrate is separated from a marine sedimentary oolitic iron ore of Dogger epsilon to Φ age (Sauer and Simon, 1975B) in the vicinity of Blumberg (Western Germany). The ooliths are somewhat larger than in the Kahlenberg case; their sizes vary between 0.8 mm and 1.4 mm. Concentric layering is predominant, considerably more than in the MKB fractions. The large MBL fractions are broken ooliths, the small fractions consist of more or less equidimensional grains, as in the MKB fractions. Traces of quartz (XRD, IRS) are present; no hematite is detected with these methods.

1.2.3 Menera (MEN)

MEN is a goethite concentrate from a sample of commercial iron ore from the Menera mining district (Spain). The goethite belongs to the oxidized caprock above a hydrothermal metasomatic siderite ore (Zitzmann and Neumann-Redlin, 1978). The mineralization is considered to be of Alpine age in predominantly Ordovician limestones and dolomites. The grains in the goethite concentrate are more or less equidimensional. Traces of quartz (XRD, IRS) and hematite (XRD, IRS) occur.

1.2.4 Sain Bel (FSB)

The FSB samples are collected from a goethite-rich gossan in the former Sain Bel mining district (France). Devonian pyritic lenses are oxidized to jarosite and ultimately to goethite and hematite in the supergene zone (Wilhelm and Kosakevitch, 1978). The goethite concentrate consists of equidimensional grains; traces of quartz and hematite (XRD, IRS) remain present.

1.2.5 Robe River (RR)

The goethite of the RR sample is separated from a commercial ore concentrate of the Robe River mining district (Western Australia). The Robe River deposits are pisolitic fluviatile replacement ores in former river channels (Harms and Morgan, 1964). A Tertiary age is suggested based on physiographic reasoning. The ore is limonitic; goethite, hematite and traces of maghemite (upper levels) occur. The pisolites generally have diameters of 1 to 3 mm; occasionally larger ones with diameters up to 10 mm are observed. Limonitized fossil wood occurs throughout the deposits, in some parts abundantly. In the goethite concentrate traces of quartz and hematite (XRD, IRS) are present. The grains are equidimensional. With simple optical observation their pisolitic origin is not recognizable anymore.

1.3 Chemistry and cell parameters

Wet-chemical and microprobe analyses of the goethite concentrates are compiled in Table I and cell constants (XRD) in Table II.

The presence of intergrowths is inferred from the differences between the wet-chemical and microprobe analyses. With the wet-chemical methods, the contents of elements other than iron are higher than in corresponding microprobe analyses. This applies specially for SiO_2 (to a lesser extent for Al_2O_3). Therefore the intergrowths are thought to be predominantly quartz-rich, which agrees with the XRD determination of traces quartz. The amount CaO in MKB goethite, determined wet-chemically, is of carbonate origin as can be deduced from the presence of CO_3 bonds in infrared absorption spectra.

All goethites approach the ideal goethite composition reasonably well; they are characterized by relatively high iron contents (calculated as Fe_2O_3), with a few weight percent Al_2O_3 and SiO_2 (microprobe analyses). The marine sedimentary goethites (MKB and especially MBL) contain more isomorphous substituted Al than the other goethites. MEN goethite contains a remarkable Mn amount, which is also isomorphously substituted in the goethite crystal lattice. Al and Mn are isomorphously substituted because they both occur as trivalent ions with a similar ionic radius as Fe^{3+} (Al^{3+}: 0.51 Å; Mn^{3+}: 0.66 Å; Fe^{3+}: 0.64 Å). Isomorphous substitution of small amounts Si in goethite is described (Norrish, 1975). The ionic radius of Si^{4+} (0.42 Å) is much smaller than that of Fe^{3+}, which limits possible substitution to insignificant levels. Moreover, the substitution of Si^{4+} requires the simultaneous substitution of a similar molar amount of divalent ions in goethite in order to maintain electro-neutrality. These ions are not available as appears from the chemical analyses. So, ignoring a possible small amount of substituted Si, only Al and Mn are substituted in the goethite lattice, and the remaining non-iron elements are sorbed onto the goethite surface and dispersed in and between goethite crystallites. MKB

goethite (and MBL goethite to a lesser extent) contain somewhat more P_2O_5 (as PO_4 sorbed onto the goethite structure) than the other three samples. Microprobe analyses indicate that the MKB and MBL goethites are more inhomogeneous than the others (larger spreading in individual spot analyses). RR goethite seems to be the most homogeneous goethite, also its excess water (determined wet-chemically, Penfield method) is minimal. The high water content determined in the FSB goethite is a total (water + sulphur) content. Trace element contents are insignificant; FSB goethite bears more Cu, Pb and Zn reflecting its origin from the oxidation of chalcopyrite-bearing pyritic ore-lenses.

Table I: Wet-chemical and microprobe analyses of the goethite concentrates

	MKB		MBL		MEN		FSB		RR	
	WC	MP	WC	MP	WC	MP	WC	MP	WC	MP
SiO_2	7.20	2.51	6.72	4.89	7.68	3.05	6.88	3.27	5.44	2.80
TiO_2	0.33	0.02	0.54	0.44	0.09	0.02	0.11	0.01	0.23	0.02
Al_2O_3	7.77	2.86	9.32	7.16	4.61	0.84	2.06	0.34	3.81	2.15
V_2O_3	nd	0.10	nd	nd	nd	0.04	nd	0.03	nd	0.04
Fe_2O_3	61.82	76.32	66.19	68.44	67.62	79.55	71.95	80.58	77.58	79.33
FeO	0.31	nd	0.53	nd	<dl	nd	0.26	nd	0.12	nd
MnO	0.20	0.24	0.13	0.06	2.88	0.93	<dl	0.02	0.12	0.05
MgO	1.13	0.92	0.85	0.86	0.98	0.95	0.09	0.10	0.12	0.09
CaO	5.45	0.27	0.57	0.26	0.24	0.17	0.07	0.08	0.14	0.07
Na_2O	0.08	0.13	0.04	nd	0.02	0.09	0.01	0.03	0.02	0.02
K_2O	0.53	0.07	0.47	nd	0.60	0.01	0.25	0.02	0.02	0.02
P_2O_5	1.31	1.79	0.74	0.84	0.23	0.28	0.17	0.07	0.12	0.07
H_2O	13.17	nd	13.43	nd	14.09	nd	17.68	nd	11.79	nd
SO_3	nd	0.81	nd	0.36	nd	0.31	nd	4.20	nd	0.33
total	99.30	86.10	99.53	83.34	99.04	86.29	99.53	88.77	99.89	85.16
Cu	60		10		60		885		30	
Zn	280		395		110		460		140	
Co	65		70		60		<dl		20	
Ni	175		235		180		40		50	
Pb	90		90		50		690		40	

WC = wet-chemical; MP = microprobe; nd = not determined; <dl = below detection limit. Contents above the dashed line in weight percentages; below the dashed line in ppm. Wet-chemical analytical methods are colorimetry for total iron (as Fe_2O_3), SiO_2, TiO_2, P_2O_5 and Al_2O_3, titrimetry for FeO (titration with $K_2Cr_2O_7$; Fe_2O_3 in Table III = total iron - FeO*1.11), atomic absorption (air-acetylene flame) for MnO, MgO, CaO, K_2O and Na_2O , the Penfield method for H_2O and atomic absorption (air-acetylene flame; Pb flameless) for trace elements. Wet-chemical analyses were done by the Service Laboratory of the Institute of Earth Sciences at the State University of Utrecht. Microprobe analyses were carried out on a TPD (Technisch Physische Dienst) microprobe fitted with a TRACOR Northern Energy Dispersive (ED) system. Operating conditions are 15 keV and 2 - 3 nA. Iron in the microprobe analyses is calculated as Fe_2O_3. ZAF matrix correction is applied.

The goethite cell constants decrease with increasing impurity content (Table II), as one would expect by comparing the ionic radius of Al^{3+} with that of Fe^{3+}. However, a linear relation between the cell dimensions and Al-content (Norrish and Taylor, 1961; Thiel, 1963) is not observed. Apparently, a straightforward relationship is hindered by simultaneous substitution of elements other than Al (i.e. Mn and possible minor Si) in the goethite structure. Also possible influence of the sorbed elements on the goethite lattice parameters is unknown, but

it is reasonable to presume that this impact will be insignificant. The FSB goethite cell constants approach best the ideal goethite cell constants (e.g. Sampson, 1969; Harrison et al., 1975), which is a further indication that the substitution of Si in the goethite lattice is insignificant or not present at all.

Table II: unit cell parameters of the natural goethites

axis	MKB	MBL	MEN	FSB	RR
a	4.585±0.003	4.586±0.004	4.612±0.004	4.611±0.004	4.596±0.004
b	9.908±0.007	9.884±0.008	9.920±0.008	9.962±0.009	9.909±0.008
c	2.995±0.002	3.000±0.002	3.011±0.002	3.008±0.003	2.998±0.002
Vol.	136.06	136.00	137.76	138.17	136.53

Lengths of the crystal axes in Å; volume (Vol.) in $Å^3$. Peak positions are taken from a Debye-Scherrer film (Fe K_α-rays). Calculation is performed with the program UNITCELLD (Strom, 1976). Ten reflections (unweighted) are entered.

1.4 Crystallite size

Broad goethite reflections in X-ray diffractograms (also the presence of intergrowths in the goethite concentrates) indicate that the goethite crystallite size is (far) smaller than the grain size of the sized goethite fractions. The crystallite size may be calculated from the line width in diffractograms. Usually, the width at half peak height corrected for the instrumental line width is used in the calculations (Klug and Alexander, 1974). Such calculations (Dekkers, 1988A) indicate that the crystallite size (in the direction of a reflection with a d_{hkl}) ranges from some 150 Å to approximately 800 Å, indeed much smaller than the grain size of the fractions. Hence, each goethite grain consists of many goethite crystallites. Reflections with a non-zero "1" index have slightly larger crystallite sizes than those with a zero "1" index. This implies some elongation of the crystallites in the direction of the crystallographical c-axis, in agreement with electron microscope observations of goethite crystals (e.g., Landa and Gast, 1973; Lewis and Schwertmann, 1979; Cornell et al., 1983). The average crystallite size for each goethite sample is as follows:

FSB 240 Å, MBL 325 Å, MEN 370 Å, RR 400 Å and MKB 480 Å.

1.5 Instrumentation for the magnetic measurements

Initial susceptibility was measured with a Jellinek KLY-1 susceptibility bridge at the paleomagnetic laboratory 'Fort Hoofddijk', State University of Utrecht (The Netherlands). High field measurements up to $16*10^6$ Am^{-1} were carried out at the High Field Magnet Laboratory of the University of Nijmegen (The Netherlands). Susceptibility measurements were done with a vibrating sample magnetometer (Foner-type) up to $1.04*10^6$ Am^{-1} (1.3 Tesla) and a ballistic magnetometer in higher fields. Measurements of remanent magnetizations were carried out with the vibrating sample magnetometer for remanences acquired in fields up to $1.04*10^6$ Am^{-1} and with a Jellinek spinner magnetometer for remanences acquired in higher fields.

2 RESULTS

The magnetic parameters measured of each goethite fraction are constituted of three contributions: 1) the magnetic contribution of goethite itself, 2) the magnetic contribution of non-goethite magnetic minerals and 3) the magnetic contribution of the matrix. Since our prime interest is in goethite magnetic properties, i.e. contribution 1), corrections have to be made to account for contributions 2) and 3). The measured parameters fall into two groups: those obtained with in-field (susceptibility) measurements (determined parameters: initial susceptibility, X_{in}; high field susceptibility, X_{hf}; saturation magnetization, J_s; coercive force, H_c; ferromagnetic coercive force, $H_{c\ ferr.}$) and those which refer to remanent magnetic properties of goethite (isothermal remanent saturation magnetization, J_{rs}; remanent coercive force, H_{cr}; remanent acquisition coercive force, $H_{cr'}$).

The coercive force (H_c) refers to the measured coercive force corrected for the diamagnetic matrix moment. The ferromagnetic coercive force ($H_{c\ ferr.}$)is the coercive force corrected for the high field susceptibility contribution. Because this contribution constitutes a large part of total magnetization, $H_{c\ ferr.}$ values, unfortunately, have a slightly larger error.

For in-field measured parameters, contribution 3) was established by means of blanks. It appeared that the (diamagnetic) matrix-moment made up a considerable part of the magnetic moment of the total sample (matrix plus goethite). The matrix contribution was up to one third of the (weak) goethite magnetic moment. To suppress contribution 2) as much as possible goethite concentrates were upgraded to a high purity; nevertheless a few percent hematite remained present in most concentrates. It is impossible to establish the goethite and hematite contributions separately at room temperature. The hematite contribution will be insubordinate because of its low abundance in the sample. The bias in X_{hf} will be negligible because the hematite and goethite X_{hf} are expected to be of the same order of magnitude. X_{in}, H_c and $H_{c\ ferr.}$ will only be slightly biased by minor hematite amounts (X_{in} upwards and both H_c and $H_{c\ ferr.}$ downward). The hematite amount in the samples can be estimated from remanent magnetization related parameters by thermal demagnetization (see below). Taking J_s of hematite 0.4 Am^2kg^{-1} (O'Reilly, 1984), with the hematite content known for each fraction, the total saturation magnetization of each fraction can be corrected for the hematite contribution, resulting in a more precisely determined goethite J_s. Traces of magnetite or maghemite, on the contrary, will strongly bias X_{in}, J_s (both upwards) and H_c and $H_{c\ ferr.}$ (both downward).

For the remanent magnetization-related parameters contribution 3) (matrix contribution) can be neglected and contribution 2) (the non-goethite part of the remanence) can be established by thermal demagnetization at 150 °C. At that temperature, the total goethite remanence is removed from the sample together with a part of the non-goethite remanence. Thermal decay curves indicate that approximately 1/9 of a room temperature induced hematite J_{rs} is removed at 150 °C (Dankers, 1978). For magnetite/maghemite this figure is approximately 1/6 (Dankers, op. cit.). Taking J_{rs} of hematite to be 0.2 Am^2kg^{-1} (Dankers, 1978, 1981; Hartstra, 1982) a calculation of the specific goethite remanence can be made. Hematite percentages are compiled in Table III. H_{cr} and $H_{cr'}$ are determined according to Fig. 1A. The hematite contribution to the total remanence is relatively large in fine-grained FSB fractions, despite the predominance of goethite in the samples (cf. Fig. 1B).

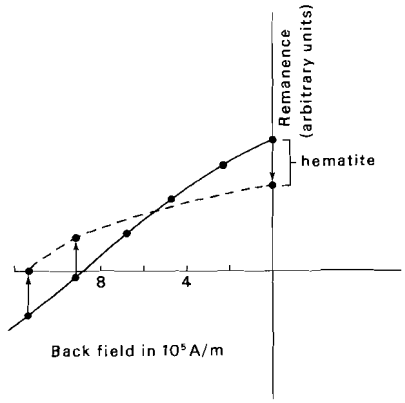

Fig. 1A. Determination of the goethite remanent coercive force and remanent acquisition coercive force. From the remanent acquisition curves it is concluded that all non-goethite minerals (hematite, maghemite) are (nearly) saturated in a field of $8*10^5$ Am^{-1}. For the determination of the goethite remanent coercive force, the non-goethite contribution (determined by thermal demagnetization) is subtracted from the measured remanent hysteresis curve (indicated with the solid line). The shape of the goethite remanent hysteresis curve is indicated with the dashed line. Between zero and minus $8*10^5$ Am^{-1} it can only be estimated; this is done by correcting the shape of the measured curves for the shape of hematite remanent hysteresis curves. For the determination of the remanent acquisition coercive force the goethite remanence itself is normalized to its (saturation) remanence; the field-strength at which half of the saturation remanence is acquired, corresponds to the remanent acquisition coercive force.

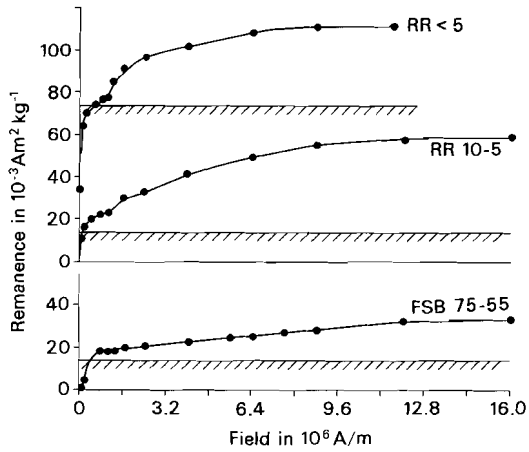

Fig. 1B. Remanent acquisition curves of some RR and FSB fractions before correction for the magnetic influence of minor hematite and traces of maghemite. The remanence below the marked horizontal line remained after thermal demagnetization at 150 °C (the actual remaining remanence is multiplied by 1.11 to correct for the part of hematite which is also thermally demagnetized; the multiplied value is shown) and can not be attributed to goethite.

Maghemite contributes to such extent to the remanence in the smallest two RR fractions, that it makes up to 75 percent of the total signal (cf. Fig. 1B). It causes a dramatic increase of the remanence at low fields, resulting in a large 'offset' of the goethite RA curve. Calculation showed that if the total non-goethite remanence is attributed to maghemite, its weight content in the sample is in the order of 0.1 per mill. Maghemite was determined by low-temperature cycling of the extremely magnetic fraction present in the raw RR goethite sample. This fraction, which constituted an extremely small weight percentage of the raw sample (far below one percent) was removed from the sample in the magnetic separation step. Traces maghemite in Robe River ore were also determined by Harms and Morgan (1964).

Table III Magnetically determined hematite weight percentages

fraction	MKB	MBL	MEN	FSB	RR	fraction	MKB	MBL	MEN	FSB	RR
250 - 150	6	<2	4	6	3	30 - 25	5	<2	5	15	5
150 - 100	4	<2	4	6	4	25 - 20	4	<2	5	14	6
100 - 75	6	<2	4	7	2	20 - 15	3	<2	5	14	6
75 - 55	6	<2	4	7	3	15 - 10	2	2	6	16	8
55 - 40	5	<2	5	11	4	10 - 5	<2	2	9	17	7
40 - 30	5	<2	4	13	4	< 5	3	2	7	14	7

Grain size of the fractions is in micrometer. During the magnetic measurements it appeared that maghemite was present in trace amount in the RR fractions. In the hematite weight percentage calculation it was assumed that approximately half of the non-goethite remanence can be attributed to maghemite, a reasonable estimate based on the shape of the RA curves. The maghemite weight content can be ignored compared to that of hematite. The finest two RR fractions contained a higher (trace) amount maghemite; therefore the hematite weight content is somewhat less precise.

Bearing the above mentioned criteria in mind, X_{in}, X_{nr}, J_s, J_{rs}, H_c, $H_{c\ ferr.}$, H_{cr} and $H_{cr'}$ as function as of grain size are compiled for each goethite sample in Table IV.

Table IV: Rockmagnetic parameters for natural goethite as a function of grain size.

	X_{in}	X_{hf}	J_s	J_{rs}	H_c	$H_{c\ ferr.}$	H_{cr}	$H_{cr'}$
MKB								
250-150	0.49	0.30	410 ± 57	99.9	21.88	59.68	222.8	135.3
150-100	0.46	0.37	210 ± 68	97.4	22.67	67.64	210.9	183.0
100-75	0.55	0.33	360 ± 82	98.2	22.28	63.66	175.1	175.1
75-55	0.56	0.34	330 ± 72	100.5	23.07	70.82	179.0	151.2
55-40	1.04	0.32	340 ± 38	103.9	17.51	46.95	151.2	143.2
40-30	1.75	0.26	470 ± 67	116.8	7.56	9.55	139.3	135.3
30-25	1.09	0.30	420 ± 74	110.6	15.12	34.22	135.3	131.3
25-20	1.15	0.29	380 ± 57	110.0	13.53	28.65	131.3	119.4
20-15	1.10	0.21	150 ± 66	85.0	14.32	25.46	135.3	135.3
15-10	0.83	0.24	270 ± 66	84.5	12.73	24.27	127.3	131.3
10-5	1.03	0.23	280 ± 59	80.8	9.15	15.12	119.4	131.3
<5	0.70	0.18	190 ± 34	89.4	16.31	27.06	115.4	131.3
MBL								
250-150	0.75	0.38	270 ± 87	57.6	3.58	9.15	75.6	107.4
150-100	0.74	0.39	360 ± 110	65.4	2.78	7.96	63.7	127.3
100-75	0.76	0.38	340 ± 66	60.9	4.38	9.95	87.5	127.3
75-55	0.76	0.42	420 ± 97	60.8	4.38	9.95	91.5	127.3
55-40	1.01	0.38	370 ± 117	62.7	3.98	7.16	87.5	135.3
40-30	1.48	0.34	430 ± 94	53.4	2.78	4.78	75.6	131.3
30-25	1.63	0.38	440 ± 97	62.1	2.39	3.18	71.6	111.4
25-20	2.05	0.28	nd	56.8	1.99	2.78	79.6	103.4
20-15	1.51	0.39	460 ± 107	59.3	2.39	3.58	75.6	111.4
15-10	1.72	0.30	350 ± 28	48.1	1.59	2.39	59.7	95.5
10-5	nd	0.29	380 ± 46	47.5	1.19	1.99	51.7	95.5
<5	1.02	0.27	290 ± 55	42.0	1.19	2.78	39.8	95.5
MEN								
250-150	0.55	0.32	58 ± 42	37.8	9.15	50.93	195.0	278.5
150-100	0.56	0.32	91 ± 52	37.2	9.15	44.56	195.0	302.4
100-75	0.61	0.24	78 ± 46	32.9	9.15	45.36	195.0	286.5
75-55	0.57	0.38	43 ± 53	41.7	9.15	62.87	195.0	310.4
55-40	1.42	0.35	140 ± 44	48.0	4.38	8.36	198.9	326.3
40-30	1.16	nd	nd	44.4	4.77	9.55	198.9	310.4
30-25	1.06	0.27	140 ± 43	41.7	4.38	7.96	183.0	286.5
25-20	0.83	0.31	95 ± 45	36.2	5.97	17.90	171.1	318.3
20-15	0.77	0.28	115 ± 33	35.0	6.37	15.92	175.1	318.3
15-10	0.76	0.28	125 ± 33	28.2	5.97	15.92	163.1	334.2
10-5	0.88	0.30	80 ± 18	30.0	4.77	9.15	155.2	334.2
<5	0.70	0.25	105 ± 31	21.0	4.38	8.75	143.2	326.3
FSB								
250-150	0.51	0.34	120 ± 45	15.4	5.57	19.89	155.2	557.0
150-100	0.56	0.36	17 ± 44	15.1	4.77	18.30	143.2	557.0
100-75	0.66	0.46	84 ± 67	21.9	5.57	18.30	139.3	533.2
75-55	0.63	0.32	36 ± 18	20.8	5.57	15.92	135.3	517.2
55-40	1.00	0.37	190 ± 68	27.5	4.78	9.55	119.4	286.5
40-30	1.65	0.32	115 ± 43	25.8	4.78	8.36	111.4	294.4
30-25	1.08	0.36	95 ± 29	27.6	3.98	5.97	103.4	274.5
25-20	1.25	0.29	180 ± 42	24.2	3.58	5.17	103.4	334.2
20-15	1.03	0.27	240 ± 57	22.6	4.38	5.97	111.4	274.5
15-10	1.41	0.27	210 ± 43	28.1	3.18	4.38	107.4	274.5
10-5	2.34	0.21	490 ± 99	27.0	2.39	2.47	83.6	198.9
<5	1.88	0.20	250 ± 53	23.0	1.99	2.23	79.6	159.2
RR								
250-150	1.10	0.30	105 ± 22	50.3	4.38	11.14	298.4	477.5
150-100	1.16	0.38	105 ± 35	57.2	3.98	11.14	318.3	493.4
100-75	1.03	0.35	64 ± 48	52.8	5.57	12.73	306.4	469.5
75-55	1.05	0.42	50 ± 52	54.6	5.18	11.94	310.4	453.6
55-40	1.45	0.33	150 ± 62	54.9	3.58	5.97	326.3	485.4
40-30	1.36	0.33	125 ± 56	52.6	3.18	5.97	310.4	453.6
30-25	1.34	0.38	78 ± 190	49.2	2.78	5.17	306.4	437.7
25-20	1.31	0.37	155 ± 37	50.0	2.78	5.17	286.5	437.7
20-15	1.40	0.20	140 ± 49	44.9	3.18	4.38	234.8	469.5
15-10	1.56	0.30	120 ± 52	36.0	2.78	3.58	238.7	433.7
10-5	2.10	0.26	225 ± 30	37.0	1.99	2.78	179.0	334.2
<5	5.92	0.24	592 ± 45	35.0	1.99	1.99	39.8	159.2

X_{in} and X_{hf} in 10^{-6} m^3kg^{-1}; J_s and J_{rs} in 10^{-3} Am^2kg^{-1}; H_c, $H_{c\ ferr.}$, H_{cr} and $H_{cr'}$ in 10^4 Am^{-1}.

2.1 Magnetization curves and related parameters (J_s, χ_{in}, χ_{hf}, H_c, $H_{c\,recr.}$)

Some examples of magnetization curves are shown in Fig. 2. Magnetization curves of MKB and MBL goethite fractions, which have a relatively large J_s (cf. Table IV), are linear above fields of approximately $3.2*10^6$ Am^{-1} (4 Tesla), those of the MEN and RR fractions above $1.6*10^6$ Am^{-1} (2 Tesla) and those of the FSB fractions already above $0.8*10^6$ Am^{-1} (1 Tesla). Fractions with perceptible slightly raised hematite content (some MKB and FSB fractions) or a mixed contribution of hematite and trace amounts maghemite (some RR fractions) are recognized by a larger magnetization in small fields than in goethite samples which contain distinctly less magnetic impurities. χ_{hf} is calculated by regression of the magnetization acquired in fields from $3.2*10^6$ up to $11.6*10^6$ Am^{-1} (4 to 14.5 Tesla). Data from lower fields are excluded to avoid influence of (possible) non-linearity of the magnetization curve at these fields. J_s is obtained by intersection of the regression line with the ordinate (indicated by the dashed lines).

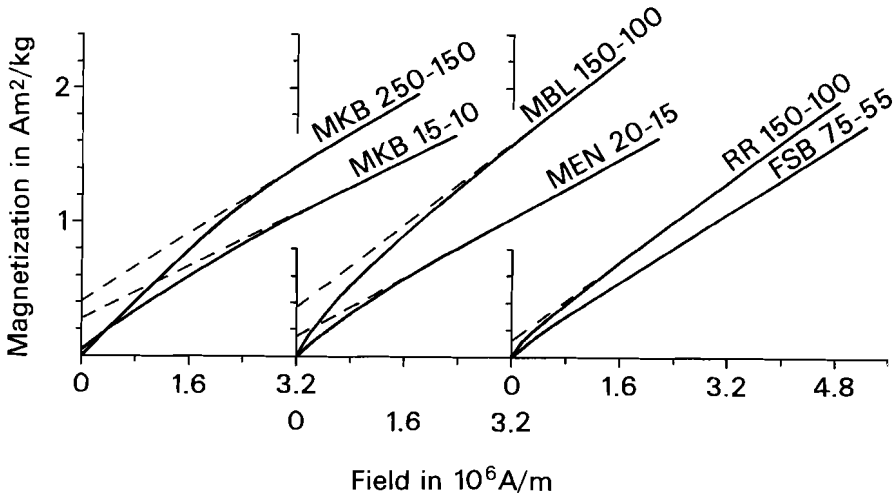

Fig. 2. Representative magnetization curves for natural goethite corrected for the diamagnetic matrix moment. MKB = Kahlenberg (West Germany), MBL = Blumberg (West Germany), MEN = Manera (Spain), FSB = Sain Bel (France), RR = Robe River (Western Australia). The numbers refer to the grain-size range in micrometer of the corresponding fractions. The dashed lines show the linear extrapolation to the ordinate; the intersection yields the saturation magnetization.

J_s figures are in general agreement with those reported for natural goethite (e.g. Hedley, 1971; Pastrana and Hopstock, 1977). Figures for MKB and MBL fractions are high for natural goethite. They approach hematite J_s figures (± 0.4 Am^2kg^{-1}, e.g. Chevallier and Mathieu, 1943; Dunlop, 1971). The figures of MEN, FSB and RR fractions are lower than the MKB and MBL fractions, uncertainties in the hematite content have the largest impact on the goethite J_s of the FSB fractions because of its low value. This contributes to the relatively large scatter in J_s for the FSB fractions.

J_s as function of grain size is plotted in Fig. 3. J_s should be a grain-size independent parameter and indeed no evident grain-size dependence is displayed. The observed irregular pattern is due to the rather large error in the J_s determination (cf. Table IV). The RR 10-5 and RR <5 fractions are contaminated with traces maghemite as could readily be deduced from their high magnetization in low fields. This obviously results in too high J_s figures.

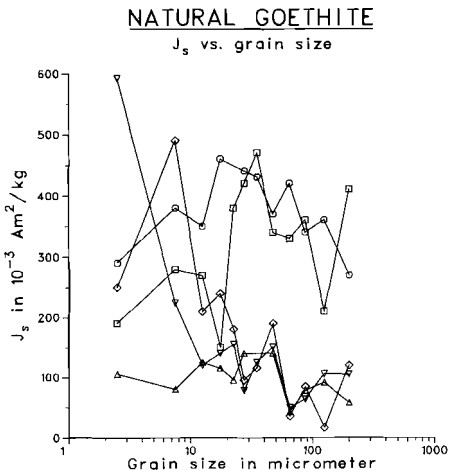

Fig. 3. Saturation magnetization (J_s) as function of grain size for the five natural goethites samples. For sample abbreviations cf. Fig. 2.

Figures for X_{in} (Fig. 4) roughly vary between $0.50 * 10^{-6}$ m^3kg^{-1} and $2.0 * 10^{-6}$ m^3kg^{-1} for all goethites. Higher susceptibilities are due to an elevated hematite content or to traces maghemite. X_{in} is approximately constant for the coarse grain-size fractions (> 55 micrometer) of each goethite sample. A remarkable increase in X_{in} is observed in 55- 40 and 40-30 micrometer range for all samples. X_{in} in smaller grain-size fractions does not show an evident trend, but there is a tendency for X_{in} to decrease with decreasing grain size.

Goethite X_{hf} figures (Fig. 5) generally are between $0.25*10^{-6}$ and $0.35*10^{-6}$ m^3kg^{-1} for all samples, somewhat lower than X_{in}. X_{hf} decreases with decreasing grain size. The scatter observed in the data is due to the relatively large error in the ballistic magnetometer measurements. X_{hf} of hematite is $0.25*10^{-6}$ m^3kg^{-1} (e.g. Collinson, 1983; O'Reilly, 1984), so goethite X_{hf} data will be less biased by hematite impurities than X_{in}.

The measured H_c varies between $1-2*10^4$ and $25*10^4$ Am^{-1} (approximately 2 to 10 times higher than H_c of small hematite grains, e.g. Chevallier and Mathieu, 1943) and decreases with decreasing grain size from 55 micrometer downward (Fig. 6) for all goethite samples. Fractions above this size have an approximately constant H_c. Absolute figures are approximately similar for MBL, FSB and RR fractions; MEN fractions have slightly higher figures; MKB fractions are characterized by the highest H_c's.

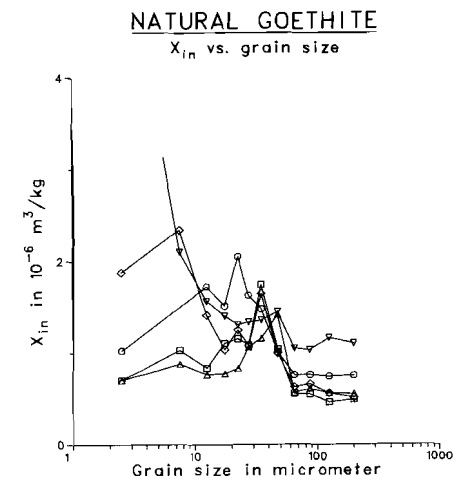

Fig. 4. Initial susceptibility per unit mass (X_{in}) as function of grain size for the natural goethites. For sample abbreviations cf. Fig. 2.

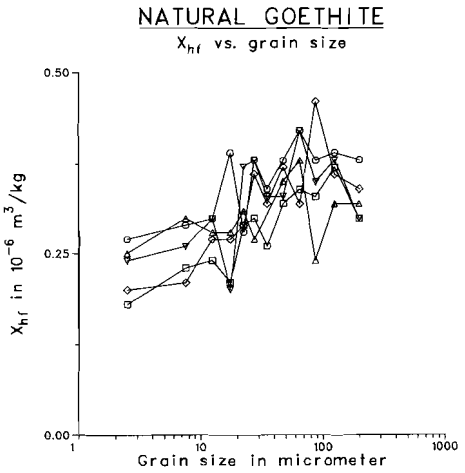

Fig. 5. High field susceptibility per unit mass (X_{hf}) as function of grain size for the natural goethites. For sample abbreviations cf. Fig. 2.

The ferromagnetic coercive force ($H_{c\ ferr.}$, Fig. 7) is approximately constant for the four coarsest grain size fractions. One should realize that even a small error in the X_{hf} determination has a large impact on the determination of $H_{c\ ferr.}$, because the contribution due to the high field susceptibility constitutes a very large part of the total sample magnetization. A (occasionally large) fall in $H_{c\ ferr.}$ is observed from the 55-40 micrometer fraction downward to some 25 micrometer for all samples. In smaller grain size fractions $H_{c\ ferr.}$ is more or less con-

stant. The fall in H_c ferr. and H_c is observed in the same grain size fractions as the increase in X_{in}. The remarkably similar grain-size dependent H_c and H_c ferr. behaviour of the goethite samples, despite large differences in absolute figures, indicates that the microcrystalline goethites should have a common mechanism explaining the behaviour of the coercive forces.

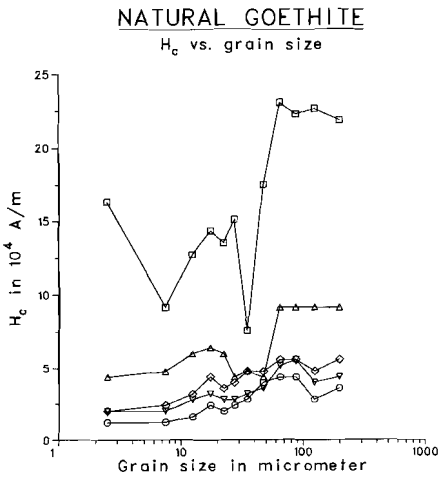

Fig. 6. Coercive force (H_c) as function of grain size for the natural goethites. For sample abbreviations cf. Fig. 2.

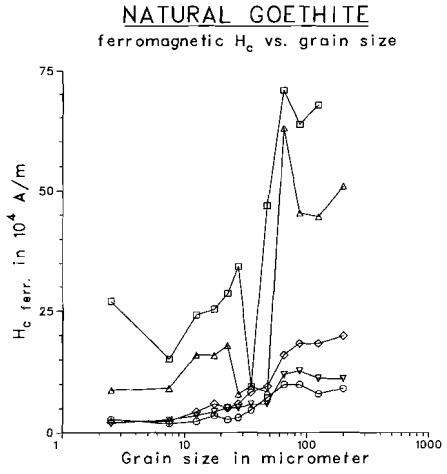

Fig. 7. Ferromagnetic coercive force (H_c ferr., i.e. H_c corrected for the high field susceptibility contribution) as function of grain size for the natural goethites. For sample abbreviations cf. Fig. 2.

2.2 Remanent acquisition curves and related parameters (J_{rs}, H_{cr}, H_{cr}')

A selection of RA curves is shown in Fig. 8A. the RA curves normalized (to the (saturation) remanence acquired in $16*10^6$ Am^{-1}) are depicted in Fig. 8B. The remanence of non-goethite minerals is subtracted from the curves. For this reason the shape of the goethite RA curves for low field remanences is somewhat approximate for those fractions which display a relatively large non-goethite remanence. The magnetic hardness of goethite is demonstrated by the low remanence acquired in fields below $0.4*10^6$ Am^{-1} (0.5 Tesla).

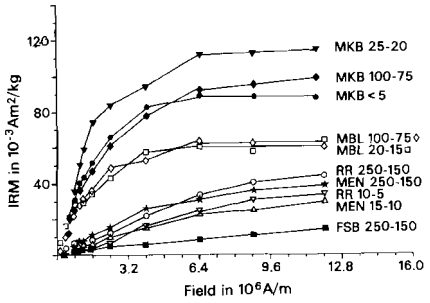

Fig. 8A. A selection of remanent acquisition (RA) curves for the natural goethites.

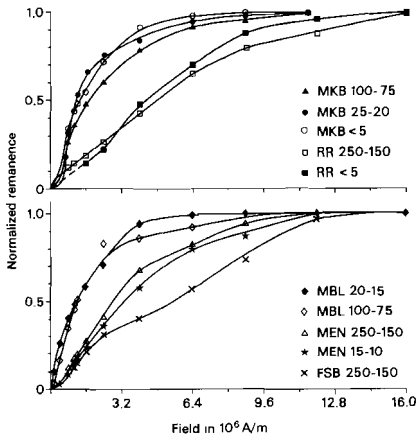

Fig. 8B. RA curves normalized to the (saturation) remanence acquired in fields of $11.6*10^6$ Am^{-1} and $16*10^6$ Am^{-1}. For sample abbreviations cf. Fig. 2; numbers designate the grain-size interval in micrometer of each fraction.

There are distinct differences between the RA curves. MKB and MBL goethite fractions acquire a larger part of their remanence in low fields than the other three goethite samples. They are also saturated in lower fields ($4*10^6$ to $6.4*10^6$ Am^{-1} (5 to 8 Tesla), especially MBL goethite) than fractions of the other goethite samples ($12*10^6$ to $16*10^6$ Am^{-1}. Most RR fractions do not even entirely saturate in $16*10^6$ Am^{-1} fields (strongest field available) apart from the three

finest grain-size fractions. MBL goethite fractions are susceptible to relaxation of the isothermal remanence; this was specially observed in the coarse grain-size fractions.

A proper goethite J_{rs} determination apparently requires much stronger fields than its J_s determination. This paradox is related to sensitivity of the susceptibility measurements: the total susceptibility consists for by far the largest part of the high field susceptibility contribution. The extremely small deviation from true linearity, which should be displayed in the magnetization curve, is lost in the error in the susceptibility determination. For the J_s and X_{hf} calculations the magnetization curve in high field is fitted as being truly linear. The error in J_s and X_{hf} due to this approximation can be neglected.

J_{rs} figures are in between 0.015 and 0.1 Am^2kg^{-1} with a tendency to decrease with grain size (Fig. 9). This is approximately 5 to 50 percent of the hematite J_{rs}, which is in the order of 0.2 Am^2kg^{-1} (e.g. Dankers, 1978, 1981; Hartstra, 1982).

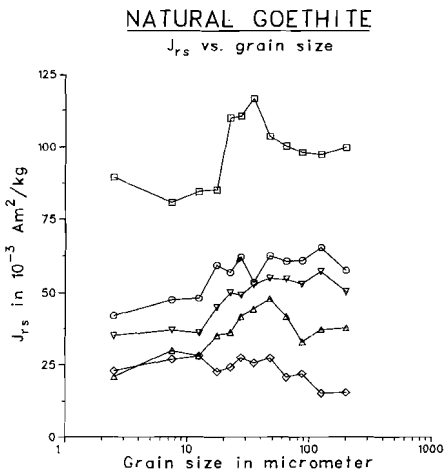

Fig. 9. Saturation remanence (J_{rs}) as function of grain size for the natural goethites. The grain- size fractions larger than 25 micrometer of the RR goethite sample are not entirely saturated. For sample abbreviations cf. Fig. 2.

H_{cr} figures vary between 50 and 300*10^4 Am^{-1}; some one to two orders of magnitude higher than hematite H_{cr} figures (± 2 - 30*10^4 Am^{-1}, e.g. Dankers, 1981; Hartstra, 1982). There are two types of goethite H_{cr} behaviour (Fig. 10): one with a decreasing H_{cr} with grain size throughout the whole investigated grain-size interval (MKB and FSB goethite) and one with a decreasing H_{cr} from approximately 40-30 micrometer downward and a more or less constant H_{cr} in coarser fractions (MBL, RR and MEN goethite).

However, during the measurements it appeared that the remanence in MBL goethite had a relatively high relaxation rate. The observed H_{cr} trend could be biased because the coarse grain-size fractions showed a stronger relaxation than the fine grain-size fractions. Also the H_{cr} trend in the RR fractions may be (slightly) biased because the coarse RR fractions are not entirely saturated, so the determined H_{cr} figures

will be (slightly?) too low. The trend observed in the MEN fractions seems not to be biased. Hence, goethite H_{cr} can show a wide variety in absolute figures with two possible grain size trends. The relation with the goethite chemical composition and crystallite size will be discussed later.

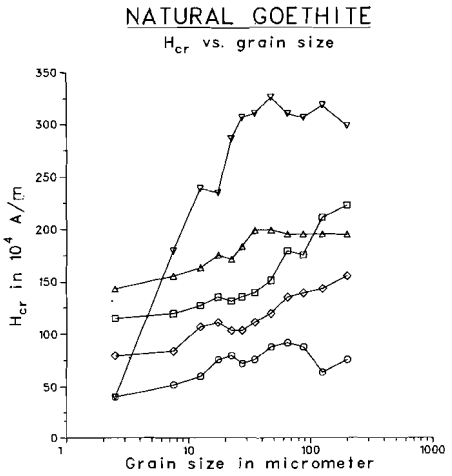

Fig. 10. Remanent coercive force (H_{cr}) as function of grain size for natural goethite. For sample abbreviations cf. Fig. 2.

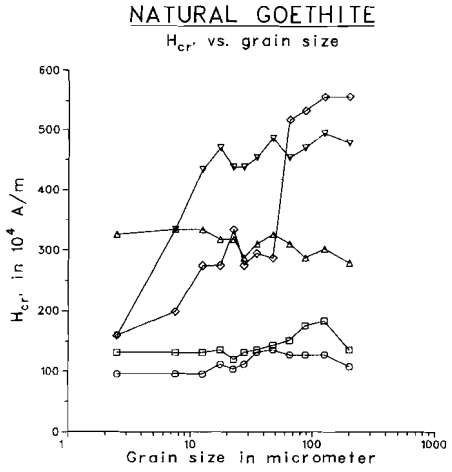

Fig. 11. Remanent acquisition coercive force ($H_{cr'}$) as function of grain size for the natural goethite. For sample abbreviations cf. Fig. 2.

$H_{cr'}$ is approximately constant throughout the investigated grain-size range in MKB, MBL and MEN goethite; it decreases with decreasing grain size in FSB and RR goethite (Fig. 11). MKB and MBL goethite have the

lowest $H_{cr'}$ figures since they acquire their saturation remanence in the lowest applied fields.

$H_{cr}/H_{cr'}$ ratios generally tend to decrease with decreasing grain-size. The ratio is about unity in MKB goethite; in between 0.4 and 0.7 in MBL, MEN and RR goethite and in between 0.25 and 0.4 in FSB goethite (Fig. 12, Table V). The extreme figures for the largest MKB fraction and the smallest RR fraction are regarded as anomalous. In four of the five goethite samples investigated, these ratios differ considerably from hematite $H_{cr}/H_{cr'}$ ratios (approximately unity; e.g. Dankers, 1978; Hartstra, 1982). Only MKB goethite has hematite-like figures for the $H_{cr}/H_{cr'}$ ratio. This indicates that goethite RA curves generally have a much smaller curvature than hematite RA curves.

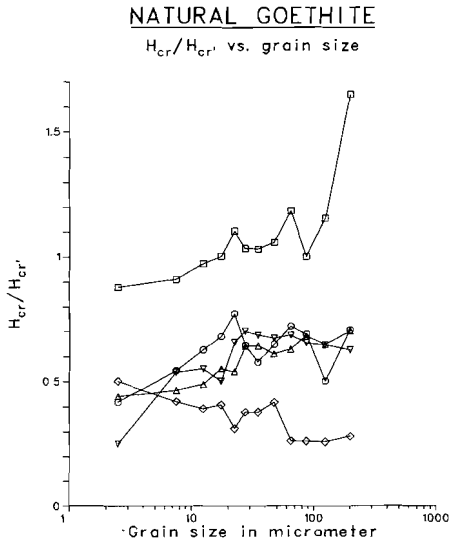

Fig. 12. Ratio of the remanent coercive force (H_{cr}) and the remanent acquisition coercive force ($H_{cr'}$) as function grain size for the natural goethites. For sample abbreviations cf. Fig. 2.

3 DISCUSSION

3.1 Ratios of some rockmagnetic parameters

The range of absolute figures of some rockmagnetic parameters of goethite partially overlaps with the hematite range. To establish more unambiguously to which mineral an observed remanence may be ascribed, ratios of rockmagnetic parameters may result in figures typical either for goethite or for hematite. A further advantage is that mass-independent parameters are obtained by taking the ratios of two mass-dependent parameters (e.g. X_{in}, J_s, J_{rs}). These ratios can directly be applied to natural samples with an unknown quantity of magnetic material.

Ratios of J_{rs}/J_s, H_{cr}/H_c, $H_{cr}/H_{c\ rev.}$ and X_{in}/J_{rs} are listed in Table V (cf. page 56). J_{rs}/J_s ratios vary between 0.1 and 0.5, generally from 0.2 to 0.35 (Fig. 13). All samples show a tendency for a declining J_{rs}/J_s ratio with decreasing grain size. MBL and FSB have the lowest ratios (generally below 0.2). The J_s determination has a rather large error (Table IV), which contributes to the observed scatter in the

J_{rs}/J_s ratios. Ratios higher than 0.6 are probably biased because of a too low figure for J_s. The goethite J_{rs}/J_s ratio generally is smaller than hematite J_{rs}/J_s ratios which are approximately 0.5 for both large single crystals (e.g. Eaton and Morrish, 1969) and fine-grained hematite powder (e.g. Dunlop, 1971). Smaller ratios have been reported for Ti-rich hematite (e.g. Westcott-Lewis and Parry, 1971), but such hematite is generally not reported in sedimentary rocks. So small J_{rs}/J_s ratios are indicative for goethite and can, as such, be used for the discrimination between goethite and hematite.

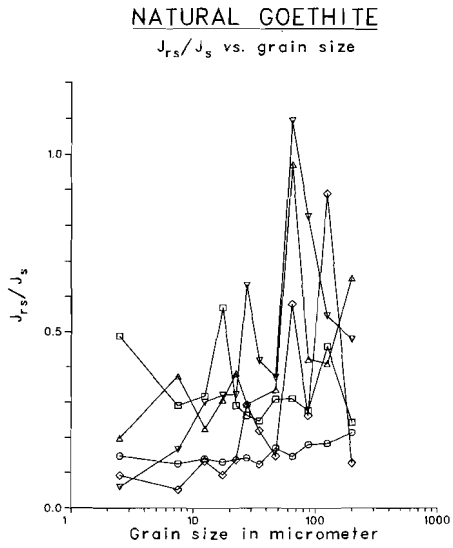

Fig. 13. J_{rs}/J_s ratios as function of grain size for the natural goethites. For sample abbreviations cf. Fig. 2.

For each individual goethite H_{cr}/H_c ratios are more or less constant throughout the grain-size range for each sample (Fig. 14). The H_{cr}/H_c ratio shows values from 10 (MKB goethite) to 40 (MBL, MEN, FSB goethite). The RR goethite values go up to about 100 for this ratio. The spreading in values for the RR fractions is due to the large difference between H_c and H_{cr} in each fraction. The H_{cr}/H_c $_{zerr.}$ ratio (Fig. 15) shows a similar pattern for four of the goethites (MBL, MEN, FSB, RR) being approximately constant for the four coarsest grain-size fractions and generally increasing in finer fractions. The increase in the 55-40 micrometer fraction is somewhat abrupt due to the fall in H_c $_{zerr.}$ in this fraction. Only the MKB goethite shows a smaller increase in its H_{cr}/H_c $_{zerr.}$ ratio, occurring in slightly finer-grained fractions (at approximately 25 micrometer). Extreme values for the H_{cr}/H_c $_{zerr.}$ are in between 3 (coarse-grained MKB goethite) and 65 (fine-grained RR goethite); usually the within-sample variation is from 7 to some 25-30. Goethite H_{cr}/H_c. $_{zerr.}$ ratios are up to two orders higher than hematite H_{cr}/H_c $_{zerr.}$ ratios, which are typically 1.5 - 2 (Dunlop, 1971). These high H_{cr}/H_c $_{zerr.}$ ratios illustrate the hardness of goethite.

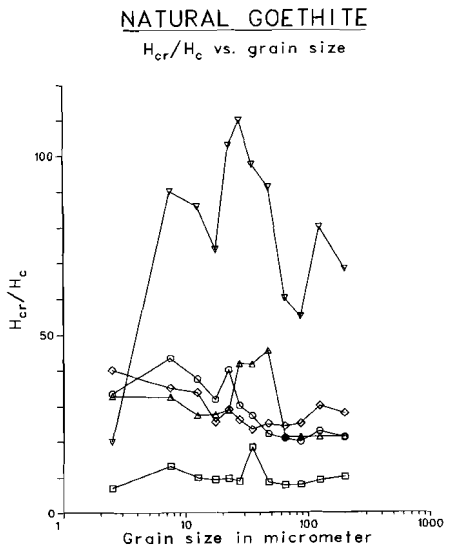

Fig. 14. H_{cr}/H_c ratios as function of grain size for the natural goethites. For sample abbreviations cf. Fig. 2.

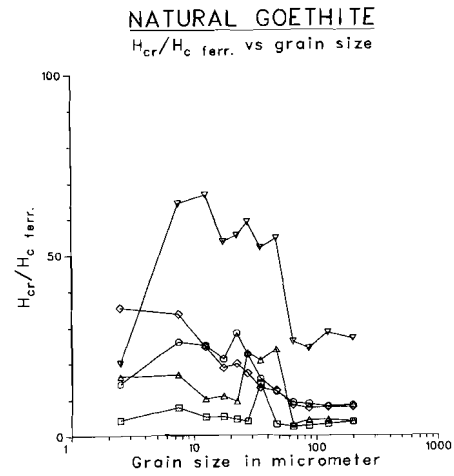

Fig. 15. $H_{cr}/H_{c\ ferr.}$ ratios as function of grain size for the natural goethites. Mark the relatively sudden fall in the 55-40 micrometer fractions. For sample abbreviations cf. Fig. 2.

J_{rs}/X_{in} decreases with grain size (Fig. 16) for all goethites. Goethite J_{rs}/X_{in} ratios are lower than such ratios for hematite (which are grain-size independent for individual hematites and between $14*10^4$ and $40*10^4$ Am^{-1}, data from Dankers, 1978). The goethite J_{rs}/X_{in} ratio approaches the ratio for fine-grained magnetite, but is one to two orders of magnitude larger than figures for coarse-grained magnetite (data from

Hartstra, 1982). Goethite and hematite may be discriminated by the absolute values for the J_{rs}/X_{in} ratio. In doubtful cases H_{cr} can be divided by this ratio. H_{cr} is larger than the J_{rs}/X_{in} ratio for goethite (cf. Table V) and smaller for hematite (data from Dankers, op. cit.). Traces maghemite or magnetite, resulting in an increased X_{in}, may noticeably lower the J_{rs}/X_{in} ratio (cf. the RR trend in Fig. 16).

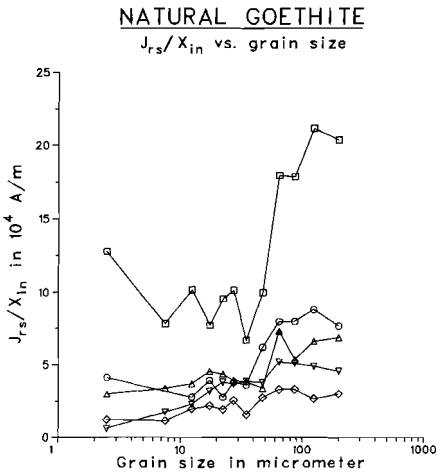

Fig. 16. Ratio of the saturation remanence (J_{rs}) and the initial susceptibility per unit mass (X_{in}) as function of grain size for the natural goethites. The coarse RR fractions are not completely saturated. For sample abbreviations cf. Fig. 2.

3.2 Influence of the chemical composition and crystallite size on the rockmagnetic parameters

Goethite rockmagnetic parameters show a wide variation, as outlined in the foregoing with emphasis on the grain-size trends for individual goethites. In the present section the influence of the goethite chemical composition and crystallite size on its rockmagnetic parameters will be examined. The non-Fe elements are divided in two groups: isomorphous substituted (Al, Mn) and sorbed, dispersed and/or intergrown (the other non-Fe elements, termed dispersed non-Fe elements) all represented by their anhydrous oxides. Trends of J_s, J_{rs}, H_c, $H_{c\ rem.}$ and H_{cr} versus isomorphous substituted non-Fe elements, non-substituted or dispersed non-Fe elements and crystallite size are shown in Fig. 17.

Goethite J_s shows an increase with increasing isomorphous substitution in the goethite, in agreement with previous observations (Hedley, 1971). The relatively high J_s figures for some of the FSB fractions (particular the fine grain-size fractions) may be due to imperfections in the hematite correction (FSB goethite has the highest hematite content, cf. Table III). The J_s trend shows no evident relation with the dispersed non-Fe element content and the crystallite size. The different relation of the two groups non-Fe elements to the goethite structure, revealed by the evaluation of the chemical and X-ray diffraction data, emerges magnetically in their J_s trends. It is reasonable to suppose that J_s is much less influenced by the dispersed non-Fe elements than by the isomorphous substituted non-Fe elements because the latter are

incorporated in the goethite structure itself. One of the two goethite magnetic sublattices preferably incorporates to some extent the substituted non-Fe ions, because J_s increases with increasing isomorphous substitution. The precise cause of this behaviour is not known, one could speculate that substitution for Fe leads to slightly extra distorted octahedra in the goethite structure and that this is better accounted for by substitution with a slight preference for alternating octahedra.

The J_{rs} dependence is much like that of J_s: it also increases with increasing isomorphous substitution. The low J_{rs} values for MBL goethite do not fit the increasing J_{rs} versus isomorphously substituted non-Fe elements trend. They are explained by the low maximum blocking temperature of MBL goethite (40 to 50 °C; the other goethites have at least 30 °C higher maximum blocking temperatures; cf. Dekkers, 1988C). In fact, the minor J_s increase in MBL, compared to the major rise in isomorphously substituted non-Fe elements, can be explained similarly. J_{rs} shows no evident relation with the content of dispersed non-Fe elements. The J_{rs} behaviour can be understood in the same framework as the J_s behaviour. Contrary to J_s, however, J_{rs} shows a relation with the crystallite size: it generally decreases with decreasing crystallite size. MBL goethite is an exception in the trend. This indicates that the saturation remanence is enhanced by isomorphous substitution (up to a certain level) and suppressed by a small crystallite size.

H_c and $H_{c\ ferr.}$ show no evident relationship with either the isomorphously substituted or the dispersed non-Fe elements. There is a tendency for H_c to first increase as the amount substituted impurities increases, and to decrease again with a further rise in substituted impurities, presumably related to distinctly lower maximum blocking temperatures in goethite with high amounts of isomorphous substitution. H_c tends to decrease with decreasing crystallite size; $H_{c\ ferr.}$ data fall into two groups: one with a high $H_{c\ ferr.}$ for its four coarsest grain-size fractions (MKB, MEN) and one with a distinctly lower $H_{c\ ferr.}$ for similar fractions (RR, FSB, MBL) without any observable crystallite-size trend.

H_{cr} first increases with increasing isomorphously substituted non-Fe elements and decreases with a further rise. This is related to falling maximum blocking temperatures with increasing substitution. H_{cr} is inversely correlated with the content dispersed non-Fe elements. The more dispersed, sorbed or intergrown non-Fe elements, reducing the crystalline order, the lower H_{cr}. Besides, the goethite crystallite size is of importance: H_{cr} decreases with decreasing crystallite size; a high content of isomorphously substituted non-Fe elements exerts an additional reducing influence (cf. MKB and MBL goethite).

Fig. 17. Saturation magnetization (J_s), saturation remanence (J_{rs}), coercive force (H_c), ferromagnetic coercive force ($H_{c\ ferr.}$) and remanent coercive force (H_{cr}) plotted versus the weight percentage isomorphously substituted impurities, dispersed impurities (microprobe analyses) and crystallite size. The grain-size range of J_s, J_{rs}, H_c, $H_{c\ ferr.}$ and H_{cr} is for each goethite sample indicated by bars. The dots in the J_s and J_{rs} plot indicate their means for each individual goethite sample. In the H_c and $H_{c\ ferr.}$ plots, values of the four coarsest grain-size fractions (which show only minor variation) are indicated by the black parts of each bar (the hatched parts of the bars in the $H_{c\ ferr.}$ plots are due to one outlying $H_{c\ ferr.}$ value). Arrows indicate the grain-size trends in the H_c, $H_{c\ ferr.}$ and H_{cr} plots. For sample abbreviations cf. Fig. 2.

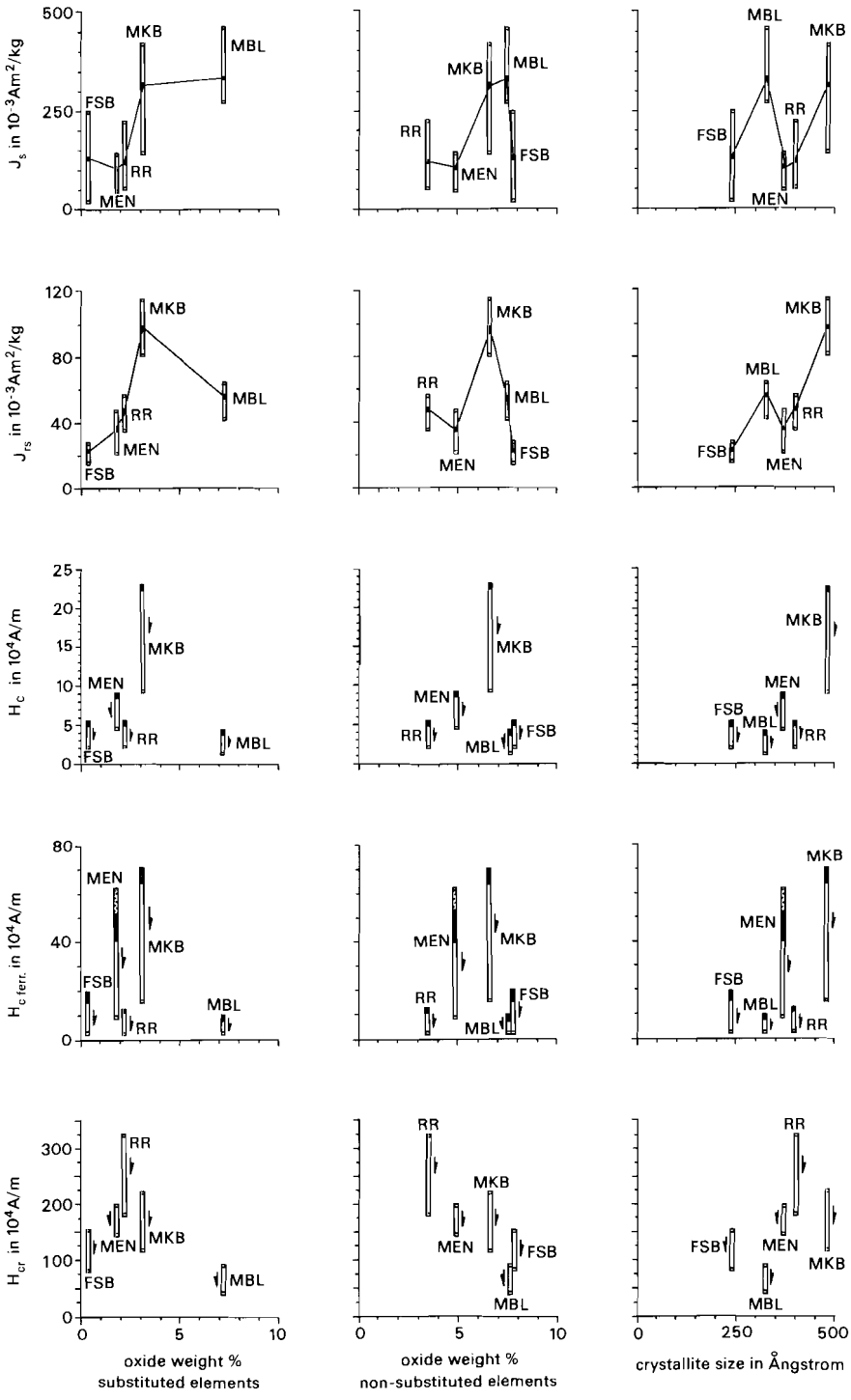
J_s in $10^{-3}Am^2/kg$
J_{rs} in $10^{-3}Am^2/kg$
H_c in $10^4A/m$
$H_{c\,ferr.}$ in $10^4A/m$
H_{cr} in $10^4A/m$
MKB
MBL
FSB
RR
MEN
oxide weight %
substituted elements
oxide weight %
non-substituted elements
crystallite size in Ångstrom

Table V: Derivative rockmagnetic parameters for natural goethite.

	H_{cr}/H_{cr}'	J_{rs}/J_s	H_{cr}/H_c	$H_{cr}/H_{c\ ferr.}$	J_{rs}/X_{in}	$H_{cr}/(J_{rs}/X_{in})$	K_a	K_b
MKB								
250-150	1.647	0.243	10.20	3.73	20.39	10.9	0.144	0.308
150-100	1.152	0.458	9.26	3.12	21.17	10.0	0.041	0.181
100-75	1.000	0.275	7.87	2.75	17.86	9.8	0.097	0.286
75-55	1.184	0.309	7.75	2.53	17.95	10.0	0.079	0.290
55-40	1.056	0.308	8.62	3.22	9.99	15.2	0.046	0.199
40-30	1.029	0.247	18.52	14.59	6.67	20.9	0.054	0.057
30-25	1.030	0.263	8.93	3.95	10.15	13.3	0.068	0.181
25-20	1.100	0.290	9.71	4.58	9.56	13.7	0.052	0.137
20-15	1.000	0.567	9.43	5.31	7.73	17.5	0.008	0.046
15-10	0.970	0.316	10.00	5.25	10.18	12.5	0.036	0.082
10-5	0.909	0.290	12.99	7.90	7.84	15.2	0.032	0.053
<5	0.879	0.487	7.09	4.26	12.77	9.0	0.020	0.062
MBL								
250-150	0.704	0.214	21.28	8.26	7.68	9.8	0.040	0.031
150-100	0.500	0.182	22.73	8.00	8.84	7.2	0.073	0.036
100-75	0.688	0.179	20.00	8.80	8.01	10.9	0.063	0.042
75-55	0.719	0.145	20.83	9.20	8.00	11.4	0.097	0.053
55-40	0.647	0.170	22.22	12.22	6.21	14.1	0.057	0.033
40-30	0.576	0.124	27.03	15.83	3.61	20.9	0.052	0.026
30-25	0.643	0.141	30.30	22.50	3.81	18.8	0.050	0.018
25-20	0.769	nd	40.00	28.57	2.77	28.7	nd	nd
20-15	0.679	0.129	31.25	21.11	3.93	19.2	0.059	0.021
15-10	0.625	0.138	37.04	25.00	2.80	21.3	0.030	0.010
10-5	0.542	0.125	43.48	26.00	nd	nd	nd	0.009
<5	0.417	0.146	33.33	14.29	4.12	9.7	0.034	0.010
MEN								
250-150	0.700	0.652	21.28	3.83	6.87	28.4	0.002	0.028
150-100	0.645	0.476	21.28	4.38	6.64	29.4	0.005	0.044
100-75	0.681	0.422	21.28	4.30	5.39	36.2	0.003	0.037
75-55	0.628	0.969	21.28	3.10	7.32	26.7	0.002	0.022
55-40	0.610	0.335	45.45	23.81	3.38	58.8	0.006	0.015
40-30	0.641	nd	41.67	20.83	3.83	51.9	nd	nd
30-25	0.639	0.293	41.67	23.00	3.93	46.5	0.008	0.014
25-20	0.538	0.382	28.57	9.56	4.36	39.2	0.005	0.021
20-15	0.550	0.305	27.78	11.00	4.54	38.5	0.007	0.023
15-10	0.488	0.225	27.03	10.25	3.71	44.0	0.009	0.025
10-5	0.464	0.374	32.26	16.96	3.41	45.5	0.003	0.009
<5	0.439	0.197	32.26	16.36	3.00	47.8	0.007	0.012
FSB								
250-150	0.279	0.127	27.78	7.80	3.02	51.4	0.012	0.030
150-100	0.257	0.888	30.30	7.83	2.70	53.1	0.001	0.001
100-75	0.261	0.261	25.00	7.61	3.32	42.0	0.004	0.019
75-55	0.262	0.578	24.39	8.50	3.30	41.0	0.001	0.003
55-40	0.417	0.147	25.00	12.50	2.75	43.4	0.015	0.023
40-30	0.378	0.220	23.26	13.33	1.56	71.2	0.003	0.012
30-25	0.377	0.293	26.32	17.33	2.56	40.5	0.003	0.007
25-20	0.310	0.135	28.57	20.00	1.94	53.4	0.011	0.012
20-15	0.406	0.093	25.64	18.67	2.19	50.8	0.024	0.018
15-10	0.391	0.132	33.33	24.54	1.99	53.9	0.013	0.012
10-5	0.420	0.053	34.48	33.87	1.15	72.4	0.042	0.016
<5	0.500	0.092	40.00	35.71	1.22	65.0	0.014	0.007
RR								
250-150	0.625	0.478	66.67	26.79	4.57	65.3	0.004	0.015
150-100	0.645	0.544	83.33	28.57	4.93	64.6	0.004	0.015
100-75	0.653	0.825	55.56	24.06	5.13	59.8	0.002	0.009
75-55	0.684	1.092	58.82	26.00	5.20	59.7	0.001	0.006
55-40	0.672	0.371	90.91	54.67	3.79	86.2	0.006	0.011
40-30	0.684	0.417	100.0	52.00	3.87	80.2	0.005	0.009
30-25	0.700	0.632	110.0	59.23	3.67	83.4	0.002	0.005
25-20	0.655	0.322	100.0	55.38	3.82	75.1	0.008	0.010
20-15	0.500	0.320	71.43	53.64	3.21	73.2	0.006	0.008
15-10	0.550	0.298	83.33	66.67	2.31	103.4	0.004	0.005
10-5	0.516	0.165	90.91	64.29	1.76	101.6	0.010	0.008
<5	0.250	0.059	20.00	20.00	0.59	67.3	0.024	0.015

H_{cr}/H_{cr}', J_{rs}/J_s, H_{cr}/H_c, $H_{cr}/H_{c\ ferr.}$ in SI units; J_{rs}/X_{in} in 10^4 Am^{-1}; $H_{cr}/(J_{rs}/X_{in})$ in SI units; K_a and K_b in Jkg^{-1}.

3.3 Weak ferromagnetism of goethite

The observed grain-size trends of H_{cr}, H_c and $H_{c\ ferr.}$ in goethite are contrary to the usual MD-PSD-SD trends which increase from low values for MD grains to high values for SD grains. Decreasing trends occur as one approaches the superparamagnetic threshold size. When this would be the case in the present goethites, the coarse grain-size fractions would be SD. With the derived rockmagnetic parameters one may calculate the anisotropy constants assuming uniaxial anisotropy. For random oriented grains two formula per unit mass (or volume) are given for uniaxial minerals (cf. Stacey and Banerjee, 1974; O'Reilly, 1984):

$K = \mu_o * 0.333 * J_s^2 * X_{in}^{-1}$ (K_a in Table V)

$K = \mu_o * J_s * H_c$ (K_b in Table V)

Both formula's yield comparable results (cf. Table V). The calculated anisotropy constants are up to three orders too low compared with goethite anisotropy constants taken from literature (0.25 to 2 Jkg^{-1}, e.g. Shinjo, 1966; Nalovic and Janot, 1979). So, apparently the SD state is not present in the actual goethites. Also the oolithic nature of some goethites and the presence of intergrowths make a SD state for coarse grains highly improbable. However, the grain-size dependence of the coercive forces - with the smallest values in the smallest grain size fractions - does not point towards MD behaviour. So mechanisms related to the microstructure of the goethite grains are needed to understand the observed behaviour.

Since (broad) X-ray reflections corresponding to goethite are recorded in the diffractograms, the present goethites are "true" goethites and not some amorphous solid. The goethites are thus not speromagnetically coupled, a fairly common coupling in amorphous solids (Coey and Schindler, 1977; see also Coey and Readman, 1973A, 1973B). The goethite crystallite size is, however, far less than its grain size, i.e. each grain consists of many crystallites.

The size of the goethite crystallites is in the range where Néel (1962) calculated that so called superantiferromagnetism occurs. If the plane in which the antiferromagnetic spin coupling is located, makes up also the outline of a crystallite, two situations may occur: one with an even number of lattice planes and one with an odd number of lattice planes. Crystallites with an even number show no magnetic moment, but have distinctly higher susceptibilities than a bulk mass of the same material. Crystallites with an odd plane number have one plane not balanced by a plane with antiparallel coupled spins and hence, carry a magnetic moment. This is usually referred to as imbalance remanence.

The present goethites show some elongation in the direction of the c-axis (derived from X-ray line broadening), so lattice planes with unbalanced spins may well occur. Indeed, crystallite-size dependence of rockmagnetic parameters is observed. However, if the size of the crystallites (combined with their chemistry) would be the only parameter determining the rockmagnetic features of the grains, there would be no grain-size dependence at all. This is in disagreement with observed grain-size dependent trends. To explain grain-size dependence, there has to be magnetic interaction amongst the crystallites. In this respect it is interesting to notice that Mössbauer spectra of microcrystalline goethite are best fitted, when exchange interaction amongst the crystallites is taken into account (Mørup et al., 1983). In goethite grains the crystallites are magnetically coupled by exchange coupling. Mørup et al.

(1983) propose the name "superferromagnetism" for this interaction regardless of the sign of the exchange coupling constant. The crystallite exchange coupling depends on the number of magnetic atoms at the crystallite interface and on the exchange coupling for individual pairs of atoms.

For H_{cr} (measured in zero applied field) this leads to the following: lower values are obtained for the crystallite exchange coupling, when the crystallite size is lowered (leading towards a lower number of magnetic atoms at their interface) or when the crystallites are less coupled by the presence of dispersed impurities. H_{cr} is decreasing with a decreasing crystallite size and also with an increasing content of dispersed non-Fe elements (Fig. 17). Isomorphous substitution, with a slight preference for one sublattice over the other (higher J_a and J_{ra}) leads first to higher exchange interaction because of higher crystallite magnetic moments, but with further substitution to a lower Néel point. H_{cr} first increases with isomorphous substitution and subsequently decreases (Fig. 17). Goethites with the most isomorphous substitution (MKB and MBL) have a relatively low H_{cr} with regard to their crystallite size (cf. the RR-MEN-FSB trend and the positions of MKB and MBL in the H_{cr} vs. crystallite size plot in Fig. 17).

For H_c and $H_{c\ ferr.}$ (measured in an applied field) the influence of this applied field is a complicating factor which obscures trends which could be traced in the H_{cr} measurements. It is remarkable that the increase in initial susceptibility in the 55-40 micrometer fraction coincides with the decrease in H_c and specially $H_{c\ ferr.}$. Tentatively, one might suggest that this increase in X_{in} (and the decrease in $H_{c\ ferr.}$?) can be explained in analogy with the superantiferromagnetism of Néel (1962) which refers to crystallites. Below a certain crystallite size the susceptibility increases up to twice the value of a bulk mass of the same material. The jump in X_{in} observed in the 55-40 micrometer fractions would then be related to a critical grain diameter below which "superantiferromagnetism" of the exchange coupling between the crystallites occurs.

By describing rockmagnetic parameters of microcrystalline goethite, crystallite exchange interaction appears to be an important factor. The great variety in goethite rockmagnetic properties may be explained as being the result of differences in goethite chemical composition, crystallite size and crystallite exchange interaction together with their interrelations.

4 CONCLUSIONS

The goethite rockmagnetic parameters reported in the present paper in a grain-size dependent framework show a considerable variety in their absolute figures and grain-size behaviour. Initial susceptibilities ($0.50*10^{-6}$ - $1.50*10^{-6}$ m^3kg^{-1}) show a maximum in the 30 to 55 micrometer range for all samples. In coarser grain-size fractions it is fairly constant and in finer grain-size fractions it tends to decrease slowly with decreasing grain size. High field susceptibilities ($0.20*10^{-6}$ - $0.40*10^{-6}$ m^3kg^{-1}) decline with decreasing grain size. The saturation magnetization ($30*10^{-3}$ - $450*10^{-3}$ Am^2kg^{-1}) is grain-size independent in the investigated grain-size range (from 250 micrometer down to <5 micrometer). It increases with increasing isomorphous substitution, in agreement with earlier observations (Hedley, 1971). The saturation remanence (acquired in $16*10^6$ Am^{-1} fields) varies between approximately $15*10^{-3}$ and $115*10^{-3}$ Am^2kg^{-1}, also increasing with a higher amount of isomor-

phous substitution in the goethite. It tends to decline with decreasing grain size.

The coercive force varies between 1-2*10⁴ and 25*10⁴ Am^{-1}, the ferromagnetic coercive force between 2*10⁴ and 70*10⁴ Am^{-1} and the remanent coercive force varies between 50*10⁴ and 300*10⁴ Am^{-1}. The remanent coercive force decreases with grain size. The remanent acquisition coercive force (100-550*10⁴ Am^{-1}) is in three of the five samples grain-size independent; in the others it decreases with grain size. The coercive force and the ferromagnetic coercive force are approximately constant for the four coarsest grain-size fractions. Both parameters tend to decrease with decreasing grain size in finer grain-size fractions. The (occasionally large) fall in coercive force and ferromagnetic coercive force coincides with the increase in initial susceptibility.

The coercive force as well as the remanent coercive force decrease with decreasing crystallite size. The remanent coercive force is inversely correlated with the content of dispersed non-Fe elements in the goethite lattice. Isomorphous substitution leads to an extra lowering of the remanent coercive force.

J_{rs}/J_s ratios typically vary between 0.2 and 0.35, depending on the goethite sample. The ratio decreases with grain size. Goethite J_{rs}/J_s ratios are smaller than such ratios for hematite (approx. 0.5). H_{cr}/H_c ratios are approximately constant for each sample throughout the grain-size range. Figures are between 10 (MKB goethite) up to 100 (RR goethite), which is one to two orders higher than hematite figures. The $H_{cr}/H_{c\ ferr.}$ ratio (3 to 60) is larger in goethite than in hematite.

J_{rs}/X_{in} decreases with decreasing grain size. Overlap may exist with the ratio for hematite. H_{cr} is larger than the J_{rs}/X_{in} ratio for goethite and smaller for hematite. X_{in} can easily be biased by impurities. So, related ratios have to be applied with a certain care.

Grain-size trends of the goethite coercive forces do not point towards MD behaviour. Calculation of the anisotropy constants yields figures up to three orders of magnitude too low for SD grains. The observed trends are qualitatively explained by taking into account exchange interaction between the crystallites making up a grain.

Differences in chemical composition (isomorphous substitution and dispersed non-Fe elements), crystallite size and crystallite exchange interaction for individual goethites with their interrelations lead to the observed wide variety in goethite rockmagnetic parameters. The relatively sudden increase in X_{in} in the 55-40 micrometer fraction is tentatively suggested to be explained by a crystallite exchange interaction analog of superantiferromagnetism (which refers to the crystallites themselves).

Acknowledgements

Dr. E. Wilhelm (Bureaux Recherches Géologiques et Minières) provided detailed information concerning the FSB sampling site. Drs. M.I. Pieters assisted during the sampling campaign for this research. Hoogovens Ltd. (Beverwijk, The Netherlands) kindly made available the raw sample material for the MEN and RR samples. The high field measurements were performed in the High Field Magnet Laboratory of the University of Nijmegen (The Netherlands) in cooperation with Dr. J.A.A.J. Perenboom and Dr. H.W. Myron (now at Argonne Nat. Lab.). C. Laman made the X-ray films and diffractograms. The manuscript was critically reviewed by Prof. Dr. J.D.A. Zijderveld. Drawings were made by J.J.J. Bergenhenegouwen. These investigations were supported by the Netherlands Foundation for Earth Science Research (AWON) with financial aid from the

Netherlands Organization for the Advancement of Pure Research (Z.W.O., grant 751-354-006).

5 REFERENCES

Bagin V.I., Gendler T.S., Kuz'min R.N., Rybak R.S., Urazayeva T.K., 1976, The weak ferromagnetism of natural hydrogoethites, Izv. Acad. Sci. USSR, Phys. Solid Earth 12, 328-33 (eng. ed.).

Banerjee S.K., 1970, Origin of thermoremanence in goethite, Earth Plan. Science Letters 8, 197-201.

Chevallier R., Mathieu S., 1943, Propriétés magnetiques des poudres d'hématites; influence des dimensions des grains, Ann. Phys. 18, 258-88.

Coey J.M.D., Readman P.W., 1973A, New spin structure in an amorphous ferric gel, Nature 246, 476-8.

Coey J.M.D., Readman P.W., 1973B, Characterization and magnetic properties of natural ferric gel, Earth Plan. Sci. Letters 21, 45-51.

Coey J.M.D., Schindler D.W., 1977, Magnetic order in fresh-water ferromanganese nodules, Physica 86-88B, 823-4.

Collinson D.W., 1983, Methods in rock magnetism and paleomagnetism, Chapman and Hall, London, New York, 503pp.

Cornell R.M., Mann S., Skarnulis A.J., 1983, A high-resolution electron microscopy examination of domain boundaries in crystals of synthetic goethite, J. C. S. Faraday I 79, 2679-84.

Creer K.M., 1962, On the origin of the magnetization of red beds, J. Geomagn. Geoelectr. 13, 86-100.

Dankers P.H.M., 1978, Magnetic properties of dispersed natural iron-oxides of known grain-size, Ph.D. thesis University of Utrecht, 143pp.

Dankers P.H.M., 1981, Relationship between median destructive field and remanent coercive forces for dispersed magnetite, titanomagnetite and hematite, Geophys. J. R. astr. Soc. 64, 447-61.

Dekkers M.J., 1988A, Some rockmagnetic parameters for natural goethite, pyrrhotite and fine-grained hematite, Ph.D. thesis State University of Utrecht, chapter 2.

Dekkers M.J., 1988B, Some rockmagnetic parameters for natural goethite, pyrrhotite and fine-grained hematite, Ph.D. thesis State University of Utrecht, appendix 1.

Dekkers M.J., 1988C, Magnetic properties of natural goethite part II: TRM behaviour during thermal and alternating field demagnetization and low-temperature treatment, in: Some rockmagnetic parameters for natural goethite, pyrrhotite and fine-grained hematite, Ph.D. thesis State University of Utrecht, chapter 4.

Dekkers M.J., Hartstra R.L., Mullender T.A.T., in prep., A device for the magnetic separation of fine-grained particles.

Dunlop D.J., 1971, Magnetic properties of fine particle hematite, Ann. Geophys. 27, 269-93.

Eaton J.A., Morrish A.H., 1969, Magnetic domains in hematite at and above the Morin transition, J. Appl. Phys. 40, 3180-5.

Forsyth J.B., Hedley I.G., Johnson C.E., 1968, The magnetic structure and hyperfine field of goethite (α-FeOOH), J. Phys. C2 1, 179-88.

Harms J.E., Morgan B.D., 1964, Pisolithic limonite deposits in North-West Australia, Proc. Australas. Inst. Min. Metall. 212, 91-124.

Harrison R.K., Aitkenhead N., Young B.R., Dagger P.F., 1975, Goethite from Hindlow, Derbyshire, Bull. Geol. Surv. Great Britain 52, 51-4.

Hartstra R.L., 1982, Some rockmagnetic parameters for natural iron-titanium oxides, Ph.D. thesis University of Utrecht, 145pp.

Hedley I.G., 1971, The weak ferromagnetism of goethite (α-FeOOH), Zeitschrift Geoph. 37, 409-20.

Heller F., 1978, Rockmagnetic studies of Upper Jurassic limestones from Southern Germany, J. Geophys. 44, 525-43.

Klug H.P., Alexander L.E., 1974, X-ray diffraction procedures, J. Wiley & sons New York, Chapman and Hall, London, 2nd edition, 966pp.

Landa E.R., Gast R.G., 1973, Evaluation of crystallinity in hydrated ferric oxides, Clays Clay Minerals 21, 121-30.

Lewis D.G., Schwertmann U., 1979, The influence of Al on iron oxides. Part III: preparation of Al-goethites in M KOH, Clay Minerals 14, 115-26.

Lowrie W., Heller F., 1982, Magnetic properties of marine limestones, Rev. Geoph. Space Phys. 20, 171-92.

Morris R.V., Lauer H.V., Lawson C.A., Gibson E.K., Nace G.A., Stewart C., 1985, Spectral and other physico-chemical properties of submicron powders of hematite (α-Fe2O3), maghemite (γ-Fe2O3), magnetite (Fe3O4), goethite (α-FeOOH) and lepidocrocite (γ-FeOOH), J. Geophys. Res. B90, 3126-44.

Mørup S., Madsen M.B., Franck J., Villadsen J., Koch C.J.W., 1983, A new interpretation of Mössbauer spectra of microcrystalline goethite: "superferromagnetism" or "super-spin-glass" behaviour?, J. Magn. Magn. Mat. 40, 163-74.

Nafovic L., Janot C., 1979, Mössbauer study of the crystallogenesis of iron hydroxides, Rev. Phys. Appl. 14, 475-80.

Néel L., 1962, Propriétés magnétiques des grains fins antiferromagnétiques: superparamagnetisme et superantiferromagnetisme, J. Phys. Soc. Japan B17, 676-84.

O'Reilly W., 1984, Rock and mineral magnetism, Blackie & Son, Glasgow and London, 220pp.

Pastrana J.M., Hopstock D.M., 1977, Magnetic properties of natural hematite and goethite, AIME Trans. 262, 1-5.

Ryabushkin P.K., 1976, Variability of magneto-mineralogical properties of iron hydroxides, Izv. Acad. Sci. USSR, Phys. Solid Earth 12, 723-6 (eng. ed.).

Sampson C.F., 1969, The lattice parameters of natural single crystal and synthetically produced goethite (α-FeOOH), Acta Cryst. B25, 1683-5.

Sauer K., Simon P., 1975A, Die Eisenerze des Aalenium und Bajocium im Oberrheingraben (Grube Kahlenberg, Grube Schönberg und kleinere Vorkommen), in: Sammelwerk Deutschen Eisenerzlagerstätten Vol 2, Eisenerze im Deckgebirge (Postvaristikum) 3) Sedimentäre Eisenerze im Süddeutschland, Geol. Jhrb. D 10, 25-68.

Sauer K., Simon P., 1975B, Die Eisenerze im Callovium von Gutmadingen, Blumberg und Waldshut, in: Sammelwerk Deutschen Eisenerzlagerstätten Vol 2, Eisenerze im Deckgebirge (Postvaristikum) 3) Sedimentäre Eisenerze im Süddeutschland, Geol. Jhrb. D 10, 104-28.

Shinjo T., 1966, Mössbauer effect in antiferromagnetic fine particles, J. Phys. Soc. Japan 21, 917-22.

Stacey F.D., Banerjee S.K., 1974, The physical principles of rock magnetism, developments in Solid Earth Geophysics Vol 5, Elsevier Scl. Publ. Comp., Amsterdam - London - New York, 195pp.

Strangway D.W., Honea R.M., McMahon B.E., Larson E.E., 1968, The magnetic properties of naturally occurring goethite, Geophys. J. R. Astr. Soc. 15, 345-59.

Strangway D.W., McMahon B.E., Honea R.M., 1967, Stable magnetic remanence in antiferromagnetic goethite, Science 158, 785-7.

Strom C., 1976, UNITCELLD, an interactive APL program for computing cell constants, unpubl. Leiden.

Thompson R., 1986, Modelling magnetization data using SIMPLEX, Phys. Earth Plan. Inter. 42, 113-27.

Westcott-Lewis M.F., Parry L.G., 1971, Magnetism in rhombohedral iron-titanium oxides, Australian J. Phys. 24, 719-34.

Wilhelm E., Kosakevitch A., 1978, Chapeaux de fer; rapport de synthèse, unpublished report BRGM, 35pp.

Zitzmann A. (ed.), 1978, The iron ore deposits of Europe and adjacent areas volume II, Bund. Geowiss. Rohst. Hannover (Schweizerbart), 386pp.

Zitzmann A., Neumann-Redling Chr., 1977, The iron ore deposits of Spain, in: Zitzmann A. (ed.), The iron ore deposits of Europe and adjacent areas Vol I, Bund. Anst. Geowiss. Rohst. Hannover (Schweizerbart), 418pp.

CHAPTER 4

MAGNETIC PROPERTIES OF NATURAL GOETHITE

PART II

TRM BEHAVIOUR DURING THERMAL AND ALTERNATING FIELD DEMAGNETIZATION AND LOW-TEMPERATURE TREATMENT

Abstract

The behaviour of a thermoremanent magnetization is reported for five natural goethites in a grain- size range of < 5 up to 250 micrometer. The TRM was induced by cooling from 140 °C in a field of 16 kAm^{-1}. The TRM grain-size dependence is different between the goethites: MEN and MBL goethite (respectively from Menera, Spain and Blumberg, Western Germany) show a maximum in the intermediate grain-size fractions. In MKB and RR goethite (from Kahlenberg, Western Germany and Robe River, Western Australia) TRM is slightly decreasing with decreasing grain size. In FSB goethite (Sain Bel, France) TRM is grain-size independent above some 30 micrometer; below that grain size it is slightly increasing with decreasing grain size. The TRM intensity shows a distinct variation between each goethite sample depending on its chemistry. The TRM intensity increases with increasing isomorphous substitution in the goethite until a certain maximum, to decrease again at higher levels of isomorphous substitution due to the lowering of the goethite Néel temperature. Besides isomorphous substitution the dispersed non-Fe elements also influence the TRM trend. A low amount of dispersed non-Fe elements lowers the TRM intensity compared to what one would expect from the amount of isomorphous substitution. With increasing isomorphous substitution the maximum blocking temperatures during continuous and stepwise thermal demagnetization are decreasing from 90-105 °C (FSB goethite) down to 45-60 °C (MBL goethite). No grain-size dependence is observed in the decay curves.

The initial susceptibility measured at room temperature generally decreases some ten percent after annealing at 140-150 °C; only FSB goethite shows a twenty percent decrease. The decrease after one time annealing and its constancy after subsequent annealings at the same temperature is a strong indication that these goethites have never been at that temperature during their geologic history. Hence, their NRM is most probably of chemical origin.

The goethites are extremely hard with respect to AF demagnetization. The remanence decay is grain- size independent for four of the goethites. It varies at 240 kAm^{-1} (300 mT, the strongest alternating field available) from 0 percent (RR goethite), via 3 percent (MEN goethite) to 6 percent (MKB and MBL goethite). Only in the fine crystalline FSB goethite the decay is larger and grain size dependence is observed: coarse-grained FSB goethite is decreasing some 18 percent and fine-grained FSB goethite some 55 percent. Only in extremely fine crystalline goethite (crystallite size close to the superparamagnetic threshold size) AF treatment results in a noticeable TRM decay.

All goethites show a steadily increasing remanence when cooling down to liquid nitrogen temperature in a zero field. Goethite is unique in this behaviour. Low-temperature treatment can thus be used for the identification of goethite remanences without the need to heat the sample. The risk of chemical alteration is avoided. The goethite remanence at room temperature decreases a few percent during the first

cooling cycle. There is no further remanence decrease upon repeated cooling. The remanence increase ratio is higher when there is more isomorphous substitution in the goethite.

1 INTRODUCTION

The increasing importance of sediments in paleomagnetic studies necessitates a thorough knowledge of remanent magnetic properties of natural goethite. To gain information on the rockmagnetic behaviour of goethite a set of artificial specimens is prepared with natural goethites from supergene environmental origin (sedimentary goethites and goethites from the weathering zone) of which the chemical composition, crystallite size and grain-size range are accurately determined. Saturation magnetization (J_s), saturation remanence (J_{rs}) and related rockmagnetic parameters of five natural goethites as a function of grain size have been described elsewhere (Dekkers, 1988A). The present study focusses on the description of the characteristics of a thermoremanent magnetization (TRM) of those goethites during routine paleomagnetic demagnetization procedures (alternating field and stepwise thermal demagnetization). Their behaviour during low-temperature treatment and continuous thermal demagnetization is also discussed. Most natural remanent magnetization (NRM) carried by goethite is thought to be a chemical remanence (CRM, acquired by growth through the blocking volume below its Néel temperature). CRM in goethite, however, is not easily simulated in an experimental set up. TRM, on the contrary, is acquired by goethite by simply cooling it from some 140 °C in a directed field. Study of the goethite TRM behaviour contributes to the understanding of goethite NRM behaviour.

Most studies concerning the magnetic properties of goethite report the saturation magnetization and related parameters (e.g. Hedley, 1971; Bagin et al., 1976). The thermomagnetic properties upon heating in a magnetic field have also been the subject of investigation (e.g. Banerjee, 1970). Mössbauer spectra of both natural and synthetic goethite are amply studied (e.g. Forsyth et al., 1968; Govaert et al., 1976, 1977; Murad, 1979, 1982; Golden et al., 1979; Goodman and Lewis, 1981; Johnston and Norrish, 1981; Fysh and Clark, 1982). There are, however, few studies on the remanent magnetic properties of goethite.

Goethite has the potential to carry a thermoremanence as was first established by Strangway et al. (1967, 1968). Their study involves J_s-T, J-H and TRM characteristics of goethite. Some goethite samples did not acquire a TRM in the geomagnetic field; however, in stronger fields a TRM was acquired (Strangway et al., 1968). The TRM was extremely stable with respect to AF demagnetization up to 80 kAm^{-1} (100 mTesla) fields. No blocking temperature spectra of the TRM are reported. Heller (1978) investigated the isothermal remanent magnetization (IRM) properties of goethite-bearing limestones in fields up to $4*10^6$ Am^{-1} (5 Tesla). He showed that during low-temperature treatment the remanence steadily increases in the temperature interval investigated (down to the liquid nitrogen temperature). He tentatively attributed this increase to lattice contraction (see also Lowrie and Heller, 1982). Continuous thermal demagnetization of the IRM indicated that some goethite samples had blocking temperatures up to approximately 60-70 °C and others up to 90 °C.

The goethites of which the magnetic properties are reported in the present contribution, have different geological origins: two marine sedimentary goethites (MKB and MBL; respectively from Kahlenberg and Blumberg, both locations in Western Germany), a fluviatile replacement

goethite (RR; Robe River mining district, Western Australia), a caprock goethite (MEN; Menera mining district, Spain) and a gossan goethite (FSB; Sain Bel, France). Chemical and crystallite size data are compiled in Table I.

Table I: Microprobe analyses, unit cell determinations and crystallite-size order of the goethite concentrates

Microprobe analyses

	MKB	MBL	MEN	FSB	RR
SiO_2	2.51	4.89	3.05	3.27	2.80
TiO_2	0.02	0.44	0.02	0.01	0.02
Al_2O_3	2.86	7.16	0.84	0.34	2.15
V_2O_3	0.10	nd	0.04	0.03	0.04
Fe_2O_3	76.32	68.44	79.55	80.58	79.33
MnO	0.24	0.06	0.93	0.02	0.05
MgO	0.92	0.86	0.95	0.10	0.09
CaO	0.27	0.26	0.17	0.08	0.07
Na_2O	0.13	nd	0.09	0.03	0.02
K_2O	0.07	nd	0.01	0.02	0.02
P_2O_5	1.79	0.84	0.28	0.07	0.07
SO_3	0.81	0.36	0.31	4.20	0.33
total	86.10	83.34	86.29	88.77	85.16
H_2O	13.17	13.43	14.09	17.68	11.79

Microprobe analyses were carried out on a TPD (Technisch Physische Dienst) microprobe fitted with a TRACOR Northern Energy Dispersive (ED) system. Operating conditions are 15 keV and 2 - 3 nA. ZAF matrix correction is applied. Contents are in weight percentages; nd = not determined; iron is calculated as Fe_2O_3. H_2O is determined with the Penfield method.

Unit cell sizes of the goethite

axis	MKB	MBL	MEN	FSB	RR
a	4.585 ± 0.003	4.586 ± 0.004	4.612 ± 0.004	4.611 ± 0.004	4.596 ± 0.004
b	9.908 ± 0.007	9.884 ± 0.008	9.920 ± 0.008	9.962 ± 0.009	9.909 ± 0.008
c	2.995 ± 0.002	3.000 ± 0.002	3.011 ± 0.002	3.008 ± 0.003	2.998 ± 0.002
Vol.	136.06	136.00	137.76	138.17	136.53

Lengths of the crystal axes in Å; volume (Vol.) in $Å^3$.

Average crystallite sizes in Å

MKB	MBL	MEN	FSB	RR
480	325	370	240	400

More detailed sample descriptions are in Dekkers (1988A, 1988B). Goethite concentrates of well-defined grain-size intervals are homogeneously dispersed in a $CaCO_3$-Al_2O_3-waterglass matrix in cylinders of 2.5 cm diameter and 2.2 cm height (standard dimensions in paleomagnetic studies) analogous to Dankers (1978, 1981) and Hartstra (1982A). Some 400 mg goethite is put in each specimen to obtain reliable magnetic measurements. Details on the preparation procedure are in Dekkers (1988C).

1.1 Instrumentation and experimental procedure

Initial susceptibilities were measured on a Jellinek KLY-1 susceptibility bridge. Remanence intensities were measured with a digital spinner magnetometer based on the Jellinek JR3 drive unit. This spinner is developed in the Utrecht Paleomagnetic Laboratory and has a sensitivity of 10^{-10} Am^2 and a reproducibility better than one degree for intensities exceeding 10^{-9} Am^2. During a later stage of the investigation measurements were performed using a 2G-Enterprises cryogenic magnetometer with a sensitivity of 10^{-11} Am^2 and a slightly better angular reproducibility than the digital spinner magnetometer.

Continuous recordings of the remanence during thermal demagnetization and low-temperature treatment were performed with a fluxgate spinner type magnetometer made suitable for measurements at high and low temperature by inserting the sample holder in a water-cooled furnace or a Dewar vessel during the measuring procedure. Periodic remanence measurements and temperature regulation were controlled with a microcomputer system (Dankers, 1978, 1981; Hartstra, 1982B, 1982C). Heating up to 145 °C takes 75 minutes; one complete cooling cycle (cooling down to -196 °C and re-heating to room temperature) takes three hours. Only moderate heating up to 145 - 150 °C is performed to avoid chemical alteration of the goethite.

Goethite generally carries an extremely weak remanence, which is easily swamped in the much stronger remanences of hematite and especially magnetite and maghemite. It appeared during the measurements on IRM-related behaviour (Dekkers, 1988A) that minor hematite is present in the goethite concentrates. Some FSB fractions contain slightly more hematite and traces of maghemite are present in RR fractions. It is, therefore, decided to focus the experiments on TRM behaviour of goethite, because - due to the very low blocking temperature spectrum of goethite - a complete TRM is acquired by goethite by cooling from some 145 °C whereas at those temperatures the partial thermoremanent magnetization (PTRM) acquired by the other magnetic minerals is low compared to the TRM of goethite.

During trial magnetization runs it appeared that the goethite remanence acquired in the geomagnetic field was extremely low, too low for a meaningful interpretation of its characteristics. Therefore TRM was induced in a somewhat stronger field of 16 kAm^{-1} (20 mTesla). This is beyond fieldstrengths for which the induced TRM is proportional with its inducing field. Hematite, with coercive forces of the same order of the present goethites, shows non-linear TRM versus H trends for induced fields stronger than approximately 800 Am^{-1} (Dunlop, 1971). So, for the present goethites only minimum values for the specific (volume) TRM may be calculated.

Superimposed on the TRM acquired by the goethite, the other magnetic minerals (present in minor amounts) simultaneously acquire a a PTRM when cooling from 145 °C (the temperature of TRM acquisition) down to room temperature. When describing goethite TRM features, the PTRM acquisition of the other minerals has to be corrected for.

2 RESULTS AND DISCUSSION

2.1 Relaxation

The relaxation of the TRM of two fractions of each goethite is followed during 35 days by measuring the remanence once a day; the interval between each measurement is enlarged after some 14 days.

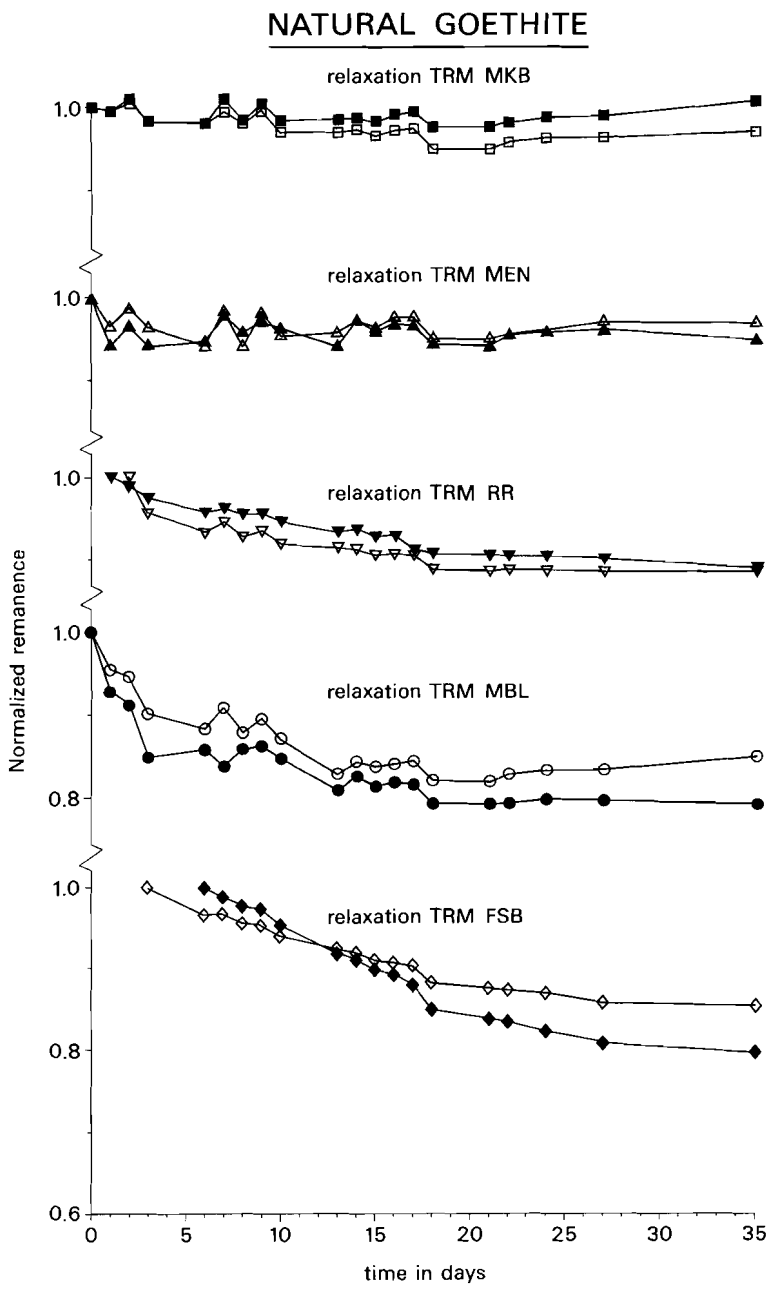

Fig. 1. Relaxation behaviour of the TRM (induced with a 16 kAm^{-1} field) of the specimens. Squares refer to MKB (Kahlenberg) fractions, circles to MBL (Blumberg) fractions, triangles to MEN (Menera) fractions, diamonds to FSB (Saln Bel) fractions and inverted triangles to RR (Robe River) fractions. open symbols denote the 150-100 micrometer fractions and full symbols 15- 10 micrometer fractions. The remanences are normalized to their initial values.

Results, normalized to the initial remanence intensity, are depicted in Fig. 1. Distinct differences exist between the goethites samples, though coarse (150-100 micrometer) and fine grain-size fractions (15-10 micrometer) for individual goethites show identical behaviour. MKB and MEN goethite show hardly any relaxation at all. RR goethite shows approximately 10 percent relaxation and MBL goethite some 15-20 percent. The remanence of FSB goethite is still decreasing at the end of the monitoring period. The fine grain-size fractions of MBL and FSB goethite show slightly more relaxation than the coarse fractions. The relaxation amount observed in the goethites correlates with the goethite crystallite size: generally more relaxation is observed with smaller crystallite size.

Goethite remanence is extremely sensitive to minute temperature variations (Heller, 1978). This explains the occasionally occurring increases in an overall decreasing remanence pattern (resulting in a saw-like appearance): relaxation is superimposed on variation in spontaneous magnetization due to (small!) temperature changes in the laboratory. After approximately 20 days the variation due to temperature fluctuation is larger than the relaxation of the remanence.

2.2 Behaviour during thermal demagnetization

Before discussing grain-size trends of the goethite TRM, the behaviour of the specimens during thermal demagnetization (continuous and stepwise) is treated, because the total remanence of the specimens is constituted of a goethite TRM and a PTRM of the other magnetic minerals. Thermal demagnetization allows for a separation of the goethite and non-goethite contributions to the total remanence. The goethite TRM behaviour during thermal demagnetization depending on its chemical composition and crystallite size is discussed in sections 2.2.1 and 2.2.2. TRM induced in virgin goethite specimens is referred to as TRM1. To study possible changes in TRM behaviour due to repeated thermal treatment in some fractions a TRM was induced a second time; this TRM is referred to as TRM2. TRM2 is acquired in the same inducing field and in the same direction as TRM1. Goethite TRM grain-size trends and the dependence of its absolute values on the chemistry and crystallite size are discussed in a separate section.

2.2.1 Continuous thermal demagnetization

Typical examples of goethite TRM behaviour during continuous thermal demagnetization are shown in Fig. 2. In Fig. 2A normalized decay curves of TRM1 are shown. The remanence can be almost exclusively attributed to goethite in the MKB, MBL and MEN samples; in the RR and FSB samples the contribution of other magnetic minerals (hematite and maghemite) to the total remanence is significant. The remanence in all goethites decreases rapidly, approximately linearly with increasing temperature. When the remanence is almost completely removed, the decay slows down, resulting in a concave part in the decay curve (see also the insets in Fig. 2A and Fig. 2B). This grain-size independent approach to the maximum blocking temperatures is notably different for each goethite. The extremes are represented in MBL and FSB versus MEN goethite: the latest goethite remanence is removed in a 10 - 15 °C temperature interval in the MBL and FSB samples and in a 50 °C interval in the MEN sample. MKB and RR goethite are intermediate (temperature interval 20 - 30 °C). The intervals are compiled in Table II. The differences between the goethite samples may be explained by differing crystallite-size spectra in these

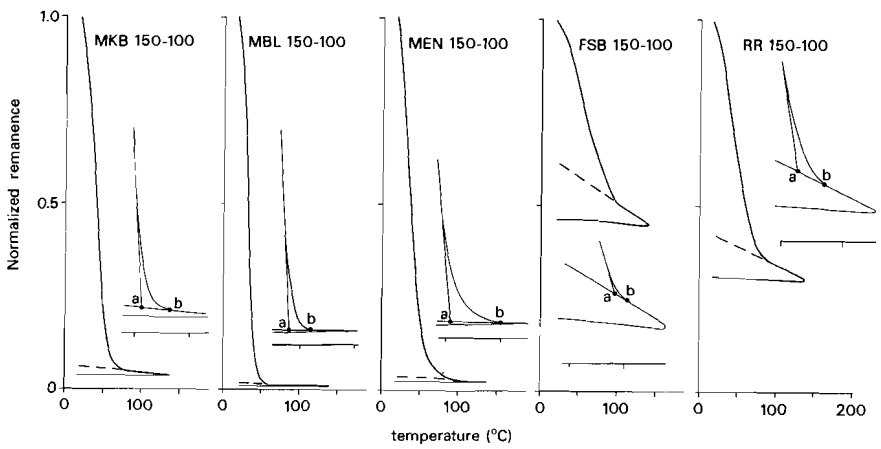

Fig. 2A. Continuous thermal decay curves of the 150-100 micrometer fractions, normalized to their initial remanence, of the first TRM, TRM1 (induced by cooling from 140 °C in a 16 kAm^{-1} field). For sample abbreviations cf. Fig. 1. The insets are enlargements of the final part of the decay curve attributed to goethite. Small a and b respectively refer to the onset and the endpoint of the 'concave part' in the decay curves; the appropriate temperatures are listed in Table II.

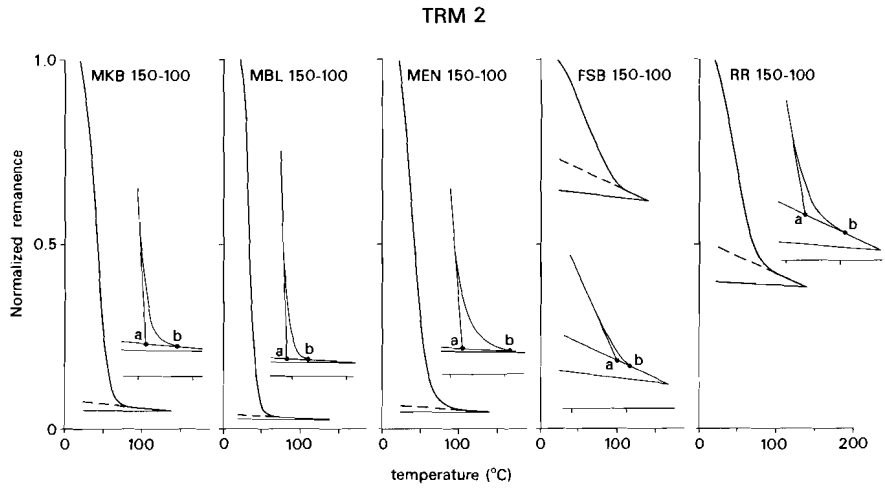

Fig. 2B. Continuous thermal decay curves of the 150-100 micrometer fractions, normalized to their initial remanence, of the second TRM, TRM2 (induced in an identical way as TRM1). Further explanation cf. Fig. 2A.

samples. The MEN goethite has apparently a relatively broad spectrum with perceptibly different blocking temperatures, which results in the observed broad temperature interval for the maximum blocking temperatures. Differential scanning calorimetry runs for this goethite (Dekkers, 1988D) show a broad decomposition temperature range (with a double peak) which points also to a broad crystallite-size spectrum.

The maximum blocking temperature of the goethites decreases with increasing isomorphous substitution. No grain-size dependence is observed. Comparison with the crystallite sizes of the goethites (cf. Table I) indicates that isomorphous substitution dominates the dependence of the blocking temperature over the crystallite size (at least in the crystallite-size range investigated), since the 'pure' FSB goethite has the smallest crystallites and nonetheless its maximum blocking temperature belongs to the group (MEN, RR, FSB) which shows the highest maximum blocking temperatures (approximately 105 °C).

Normalized decay curves of TRM2 are shown in Fig. 2B. TRM2 was induced in the same fractions after thermal demagnetization of TRM1. TRM2 is somewhat weaker than TRM1 (the contribution of the non-goethite minerals to the total remanence is slightly higher). Its behaviour during thermal demagnetization is identical to TRM1. The maximum blocking temperatures and concave parts of the decay curves are observed at (nearly) identical temperatures and temperature intervals as in TRM1.

Table II: Temperature intervals of the concave part in the goethite remanence decay curves during continuous thermal demagnetization, representing the highest part of the goethite blocking temperature spectrum

	150 - 100	55 - 40	40 - 30	20 - 15	15 - 10
MKB TRM1	55 - 79	---	---	57 - 78	---
MKB TRM2	59 - 80	±65	69 - 114	---	61 - 79
MBL TRM1	40 - 61	41 - 60	---	40 - 60	---
MBL TRM2	45 - 63	45 - 60	44 - 61	---	43 - 61
MEN TRM1	54 - 105	52 - 99	---	54 - 100	---
MEN TRM2	62 - 104	56 - 103	54 - 100	---	58 - 102
FSB TRM1	95 - 106	76 - 98	---	90 - 100	---
FSB TRM2	89 - 104	89 - 109	81 - 97	---	76 - 90
RR TRM1	70 - 95	68 - 98	---	67 - 100	---
RR TRM2	72 - 103	72 - 106	71 - 100	---	72 - 96

MKB, MBL, MEN, FSB and RR refer to the goethite sample abbreviations (respectively for Kahlenberg, Blumberg, Menera, Sain Bel and Robe River). TRM1 is induced in virgin specimens; TRM2 in the same specimens after thermal demagnetization of TRM1. The numbers refer to the grain size in micrometer for the fractions. Temperatures are in degrees Centigrade.

2.2.2 Stepwise thermal demagnetization

Representative normalized decay curves of stepwise thermal demagnetization for each goethite are given in Fig. 3; the curves recalculated to 100% goethite are shown in Fig. 4. Trial runs indicated that demagnetization steps of 10 °C are necessary for a good representation of the curves.

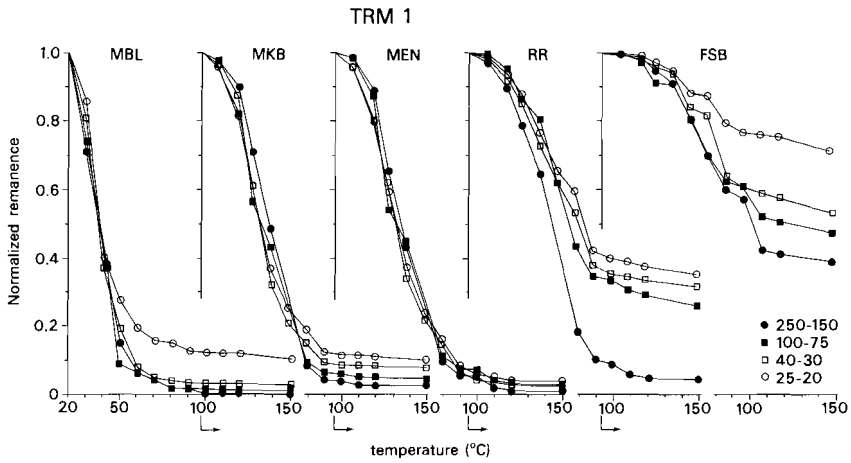

Fig. 3. Decay curves of stepwise thermal demagnetization of TRM1, normalized to their initial remanence, showing that the non-goethite contribution to the total remanence is different in each goethite sample and somewhat increasing with decreasing grain size. For sample abbreviations cf. Fig. 1.

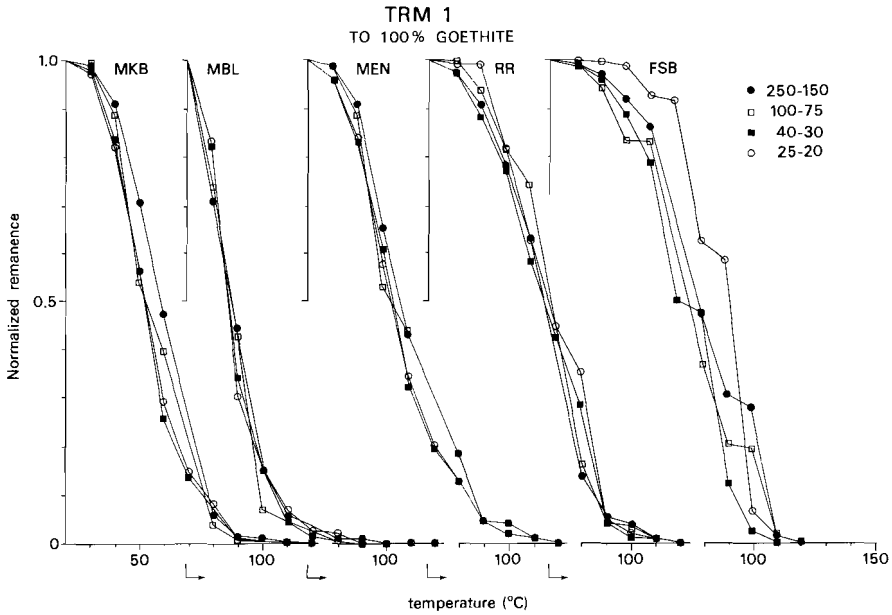

Fig. 4. Curves of Fig. 3 corrected for the non-goethite remanence. The thermal behaviour of each goethite is grain-size independent.

Generally, the non-goethite contribution to the total remanence increases with decreasing grain size due to a slightly raised hematite content in the finer fractions (cf. Dekkers, 1988A: Table III). The behaviour of the non-goethite part of the remanence is approached by comparing thermal demagnetization curves of a 16 kAm^{-1} IRM in similar samples and by comparing J_{rs} thermal decay curves of hematite from literature data (Dankers, 1978; Hartstra, 1982). The normalized goethite decay curves are clock-shaped and have a (nearly) identical shape for all grain sizes. The somewhat stoping appearance of the FSB curves is due to the normalization procedure, since the non-goethite contribution is large in those samples.

Decay curves obtained with the stepwise thermal demagnetization method also indicate that the goethite blocking temperature spectra correlate inversely with their isomorphous substitution: MBL with most isomorphous substitution has the lowest blocking temperature spectrum (maximum blocking temperatures approximately 60 °C), followed subsequently by MKB (80-90 °C), MEN and RR (90-100 °C) and finally by FSB (100-110 °C). As with the continuous method no crystallite-size dependence is traced. The small part of goethite remanence remaining at higher temperatures, representing at most up to a few percent of the initial goethite remanence, could be due to the estimation method for the non-goethite remanence. When this part reflects real goethite behaviour, this small tail can hardly be observed with the continuous thermal demagnetization method because of the decay in goethite spontaneous magnetization with increasing temperatures. Maximum blocking temperatures for goethite obtained with both methods can thus be considered as in good agreement.

2.3 TRM versus grain size

To calculate the goethite TRM per unit mass, the non-goethite part of the remanence is subtracted from the total remanence. The sample weight is subsequently corrected for the hematite weight content (calculated from remanent acquisition curves (Dekkers, 1988A), taking the saturation magnetization of 0.2 Am^2kg^{-1} for hematite; e.g. Dankers, 1981; Hartstra, 1982). Maghemite is negligible with respect to weight content. In decay curves determined with continuous thermal demagnetization, the magnetic non-goethite amount is established by linear extrapolation of the decay curve from temperatures above the bending point (corresponding to the removal of the latest goethite remanence) backwards to 20 °C. Continuous thermal decay curves of hematite and maghemite IRM are approximately linear at least in the temperature range of interest (Dankers, 1978; Hartstra, 1982). In decay curves determined with the stepwise method, the hematite behaviour during thermal demagnetization is allowed for as outlined in the foregoing section.

The TRM per unit mass versus grain size is tabulated in Table III and plotted in Fig. 5 and Fig. 6 (TRM1 and TRM2 resp.). TRM2 is (nearly) identical to TRM1 for MKB goethite. It is slightly lower than TRM1 for MBL, MEN and RR goethite and distinctly lower than TRM1 in FSB goethite (cf. Table III).

Individual goethite samples show different grain-size trends for their thermoremanences. TRM1 as well as TRM2 are decreasing with grain size for MKB goethite. A slight tendency to decrease with grain size is found for TRM1 and TRM2 in RR goethite. TRM1 and TRM2 show their highest values in the intermediate grain-size fractions for MBL and especially MEN goethite. TRM2 exhibits the maximum weaker than TRM1 in MEN goethite and stronger in MBL goethite. In FSB goethite the extremely weak TRM1 is

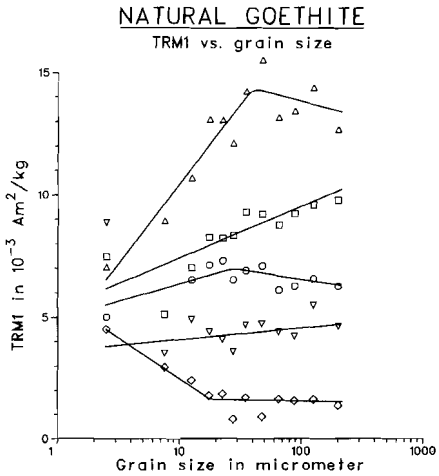

Fig. 5. TRM1 (per unit mass) versus grain size for the natural goethites. For sample abbreviations cf. Fig. 1.

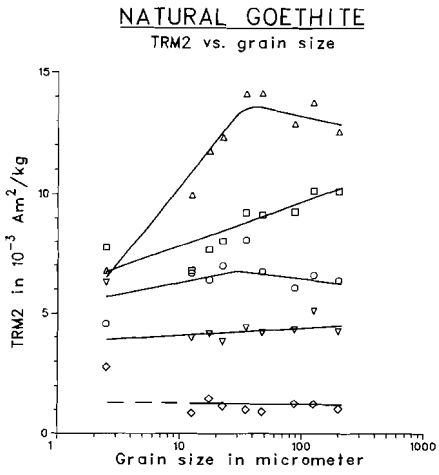

Fig. 6. TRM2 (per unit mass) versus grain size for the natural goethites. For sample abbreviations cf. Fig. 1.

grain-size independent in the investigated grain-size range in fractions down to 20 micrometer, in smaller fractions it slightly increases with decreasing grain size. The even weaker TRM2 shows hardly any grain-size dependence over the whole investigated grain-size range.

FSB goethite has the lowest TRM per unit mass followed by RR, MBL, MKB and finally by MEN goethite. Plots of TRM1 versus the amount of isomorphously substituted non-Fe elements, the amount of dispersed non-

Fe elements and the crystallite size are shown in Fig. 7. TRM intensities show a complex pattern with respect to these variables.

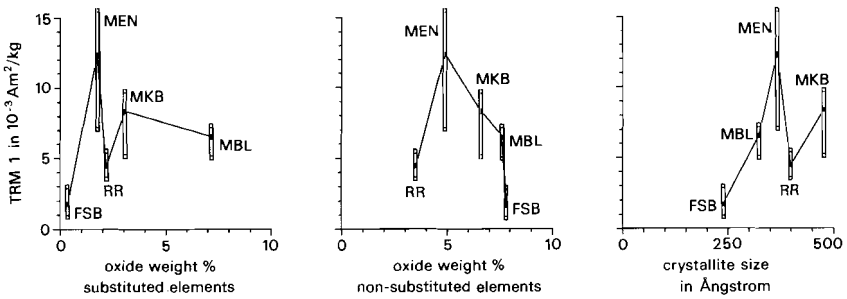

Fig. 7. TRM1 (per unit mass) versus the oxide weight percent isomorphously substituted non-Fe elements, the oxide weight percent dispersed non-Fe elements and the average crystallite size for each goethite. The TRM range is indicate by bars; the average for each bar is connected by straight lines.

Table III: TRM intensities (16 kAm^{-1} inducing field) for the natural goethites.

MKB				MBL				MEN			
fraction	TRM1	TRM2	$T_{1/2}$	fraction	TRM1	TRM2	$T_{1/2}$	fraction	TRM1	TRM2	$T_{1/2}$
250 - 150	9.78	10.11	0.97	250 - 150	6.26	6.36	0.98	250 - 150	12.69	12.54	1.01
150 - 100	9.59	10.12	0.95	150 - 100	6.58	6.59	1.00	150 - 100	14.42	13.74	1.05
100 - 75	9.22	9.27	0.99	100 - 75	6.28	6.05	1.04	100 - 75	13.42	12.89	1.04
75 - 55	8.75	nd	--	75 - 55	6.11	nd	--	75 - 55	13.17	nd	--
55 - 40	9.20	9.14	1.01	55 - 40	7.09	6.73	1.05	55 - 40	15.54	14.13	1.10
40 - 30	9.30	9.23	1.01	40 - 30	6.90	8.08	0.85	40 - 30	14.25	14.12	1.01
30 - 25	8.33	nd	--	30 - 25	6.54	nd	--	30 - 25	12.13	nd	--
25 - 20	8.22	8.05	1.02	25 - 20	7.31	6.96	1.05	25 - 20	13.07	12.32	1.06
20 - 15	8.26	7.65	1.08	20 - 15	7.13	6.38	1.12	20 - 15	13.09	11.75	1.11
15 - 10	7.03	6.79	1.04	15 - 10	6.53	6.67	0.98	15 - 10	10.70	9.98	1.07
10 - 5	5.13	nd	--	10 - 5	nd	nd	--	10 - 5	8.94	nd	--
< 5	7.46	7.75	0.98	< 5	5.01	4.55	1.10	< 5	7.05	6.79	1.04

FSB				RR			
fraction	TRM1	TRM2	$T_{1/2}$	fraction	TRM1	TRM2	$T_{1/2}$
250 - 150	1.38	1.05	1.31	250 - 150	4.63	4.25	1.09
150 - 100	1.63	1.23	1.32	150 - 100	5.50	5.10	1.08
100 - 75	1.58	1.25	1.26	100 - 75	4.22	4.32	0.98
75 - 55	1.63	nd	--	75 - 55	4.40	nd	--
55 - 40	0.91	0.92	1.00	55 - 40	4.74	4.21	1.12
40 - 30	1.70	1.01	1.68	40 - 30	4.69	4.41	1.06
30 - 25	0.81	nd	--	30 - 25	3.58	nd	--
25 - 20	1.86	1.15	1.62	25 - 20	4.10	3.84	1.07
20 - 15	1.78	1.46	1.22	20 - 15	4.40	4.16	1.06
15 - 10	2.40	0.88	2.70	15 - 10	4.91	3.98	1.23
10 - 5	2.95	nd	--	10 - 5	3.52	nd	--
< 5	4.50	2.76	1.63	< 5	8.86	6.28	1.41

Intensities in 10^{-3} Am^{2}kg^{-1}. TRM1 refers to the TRM induced in virgin samples; TRM2 to the TRM induced after thermal demagnetization of TRM1. The ratio of TRM1 and TRM2 is denoted with $T_{1/2}$. nd = not determined. Grain size ranges are in micrometer. For sample abbreviations cf. Table II.

The TRM intensity seems to be enhanced by increasing isomorphous substitution until a certain maximum value; it is decreasing with further isomorphous substitution due to lower Néel points in highly substituted goethites. However, RR goethite, with its relatively low TRM, does not fit in this trend. The observed TRM pattern can qualitatively be explained by taking into account the non-substituted or dispersed non-Fe elements. The RR goethite has the least dispersed non-Fe elements, which leads to a relatively high antiferromagnetic exchange coupling between its crystallites. This should result in the relatively low observed TRM. The influence of the crystallite size is difficult to evaluate. With decreasing crystallite size the TRM intensity should decrease because of the approach to the superparamagnetic threshold size (Mössbauer results indicate it to be approximately 200 Å). The trends in the present goethites, however, seem to be dominated by their chemistry.

A minimum specific volume TRM can be calculated for each goethite by dividing the TRM per unit volume by its inducing field. In the present case, the TRM versus H curve is probably not linear anymore at the inducing field of 16 kAm^{-1}, so this specific volume TRM (SI units) is a minimum one. For each sample the average TRM1 (the highest and lowest value for each goethite were excluded when calculating the average TRM) was taken and the specific density of goethite was set at 3700 kgm^{-3}. The following average minimum specific volume TRM values are obtained for each goethite sample: MKB: $1.9*10^{-3}$; MBL: $1.5*10^{-3}$; MEN: $2.9*10^{-3}$; FSB: $0.4*10^{-3}$ and RR: $1.0*10^{-3}$. These minimum values are two orders less than hematite specific volume TRM (approximately 0.4; Dunlop, 1971).

2.4 Initial susceptibility after annealing

Initial susceptibilities for each fraction, measured at room temperature after annealing at 140 °C, are listed in Table IV. The values refer to goethite; i.e. they are corrected for the diamagnetic moment of the matrix, which alters after one heat treatment due to liberation of water from the calciumcarbonate-waterglass mixture. This was checked by comparing the weights of each specimen before and after annealing. The change in diamagnetic moment of the matrix per unit mass was established by means of blanks. The initial susceptibilities decrease during the first annealing; repeated annealing at the same temperature hardly changes the susceptibility further. The ratio of the initial susceptibility after two times annealing and that prior to annealing as function of grain size is shown in Fig. 8.

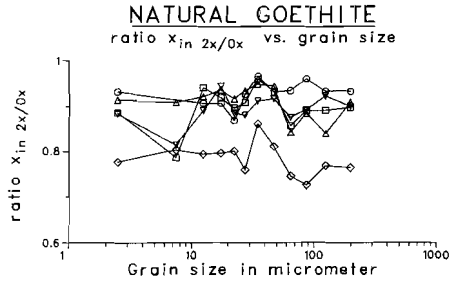

Fig. 8. Ratio of the initial susceptibility of the natural goethites after two times annealing and prior to any annealing (2x/0x) versus grain size. For sample abbreviations cf. Fig. 1.

Generally, the susceptibility decreases some ten percent, regardless of the grain size of the goethite. Only in the FSB fractions a decrease of some twenty percent is observed.

The lower initial susceptibility after annealing reflects a more ideal antiferromagnetic goethite structure. Apparently, annealing at moderate temperatures already gives rise to changes in the goethite lattice, such as the loss of loosely bonded water. The change in initial susceptibility after one time annealing at 140 °C and its constancy after further annealing at the same temperature is a strong indication that the goethite has never been at that temperature in nature, i.e. the NRM carried by these goethites is most probably a chemical remanence (CRM). A further indication in this direction is the fact that the TRM acquired by the artificial specimens in the geomagnetic field is hardly measurable, despite the relatively large amounts of goethite in these specimens.

Table IV: Initial susceptibilities prior to after annealings at 140 °C.

	MKB						MBL						MEN					
grain size	0x	1x	2x	3x	4x	5x	0x	1x	2x	3x	4x	5x	0x	1x	2x	3x	4x	5x
250 - 150	0.49	--	0.44	0.44	0.43	--	0.75	--	0.70	0.69	0.70	--	0.55	--	0.50	0.48	0.51	--
150 - 100	0.46	--	0.41	0.41	0.40	0.42	0.74	--	0.69	0.68	0.67	0.68	0.56	--	0.47	0.48	0.48	0.50
100 - 75	0.55	--	0.49	0.49	0.49	--	0.76	--	0.73	0.71	0.72	--	0.61	--	0.54	0.53	0.54	--
75 - 55	0.56	0.48	0.48	--	--	--	0.76	0.70	0.71	--	--	--	0.57	0.49	0.48	--	--	--
55 - 40	1.04	--	0.97	0.96	0.98	0.97	1.01	--	0.94	0.93	0.94	0.94	1.42	--	1.34	1.33	1.34	1.34
40 - 30	1.75	--	1.68	--	1.70	1.71	1.48	--	1.43	--	1.42	1.42	1.16	--	1.10	--	1.09	1.09
30 - 25	1.09	1.02	0.99	--	--	--	1.63	1.52	1.51	--	--	--	1.06	0.99	0.99	--	--	--
25 - 20	1.15	--	1.03	0.98	1.02	--	2.05	--	1.78	1.74	1.79	--	0.83	--	0.76	0.76	0.79	--
20 - 15	1.10	--	1.01	0.98	0.99	--	1.51	--	1.37	1.34	1.39	--	0.77	--	0.72	0.70	0.73	--
15 - 10	0.83	--	0.78	0.76	0.76	0.77	1.72	--	1.56	1.50	1.51	1.50	0.76	--	0.70	0.69	0.69	0.68
10 - 5	1.03	0.83	0.81	--	--	--	--	--	--	--	--	--	0.88	0.82	0.80	--	--	--
< 5	0.70	--	0.62	0.62	0.63	--	1.02	--	0.95	0.95	0.99	--	0.70	--	0.64	0.66	0.63	--

	FSB						RR					
grain size	0x	1x	2x	3x	4x	5x	0x	1x	2x	3x	4x	5x
250 - 150	0.51	--	0.39	0.41	0.41	--	1.10	--	0.99	0.99	0.95	--
150 - 100	0.56	--	0.43	0.42	0.42	0.42	1.16	--	1.07	1.02	1.04	1.04
100 - 75	0.66	--	0.48	0.48	0.52	--	1.03	--	0.92	0.92	0.95	--
75 - 55	0.63	0.48	0.47	--	--	--	1.05	0.98	0.92	--	--	--
55 - 40	1.00	--	0.81	0.78	0.81	0.80	1.45	--	1.33	1.27	1.30	1.30
40 - 30	1.65	--	1.42	--	1.42	1.43	1.36	--	1.24	--	1.24	1.26
30 - 25	1.08	0.91	0.82	--	--	--	1.34	1.28	1.18	--	--	--
25 - 20	1.25	--	1.00	0.98	1.02	--	1.31	--	1.16	1.17	1.20	--
20 - 15	1.03	--	0.82	0.76	0.78	--	1.40	--	1.32	1.24	1.20	--
15 - 10	1.41	--	1.12	1.13	1.13	1.14	1.56	--	1.39	1.39	1.38	1.40
10 - 5	2.34	2.11	1.88	--	--	--	2.10	2.03	1.71	--	--	--
< 5	1.88	--	1.46	1.45	1.42	--	5.92	--	5.22	5.20	4.94	--

0x: Initial susceptibility (in 10^{-6} m^3kg^{-1}) of virgin samples; 1x up to 5x: initial susceptibility measured at room temperature after the respective times annealing at 140 °C. Grain size ranges in micrometer; for sample abbreviations cf. Table II.

2.5 Behaviour during alternating field (AF) demagnetization

To evaluate the goethite behaviour during alternating field demagnetization TRM1 was subjected to increasing alternating fields up to 240 kAm^{-1}. Two fractions of each sample - with grain-size ranges of

250- 150 and 20-15 micrometer - were selected to investigate grain size effects upon AF demagnetization. Differences between the fractions of individual goethite samples are minor. There are, however, distinct differences between the goethite samples (Fig. 9A). It might be that these sample differences are caused by different contributions of the non-goethite minerals to the observed remanence (which is constituted of a goethite and a non-goethite part). To evaluate the influence of the non-goethite minerals on the AF behaviour of the total remanence, two neighbouring fractions of each goethite (150-100 and 15-10 micrometer fractions) were thermally demagnetized at 135 °C to remove the goethite contribution to the remanence. A part of the non-goethite remanence is also removed. To correct as much as possible for this decay, an IRM was given to these samples in the same direction and with the same inducing field as the original TRM after the thermal demagnetization. It appeared that the remanence after IRM acquisition was slightly higher than before. This remanence, i.e. the remainder after thermal demagnetization at 135 °C plus the room temperature induced IRM, was also subjected to alternating field demagnetization. The remanence decay during AF treatment was subtracted from the original sample TRM (constituted of a goethite and a non-goethite part) and subsequently normalized. In this way the behaviour of the non-goethite part of the total remanence during AF demagnetization can be determined (Fig. 9B).

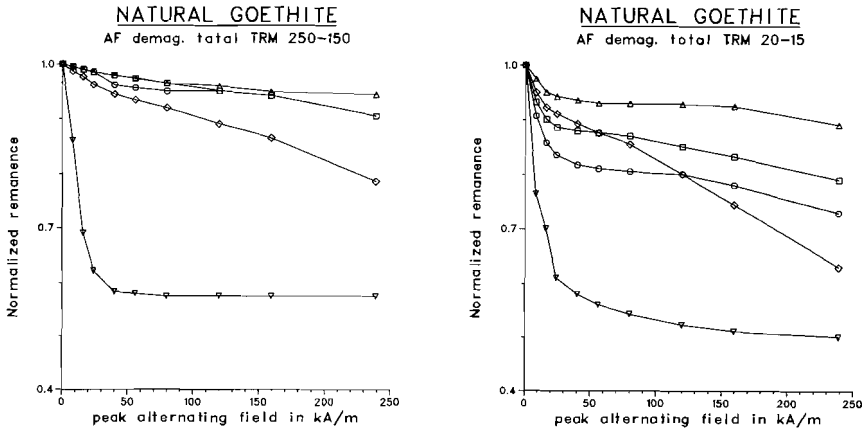

Fig. 9A. Behaviour of the total thermoremanence (acquired by cooling from 140 °C in a 16 kAm^{-1} field) during AF demagnetization of two fractions of each goethite sample, normalized to their initial remanences. The numbers indicate the grain-size fractions of each goethite. For sample abbreviations cf. Fig. 1.

The large similarity of the curves in Fig. 9A and Fig. 9B indicates that the differences between the goethite samples are predominantly due to the non-goethite contribution to the remanence. After thermal demagnetization, the remaining remanence of the AF demagnetized specimens indeed was much lower than that of non-AF demagnetized specimens. When the composition of neighbouring fractions is exactly equal, the relative decay of the total remanence and that of the non-goethite remanence can directly be subtracted from each other to establish the goethite behaviour during AF demagnetization. When the composition is not exactly equal, the decay of the non-goethite curve (Fig. 9B) should be "normalized" to the decay curve of the corresponding "total" curve (Fig. 9A).

In practice, this appeared only necessary for the MBL 20-15 and 15-10 micrometer fractions. Above 80 kAm^{-1} the non-goethite minerals showed no decrease anymore (Fig. 9B), so the decrease in the total curve (Fig. 9A) is due to goethite. The minor differences in corresponding RR fractions are due to minute variations in maghemite content of the goethite concentrates.

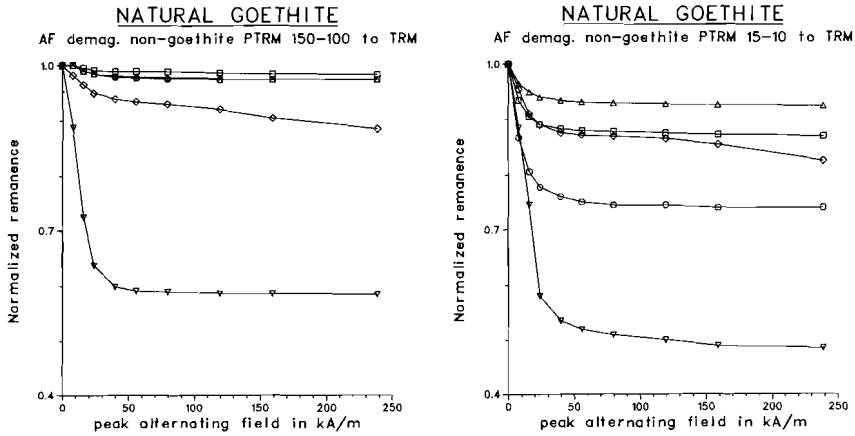

Fig. 9B. Behaviour of the non-goethite part (i.e. their PTRM remaining after thermal demagnetization at 140 °C plus their IRM acquired in the same field after thermally demagnetizing the goethite TRM part) of the remanence during AF demagnetization. The decay is normalized to the initial total thermoremanence (goethite TRM plus non-goethite PTRM) to compare the non-goethite behaviour with the behaviour of the total thermoremanence to evaluate the goethite behaviour. The numbers refer to the grain-size fractions of each goethite. For sample abbreviations cf. Fig. 1.

The relative goethite decay normalized to the initial value of the goethite TRM sensu stricto (= total TRM corrected for the non-goethite contribution) is shown in Fig. 9C. Four of the five goethites investigated (RR, MEN, MKB, MBL) show an extreme hardness in agreement with general observations (e.g. Strangway et al., 1968; Heller, 1977, 1978). Coarse and fine fractions behave alike. The RR goethite fractions do not show any decrease up to 240 kAm^{-1}; the MEN fractions decrease approximately 3% at the maximum applied alternating field; the MKB and MBL fractions 7% to 8%. The decrease for all goethites is negligible in alternating fields up to 80 kAm^{-1}.

The FSB fractions show more decrease and a perceptible grain-size dependence: at 240 kAm^{-1} the 250-150 micrometer fraction decreases 18% and the 20-15 micrometer fraction 55%. The onset of the decrease occurs also at lower applied fields, down to 40 kAm^{-1}. Apparently, remanences in extremely fine crystalline goethite (as FSB) can be broken down with alternating fields to a varying, but reasonably large extent depending on the grain size.

The observed behaviour indicates that the goethite AF properties are dominated by its crystallite size. AF demagnetization can only cope with thermoremanences in extremely fine crystalline goethite with crystallite sizes close to the superparamagnetic threshold size. In these fine crystalline goethites, exchange interaction between crystallites is important, since grain-size dependence of the decay during AF treatment is observed. The exchange interaction in goethite with slightly coarser

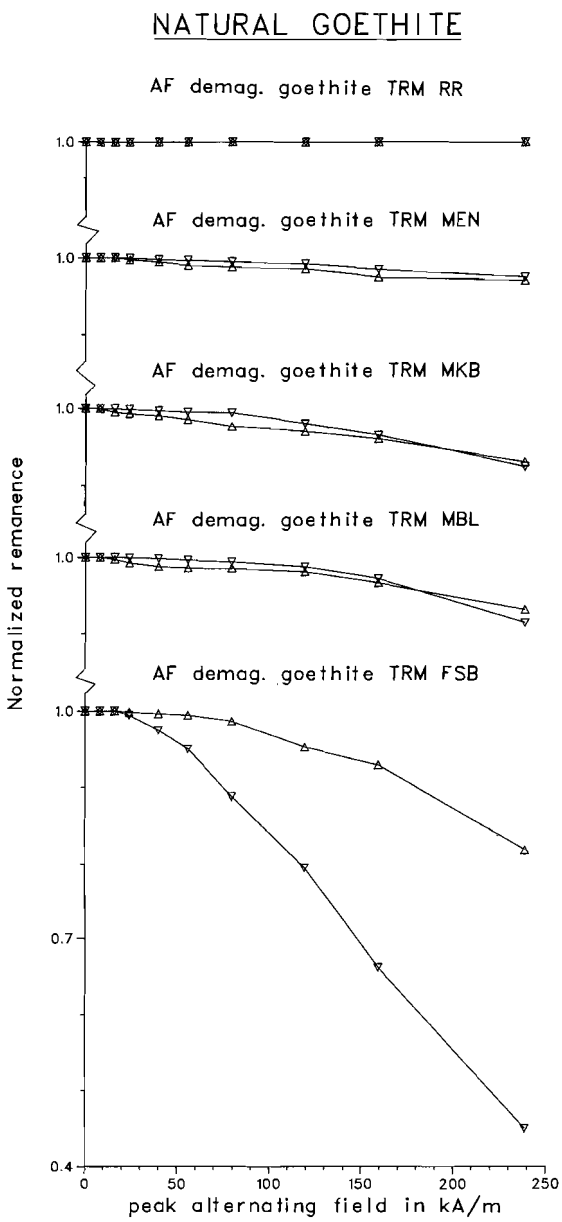

Fig. 9C. Behaviour of the goethite thermoremanence during AF demagnetization. The goethite behaviour is obtained by subtracting the non-goethite behaviour (Fig. 9B) from the behaviour of the total remanence (Fig. 9A) of neighbouring grain-size fractions and normalizing the decay to the goethite sensu stricto TRM. For sample abbreviations cf. Fig. 1.

crystallites is apparently already that large that hardly any remanence decrease is observed anymore in available alternating fields. Slight differences in AF behaviour in these goethites are due to their chemical composition. Isomorphous substitution enhances the magnetic moment of the crystallites and, as such, their exchange interaction, but lowers the Néel point. Dispersed non-Fe elements lower the crystallite exchange interaction. RR goethite contains a low amount dispersed non-Fe elements; its crystallites are rigidly coupled and no decrease of the TRM is observed even after treatment in 240 kAm^{-1} alternating fields. MEN, MKB and MBL goethite contain increasingly more dispersed non-Fe elements. The amount of isomorphous substitution is also increasing in this sequence. A slightly increasing remanence decay is observed from MEN to MKB and MBL.

It follows from the AF decay curves after thermal demagnetization of the goethite thermoremanence (at 140 °C) followed by IRM acquisition in a 16 kAm^{-1} field normalized to their remanence after this treatment (Fig. 9D), that a PTRM residing in hematite shows markedly different AF properties as an IRM acquired in the same field. An IRM induced in a 16 kAm^{-1} field is obviously removed by AF demagnetization in fields with peak values of the same order. A PTRM induced at 140 °C also in a 16 kAm^{-1} field, is not completely removed in alternating fields of the same order at room temperature. There is still a (large) part of hematite PTRM present after AF treatment in 240 kAm^{-1} fields! The difference in behaviour of the maghemite PTRM and IRM is minor: most maghemite is removed with 16 kAm^{-1} alternating fields (cf. the RR decay curve in Fig. 9D); the minor further decay is attributed to hematite which is a minor phase in the RR goethite concentrate.

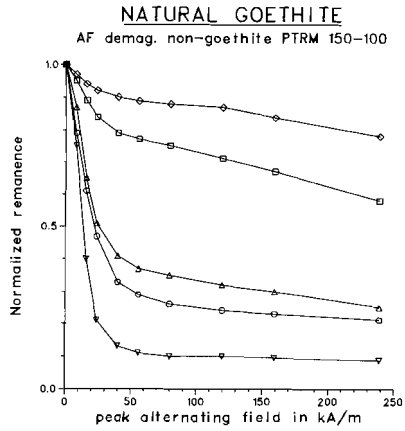

Fig. 9D. Behaviour of the goethite thermoremanence during AF demagnetization, normalized to its figure after thermal demagnetization. It is apparent from the curves that the room temperature AF behaviour of a PTRM induced at 140 °C in a 16 kAm^{-1} field is significantly different from a room temperature IRM induced with the same field. Part of the remanence is not removed even with a 240 kAm^{-1} alternating field, which is considerably larger than the inducing field of only 16 kAm^{-1}. For maghemite (RR fractions) the difference in behaviour due to the temperature of IRM acquisition is less.

2.6 Low-temperature behaviour

Goethite thermoremanences steadily increase, when cooled down from room temperature to -196 °C (Fig. 10). This behaviour is typical for goethite and low-temperature treatment is, as such, a powerful technique to identify a goethite remanence without heating the sample (chemical alterations are thus avoided). Remanence behaviour during the first cooling cycle is shown in Fig. 10A. After the first complete cooling cycle, the remanence has decayed some 3 to 10%. This indicates that the exchange coupling regime is slightly altered during the first cooling. Generally, in small grain size fractions the decay is slightly larger than in coarse grain size fractions. MEN goethite shows a smaller decay than the others: it behaves more or less reversibly already during the first rewarming. All goethites show reversible remanence behaviour from the second cooling cycle onwards (Fig. 10B).

Table V: Ratio of the thermoremanences at -196 °C and the remanence before the first cooling cycle for all cooling cycles of a specific specimen together with the remanence ratio before and after each individual cooling cycle.

	MKB		MBL		MEN		FSB		RR	
	RI	RBA	RI	RBA	RI	RBA	RI	RBA	RI	RBA
150 - 100 A	3.05	0.95	3.39	0.99	2.65	0.98	2.15	1.00	3.00	0.93
150 - 100 B	3.22	1.00	3.34	1.00						
40 - 30 A	2.82	0.87	3.28	0.96	2.49	0.97	2.12	1.00	2.75	0.89
40 - 30 B	3.20	1.00								
15 - 10 A	2.87	0.89	3.03	0.91	2.56	1.00	1.56	0.90	2.45	0.86
15 - 10 B	3.25	1.00	3.35	1.00	2.56	1.00	1.72	1.00	2.82	1.00
15 - 10 C	3.23	1.00	3.32	1.00	2.54	1.00				
15 - 10 D	3.22	1.00			2.57	1.00				
< 5 A	2.95	0.94	3.12	0.94	2.44	0.96	1.58	0.89	1.86	0.88
< 5 B	3.19	1.00					1.74	1.00		

MKB, MBL, MEN, FSB and RR denote the goethite sample abbreviations. The numbers refer to the grain size of the fractions in micrometer; "A" refers to the first cooling curve, "B" to the second of the same sample, "C" to the third and "D" to the fourth. The remanence increase at -196 °C (RI) divided by the initial remanence (i.e. the remanence prior to the "A" curve) is listed in the first column. The second column refers to the ratio of the remanence before and after each individual cooling cycle (RBA).

Possible changes in the cooling curves due to hematite are negligible, since the hematite part of the remanence in the samples is small. The hematite contribution to the remanence is only significant in the FSB samples. The Morin transition is transferred to low temperatures and largely or completely suppressed in extremely fine crystalline hematite (e.g. Bando et al., 1965). The FSB samples show hardly, or not at all, a remanence decrease associated with the Morin transition, so the hematite contribution to the total remanence is taken as constant throughout the investigated temperature range. The changes in behaviour of the remanence due to the maghemite contribution in the RR fractions is more difficult to assess. When cooling down there is no change in the maghemite remanence (Dankers, 1978). The maghemite remanence is slightly decreasing up to some 10% without any clear transition point, when reheating from -196 °C (Dankers, op. cit.). The observed slightly larger remanence decay in the RR fractions after the first cooling cycle could be caused by simultaneous goethite and maghemite decay. The complete reversibility of the remanence behaviour during a second cooling cycle (Fig. 10B) would indicate that maghemite behaves also reversibly. Data

on second cooling cycles for pure maghemite samples to check this possible reversibility, however, have not been traced by the author.

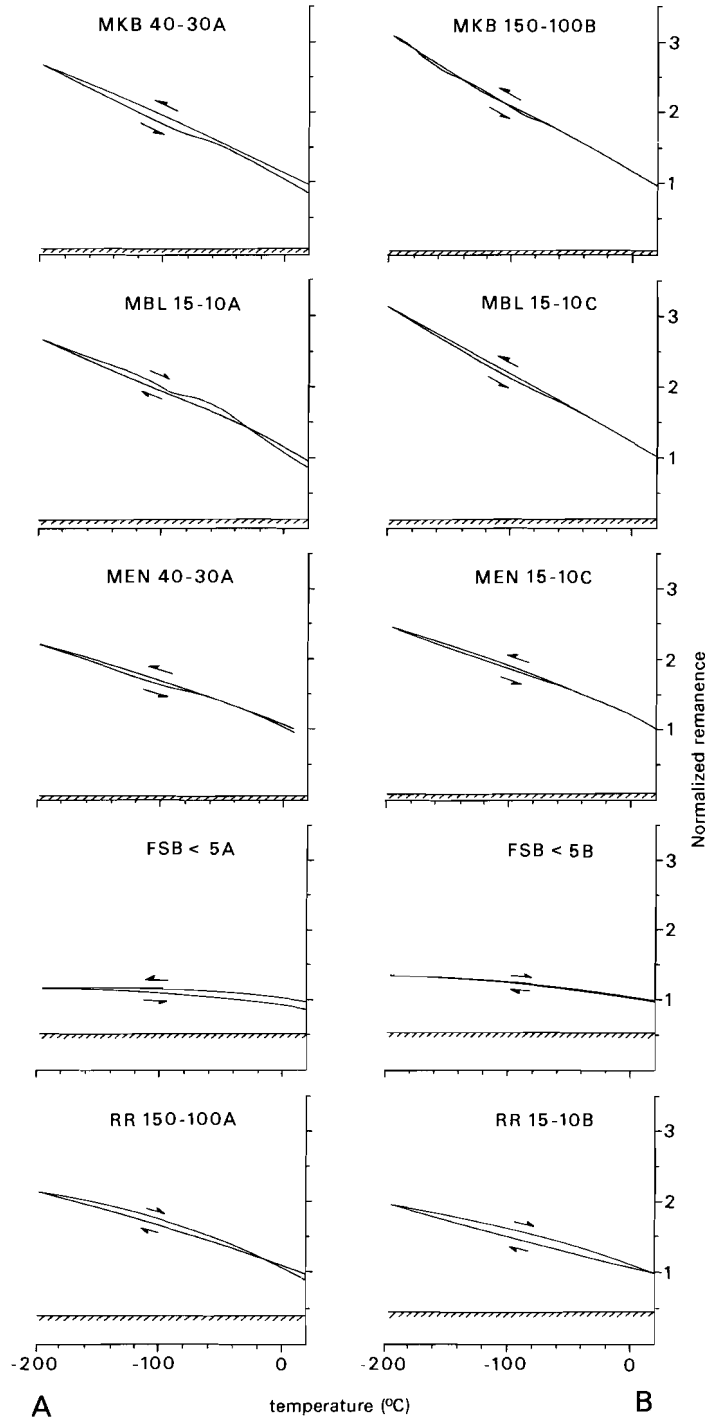

During the first cooling cycle the increase ratios tend to decrease with decreasing grain size in FSB, RR and MEN goethite. In MBL and MKB goethite this trend is absent or only weakly developed (Table V). For all goethites, in repeated cooling cycles this grain-size dependence is absent or much weaker developed than in corresponding first cooling cycles.

The remanence increase is due to an increase in spontaneous magnetization, which is a combination of within- and between-crystallite properties. Upon cooling, the atomic movement due to temperature excitation decreases, which results in an increasing remanence. Upon rewarming, the temperature excitation increase again, which results in the observed (nearly) reversible remanence behaviour during cooling cycles. The remanence increase will be larger when there is more isomorphous substitution in the goethite, because of the increased magnetic moments. An increase in remanence ratio is observed from FSB via MEN, RR, MKB and finally MBL goethite (remanence increase ratios referring to reversible behaviour respectively 1.8–2.1, 2.5, 2.8–3.0, 3.2 and 3.35). However, an approximately linear correlation between the remanence increase ratio and isomorphous substitution is not observed, so the isomorphously substituted non-Fe elements are not the sole factor explaining the increase. Dispersed non-Fe elements lower the exchange coupling and will suppress the remanence increase. So, goethites with relatively few dispersed non-Fe elements will show a relatively large increase ratio. In RR goethite with the least dispersed non-Fe elements content of the goethites investigated, indeed a relatively large increase ratio is observed with respect to its isomorphous substitution.

The goethite investigated by Heller (1978) also shows a steady increase upon cooling down to -196 °C. It was tested whether comparison of Hellers results, which refer to IRM properties, and the results of the present investigation, which deal with TRM properties, is allowed. Trial runs showed that, for individual goethites, IRM increased with the same ratio as TRM.

The crystallite size of the goethite investigated by Heller is extremely small, since it contains no isomorphously substituted non-Fe elements (non-Fe elements below limit of detection except Si, microprobe analyses) and its maximum blocking temperature is nonetheless only 55 to 90 °C (Heller, 1978). The large relative remanence increase upon cooling in Hellers goethite might be explained by its relatively low amount dispersed non-Fe elements (approximately 3.5 weight percent SiO_2) and by the fact that the remanence at the onset of cooling treatment is low because of the vicinity of the maximum blocking temperatures (goethite with maximum blocking temperatures of 60 °C has an increase ratio of 3.7 and a chemically similar goethite with maximum blocking temperatures of 100 °C has an increase ratio of 2.5; cf. Figs. 3 and 4 of Heller, 1978).

Fig. 10. The non-goethite part of the remanence (as determined by thermal demagnetization) is indicated by the shaded line in Fig. 10A and 10B.

Fig. 10A: Examples of the behaviour of TRM1 during the first cooling cycle. The remanence is steadily increasing throughout the whole temperature range. At room temperature there is generally a small decrease in remanence after completing the cooling cycle. The numbers behind the goethite sample abbreviation refer to the grain size in micrometer; 'A' stands for the first cooling cycle.

Fig. 10B: Behaviour of TRM1 during repeated low-temperature treatment. The behaviour is reversible: at room temperature there is no further remanence decrease anymore when rewarming from the liquid nitrogen temperature. Numbers behind goethite sample abbreviations refer to the grain size in micrometer; 'B' stands for the second cooling cycle, 'C' for the third.

3 CONCLUSIONS

The grain-size trends of TRM in goethite (induced with a 16 kAm^{-1} field for experimental reasons) are different for individual goethites. It is decreasing with grain size in MKB goethite; approximately grain-size independent in FSB and RR goethite and it shows a maximum in the intermediate grain-size range for MEN and MBL goethite. FSB goethite has the lowest TRM per unit mass, followed in increasing order by RR, MBL, MKB and MEN goethite (average values respectively $1.7*10^{-3}$, $4.4*10^{-3}$, $6.5*10^{-3}$, $8.4*10^{-3}$ and $12.4*10^{-3}$, all in Am^2kg^{-1}). This trend in TRM values for individual goethites can be understood as being the result of isomorphous substituted and dispersed non-Fe elements in the goethite. Isomorphous substitution enhances the TRM until a certain maximum value, with further isomorphous substitution the TRM declines again due to lowering of the goethite Néel point. Relatively modest amounts of dispersed non-Fe elements result in relatively tightly antiferromagnetically coupled crystallites and the observed TRM value is lower than one would suppose when taking only isomorphous substitution into account. The TRM trends are predominantly determined by the chemical characteristics of the goethite; crystallite-size dependence is a second order effect.

Minimum specific volume TRM's are for MKB, MBL, MEN, FSB and RR goethite respectively: $1.9*10^{-3}$, $1.5*10^{-3}$, $2.9*10^{-3}$, $0.4*10^{-3}$ and $1.0*10^{-3}$ (SI units). These figures are two orders less than hematite figures.

The maximum blocking temperature of the goethites is dominated by their isomorphous substitution over their crystallite size. FSB goethite has the highest maximum blocking temperature despite its small crystallite size. MBL goethite, with the largest isomorphously substituted content of the goethites investigated, has the lowest maximum blocking temperature (45 to 60 °C), followed in upward direction by MKB (55 to 80 °C), MEN (55 to 105 °C), RR (70 to 100 °C) and FSB (90 to 105 °C). Both with stepwise and continuous thermal demagnetization no grain-size dependence was observed. Continuous thermal demagnetization curves show a rapid, approximately linear decrease with increasing temperature, evolving into a concave part when the remanence is almost completely removed. The lowest temperatures listed above after each goethite sample correspond to the beginning of the concave part in the decay curve. The highest temperatures correspond to the temperatures where no goethite remanence is observed anymore. Stepwise thermal demagnetization revealed the same maximum blocking temperature order with similar temperatures for individual goethites. It was obligatory to take demagnetization steps of only 10 °C for a good representation of the decay curves.

A second TRM (TRM2), induced in the same specimens with the same inducing field and direction as the first TRM (TRM1), is identical (MKB, MBL, MEN goethite) to TRM1 or has a slightly weaker intensity (RR, FSB goethite). This is most prominent in the fine-crystalline FSB goethite. There is, apparently, a re-ordering in the goethite lattice, which results in a better crystal structure. Consequently, the TRM after repeated annealing is slightly weaker.

The initial susceptibility of goethite measured at room temperature decreases some 10 percent during annealing at 140 °C for the first time in the MKB, MBL, MEN and RR fractions. The initial susceptibility of the FSB fractions shows a decrease of some 20 percent. Repeated annealing at the same temperature hardly changes the initial susceptibility further. This is a strong indication that the natural remanence (NRM) carried by these goethites, is of chemical remanent origin.

The goethites are extremely hard with respect to AF demagnetization, illustrated by their small decay in TRM after treatment with 240 kAm^{-1} alternating fields (maximum fields available). RR goethite fractions do not show any decay at all. MEN, MBL and MKB goethite decay three to six percent, without any grain-size dependence. Only FSB goethite shows a larger decay and grain-size dependence is observed. The decay is 18 percent in the 250-150 micrometer fraction and 55 percent in the 20-15 micrometer fraction. Only thermoremanences in extremely fine crystalline goethite with crystallite sizes close to the superparamagnetic threshold size can be (partially) broken down with AF treatment in available fields.

The goethites show a continuous remanence increase when cooling it in a field-free space. Goethite is unique in this low-temperature behaviour and low-temperature treatment is, as such, an elegant technique to identify goethite remanences without the need to heat a specimen which may result in alterations in the goethite. The remanence increase ratio is higher with rising content of isomorphously substituted non-Fe elements in the goethite. The steady remanence increase with decreasing temperature is due to an increase in spontaneous magnetization. The exchange coupling within and between the goethite crystallites increases during cooling because the temperature excitation of the atoms decreases.

Acknowledgements

Prof. Dr. J.D.A. Zijderveld critically reviewed the manuscript. It would have been hardly possible to keep the HALT spinner (High And Low Temperature spinner) in top running condition without the help of T.A.T. Mullender. J.J.J. Bergenhenegouwen made the drawings. These investigations were supported by the Netherlands Foundation for Earth Science Research (AWON) with financial aid from the Netherlands Organization for the Advancement of Pure Research (Z.W.O., grant 751-354-006).

4 REFERENCES

Bagin V.I., Gendler T.S., Kuz'min R.N., Rybak R.S., Urazayeva T.K., 1976, The weak ferromagnetism of natural hydrogoethites, Izv. Acad. Sci. USSR, Phys. Solid Earth 12, 328-33 (eng. ed.).

Bando Y., Kiyama M., Yamamoto N., Takada T., Shinjo T., Takaki H., 1965, The magnetic properties of α-Fe_2O_3 fine particles, J. Phys. Soc. Japan 20, 2086.

Banerjee S.K., 1970, Origin of thermoremanence in goethite, Earth Plan. Science Letters 8, 197-201.

Dankers P.H.M., 1978, Magnetic properties of dispersed natural iron-oxides of known grain-size, Ph.D. thesis University of Utrecht, 143pp.

Dankers P.H.M., 1981, Relationship between medlan destructive field and remanent coercive forces for dispersed magnetite, titanomagnetite and hematite, Geophys. J. R. astr. Soc. 64, 447-61.

Dekkers M.J., 1988A, Magnetic properties of natural goethite part I: grain-size dependence of some low- and high-field related rockmagnetic parameters measured at room temperature, in: Some rockmagnetic parameters for natural goethite, pyrrhotite and fine-grained hematite, Ph.D. thesis University of Utrecht, chapter 3.

Dekkers M.J., 1988B, Some rockmagnetic parameters for natural goethite, pyrrhotite and fine-grained hematite, Ph.D. thesis University of Utrecht, appendix 1.

Dekkers M.J., 1988C, Goethite: separation procedure, characteristics and preparation of the artificial samples, in: Some rockmagnetic parameters for natural goethite, pyrrhotite and fine-grained hematite, Ph.D. thesis University of Utrecht, chapter 2.

Dekkers M.J., 1988D, Magnetic properties of natural goethite part III: Investigation of the magnetic behaviour of the magnetic minerals originating from goethite dehydration during thermal demagnetization, in: Some rockmagnetic parameters for natural goethite, pyrrhotite and fine-grained hematite, Ph.D. thesis University of Utrecht, chapter 5.

Forsyth J.B., Hedley I.G., Johnson C.E., 1968, The magnetic structure and hyperfine field of goethite (α-FeOOH), J. Phys. C2 1, 179-88.

Fysh S.A., Clark P.E., 1982, Aluminous goethite: A Mössbauer study, Phys. Chem. Minerals 8, 180-7.

Golden D.G., Bowen L.H., Weed S.B., Bigham J.M., 1979, Mössbauer studies of synthetic and soil-occurring aluminum substituted goethites, Soil Sci. Soc. Am. J. 43, 802-8.

Goodman B.A., Lewis D.G., 1981, Mössbauer spectra of aluminous goethites (α-FeOOH), J. Soil Sci. 32, 351-63.

Govaert A., Dauwe C., De Sitter J., De Grave E., 1976b, On the surface contribution to the line profile of small particles of goethite, J. Phys. Coll. C6 37, 291-2.

Govaert A., Dauwe C., De Sitter J., De Grave E., Robbrecht G., 1977, On the bulk and surface contributions to the magnetic hyperfine field of small particles of goethite (α-FeOOH), Physica B & C 86-88B, 1427-8.

Govaert A., Dauwe C., Plinka P., De Grave E., De Sitter J., 1976a, A classification of goethite minerals based on the Mössbauer behaviour, J. Phys. Coll. C6 37, 825-7.

Hartstra R.L., 1982A, Some rockmagnetic parameters for natural iron-titanium oxides, Ph.D. thesis University of Utrecht, 145pp.

Hartstra R.L., 1982B, High-temperature characteristics of a natural titanomagnetite, Geophys. J. R. astr. Soc. 71, 455-76.

Hartstra R.L. 1982C, A comparative study of the ARM and I_{sr} of some natural magnetites of MD and PSD grain size, Geophys. J. R. astr. Soc. 71, 497-518.

Hedley I.G., 1971, The weak ferromagnetism of goethite (α-FeOOH), Zeitschrift Geoph. 37, 409-20.

Heller F., 1977, Paleomagnetism of Upper Jurassic Limestones from Southern Germany, J. Geophys. 42, 475-88.

Heller F., 1978, Rockmagnetic studies of Upper Jurassic limestones from Southern Germany, J. Geophys. 44, 525-43.

Johnston J.H., Norrish K., 1981, A ^{57}Fe Mössbauer spectroscopic study of a selection of Australian and other goethites, Aust. J. Soil Res. 19, 231-7.

Lowrie W., Heller F., 1982, Magnetic properties of marine limestones, Rev. Geoph. Space Phys. 20, 171-92.

Mørup S., Madsen M.B., Franck J., Villadsen J., Koch C.J.W., 1983, A new interpretation of Mössbauer spectra of microcrystalline goethite: "superferromagnetism" or "super-spin-glass" behaviour?, J. Magn. Magn. Mat. 40, 163-74.

Murad E., 1979, Mössbauer spectra of goethite: evidence for structural imperfections, Min. Mag. 43, 355-61.

Murad E., 1982, The characterization of goethite by Mössbauer spectroscopy, Am. Min. 67, 1007-11.

O'Reilly W., 1984, Rock and mineral magnetism, Blackie & Son, Glasgow and London, 220pp.

Strangway D.W., Honea R.M., McMahon B.E., Larson E.E., 1968, The magnetic properties of naturally occurring goethite, Geophys. J. R. Astr. Soc. 15, 345-59.

Strangway D.W., McMahon B.E., Honea R.M., 1967, Stable magnetic remanence in antiferromagnetic goethite, Science 158, 785-7.

CHAPTER 5

MAGNETIC PROPERTIES OF NATURAL GOETHITE

PART III

INVESTIGATION OF THE MAGNETIC BEHAVIOUR OF THE MAGNETIC MINERALS ORIGINATING FROM GOETHITE DEHYDRATION DURING THERMAL DEMAGNETIZATION.

Abstract

The behaviour during stepwise thermal demagnetization of a set of artificial samples, containing well-defined natural goethite from five locations (chemical composition, crystallite and grain size are known) is reported. The goethite converts to hematite in a 260-360 °C temperature interval as was observed through monitoring the initial susceptibility. During the conversion reaction the initial susceptibility slightly decreases. The temperature range for the conversion reaction inferred from the initial susceptibility decrease corresponded well with the temperature interval determined by Differential Scanning Calorimetry measurements. Due to recrystallization of minor hematite already present in the original goethite concentrates during the goethite/hematite conversion reaction, an extra remanence decrease is observed during this reaction, facilitated by the free water available in the direct vicinity of the original hematite. The extra bending point in the decay curve might be erroneously interpreted as evidence for the presence of titanomagnetite or pyrrhotite in the specimens. At temperatures from 380 °C upwards (depending on the grain size of the original goethite) the initial susceptibility increases with widely varying extents, due to the creation of trace amounts of magnetite.

Differences in magnetite/hematite ratio as well as in the properties of both minerals were inferred from rockmagnetic investigations after the 400 °C and 685 °C demagnetization steps (IRM acquisition in fields up to $11.2*10^6$ Am^{-1}, AF demagnetization and low-temperature cycling of J_{rs}). Traces magnetite appeared to be already present after the 400 °C step; after the 685 °C step the magnetic mineralogy was usually dominated by magnetite. The magnetic behaviour of both hematite and magnetite seems not to be determined by compositional differences in their precursor goethite.

After the 400 °C step the hematite showed no Morin transition during low-temperature treatment, indicative for an extremely fine crystallite size. J_{rs} varied between 0.007 and 0.064 Am^2kg^{-1}, distinctly lower than J_{rs} of well crystalline hematite. After the 685 °C step a weak Morin transition was observed and J_{rs} was slightly increased. Large magnetic fields are necessary to saturate the hematite after the 400 °C step (up to $10.4*10^6$ Am^{-1}); after the 685 °C step considerably smaller fields are needed ($3.2*10^6$ to $4.8*10^6$ Am^{-1}).

The magnetite-dominated specimens showed during low-temperature cycling an isotropic point transition related remanence decrease only in the fine grain-size fractions. Magnetite growth in these fine fractions took place over a rather large number of thermal demagnetization steps, giving rise to relatively coarse magnetite crystallites. In the coarse grain-size fractions magnetite growth took place predominantly during one or two thermal demagnetization steps resulting in aggregates of extremely small SD magnetite crystallites within a larger hematite crystallite aggregate. Combination of the magnetic magnetite percentage (obtained from RA curves) and the magnetite weight percentage (calcu-

lated from the initial susceptibility) yields high figures for the ratio of the magnetite and hematite saturation remanences. This points to extremely fine grain sizes for the magnetite (from very close to the superparamagnetic threshold size to approximately 1 micrometer).

The large differences in magnetic magnetite and hematite contents of the samples are the result of extremely local differences in vapour phase amount (and composition?) within the specimens. The vapour phase is formed by chemical reactions of the matrix constituents ($CaCO_3$ and waterglass) leading to a CO_2/H_2O vapour phase. Reducing capacity is presumably created by decomposition of trace amounts organic matter. Other factors in explaining the differences between the samples are the presence of seeding crystals and the crystallinity of the precursor goethite. A self-reversal is observed in most specimens in the 600 °C temperature interval.

1 INTRODUCTION

Progressive demagnetization to evaluate the natural remanent magnetization which was acquired by rocks during the geological history, is increasingly performed by means of thermal methods. However, chemical reactions occur in the specimens during heating. This can lead to the introduction of new magnetic minerals, which may acquire a spurious remanence during the demagnetization procedure. When studying volcanic rocks, the amount of chemical alterations introduced in the specimens during annealing, will generally be minor, because volcanics were at high temperatures during their formation.

The situation is completely different in sediments, however, since they were formed at low temperatures. Sediments have a composite nature: they consist of varying amounts of detrital and authigenic material. A wide variety is possible in the clay-mineral type(s) and quantity. The quantity and composition of organic matter may also show a considerable variation. So, it is to be expected that sediments will react considerably during annealing due to the decomposition of organic matter and unstable mineral phases. For paleomagnetic purposes, the thermal behaviour of hydrous iron(hydr)oxides and iron sulphides is of special interest, because magnetic minerals are involved.

During thermal demagnetization, sediments are for the first time at elevated temperatures. The original sedimentary mineral suite becomes (partly) unstable and chemical reactions occur between the sample constituents. Apart from mere thermodynamic arguments regarding mineral stability, kinetic aspects are of prime importance in explaining the reactions occurring in the specimens, because the heating time is short. The presence of a vapour phase within the specimens has a tremendous impact on reaction kinetics, because a vapour phase offers a reactive medium. It can accelerate chemical reactions by several orders of magnitude by increasing the availability of reacting components, acting analogous to a catalyst.

Interstitially absorbed water, which is present in all sediments, is by and large removed at approximately 100 °C. Its influence on reactions occurring in the samples is minor, because reaction kinetics are generally slow at those relatively low temperatures. At higher temperatures, on the contrary, the effect of a flux of water vapour or, in general, a composite vapour phase in the specimens is significant. This flux can be created by dehydration and/or decomposition of minerals and/or organic matter at elevated temperatures. The mineral phases and the organic matter each have their own dehydration or decomposition temperature. The subsequent (partial) break-down of the mineral phases, accompanied by

the decomposition of organic matter, ensures the presence of a (complex) vapour phase in minute quantities in the specimens, when annealing stepwise up to 700 °C.

Natural samples are less suitable for the discrimination in behaviour of specific magnetic minerals in the specimens during thermal demagnetization. This is, because the composition of the (magnetic) mineral suite and of the reactive vapour phase are both relatively poorly defined. Artificial samples, which contain known quantities of a well-defined magnetic mineral, offer the potential to relate processes which occur during annealing, to alterations of that specific mineral. Suchlike investigations ultimately lead to a better understanding of the behaviour of natural samples, which contain varying combinations of reactive components. By heating goethite (α-FeOOH) bearing artificial samples, the magnetic behaviour exclusively due to goethite alterations can be studied.

The series of goethite bearing artificial samples of which the magnetic properties have been reported in Dekkers (1988A, 1988B), is subjected to temperatures up to 700 °C to investigate the magnetic properties of the minerals which originate from the goethite. The goethites comprise two marine sedimentary oolithic iron ores (MKB and MBL, respectively from Kahlenberg and Blumberg in Western Germany), a fluviatile replacement ore (RR, from Robe River mining district, Western Australia), a caprock goethite (MEN, from Menera mining district, Spain) and a gossan goethite (FSB, from Sain Bel, France). Detailed sample descriptions are in Dekkers (1988A, 1988C). Some important chemical and X-ray characteristics of the goethites are compiled in Table I.

Table I: Microprobe analyses, unit cell determinations and crystallite size order of the goethite concentrates

Microprobe analyses

	MKB	MBL	MEN	FSB	RR
SiO_2	2.51	4.89	3.05	3.27	2.80
TiO_2	0.02	0.44	0.02	0.01	0.02
Al_2O_3	2.86	7.16	0.84	0.34	2.15
V_2O_3	0.10	nd	0.04	0.03	0.04
Fe_2O_3	76.32	68.44	79.55	80.58	79.33
MnO	0.24	0.06	0.93	0.02	0.05
MgO	0.92	0.86	0.95	0.10	0.09
CaO	0.27	0.26	0.17	0.08	0.07
Na_2O	0.13	nd	0.09	0.03	0.02
K_2O	0.07	nd	0.01	0.02	0.02
P_2O_5	1.79	0.84	0.28	0.07	0.07
SO_3	0.81	0.36	0.31	4.20	0.33
total	86.10	83.34	86.29	88.77	85.16
H_2O	13.17	13.43	14.09	17.68	11.79

MKB, MBL, MEN, FSB and RR are abbrevietions of the goethite sample locations, respectively of Kahlenberg (Western Germany), Blumberg (Western Germany), Menera (Spain), Sain Bel (France) and Robe River (Western Australia). Microprobe analyses were carried out on a TPD (Technisch Physische Dienst) microprobe fitted with a TRACOR Northern Energy Dispersive (ED) system. Operating conditions are 15 keV and 2 - 3 nA. ZAF matrix correction is applied. Contents are in weight percentages; nd = not determined; iron is calculated as Fe_2O_3. H_2O is determined with the Penfield method.

Unit cell sizes of the goethite

axis	MKB	MBL	MEN	FSB	RR
a	4.585±0.003	4.586±0.004	4.612±0.004	4.611±0.004	4.596±0.004
b	9.908±0.007	9.884±0.008	9.920±0.008	9.962±0.009	9.909±0.008
c	2.995±0.002	3.000±0.002	3.011±0.002	3.008±0.003	2.998±0.002
Vol.	136.06	136.00	137.76	138.17	136.53

Lengths of the crystal axes in Å; volume (Vol.) in $Å^3$.

Average crystallite sizes in Å

MKB	MBL	MEN	FSB	RR
480	325	370	240	400

1.1 Temperature range of the goethite/hematite conversion reaction acquired with differential scanning calorimetry

Goethite is thermodynamically stable with respect to hematite plus water in a temperature interval of 80 °C at 1 bar up to 140 °C at 4 kbar (Langmuir, 1971, 1972). Langmuir's data refer to pure goethite. Assuming ideal mixing of goethite and diaspore, Yapp (1983) calculated that Al-substitution in goethite would increase its thermodynamic stability with respect to hematite plus water. The influence of Al-incorporation on the thermodynamic properties is so overwhelming that the oversimplification of the ideal mixing model is regarded to be of minor influence.

Goethite is known to dehydrate to hematite at a temperature interval of 250 to 400 °C in differential thermal analysis (DTA) runs, depending on its crystallinity and chemical composition (e.g. Smykatz-Kloss, 1974). These temperatures are indeed much higher than those one would expect on thermodynamic grounds, an indication for the importance of reaction kinetics. Differential scanning calorimetry - DSC, a slightly modified differential thermal technique, measuring the amount of heat required to maintain a constant heating rate of a sample - runs of the goethites are presented in Fig. 1.

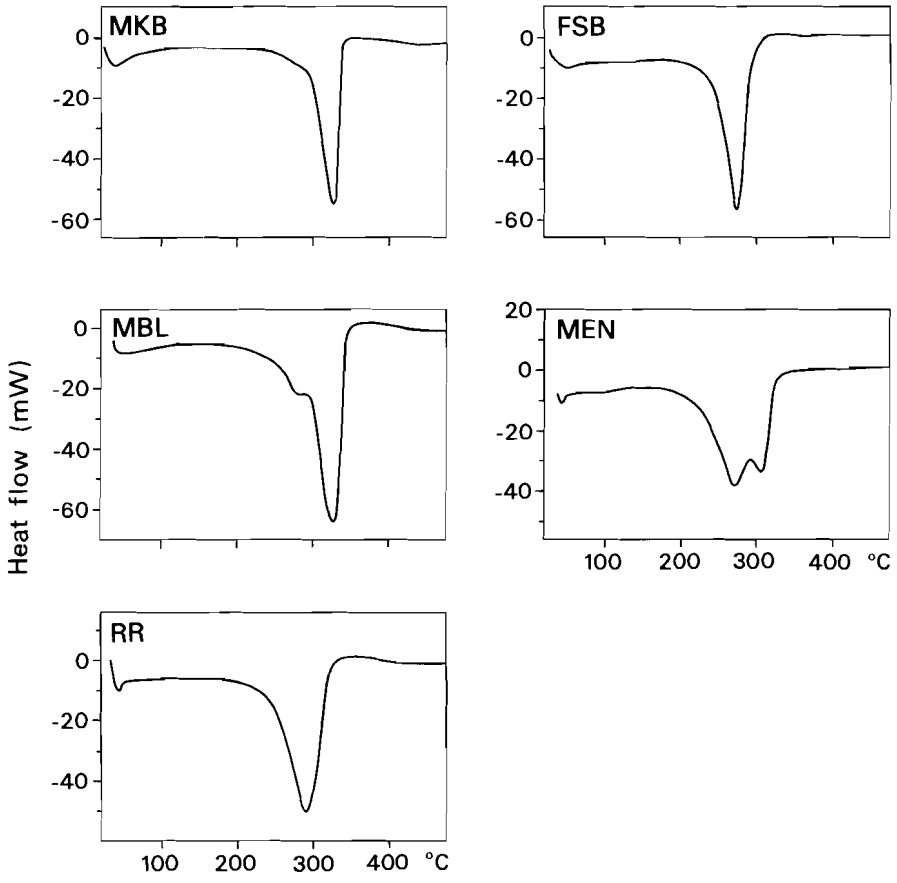

Fig. 1. Differential Scanning Calorimetry (DSC) curves of the natural goethite samples. Heating was performed in air with a rate of 10 °C/min. MKB = Kahlenberg (Western Germany), MBL = Blumberg (Western Germany), MEN = Menera (Spain), FSB = Sain Bel (France), RR = Robe River (Western Australia).

Distinct differences in DSC behaviour exist between the samples. MKB and FSB goethite display relatively sharp peaks despite large differences in crystallinity. The peak of FSB goethite lies at a considerably lower temperature than that of MKB goethite. RR goethite has a relatively broad peak although its crystallinity is equivalent to MKB goethite. A small shoulder is developed on the lower temperature side of the peak in the DSC curve of MBL goethite. The DSC curve of MEN goethite actually

consists of two peaks close to each other. The onset of the peaks is in all samples already at approximately 200 °C.

The aluminous MKB and MBL goethite (cf. Table I) decompose at higher temperatures than the other goethites. This is remarkable since Al-goethite is known to decompose at lower temperatures than pure goethite (e.g. Smykatz-Kloss, 1974). The presence of escape conduits for the liberated water is important in explaining goethite DTA characteristics. Less escape conduits lead to higher decomposition temperatures (Murad, 1979). However, of more importance is the thermodynamic stability of the goethite. Al-goethite is thermodynamically more stable than Al-free goethite with respect to hematite plus water (Yapp, 1983) and this obviously leads to higher decomposition temperatures for Al-goethites when the goethites have crystallite sizes of the same order. The general observation that Al-goethite decomposes at lower temperatures than Al-free goethites is thus not due to its Al content but to the fact that Al-goethites generally have a smaller crystallite size than Al-free goethite.

1.2 Experimental procedure

The goethite concentrates contain trace amounts of non-goethite minerals (hematite and in the RR fractions also maghemite). A thermoremanence was induced in the specimens by cooling from 145 °C in a field of 16 kAm^{-1} (20 mTesla) to suppress the non-goethite contribution to the total remanence. This TRM was thermally demagnetized with the stepwise method. Goethite remanence is already removed at some 100 °C; the non-goethite remanence will persist up to much higher temperatures. The measuring procedure was designed to allow for the detection of possible viscous behaviour due to newly-formed minerals formed by the goethite break-down.

Since the goethite break-down occurs at temperatures higher than its Néel temperature, the goethite break-down reaction cannot be monitored by goethite remanence measurements. However, the goethite break-down may influence the remanence behaviour of the non-goethite minerals (hematite and maghemite). The goethite break-down reaction was therefore monitored by measuring the initial susceptibility at room temperature after each thermal demagnetization step up to 685 °C. Special attention was paid to the 200-400 °C temperature interval.

To study the magnetic properties of the newly formed minerals (i.e. hematite and a magnetite-like mineral in varying amounts, depending on the temperature) the thermal demagnetization was stopped for half of the fractions after the 400 °C step, i.e. shortly after the complete goethite/hematite conversion. Isothermal remanent magnetization (IRM) acquisition curves (RA curves; in magnetic fields up to $11.2*10^6$ Am^{-1} or 14 Tesla) and the remanent coercive force (H_{cr}) were determined at room temperature to evaluate the magnetic characteristics of the newly formed hematite. Low-temperature cycling of J_{rs}, induced at room temperature was carried out for further evaluation. The AF behaviour of a $1.6*10^6$ Am^{-1} (2 Tesla) induced IRM was also studied.

To study possible changes in the hematite magnetic properties and to evaluate the characteristics of the magnetite-like phase, the aforementioned experiments were carried out after the 685 °C step for the remainder of the fractions.

Initial susceptibility measurements were carried out with a Jellinek KLY-1 susceptibility bridge. Remanences were measured with a digital spinner magnetometer developed in the Utrecht Paleomagnetic Laboratory based on the Jellinek JR3 drive unit. IRM acquisition curves up to

11.2*10^{6} Am^{-1} (14 Tesla) fields were determined with a Förster fluxgate magnetometer type 1.107, which was calibrated with the digital spinner magnetometer or with an astatic magnetometer. Heating was performed in air in a thermal demagnetizer constructed in the Paleomagnetic Laboratory; the field in the heating and cooling compartments was less than 40 γ. Low-temperature measurements were done with a fluxgate spinner type made suitable for measurements at high and low temperatures by inserting the sample holder in a water-cooled furnace or in a dewar vessel throughout the measuring procedure. Periodic remanence measurements and temperature control is performed by a microcomputer system (Dankers, 1978, 1981; Hartstra, 1982A, 1982B).

2 RESULTS

For each goethite sample, identical grain-size fractions throughout the whole investigated grain-size range were stepwise thermally demagnetized to evaluate grain-size effects: the 250-150, 30-25 and <5 micrometer fractions were demagnetized up to 685 °C; the 75-55, 20-15 and 10-5 micrometer grain-size fractions up to 400 °C. The maximum blocking temperatures of the goethite are dominated by their chemical composition (Dekkers, 1988B); in the present contribution the magnetic impact of goethite dehydration on the behaviour of the (small) non-goethite part of the original TRM will be discussed.

2.1 Remanence behaviour

Representative decay curves are shown in Fig. 2. Because of the goethite predominance in the samples, the remanence is by and large removed at temperatures well below 150 °C. The non-goethite contribution to the remanence is larger in the FSB and RR fractions because of an extremely low specific goethite remanence and slightly raised hematite contents in the former and the presence of minute amounts maghemite in the latter (cf. Dekkers, 1988A, 1988B). There were no indications of viscous remanence behaviour after demagnetization steps up to 685 °C, due to creation of new magnetic minerals.

There are distinct differences among the samples in remanence behaviour during thermal demagnetization at temperatures above 150 °C. The within-sample variation is distinctly smaller than the between-sample variation. The non-goethite remanence part in the MBL fractions is generally too small to allow for a more definite interpretation, but it seems that there is an approximately linear remanence decrease from 100-150 °C upwards. The remanence is completely removed at temperatures down to 550 °C, considerably lower than 685 °C, the Curie temperature of hematite, pointing towards extremely small hematite crystallites.

The MKB fractions have linear decay curves from 150 °C upwards with occasionally a minute bending at the onset of the goethite/hematite conversion reaction. MEN fractions show a similar bending during the temperature range of the conversion reaction itself. The remanence is completely removed in both samples at 660 °C.

In decay curves of FSB and RR goethite two distinct bending points are present. The first bending point at approximately 100 °C obviously corresponds to the removal of the goethite remanence.

The second bending point is at first sight likely to be explained by the presence of a previously undetermined magnetic phase with a maximum blocking temperature of 280-300 °C. Pyrrhotite or titanomagnetite could be possible candidates. However, careful mineralogical and magnetic determinations of the original FSB and RR goethite concentrates did not

reveal their presence (Dekkers, 1988A). The second bending point in their decay curves corresponds closely with the goethite/hematite conversion interval (cf. Fig. 2), so they might well be related.

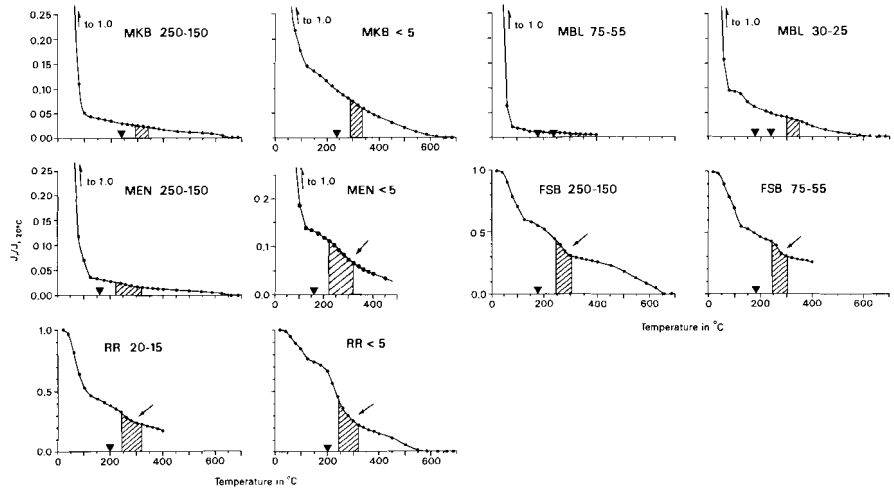

Fig. 2. Representative examples of goethite remanence behaviour upon stepwise thermal demagnetization of a 16 kAm^{-1} (20 mT) thermoremanence (induced at 145 °C). Remanences are normalized to their initial values. The temperature interval of the goathite/hematite conversion reaction, extracted from the DSC determination, is indicated with a hatched area. The onset of the conversion reaction is indicated with a triangle on the temperature axis (MBL samples have a discernable two-stage onset of the conversion reaction). The grain-size range of the initial goethite fractions is denoted in micrometer. The extra bending point related to the goethite/hematite conversion reaction is indicated with arrows. Note that the ordinate scale of the Kahlenberg, Blumberg and Menera fractions is four times expanded compared to those of Sain Bel and Robe River.

The dehydration of goethite in the 260-300 °C temperature interval creates a flux of water vapour within the specimens in the immediate vicinity of the original hematite parts of the goethite grains (goethite and hematite are intimately intergrown). This extra free water facilitates diffusion - anyhow necessary for any re-arrangement - within the minor originally existing hematite. Hence, besides new-formation of hematite, also re-arrangement of originally existing hematite occurs during the goethite/hematite conversion reaction. The re-arrangement takes place in a field-free space and results in a hardly magnetic hematite type (cf. section 4.3.1.2), so an extra remanence decay during the goethite/hematite conversion reaction is plausible. The lattice re-arrangement of the hematite is considerably slowed down when the free water supply stops, which is actually happening when all goethite is converted to hematite. This results in the observed second bending point at approximately 300 °C in the decay curves. Especially originally poorly crystalline hematite (as in the FSB goethite concentrate) is sensitive to lattice re-arrangements, because in such material the driving force to a more ideal crystalline structure with a lower Gibbs energy is relatively large.

RA curves of FSB samples after the 400 °C demagnetization step (cf. Fig 4) show that the hematite acquires considerably less remanence at

the same inducing field than the original hematite. The "400 °C" hematite is saturated in considerably higher fields than the original hematite. This indicates that the "400 °C" hematite has an other structure than the original hematite.

2.2 Initial susceptibility

The initial susceptibility (X_{in}) was measured at room temperature after each demagnetization step to evaluate changes in the magnetic mineralogy in the specimens. Representative results, corrected for matrix changes (established by blanks) are shown in Fig. 3. The initial susceptibility before the thermal demagnetization procedure, after the 400 °C demagnetization step and after the 685 °C step (temperatures after which room and low-temperature magnetic experiments were carried out to assess the magneto-mineralogy of the samples) are tabulated in Table II to show the differences among the specimens. After the 685 °C step large differences exist between the specimens.

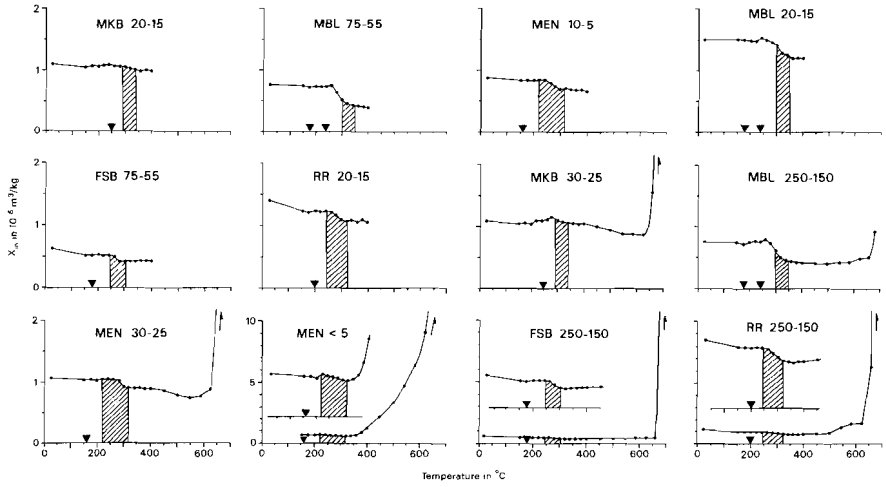

Fig. 3. Representative examples of the changes in initial susceptibility during the stepwise thermal demagnetization procedure. DSC data are visualized similar to Fig. 2. Susceptibilities, calculated per unit mass, refer to the original goethite weight. Grain-size fractions are indicated in micrometer. Note occasionally expanded ordinate scales. In plots with two curves, the upper curve is the same as the lower curve only with a five times exaggerated vertical scale. The initial susceptibility after the 685 °C step is indicated near the arrow, when it is (much) larger than the vertical scale shown.

X_{in} does not show a significant change up to 240-260 °C (observed variations are due to the noise level of the susceptibility bridge). In the temperature range of 250 to 350 °C interval there is a small but distinct decrease in X_{in}. Only in the MKB samples there is hardly any decrease. The actual temperature range of the X_{in} decrease is closely related to goethite/hematite conversion reaction temperature range determined with DSC. X_{in} of the <5 micrometer fractions starts to increase from 400 °C upwards, first rather slowly but above some 600 °C a strong increase is observed. The increase is due to the creation of an extremely magnetic phase, presumably magnetite. Blocking temperature spectra of J_{rs} of some pilot samples induced after a complete thermal demagnetiza-

tion procedure, revealed maximum blocking temperatures of 560 °C for the magnetite phase, i.e. well below 578 °C. This is indicative for fine-grained rather pure magnetite (Dunlop, 1973A), rather than for the presence of highly cation-deficient magnetites with much more elevated maximum blocking temperatures (e.g. Nishitani and Kono, 1983; Özdemir and Banerjee, 1984; Heider and Dunlop, 1987). In the coarse grain-size fractions X_{in} starts increasing at higher temperatures and its magnitude is highly variable (cf. Fig. 3 and Table II). The results indicate that in natural samples magnetite, besides being created from non-magnetic minerals, can also be produced from hematite (or goethite) as precursor mineral. When dealing with goethite/hematite aggregates with small grain sizes, which is the case in many natural samples, one has to take into account that there could already be some magnetite produced in specimens from temperatures as low as some 400 °C. This is a considerably lower temperature than 550 °C at which there is magnetite production according to Heller (1978).

Table II: Initial mass susceptibility at room temperature before the thermal demagnetization procedure, after the 400 °C step and after the 685 °C step.

	25 °C	400 °C	685 °C		25 °C	400 °C
MKB 250-150	0.49	0.37	6.60	MKB 75-55	0.56	0.44
MKB 30-25	1.09	1.04	4.85	MKB 20-15	1.10	0.99
MKB <5	0.70	0.80	17.29	MKB 10-5	1.03	0.30
MBL 250-150	0.75	0.42	0.94	MBL 75-55	0.76	0.41
MBL 30-25	1.63	1.29	5.53	MBL 20-15	1.51	1.21
MBL <5	1.02	0.95	23.28	MBL 10-5	--	--
MEN 250-150	0.55	0.39	1.91	MEN 75-55	0.57	0.36
MEN 30-25	1.06	0.89	35.06	MEN 20-15	0.77	0.36
MEN <5	0.70	1.28	17.26	MEN 10-5	0.88	0.65
FSB 250-150	0.51	0.34	31.41	FSB 75-55	0.63	0.43
FSB 30-25	1.08	0.86	1.38	FSB 20-15	1.03	0.73
FSB <5	1.88	2.08	26.76	FSB 10-5	2.34	1.80
RR 250-150	1.10	0.77	86.97	RR 75-55	1.05	0.73
RR 30-25	1.34	1.06	1.88	RR 20-15	1.40	1.05
RR <5	5.92	4.46	15.18	RR 10-5	2.10	1.57

Initial susceptibilities (in 10^{-6} m^3kg^{-1}) have been calculated per unit mass with respect to the weight content of the original goethite in the samples.

The decrease in X_{in} during the goethite/hematite conversion reaction is also observed by Strangway et al. (1968). They detected also that some goethites showed hardly any decrease during the conversion eaction (like the MKB goethite). They could relate this different susceptibility behaviour to the spontaneous magnetization of the produced hematite. The hematite type which originated from goethite with an approximately equal susceptibility had a definite spontaneous magnetization, whereas the type with a smaller susceptibility showed hardly any spontaneous magnetization.

The MKB goethite which shows hardly any decrease in X_{in} during the conversion to hematite has the highest saturation remanence after the 400 °C step. The other samples showed much lower saturation remanences (cf. Table IV). This agrees well with the data of Strangway et al. (1968). The present study infers a trend for the decrease in X_{in} with grain size. Small grain sizes generally show less decrease in X_{in} than coarse grain size of the same goethite sample (cf. Table II).

2.3 Magnetic properties after the 400 and 685 °C thermal demagnetization step

The specimens became extremely fragile during the thermal demagnetization despite careful sample handling. Therefore, it was decided to perform only room and low-temperature measurements on the samples for the evaluation of the rockmagnetic characteristics of the magnetic minerals, which were formed during the thermal treatment. Rockmagnetic investigation was performed after the 400 °C step, to study the hematite characteristics shortly after its formation and after the 685 °C step to detect possible changes in the hematite due to further thermal treatment and to get information on the rockmagnetic parameters of the magnetite-like phase, which is especially produced during the high temperature demagnetization steps (above some 600 °C). The term "magnetite" is used for all types of magnetite despite possible varying vacancy contents among the samples. Because of the reducing conditions within the specimens the formation of maghemite "proper" is unlikely, a statement which is supported by the low-temperature behaviour of the specimens, by the low maximum blocking temperatures during a second thermal demagnetization of J_{rs} induced after the first thermal demagnetization and by the fact that most "magnetite" is created above the maghemite inversion temperature.

Examples of RA curves after thermal treatment at 400 and 685 °C are shown in Fig. 4. After the 400 °C demagnetization step all samples behave alike. The hematite derived from goethite is hardly magnetic compared to the original hematite (compare for instance FSB_{400} with FSB_{25} in Fig. 4A), in agreement with findings of Dunlop (1971). Differences in remanence increase in low applied fields between the specimens are due to minute amounts of a magnetite-like phase created in the specimens (cf. also Fig. 4B, showing some normalized RA curves). After the 685 °C step there are large differences in remanence due to a varying amount of magnetite created in the specimens (cf. Table III; Figs. 4A and 4B). Considerable differences in X_{in} (cf. Table II) also indicate varying magnetite amounts. These large differences indicate that magnetite nucleation and growth depend on extremely local conditions existing within the specimens.

The hematite and magnetite amounts created in each specimen during thermal demagnetization of the goethite are listed in Table III. The percentages refer to the abundances as defined by their saturation remanence, since they were derived from RA curves (Fig. 5A). The magnetite amount, expressed in weight percentages, is obviously much lower because of the high magnetite saturation remanence compared to that of hematite (cf. Fig. 5B)

After the 400 °C step, the magnetic mineralogy is dominated by hematite. The magnetite content is slightly increasing with decreasing grain size. The RR fractions contain a much larger percentage magnetite at this temperature, because of the presence of maghemite seeding crystals, which enhance magnetite (with a relatively high vacancy content?) formation. After the 685 °C step, the <5 micrometer fractions are dominated by magnetite, but in the coarse-grained fractions the magnetite contents are extremely variable.

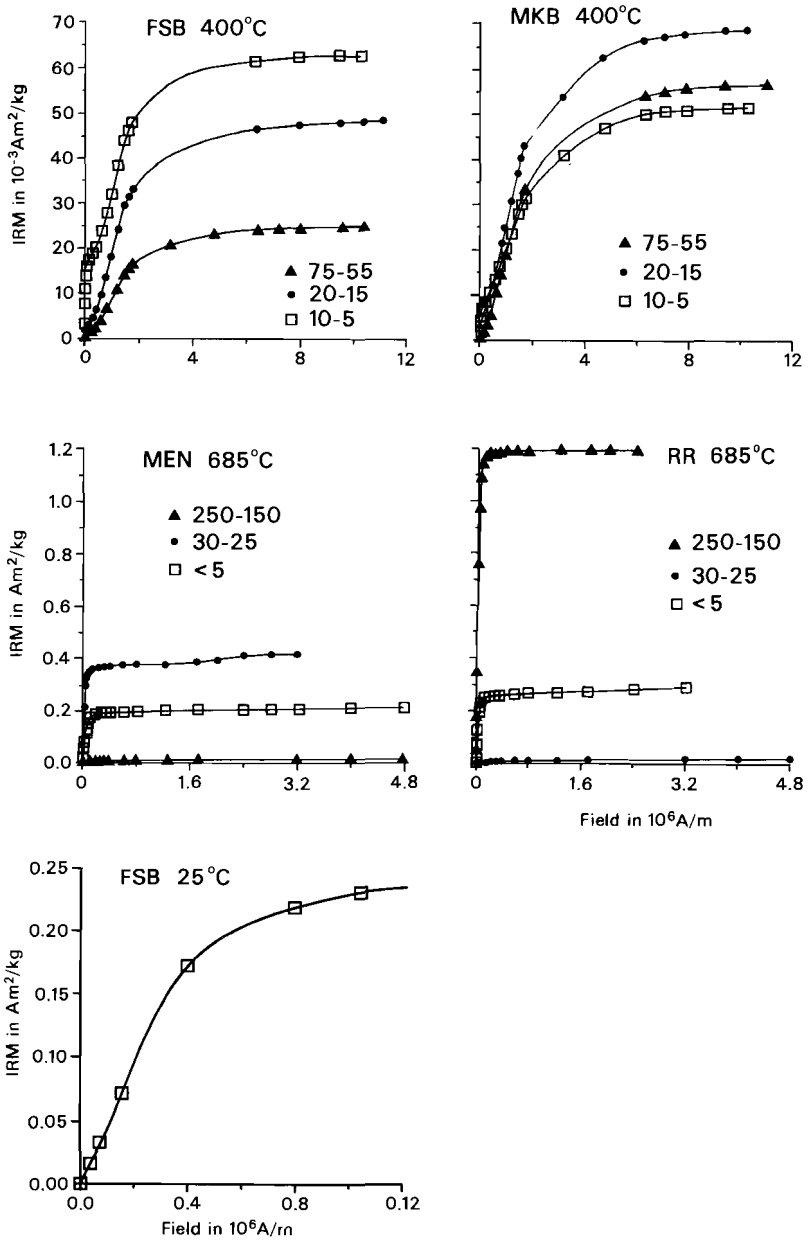

Fig. 4A. Examples of acquisition curves of the isothermal remanence at room temperature (RA curves) after the 400 and 685 °C demagnetization step. For the FSB hematite also the RA prior to thermal treatment is shown. For sample abbreviations cf. Fig. 1. The numbers refer to the grain-size range of the original goethite fractions in micrometer. After the 400 °C step a hardly magnetic hematite type shows up (compare the ordinate scales of FSB_{25} and FSB_{400}). After the 685 °C the remanence is highly variable due to different amounts magnetite produced in the specimens.

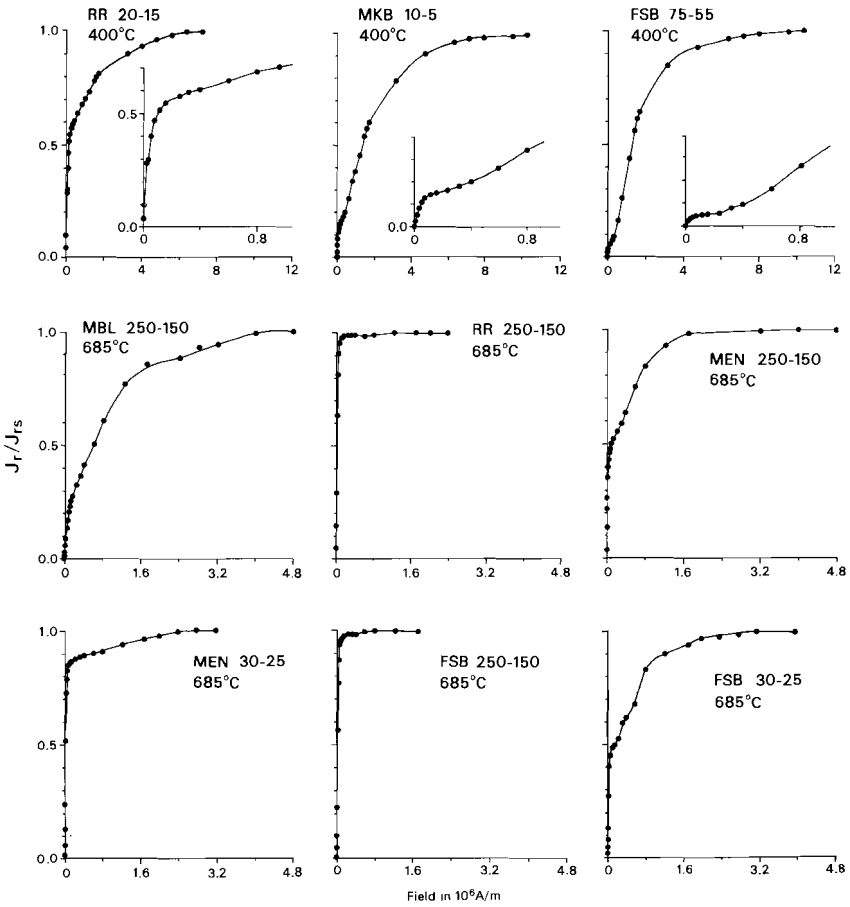

Fig. 4B. Normalized RA curves after the 400 °C and 685 °C steps. The insets in the 400 °C examples show the relatively large increase after extremely low applied fields, pointing towards the presence of minute amounts of a magnetite-like phase already at that temperature. Note the considerable differences in fractions of the same sample after the 685 °C step.

The large sample differences are also displayed in their remanent coercive force (Table IV). The decrease in H_{cr} after the 400 °C step reflects the slightly increased magnetite content. The widely different H_{cr} after the 685 °C step is obviously due to varying impact of the magnetite phase. The hematite and magnetite contributions to the RA curves are separated (Fig. 5A) to allow for a more precise evaluation of their rockmagnetic characteristics.

Table III: Magnetic magnetite and hematite percentage in the specimens

grain size	Temp.	MKB M	MKB H	MBL M	MBL H	MEN M	MEN H	FSB M	FSB H	RR M	RR H
75 - 55	400°C	0	100	5	95	7	93	2	98	52	48
20 - 15	400°C	4	96	40	60	10	90	5	95	52	48
10 - 5	400°C	10	90	-	-	20	80	24	76	68	32
250 - 150	685°C	58	42	18	82	44	56	97	3	100	0
30 - 25	685°C	8	92	54	46	86	14	45	55	27	73
< 5	685°C	84	16	89	11	90	10	47	53	90	10

Contents in percentages. Grain size in micrometer; M = megnetite; H = hematite. For sample abbreviations see Table I.

Table IV: Remanent coercive force of the samples

grain size	Temp.	MKB H_{cr}	MBL H_{cr}	MEN H_{cr}	FSB H_{cr}	RR H_{cr}
75 - 55	400 °C	1528	1289	780	1074	430
20 - 15	400 °C	1401	501	644	804	87.5
10 - 5	400 °C	1377	--	462	541	43.0
250 - 150	685 °C	19.9	613	171	17.5	14.3
30 - 25	685 °C	748	42.9	17.5	73.2	214.8
< 5	685 °C	41.4	36.6	37.4	32.6	34.2

H_{cr} in kAm^{-1}. Grain size = grain-size interval of the original goethite in micrometer; Temp. = temperature of the last thermal demagnetization step prior to the determination of the remanent coercive force. For sample abbreviations see Table I.

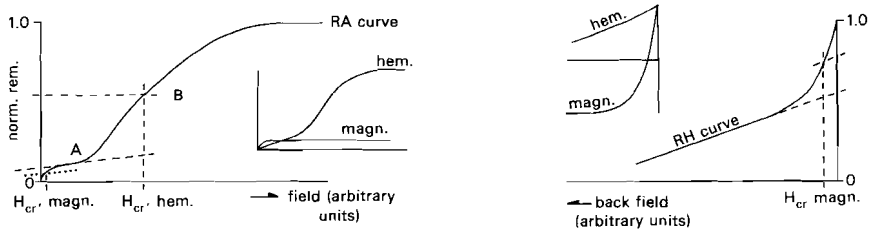

Fig. 5A. The magnetite and hematite magnetic percentages were derived by linear extrapolation of the RA curve after the bending point (A) to the ordinate. RA curves of hematite without any magnetite are linear during the field range of interest. The measured RA curve is the sum of the magnetite and hematite RA curves, schematically shown in the inset. The magnetite remanent acquisition coercive force is determined by correcting the measured RA curve for the (linear) hematite contribution, followed by reading the fieldstrength at which half of the magnetite remanence is acquired. The hematite remanent acquisition coercive force is determined by subtracting the magnetite part of the total remanence and dividing the hematite part into two equal segments (line B). The fieldstrength corresponding to the point where line B intersects the measured RA curve is the hematite remanent acquisition coercive force. The magnetite coercive force is determined from the remanent hysteresis (RH) curves corrected for the (linear) hematite contribution in the small fields of interest. The measured RH curve is the sum of the magnetite and hematite contribution, schematically indicated in the inset. The total magnetite contribution is divided into two equal parts; the fieldstrength corresponding to half of the magnetite contribution is the remanent coercive of magnetite.

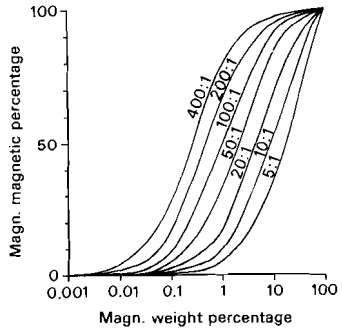

Fig. 5B. To illustrate the magnetic dominance of trace amounts magnetite over hematite, the magnetite weight percentage is plotted versus the magnetite magnetic percentage - based on saturation remanences - for a series of magnetite/hematite J_{rs} ratios in Fig. 5B. Note the logarithmic scale of the abscissa and the linear scale of the ordinate. For single domain (SD) magnetite and poorly crystalline hematite a ratio in the order of 400:1 is appropriate; for multidomain (MD) magnetite and well-crystalline hematite the ratio is approximately 5:1. It is apparent that the magnetic determination of the magnetite content is extremely suitable for the determination of trace amounts magnetite in hematite, but that magnetite weight contents larger than some 10 percent are less precise determined.

2.3.1 Hematite

2.3.1.1 Remanent acquisition coercive force

Large magnetic fields, up to $10.4*10^6$ Am^{-1} (13 Tesla), are necessary to saturate the hematite after the 400 °C demagnetization step. This, together with the absence of a Morin transition (cf. Fig. 6), points to extremely fine-crystalline hematite. The canted antiferromagnetic structure, typical for well-crystallized hematite, is not developed. The remanence in the hematite is carried by defects in the crystal structure. The hematite saturates in considerably lower magnetic fields ($3.2*10^6$ to $4.8*10^6$ Am^{-1}, i.e. 4 to 6 Tesla) after the 685 °C demagnetization step. Lattice re-arrangements, occurring continuously within the hematite during thermal treatment at successively higher temperatures, lead to the development of a better crystalline hematite. There is also a faint appearance of a Morin transition after treatment at 685 °C in samples with a magnetic mineralogy still dominated by hematite (Fig. 6).

For hematite only H_{cr}· was determined since H_{cr} and H_{cr}· are approximately equal for this mineral (Dankers, 1981). H_{cr}· is more or less grain-size independent or slightly decreasing after the 400 °C step. This indicates that the hematite grains are aggregates of small crystallites since one would expect an H_{cr}· increase with decreasing grain size when the actual grain size would reflect grain sizes of rather coarse-crystalline hematite (Dankers, 1981). Chemical differences of the original goethites do not show up in distinct hematite H_{cr}· trends; only the Mn-bearing MEN goethite result in a hematite type with markedly lower H_{cr}· than the others.

After the 685 °C step, the hematite H_{cr}· is usually lower than after 400 °C step. Only in the MEN fractions, H_{cr}· after the 400 and 685 °C steps is hardly different. No evident relation with the original goethite chemistry exists. H_{cr}· tends to decrease with decreasing grain

size. The general decrease in H_{cr}' could be related to a decrease in stress within the hematite aggregates due to the repeated annealing. The decrease with decreasing grain size would then be related to the fact that smaller grain sizes are more prone to stress release than larger ones because they are more easily accessible to vapour fluxes from the matrix.

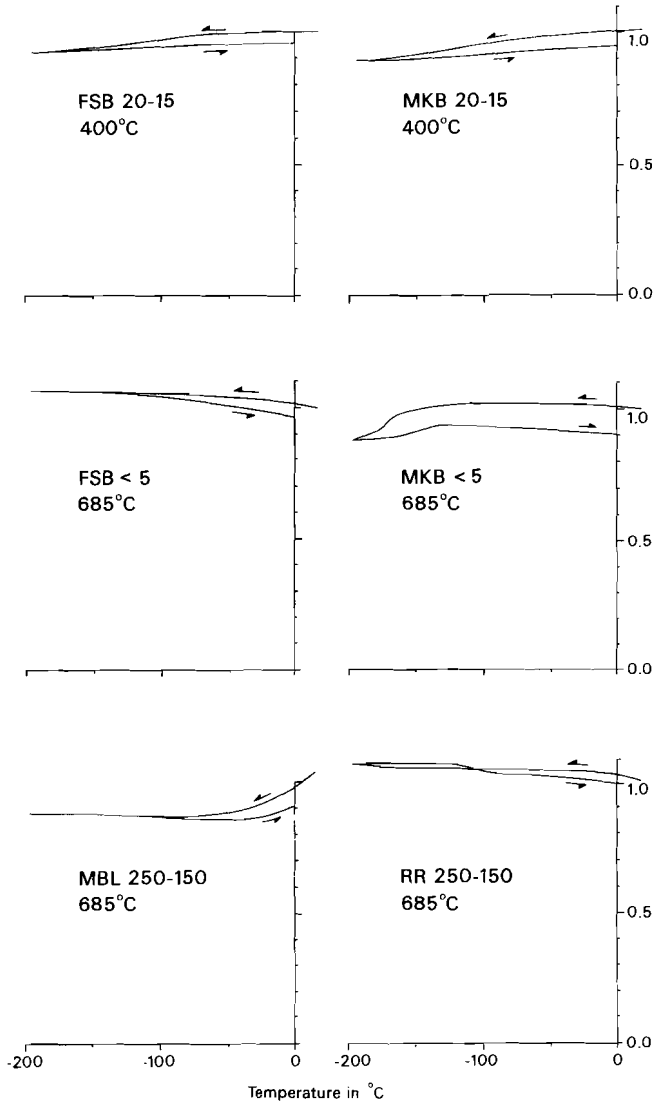

Table V: Hematite remanent acquisition coercive forces

grain size	Temp.	MKB	MBL	MEN	FSB	RR
75 - 55	400 °C	1424	1200	816	1296	1496
20 - 15	400 °C	1376	1120	720	1224	1400
10 - 5	400 °C	1440	--	544	1304	1288
250 - 150	685 °C	872	768	568	np	np
30 - 25	685 °C	680	656	1120*	544	880
< 5	685 °C	408	1040*	816	464	1200*

H_{cr}, in kAm^{-1}; figures with an asterisk are only very approximate because of the small (magnetic) hematite percentage present. Grain sizes in micrometer, referring to the grain size of the original goethite fractions. Temp. indicates the maximum temperature step in the thermal demagnetization before the determination of the remanent acquisition coercive force (at room temperature). np = not present (i.e. below limit of detection); for sample abbreviations cf. Table I.

2.3.1.2 Saturation remanence

When calculating the saturation remanence per unit mass for the hematites (Table VI), it is assumed that the goethite lost 12 percent water, in order to attain more realistic hematite weight contents for individual specimens. After the 400 °C demagnetization step, the magnetite weight content can be ignored because of its high magnetization per unit mass (cf. Fig. 5B). It is reasonable to suppose that the trace amount of magnetite present in the specimens at this stage consists of single domain (SD) or extremely small pseudo single domain (PSD) grains. J_{rs} figures after the 685 °C step in Table VI are minimum ones, because the magnetite weight is ignored. After the 400 °C step, one may safely ignore the weight of the trace amounts magnetite present, but after the 685 °C step this may lead to a minor underestimation of the hematite saturation remanence.

Fig. 6. J_{rs} behaviour during low-temperature cycling of some specimens after the 400 °C and 685 °C demagnetization step. The indicated grain-size ranges refer to the grain size of the original goethite fractions in micrometer. The cooling and rewarming curves are indicated with arrows. For sample abbreviations cf. Fig. 1. A Morin transition is absent in the hematites after the 400 °C step (FSB 20-15, MKB 20-15) pointing towards extremely fine crystalline hematite grains. After the 685 °C step, hematite-dominated specimens show a "weak" Morin transition (MBL 250-150). Magnetite-dominated specimens show a remanence decrease associated with the isotropic point transition (IPT) only in the smallest grain size fractions (MKB <5) in which the magnetite grew over a considerable number of thermal steps as inferred from the X_{in} increase (Fig. 3). Only in the extremely fine crystalline FSB <5 fraction no such IPT-related remanence decrease is observed. In FSB material the crystallites are apparently too small for a IPT-associated remanence decrease to occur. In originally coarse grain size fractions no IPT-related remanence decrease is detected (RR 250-150). This indicates that the magnetite (which grew almost completely during only one or two thermal demagnetization steps) in the coarse grain-size hematite crystallite aggregates consists of a series closely spaced, magnetically interacting SD crystallites. The some 10 percent increase of the remanence is due to an increase in spontaneous magnetization with decreasing temperature. In the relatively "dry" conditions existing within the specimens the magnetite crystallites have not (yet) been recrystallized to larger magnetite grains.

Table VI: Hematite saturation remanence after thermal treatment at 400 and 685 °C.

Temp.	grain size	MKB	MBL	MEN	FSB	RR
400 °C	average	0.064	0.007	0.017	0.045	0.011
685 °C	250 - 150	>0.062	>0.012	>0.010	>0.018	np
	30 - 25	>0.078	>0.013	>0.047	>0.057	>0.018
	< 5	>0.073	>0.021	>0.024	>0.114	>0.0325

J_{rs} in Am^2kg^{-1}. Averages after the 400 °C thermal demagnetization step refer to the 75 - 55, 20 - 15 and 10 - 5 micrometer fractions. For sample abbreviations see Table I. np = not present. The saturation remanence figures after the 685 °C demagnetization step are minimum ones. Further explanation in text.

The hematite saturation remanence per unit mass (Table VI) is distinctly lower than that of "model" hematite (some 0.2 Am^2kg^{-1}, e.g. Dankers, 1978; O'Reilly, 1984). Especially shortly after its formation, after the 400 °C step, the saturation remanence is extremely low. This points to fine crystalline hematite, which agrees with the absence of a Morin transition during low-temperature cycling. The hematite saturation remanence does not show any correlation with the chemical composition of the parent goethite. Hematite derived from the goethite with the largest impurity content (MBL) has the lowest J_{rs}, whereas hematite from goethite with the second largest impurity content (MKB) has the highest J_{rs}. The fine-crystalline FSB goethite converts to a hematite with a relatively high J_{rs}. After the 400 °C step no grain-size dependence is observed in the hematite J_{rs}.

After the 685 °C step, J_{rs} is slightly increased compared to figures after the 400 °C step. There is a tendency for J_{rs} to increase with decreasing grain size.

Summarizing, after the 685 °C demagnetization step the following differences in rockmagnetic characteristics of the hematite are detected compared with the 400 °C step:

1) A considerable decrease of the induced field necessary to saturate the hematite at room temperature.
2) An increase of its saturation remanence.
3) A decrease in H_{cr}'.
4) The appearance of a faint Morin transition during low-temperature cycling.

These facts are all indications that the hematite lattice is approaching a well-crystallized hematite structure.

2.3.2 Magnetite characteristics

2.3.2.1 Remanent (acquisition) coercive force

H_{cr} and H_{cr}' for the magnetite in the specimens (determined according to Fig. 5A) are listed in Table VII. Chemical differences in the precursor goethite (and hematite) do not show up in the magnetite H_{cr} and H_{cr}' trends, indicating that the magnetite in each sample will have an approximately similar chemistry. Ranges for the magnetite saturation remanence per unit mass will be determined in section 3.2.

When using the derived hysteresis parameters for granulometric purposes, one should compare the present data with magnetites prepared in a similar way. Basically, magnetite reference data have been acquired in three different ways: 1) by grinding and sizing larger synthetic or natural grains (e.g. Parry, 1965, Day et al., 1977,

Hartstra, 1982C, 1983); 2) by precipitation from aqueous solution (e.g. Dunlop, 1973B; Levi and Merrill, 1978), leading to extremely small magnetite crystals. This method can be extended to obtain larger grain sizes by hydrothermal recrystallization (Heider et al. 1987); 3) Non aqueous synthesis at high temperatures i.e. by reducing hematite (e.g. Schmidbauer and Schembera, 1987) or by precipitation in a silicate matrix (Worm and Markert, 1987A).

Table VII: Remanent (acquisition) coercive force for the magnetite in the specimens

		MKB		MBL		MEN		FSB		RR	
grain size	Temp.	H_{cr}'	H_{cr}	H_{cr}'	H_{cr}	H_{cr}'	H_{cr}	H_{cr}'	H_{cr}	H_{cr}'	H_{cr}
75 - 55	400 °C	np	np	30.5	16.7	41.1	23.1	22.5	17.5	27.8	23.9
20 - 15	400 °C	27.8	22.3	35.8	19.9	30.5	19.1	25.2	19.9	34.4	22.3
10 - 5	400 °C	31.8	21.5	--	--	26.6	23.1	27.8	21.5	29.2	22.3
250 - 150	685 °C	20.2	19.9	52.8	33.4	17.0	12.7	23.2	17.5	23.5	14.3
30 - 25	685 °C	15.9	13.9	15.9	11.5	24.4	17.5	22.3	17.5	28.7	19.1
< 5	685 °C	45.8	41.4	41.1	36.6	44.4	37.4	22.3	19.0	42.2	34.2

H_{cr}' and H_{cr} in kAm^{-1}. Grain size = grain-size range of the original goethite in micrometer; Temp. = temperature of the last thermal demagnetization step prior to the determination of H_{cr}' and H_{cr}. np = not present. For sample abbreviations see Table I.

The present magnetite data can best be compared with data acquired in the third way because they were obtained in a similar way. Grinding leads to internal stress within magnetite grains and hydrothermal recrystallization results in nearly perfect stress-free magnetite crystals.

After the 400 °C step, H_{cr}' and H_{cr} of the magnetite have relatively low values without clear grain-size dependence. For all magnetites H_{cr} values are in between 17 and 24 kAm^{-1}. H_{cr}' is larger than H_{cr} and exhibits a wider range in its values (27-40 kAm^{-1}). The relatively small H_{cr} and H_{cr}' after the 400 °C demagnetization step do not point to MD magnetite for three reasons.

1) It is unlikely that the trace amount of magnetite present (cf. Table III and Fig. 5B) resides in a relatively small number of large MD crystals.
2) There is no grain-size dependence at 400 °C, which is in disagreement with a supposed existence of MD magnetite.
3) H_{cr} and H_{cr}' after the 400 °C demagnetization step are smaller than those parameters for the <5 micrometer fractions after the 685 °C step.

Comparison with Schmidbauer and Schembera's (1987) data for extremely small, roughly spherical, magnetite particles and Worm and Markert's (1987B) data for equidimensional particles (the latter would result in slightly higher H_{cr}'s for similar grain sizes when the Schmidbauer and Schembera's H_{cr}/H_c ratio (approx. 1.5) is adopted), reveals grain sizes close to the superparamagnetic (SP) threshold size for the present magnetites. In both aforementioned papers a decrease in H_{cr} is found when approaching the SP threshold size. Because H_{cr} after the 685 °C step in the <5 micrometer fractions is larger than after the 400 °C step, it is believed that the extremely small particles span the lowermost tail of the SD grain-size region. Due to their extremely low concentration magnetic inter-particle interaction will be insignificant.

After the 685 °C step, H_{cr} and $H_{cr'}$ increase with decreasing grain size for all samples except the FSB sample, in which no grain-size dependence is observed. $H_{cr'}$ is larger than H_{cr}, a common magnetite feature (Dankers, 1981). Both parameters generally are lower in the 250-150 and 30-25 micrometer fractions than after the 400 °C step and higher in the <5 micrometer fractions. The increase in hysteresis parameters with decreasing grain size is inherent to magnetite grains. In this case, however, it can also be explained by magnetic interaction between closely spaced magnetite crystallites of a certain size. In large grains much more crystallites are present than in small grains, resulting in lower hysteresis parameters. H_{cr} and $H_{cr'}$ are approximately equal for all FSB fractions. The original FSB goethite is extremely finely crystalline. It might well be that FSB grains are composites of fine-crystalline magnetite with such a small size that the relatively high hysteresis parameters of the other samples can not be reached.

2.3.2.2 Median destructive field of the saturation remanence

AF decay curves of the hematite are (virtually) linear in fields up to 240 kAm^{-1} (300 mT; cf. MKB 75-55 in Fig. 7). The hematite is magnetically "hard" as inferred from the small decay, which is only slightly larger than the original goethite in comparable alternating fields (Dekkers, 1988B). The clock-shaped parts in the decay curves at low alternating fields can thus be attributed to magnetite. AF decay curves after the 685 °C step show a considerably larger decrease in low alternating fields than after the 400 °C step, obviously related to the increased magnetite amount.

Table VIII: Magnetite median destructive field

		MKB		MBL		MEN		FSB		RR	
grain size	Temp.	$H_{1/2I}$	rat	$H_{1/2I}$	rat	$H_{1/2I}$	rat	$H_{1/2I}$	rat	$H_{1/2I}$	rat
75 - 55	400 °C	np	--	16.7	0.71	17.5	0.79	15.9	0.91	17.5	1.06
20 - 15	400 °C	11.9	1.12	15.1	0.78	10.3	0.94	9.6	1.14	15.1	0.90
10 - 5	400 °C	12.7	0.97	--	--	13.5	1.15	9.6	1.15	15.9	0.99
250 - 150	685 °C	9.6	1.34	28.6	0.82	9.6	0.95	12.7	0.97	8.8	0.89
30 - 25	685 °C	19.1	0.79	11.9	0.83	12.7	0.94	11.9	1.02	15.9	0.86
< 5	685 °C	28.6	1.11	27.8	1.06	23.1	1.11	15.9	0.99	21.5	1.07

$H_{1/2I}$ in kAm^{-1}. np = not present. rat = $2*H_{cr}/(H_{1/2I} + H_{cr'})$, i.e. empirical relation derived by Dankers (1981). Temp. = temperature of the last thermal demagnetization step before determination of $H_{1/2I}$. For sample abbreviations see Table I.

$H_{1/2I}$ (Table VIII) after the 400 °C demagnetization step shows minor grain-size dependence. The 75-55 micrometer fractions have a (slightly) larger $H_{1/2I}$ than the others. After the 685 °C step $H_{1/2I}$ decreases with increasing grain size (the deviating behaviour of the MBL 250-150 micrometer fraction is caused by the distinctly lower magnetite content of that fraction). $H_{1/2I}$ of the <5 micrometer fractions is larger than any $H_{1/2I}$ after the 400 °C demagnetization step except for the FSB fractions. $H_{1/2I}$ of the 250-150 micrometer fractions is approximately two times larger than $H_{1/2I}$ of MD type magnetite (Dunlop, 1983; Hartstra, 1983), which points to the existence of smaller magnetite crystallites in the original 250-150 micrometer goethite grains (which are converted to hematite). Low-temperature investigation supports this conclusion.

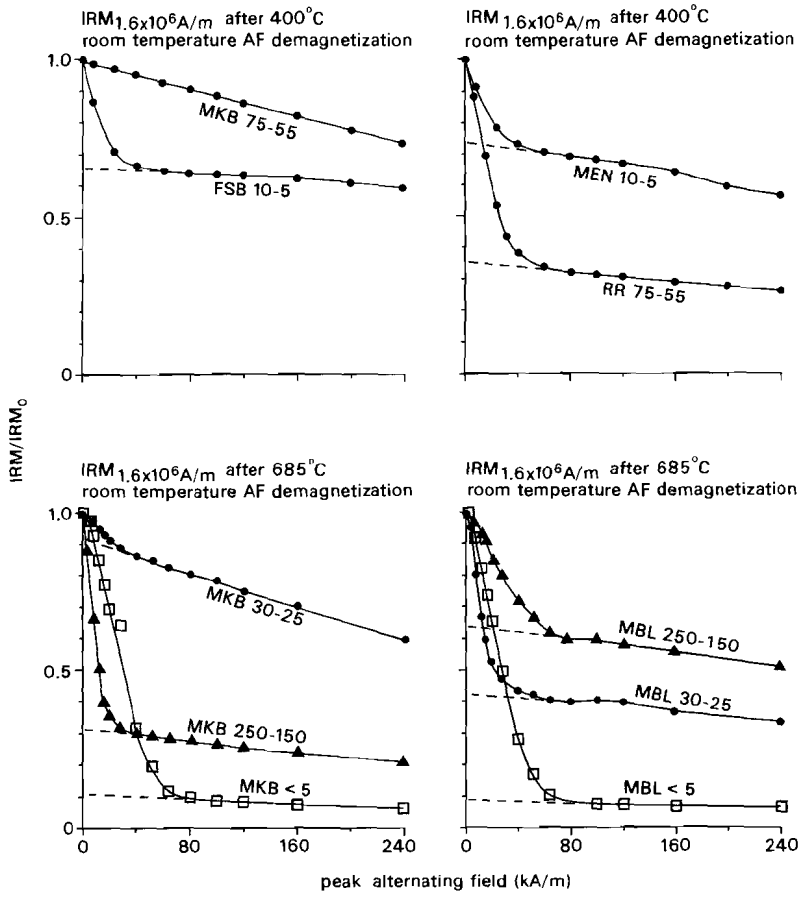

Fig. 7. AF decay curves of an IRM induced with a $1.6*10^6$ Am^{-1} field. Grain-size ranges refer to the original goethite grain-size range in micrometer. For sample abbreviations cf. Fig. 1. The hematite derived from the goethite shows linear AF decay curves up to the maximum peak value applied (24 kAm^{-1}) as is illustrated by the MKB 75-55 specimen. The clock-shaped parts of the decay curves in small alternating fields is thus due to magnetite. The magnetite remanence part is saturated in the inducing field of $1.6*10^6$ Am^{-1}, so linear extrapolation of the hematite behaviour to the ordinate allows for the establishment of the magnetite part. By dividing this part into two equal segments and drawing a line parallel to the extrapolated hematite behaviour to the AF decay curve, the fieldstrength at which this line intersect the AF decay curve, corresponds to the median destructive field of the saturation remanence of the magnetite ($H_{1/2I}$). The magnetite content is extremely small after the 400 °C step and considerably increased after the 685 °C step. Note the considerable differences in magnetite content between fractions of the same sample.

$H_{1/2I}$ is smaller than H_{cr} which again is smaller than $H_{cr'}$. The present magnetites roughly obey the relation $H_{1/2I} + H_{cr'} = 2*H_{cr}$, derived by Dankers (1981). Occasionally deviations over twenty percent are observed. The $H_{1/2I}/H_{cr}$ ratio is larger than the ratios reported for magnetite by Dankers (1978, 1981) and Hartstra (1983), but approximately equal to the ratios calculated from Dunlop's (1983) data.

2.3.2.3 Low-temperature behaviour

Low-temperature cycling of J_{rs} (cf. Fig. 6) revealed remarkable magnetite characteristics. There is only an isotropic point transition (IPT) observed in most <5 micrometer fractions (the crystallites in FSB <5 are apparently too small to show such behaviour, cf. Fig. 6C), in which the magnetite grew over a considerable temperature trajectory as is deduced from X_{in} behaviour (cf. Fig. 3). The originally coarse-grained fractions did not show any remanence collapse related to the magnetite lattice conversion from a cubic to an orthorhombic lattice at the so called isotropic point (-150 °C). The slight increase of the remanence observed in the coarse fractions during cooling could be caused by an increase of the spontaneous magnetization of the extremely fine-grained magnetite. Dunlop (1973A) demonstrated that small (0.04 micrometer diameter) magnetite grains had not yet reached a "completely blocked" domain state at room temperature. This indicates that coarse grain-size fractions are aggregates of small magnetite crystallites which show relatively low coercive forces due to magnetic interaction. The small (SD or small PSD) crystallites will not exhibit an IPT-related remanence collapse. Magnetite will mainly occur as crystallite aggregates rather than as grains for three reasons:

1) Silicate impurities within the original goethite samples remain present.
2) Fine-crystalline hematite is formed through goethite dehydration.
3) The hematite crystallites are usually not totally converted to magnetite under the relatively "dry" conditions at high temperatures: fine crystalline non-reacted hematite remnants remain present in the magnetite-rich aggregates.

The large difference between the coarse and the fine grain sizes lies in the temperature trajectory during which magnetite is formed. When the bulk is formed almost exclusively during one or two steps in the thermal demagnetization procedure (as in the coarse fractions) this leads to many small crystallites. When formed over a rather large number of steps (as in the fine fractions) this leads to a relatively low amount of seeding crystals which grow during successive steps to larger (but still small), relatively well-crystalline, grains.

Even well-crystallized magnetite shows some vacancies in their structure when annealed to temperatures above 600 °C (e.g. Lowrie and Fuller, 1969). It is not known at which vacancy content in magnetite the IPT is not observed anymore during low-temperature cycling.

3 DISCUSSION

3.1 Sample reactivity

The large differences in X_{in} and RA curves after the 685 °C step among the fractions, also among fractions of the same sample (cf. Table III), indicate that hematite recrystallization and the formation of magnetite occur in principle simultaneously. The extent to which each process occurs in the specimens, depends on factors which may vary on an extremely localized scale within the specimens. It is well possible that variations occur within a single grain (or crystallite aggregate).

The conditions which promote local magnetite growth are the result of the following factors:

1) The presence of a vapour phase, creating locally reducing conditions.
2) The reaction surface of the vapour phase with the magnetic mineral grains or crystallite aggregates.
3) The presence of seeding crystals.
4) The original inclusion pattern (e.g. oolithic versus non-oolithic goethite).
5) The crystallinity of the hematite created by dehydration of the original goethite.

The magnetic mineralogy of the <5 micrometer fractions after the 685 °C step is magnetically dominated by magnetite as appears from the RA curves (cf. Fig. 4 and Table III). The relatively small hematite crystallite aggregates with a large reaction surface ensure a relatively good contact with the (reducing) vapour phase, which promotes magnetite growth. All <5 micrometer fractions display a large (magnetic) magnetite percentage (Table III).

However, the coarser grain-size fractions do not show such a simple pattern. In some samples the magnetic mineral suite is dominated by magnetite (e.g. FSB 250-150, RR 250-150 and MEN 30-25), whereas magnetite is present in much smaller amounts in other samples (e.g. MBL 250-150, MEN 250-150 and FSB 30-25, cf. Fig. 4). There is no evident correlation between the crystallite size of the original goethite and the amount of magnetite production. Also there is no straightforward relationship between the reaction surface and the magnetite production. One expects that a reaction is facilitated when the size of the reactant crystallite aggregate is smaller because of the larger reactive surface. Apparently, the crystallite aggregate surface is only rate-determining in the smallest grain-size fractions.

In coarse grain-size fractions, the amount of magnetite production depends on the incidental creation of seeding crystals and the availability of a vapour phase at the reaction site. Even in extremely fine-crystalline material such as FSB, the reaction surface of the hematite is not rate-determining as is demonstrated by the 30-25 and 250-150 micrometer fractions. Usually, in the coarse grain-size fractions, magnetite is created in relatively large quantities during a single thermal demagnetization step.

The presence of a vapour phase is inferred from the weight-loss of the specimens: 11 percent of their initial weight after the 400 °C and 24 percent after 685 °C steps respectively. The importance of a vapour phase may be demonstrated by the following example: a test sample consisting of hematite dispersed in a "non-reactive" Al_2O_3-waterglass matrix was annealed at 700 °C when the specimen was not completely dry. After annealing, the saturation remanence indicated that the hematite was (virtually) completely converted to an extremely magnetic magnetite-like phase. However, there occurred no reaction at all in an other test sample which consisted of the same hematite fraction in the same matrix, but which was completely hardened out and stepwise heated up to 700 °C.

A CO_2/H_2O vapour phase is present in the 500-700 °C temperature range in the carbonaceous specimens because there are chemical alterations in the matrix: the $CaCO_3$ reacts with the waterglass to α-Ca_2SiO_4 (poorly crystalline, broad X-ray lines) under liberation of an CO_2/H_2O vapour phase. Wollastonite ($CaSiO_3$), spurrite ($2Ca_2SiO_4.CaCO_3$) and $Na_2Ca_3Si_6O_{16}$ are tentatively determined. Wollastonite, spurrite and Ca_2SiO_4 (β-structure: larnite) are known as metamorphic minerals characteristic for siliceous chalks in a high temperature very low pressure regime (e.g. Winkler, 1979). For magnetite production, the

availability of the vapour phase in the immediate vicinity of the hematite crystallite aggregates is important, rather than the total amount vapour phase produced within a specimen. Reducing capacity is afforded by decomposition of organic matter, which is present in trace amounts. Differences in this local availability result in the scattered pattern of magnetite quantities observed. This shows that, even in such relatively simple artificial systems, reaction rates are determined by different factors which appear to be difficult to quantify. The exact composition of the magnetite needs further examination. This will lead to a better understanding of the reaction mechanism for its production. The situation in natural samples is expected to be (considerably) more complex (e.g. the impact of dehydration of clay minerals), giving rise to a wide variety of reaction possibilities, which will be hard to characterize in detail.

3.2 Magnetite saturation remanence and grain-size estimate

The initial susceptibility of the specimens can be used to calculate their magnetite weight percentage. An exact calculation can only be performed, when the susceptibilities of the constituting magnetite and hematite are known. Precise data, however, are not available, so approximations have to be made for the magnetite and hematite susceptibilities. The initial susceptibility of magnetite is in between $3.6*10^{-4}$ and $7.2*10^{-4}$ m^3kg^{-1} depending on grain size and preparation method (Dunlop, 1986). Reasonable values for the hematite susceptibility after 685 °C are in between $0.5*10^{-6}$ and $1*10^{-6}$ m^3kg^{-1}. After the 400 °C step the susceptibility is smaller: a range between $0.15*10^{-6}$ and $0.5*10^{-6}$ is adopted. Combination of these data with the measured initial susceptibility (Table II) yields a range for the magnetite weight percentage of each specimen. These percentages are small, usually between 0.1 and 1 percent. Intersection of the magnetite weight percentage with the magnetic magnetite percentage (Table III) leads to a ratio for the magnetite and hematite saturation remanence. This is done for each specimen (cf. Fig. 8). High ratios (from 50:1 to over 800:1) are obtained. The ratios are higher after the 685 °C thermal demagnetization step than after the 400 °C step. Using the hematite J_{rs} (Table VI), ranges for the magnetite J_{rs} can be calculated (Table IX).

Table IX: Isothermal saturation remanent magnetization (J_{rs}) ranges for the magnetite.

Grain size	Temp.	MKB	MBL	MEN	FSB	RR
75 - 55	400 °C	---	0.7 - 1.4	3.5 - 5	2.2 - 4.5	> 9
20 - 15	400 °C	2 - 4	2 - 5	3.5 - 7	1.0 - 2.2	4.5 - 9
10 - 5	400 °C	13 - 26	---	3.5 - 7	2.2 - 4.5	9
250 - 150	685 °C	6 - 12	2.5 - 5	2 - 6	29 - 50	---
30 - 25	685 °C	0.8 - 1.6	1.3 - 2.6	3.5 - 7	23 - 46	2 - 3.5
< 5	685 °C	11 - 22	3 - 4.5	5 - 10	17 - 26	6.5 - 13

J_{rs} in Am^2kg^{-1}. The grain size refers to the grain size of the original goethite. Temp. = temperature of the last thermal demagnetization step before the RA curves and initial susceptibility were determined. The ranges have to be regarded as somewhat approximate.

The obtained values for the "magnetite" can in principle be used for their grain-size determination. Application of pure magnetite data have to be done with a certain care because the exact composition of the present "magnetite" is not known. The vacancy content is known to influence the magnetite saturation remanence (e.g. Lowrie and Fuller,

1969). Blocking temperature spectra of the present magnetite do not point to a high vacancy content.

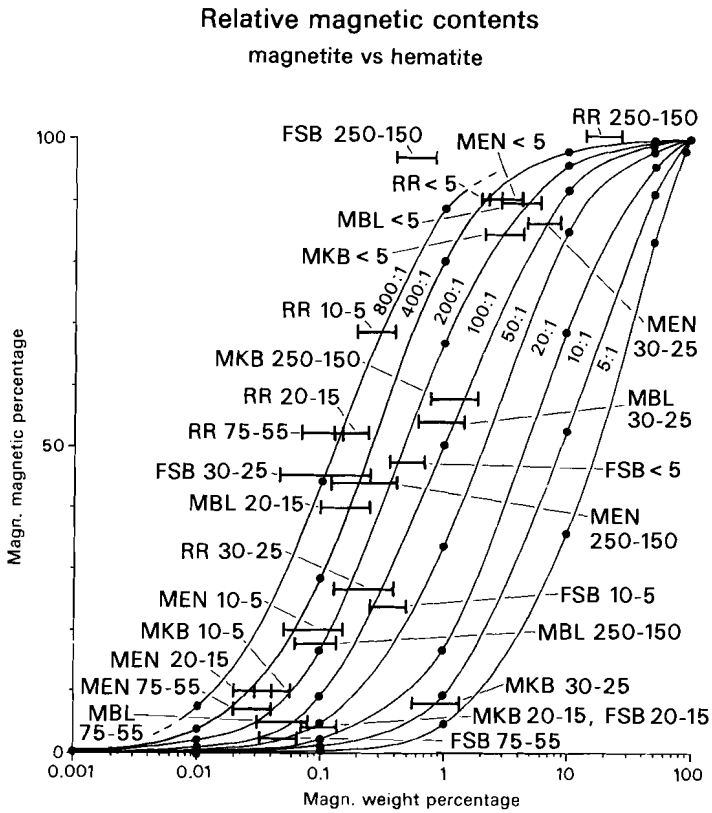

Fig. 8. Determination of the ratio of the magnetite/hematite saturation remanence for the specimens. The magnetic magnetite percentage is determined with RA curves and the magnetite weight percentage is calculated from the initial susceptibility.

The low saturation remanence after the 400 °C step indicates that the magnetite grains have sizes very close to the superparamagnetic threshold size. Low saturation remanences are characteristic for such magnetite grains (Worm and Markert, 1987B). Calculation of J_{rs} per unit mass from Schmidbauer and Schembera's (1987) data for extremely fine-grained magnetite assuming the magnetite J_s to be 90 Am^2kg^{-1} reveals approx. 32 Am^2kg^{-1} for 0.061 micrometer grains, approx. 40 Am^2kg^{-1} for 0.085 micrometer grains, approx. 30 Am^2kg^{-1} for 0.127 micrometer grains and approx. 22.5 Am^2kg^{-1} for 0.162 micrometer grains. The high J_{rs} after the 685 °C step for FSB "magnetite" corresponds with such fine grain sizes. Lower values indicate extremely small grain sizes when the magnetic magnetite percentage is small (below 20-30 percent). Grain sizes in the order of 0.2-1 micrometer are appropriate when the magnetic magnetite percentage is large.

3.3 Observation of a self-reversal in artificial samples

During stepwise thermal demagnetization of the original 16 kAm^{-1} TRM it appeared that a small component with a reversed direction was present in most specimens. This is remarkable because a single component TRM was induced in the specimens. The reversed component occurs at temperatures above 500 °C, generally between the 585 °C and 625 °C demagnetization steps (cf. Fig. 9). Its magnitude correlates with the remanence present in the specimens just before the reversal is observed. It is thus likely that the reversal is related to a process occurring in the specimens.

When the self-reversal would be related to the dehydration of goethite, i.e. the creation of hematite at some 250-300 °C, it would occur in all specimens. This is not the case, so the self-reversal is probably related to the magnetite growth, which occurs predominantly at elevated temperatures. Magnetite crystallites are growing within their precursor hematite crystallite aggregates. The demagnetizing field existing within the hematite aggregates, though macroscopically small, is significant at the short distances under consideration.

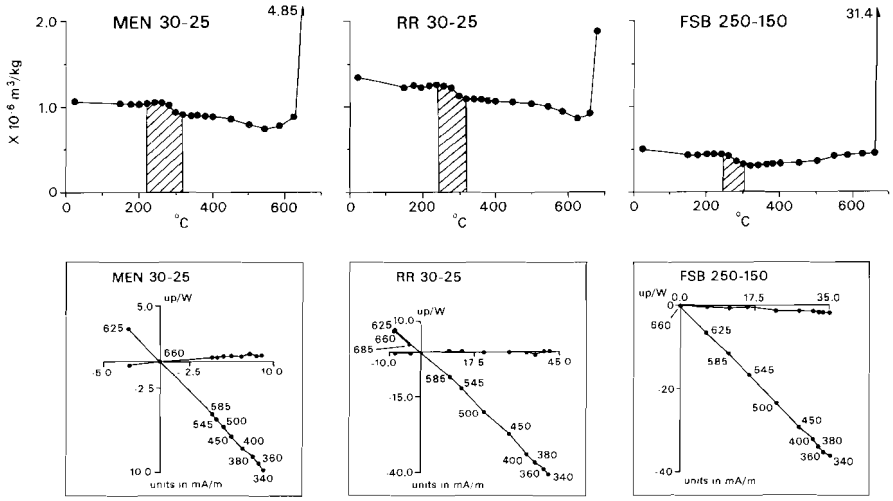

Fig. 9. Plots of X_{in} behaviour during the stepwise thermal demagnetization with corresponding vector demagnetization diagrams (Zijderveld, 1967). Only the remanence from 340 °C upwards is shown. The grain-size ranges refer to the original goethite grain size in micrometer. For sample abbreviations cf. Fig. 1. The X_{in} plots are similar to those in Fig. 3 (cf. caption Fig. 3 for explanation). In most specimens a self-reversal is observed. The magnitude of the (small) reversed component correlates with the remanence just before the reversal is observed. The initial susceptibility is low at temperatures at which the reversal is observed. In FSB 250-150 the magnetite amount is apparently too small for the development of a reversed component. Further explanation in text.

When the magnetite crystallites reach SD grain sizes above the blocking temperature, they acquire a TRM which is induced by the hematite demagnetizing field, when cooled through their blocking temperature spectrum down to room temperature. The magnetite crystallites acquire a combined PTRM/CRM when growing through their blocking volume below the blocking temperature (magnetite SD grains typically have

diameters of 30 to 60 nm). The paradoxical situation exists that a magnetite remanence is traced at temperatures higher than its maximum blocking temperature. This is, however, implicitly hidden in the cooling to room temperature, well below the maximum blocking temperature of magnetite.

Measurements of X_{in} indicate that the self-reversal is only observed when the magnetite formation is minimal. The created magnetite will be SD. SD magnetite has the highest specific volume TRM (approximately 100, cf. O'Reilly, 1984), and will be most sensitive for the inducing field of the hematite (Calculation of the amount of magnetite needed for observed reverse components under the assumption of induction by the rest-field of thermal demagnetizer yields unreasonably large magnetite quantities). When the magnetite crystallites become larger, their specific volume TRM decreases. Also, crystallite growth at successive thermal demagnetization steps will be accompanied by nucleation of new crystallites. So, besides that the magnetite is less sensitive for the hematite inducing field, this field itself will become (much?) smaller by enhanced magnetite growth. At temperatures close to the maximum blocking temperature of the hematite, the demagnetizing field will anyhow be low because of the approach of the maximum blocking temperature. At such temperatures the induced field for the reversed component diminishes and its magnitude will become smaller. This leads to the actual observation of a reversed component. At the hematite Curie temperature, the induced field becomes zero; the remanence vector is in the origin of the orthonormal vector demagnetization diagram. This also occurs, when the hematite is totally converted to magnetite.

The foregoing explanation for the self-reversal implies a magnetostatic self-reversal mechanism. For the moment a magnetostatic mechanism is preferred over a magnetocrystalline self-reversal mechanism which involves a strict crystallographical relation between parent and daughter minerals, because the self-reversal is observed above the Curie point of magnetite. Experiments will be designed to unravel the self-reversal mechanism more definitely.

The observation of this self-reversal, regardless of its exact mechanism, implies that reversals observed in the ultimate part of demagnetization diagrams (when the original NRM is almost completely removed) in goethite-bearing sediments treated with the stepwise thermal demagnetization procedure may be self-reversals.

4 SUMMARY AND CONCLUSIONS

This study demonstrates that the reaction goethite = hematite + H_2O during a stepwise thermal demagnetization procedure can well be monitored by X_{in} measurements at room temperature. Generally, X_{in} is slightly decreasing in the temperature interval of the goethite/hematite conversion reaction. The temperature interval for the conversion reaction determined by initial susceptibility measurements corresponds closely to that determined by DSC measurements.

Goethite crystallite aggregates usually occur with minor hematite intergrown. During the goethite/hematite conversion reaction, there is an amount of free water available within these crystallite aggregates in the direct vicinity of the hematite. This locally present water vapour flux facilitates to some extent the recrystallization of the minor originally present hematite. This may lead to an extra remanence decrease, especially in extremely poorly crystalline material, because the recrystallization is occurring in a field-free space and results in a hardly magnetic hematite type. When the goethite is completely con-

verted to hematite, the amount of vapour available within the grains decreases considerably and the lattice recrystallization is considerably slowed down, which leads to the observed bending points in the decay curves at some 250-300 °C.

X_{in} measurements indicate that a phase with a high susceptibility is created within the specimens during thermal demagnetization, in the coarse grain-size fractions generally at temperatures above some 550 °C but in the fine grain-size fractions (<5 micrometer) already at temperatures of some 400 °C. Because of the reducing conditions within the specimens the formation of magnetite is inferred. This is supported by the low maximum blocking temperatures of the saturation remanence of the magnetite-like phase (approximately 560 °C), induced after a complete thermal demagnetization. The rockmagnetic properties of the hematite and magnetite which formed during the thermal demagnetization procedure, were investigated after the 400 °C and 685 °C steps.

After the 400 °C step, the hematite has a considerably lower specific J_{rs} than well-crystallized hematite, indicative for an extremely fine-crystalline hematite type. This is also indicated by the absence of a Morin transition during low-temperature cycling. Applied fields up to $10.4*10^6$ Am^{-1} were necessary for the induction of J_{rs}. No distinct grain-size dependence is observed for H_{cr}' in all samples. It varies from 1100 to 1500 kAm^{-1} for four of the samples; only the MEN sample has a lower H_{cr}' (approximately 700-800 kAm^{-1}).

After the 685 °C demagnetization step, the specific J_{rs} of hematite is higher than after the 400 °C demagnetization step but still smaller than well-crystalline hematite. Considerably smaller fields ($3.2*10^6$ to $4.8*10^6$ Am^{-1}) are needed for J_{rs} acquisition. H_{cr}' decreases also considerably: it varies between 500 and 800 kAm^{-1}. A "weak" Morin transition is detected in hematite-dominated samples, indicative for a coarsening of the hematite crystallites. The differences in hematite rockmagnetic properties after both thermal demagnetization steps indicate that the hematite lattice is (continuously) re-arranging during successive steps in the stepwise thermal demagnetization.

The magnetite formed in the specimens after the 400 °C step is extremely fine-crystalline. Trace amounts were only detectable by RA curves, only in the <5 micrometer fractions a minute increase in X_{in} points to their creation. RA curves can thus successfully be used for determination of traces of magnetite which do not show up by a marked increase in initial susceptibility.

$H_{cr}' > H_{cr} > H_{1/2r}$ for magnetite in all specimens, roughly obeying the empirical relation derived by Dankers (1981). After the 400 °C step, they are approximately similar for all samples without any evident grain-size dependence (H_{cr}': some 25-35 kAm^{-1}, H_{cr}: 20-24 kAm^{-1} and $H_{1/2r}$: 10-15 kAm^{-1}). After the 685 °C step, the magnetite properties are governed by their (highly variable) amount formed during the thermal demagnetization. Basically, all three parameters show an increase with decreasing grain size. H_{cr}', H_{cr} and $H_{1/2r}$ (respectively: 45, 35-40 and 25-30) of the <5 micrometer fractions are larger than corresponding parameters obtained after the 400 °C step. Only the fine-crystalline FSB specimens revealed similar values for the hysteresis parameters for both temperatures without any evident grain-size dependence.

The IPT typical for MD magnetite during low-temperature cycling of J_{rs} occurred only in the <5 micrometer fractions. Coarser grained specimens showed a slightly increasing remanence without the occurrence of an isotropic point-related remanence decrease at approximately -150 °C. This different behaviour is related to the rate of magnetite formation. The magnetite growth in the <5 micrometer fractions occurs over a large

temperature interval giving rise to relatively well-crystalline rather "coarse" magnetite crystallites. The magnetite in the coarse grain-size fractions formed almost exclusively during one or two thermal demagnetization steps. Diffusion rates are low in the relatively "dry" environment, so magnetite within a large crystallite aggregate will prevail as closely spaced extremely small, magnetically interacting magnetite crystallites, rather than much larger magnetite grains. Magnetic interaction lowers the coercive forces and saturation remanence, but the small crystallites will not show an IPT during low-temperature cycling. Combination of the magnetite weight percent (usually between 0.1 and 1 percent, calculated from the initial susceptibility) and the magnetic magnetite percentage (between a few and 100 percent, determined from the RA curves) yields high ratios for the saturation remanence of the magnetite and hematite. This indicates grain sizes for the magnetite from very close to the superparamagnetic threshold size up to approximately 1 micrometer.

RA curves after the 400 °C demagnetization step showed similar behaviour for all specimens, regardless of the origin of the original goethite. In fine fractions the amount of magnetite is slightly larger than in coarse fractions. After the 685 °C demagnetization step large differences were noticed between samples as well as between fractions of the same sample. These differences were also exhibited in large differences in X_{in} between the specimens. The <5 micrometer fractions were magnetically dominated by magnetite after the 685 °C step, but the coarser grain-size fractions showed varying magnetite contents. These large differences indicate that magnetite formation is not governed by a single process: in small grain-size fractions the reaction surface of the crystallite aggregates making up the grains appears to be rate-determining, but in coarse grain-size fractions the amount of magnetite is dependent on subtle processes such as the local presence of a reducing vapour phase and the presence of seeding crystals within the reacting aggregates. A reducing vapour phase is inferred from the decomposition of trace amounts of organic matter. Chemical reactions between the matrix $CaCO_3$ and the waterglass under release of CO_2/H_2O vapour ensure a relatively long contact time between the reducing agent at the reaction site, so that actual reduction can take place.

Usually, a self-reversal is observed between the 585 and 625 °C demagnetization steps. Its magnitude correlates with the hematite remanence just before the reversal is observed. This implies that, when dealing with fine crystalline goethite/hematite aggregates in sediments demagnetized with stepwise thermal demagnetization, small reverse components observed in the ultimate part of demagnetization diagrams should be regarded with care.

Acknowledgements

H.J. Meijer and P.J. Verplak carried out the majority of the magnetic measurements for this investigation. P. van Krieken (department of sedimentology, University of Utrecht) performed the DSC measurements. The high field measurements were carried out in the High Field Magnet Laboratory of the University of Nijmegen (The Netherlands) in cooperation with Dr. J.A.A.J. Perenboom. Prof. Dr. J.D.A. Zijderveld carefully reviewed the manuscript. J.J.J. Bergenhenegouwen made the drawings. These investigations were supported by the Netherlands Foundation for Earth Science Research (AWON) with financial aid from the Netherlands Organization for the Advancement of Pure Research (Z.W.O., grant 751-354-006).

5 REFERENCES

Dankers P.H.M., 1978, Magnetic properties of dispersed natural iron-oxides of known grain size, Ph.D. thesis University of Utrecht, 143pp.

Dankers P.H.M., 1981, Relationship between median destructive field and remanent coercive forces for dispersed magnetite, titanomagnetite and hematite, Geophys. J. R. astr. Soc. 64, 447-61.

Day R., Fuller M., Schmidt V.A., 1977, Hysteresis properties of titanomagnetites: grain size and compositional dependence, Phys. Earth Plan. Inter. 13, 260-7.

Dekkers M.J., 1988A, Magnetic properties of natural goethite part I: Grain-size dependence of some low- and high-field related rockmagnetic parameters measured at room temperature, in: Some rockmagnetic parameters for natural goethite, pyrrhotite and fine-grained hematite, Ph.D. thesis University of Utrecht, chapter 3.

Dekkers M.J., 1988B, Magnetic properties of natural goethite part II: TRM behaviour during thermal and alternating field demagnetization and low-temperature treatment, in: Some rockmagnetic parameters for natural goethite, pyrrhotite and fine-grained hematite, Ph.D. thesis University of Utrecht, chapter 4.

Dekkers M.J., 1988C, Some rockmagnetic parameters for natural goethite, pyrrhotite and fine-grained hematite, Ph.D. thesis University of Utrecht, appendix 1.

Dunlop D.J., 1971, Magnetic properties of fine particle haematite, Ann. Géophys. 27, 269-93.

Dunlop D.J., 1973A, Thermoremanent magnetization in submicroscopic magnetite, J. Geophys. Res. 78, 7602-13.

Dunlop D.J., 1973B, Superparamagnetic and single-domain threshold sizes in submicroscopic magnetite, J. Geophys. Res. 78, 1780-93.

Dunlop D.J., 1983, Determination of domain structure in igneous rocks by alternating field and other methods, Earth Plan. Sci. Letters 63, 353-67.

Dunlop D.J., 1986, Hysteresis properties of magnetite and their dependence on particle size: a test of pseudo-single-domain remanence models, J. Geophys. Res. B 91, 9569-84.

Hartstra R.L., 1982A, High-temperature characteristics of a natural titanomagnetite, Geophys. J. R. astr. Soc. 71, 455-76.

Hartstra R.L., 1982B, A comparative study of the ARM and I_{sr} of some natural magnetites of MD and PSD grain size, Geophys. J. R. astr. Soc. 71, 497-518.

Hartstra R.L., 1982C, Grain-size dependence of initial susceptibility and saturation magnetization-related parameters of four natural magnetites in the PSD-MD range, Geophys. J. R. astr. Soc. 477-95.

Hartstra R.L., 1983, TRM, ARM and I_{sr} of two natural magnetites of MD and PSD grain size, Geophys. J. R. astr Soc. 73, 719-37.

Heider F., Dunlop D.J., 1987, Two types of chemical remanent magnetization during the oxidation of magnetite, Phys. Earth Plan. Inter. 46, 24-45.

Heider F., Dunlop D.J., Suglura N., 1987, Magnetic properties of hydrothermally recrystallized magnetite crystals, Science 236, 1287-90.

Heller F., 1978, Rockmagnetic studies of Upper Jurassic limestones from Southern Germany, J. Geophys. 44, 525-43.

Langmuir D., 1971, Particle size effect on the reaction goethite = hematite + water, Am. J. Sci. 271, 147-56

Langmuir D., 1972, Correction: particle size effect on the reaction goethite = hematite + water, Am. J. Sci. 272, 972.

Levi S., Merrill R.T., 1978, Properties of single-domain, pseudo-single-domain and multidomain magnetite, J. Geophys. Res. 83, 309-23.

Lowrie W., Fuller M., 1969, Effect of annealing on coercive force and remanent magnetization in magnetite, J. Geophys. Res. 74, 2698-2710.

Murad E., 1979, Mössbauer spectra of goethite: evidence for structural imperfections, Min. Mag. 43, 355-61.

Nishitani T., Kono M., 1983, Curie temperature and lattice constant of oxidized titanomagnetite, Geophys. J. R. astr. Soc. 74, 585-600.

O'Reilly W., 1984, Rock and Mineral Magnetism, Blackie and Son Ltd., Glasgow, 220pp.

Özdemir Ö., Banerjee S.K., 1984, High-temperature stability of maghemite (γ-Fe_2O_3), Geophys. Res. Lett. 11, 161-4.

Parry L.G., 1965, Magnetic properties of dispersed magnetite powders, Philos. Mag. 11, 303-12.

Schmidbauer E., Schembera N., 1987, Magnetic hysteresis properties and anhysteretic remanent magnetization of spherical Fe_3O_4 particles in the grain size range 60-160 nm, Phys. Earth Plan. Inter. 46, 77-83.

Smykatz-Kloss W., 1974, Differential thermal analysis, Minerals and rocks Vol. 11, Springer Verlag, Berlin-Heidelberg-New York, 185pp.

Strangway D.W., Honea R.M., McMahon B.E., Larson E.E., 1968, The magnetic properties of naturally occurring goethite, Geophys. J. R. astr. Soc. 15, 345-59.

Winkler H.G.F., 1979, Petrogenesis of metamorphic rocks, Springer Verleg, New York, Heidelberg, Berlin, 5^{th} edition, 348pp.

Worm H.-U., Markert H., 1987A, The preparation of dispersed titanomagnetite particles by the glass-ceramic method, Phys. Earth Plan. Inter. 46, 263-9.

Worm H.-U., Markert H., 1987B, Magnetic hysteresis properties of fine particle titanomagnetites precipitated in a silicate matrix, Phys. Earth Plan. Inter. 46, 84-92.

Yapp C.J., 1983, Effects of AlOOH-FeOOH solid solution on goethite-hematite equilibrium, Clays Clay Minerals 31, 239-40.

Zijderveld J.D.A., 1967, AC demagnetization of rocks: analysis of results, in Collinson et al., Methods in Paleomagnetism, Elsevier Amsterdam, 254-86.

CHAPTER 6

PYRRHOTITE: SOME LITERATURE DATA

1 INTRODUCTION

Some general background information and a short outline of the magneto-mineralogical data concerning pyrrhotite are given in this chapter, before the experimental details and results are reported in the next three chapters.

The series of iron-sulphur compounds with compositions varying between Fe_7S_8 and $Fe_{11}S_{12}$ is generally referred to as pyrrhotite. A general formula for the troilite - pyrrhotite series is $Fe_{1-x}S$ with x varying between zero and 0.125. Troilite approaches truly stoichiometric FeS: a finite non-stoichiometry always exists (Ward, 1970; Goodenough, 1978). The specific density of pyrrhotite varies between 4580 and 4650 $kg*m^3$. Pyrrhotite has unique properties: it is by far the most magnetic and has the highest electrical conductivity of all sulphide minerals. Its crystal structure consists of a series of alternating iron and sulphur layers based on the NiAs-structure with the iron layers partially occupied by vacancies. This results in a monoclinic structure (pseudo-hexagonal) for the most iron-deficient pyrrhotite and in a hexagonal crystal structure for iron-richer pyrrhotite. The vacancies are distributed in a regular way, giving rise to various possible superstructures depending on the pyrrhotite composition. Pyrrhotite with an overall composition in the intermediate pyrrhotite compositional range usually consists of intimate intergrowths of several superstructures. This so called intermediate pyrrhotite frequently occurs in nature (e.g. Arnold, 1967). There are large differences in magnetic behaviour between monoclinic and hexagonal pyrrhotite.

Fresh pyrrhotite crystals are macroscopical brass-brown coloured. They tarnish easily; specially in the presence of oxygen and water. The colour becomes deep black-brown. In the weathering zone pyrrhotite is generally completely altered to pyrite and/or marcasite due to the removal of iron from the lattice.

Microscopically, under reflected light, pyrrhotite has a pinkish-yellow colour with a reflection of 38 to 45 percent (e.g. Schouten, 1962). It is strongly anisotropic. With etching techniques it is possible to distinguish between hexagonal and monoclinic pyrrhotites (e.g. Naldrett and Kullerud, 1967). However, with the same etching fluid sometimes hexagonal pyrrhotite is darker than monoclinic pyrrhotite, whereas in other cases the reverse is true. This drawback has hindered a straightforward application of etching techniques in pyrrhotite determination.

2 GEOLOGICAL OCCURRENCE

Pyrrhotite is well-known as an important constituent of a wide variety of ore-parageneses. Moreover, there is accumulating evidence that it is far more common in ordinary rocks than previously assumed. Its occurrence is reported in igneous rocks without any relation to ore-bearing assemblages (e.g. Soffel, 1977), in metamorphic rocks (e.g. Carpenter, 1974; Rochette, 1987) and also in sediments (e.g. Kligfield and Channell, 1981; Freeman, 1986). Pyrrhotite - capable in carrying a stable NRM - can thus occur also without any direct spatial relationship to the rather specific sulphidic ores. Its paleomagnetic importance therefore significantly increases. Pyrrhotites related to ore-deposits

are sampled for the present study to obtain pyrrhotite in workable quantities, because pyrrhotite occurs only in trace amounts in sediments and metamorphic rocks.

Pyrrhotite-bearing ore-parageneses are found in several genetically different ore types. A crude classification of pyrrhotite-bearing ores is the division into orthomagmatic ores, skarn ores with massive replacement (pyrometasomatic ores), hydrothermal vein-type ores (hypothermal) and (reheated) pyritic ores of volcano-sedimentary origin. The paragenesis: pyrrhotite ± pentlandite ± chalcopyrite ± (titano)-magnetite is dominant in the orthomagmatic Ni-Cu-Fe ores. In the other types pyrrhotite is found associated with sphalerite, galena, pyrite, arsenopyrite, chalcopyrite and magnetite. Associations with chalcopyrite and specially magnetite reflect a higher ore-formation temperature than parageneses with the other minerals. A much wider spectrum of minerals in pyrrhotite-bearing ore-parageneses can be encountered in ore deposits with a special composition or in deposits with a complex multi-phase evolution.

3 SOME MINERALOGICAL AND CRYSTALLOGRAPHICAL CHARACTERISTICS

3.1 Chemical composition

Pyrrhotite chemical compositions are usually determined with a microprobe. Natural pyrrhotite does not show much isomorphous replacement. Minor copper, manganese, nickel and cobalt contents are reported (generally below 0.2 weight percent, e.g. Arnold and Reichen, 1962; Engel et al., 1978). Traces of zinc are possible. Occasionally higher isomorphous replacement in pyrrhotite has been found (e.g. Vaughan et al. (1971) report nickel contents up to one weight percent and Thompson et al. (1980) up to three weight percent).

The pyrrhotite iron/sulphur ratio can also be determined with X-ray techniques. This method involves quenching of the high-temperature hexagonal pyrrhotite structure (cf. section 6.4) followed by the determination of the position of the composition-dependent d_{102} reflection for hexagonal pyrrhotite (Yund and Hall, 1969). Monoclinic pyrrhotite has to be converted to a hexagonal structure by annealing in vacuo at 350 °C, followed by quenching of the high-temperature hexagonal structure - with the same chemical composition as its low-temperature monoclinic equivalent. The d_{102} reflection is represented by a doublet in monoclinic pyrrhotite, which has to be changed to a single hexagonal d_{102} reflection for a proper determination of the iron/sulphur ratio. One should bear in mind that only the average composition of the pyrrhotite sample (pyrrhotite is, at low temperatures, frequently a composite of several superstructures) is obtained with this X-ray technique. The isomorphous substitution of non-Fe elements should be insignificant because the Yund and Hall (1969) calibration curve is derived for pyrrhotite synthesized from analytical grade chemicals. X-ray methods for the discrimination between the amounts of hexagonal and monoclinic pyrrhotite may lead to spurious results (e.g. Kissin and Scott, 1982). Relative amounts of hexagonal and monoclinic pyrrhotites are preferably determined by optical methods applying etching fluids (e.g. Naldrett and Kullerud, 1967; Schwarz and Harris, 1970) or magnetic colloids (e.g. Chikazumi, 1964).

3.2 Crystal structure

The crystal structures of troilite and pyrrhotite are based on the NiAs-structure (Fig. 1). The troilite and pyrrhotite structures consist of hexagonal close-packed iron and sulphur layers. There are two different types of interstitial spaces in a close-packed structure (Fig. 2): one in four-fold coordination (tetrahedral site) and one in six-fold coordination (octahedral site). In the troilite and pyrrhotite structures, both iron and sulphur occupy the octahedral sites; the tetrahedral sites are vacant.

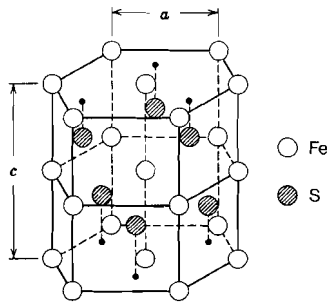

Fig. 1. The pyrrhotite structure (NiAs-structure), consisting of hexagonal close-packed S layers with Fe occupying the octahedral interstitial sites. The a-axis is approximately 3.45 Å and the c-axis 5.75 Å (e.g. Nakazawa and Morimoto, 1971).

In a hexagonal close-packed structure (with ABAB layer stacking), the interstitial tetrahedral and octahedral sites each form chains perpendicular to the close-packed layers. In a cubic close-packed structure (with ABCABC stacking) the tetrahedral and octahedral sites alternate within each chain (cf. Fig. 2). In a hexagonal close-packed structure consisting of alternate layers of larger and smaller ions as is the case with troilite and pyrrhotite, it is thus relatively easy for the smaller ions (iron) to move from one octahedral interstitial site to another, because the octahedral sites are bigger than the tetrahedral sites.

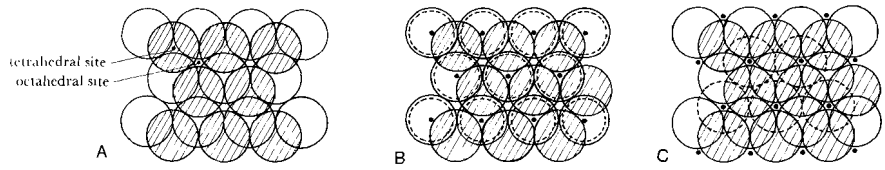

Fig. 2. Close-packed structure showing the tetrahedral and octahedral sites. Two layers are shown (Fig. 2A). Adding a third layer, in a hexagonal close-packed structure (with ABAB layer stacking) the tetrahedral and octahedral sites each form chains perpendicular to the basal plane (Fig. 2B); in a cubic close-packed structure (with ABCABC layer stacking) tetrahedral and octahedral sites alternate within each chain (Fig. 2C).

The atoms within each Fe-layer are ferromagnetically coupled in troilite and pyrrhotite; antiferromagnetic coupling exists between each iron neighbour layer. In a stoichiometric structure the magnetic moments

of each magnetic sublattice cancel each other and the crystal has an antiferromagnetic structure. When the structure is non-stoichiometric, there are several ways to distribute the vacancies throughout the lattice. Cancellation of the sublattice magnetic moments, as in stoichiometric structures, is also achieved when there is an ordered vacancy distribution with an equal number of vacancies in each sublattice. Hence, ordered vacancy distributions with a certain preference for one of the sublattices are needed to explain the magnetic properties of pyrrhotite. In such cases, the magnetic moments of each sublattice no longer cancel each other and ferrimagnetism results.

The ordered vacancy distributions of pyrrhotite can be described by so called superstructures: the appearance of vacancies at specific lattice positions is repeated at intervals with an integer number of cell units in a certain direction. These superstructures are referred to as commensurate. The number of vacancies determines the chemical composition of the pyrrhotite, so that pyrrhotite superstructure and chemical composition are related. The more common superstructures are visualized in Fig. 3. Monoclinic pyrrhotite has most vacancies; due to the large vacancy content the crystal symmetry degenerates from a hexagonal to a monoclinic structure. It has the so called 4C supercell (Bertaut, 1953): each other iron layer contains vacancies at one quarter of the iron lattice positions. Starting with a certain iron layer, exactly the same iron layer is repeated with an interval of four times the c-axis of the (psuedohexagonal) unit cell. In the direction of the a-axis the same vacancy positions are repeated with an interval of two unit cells. The 4C notation is a short notation for the 4C, 2A superstructure. Other commensurate superstructures reported at low temperatures are the 5C, 6C and 11C structures (e.g. Morimoto et al., 1970, 1975A; Fleet and MacRae, 1969). Those superstructures have also a 2A symmetry interval. Also non-integral (incommensurate) superstructure types are reported at low temperature, the so called NC types (e.g. Morimoto et al., 1975A, 1975B).

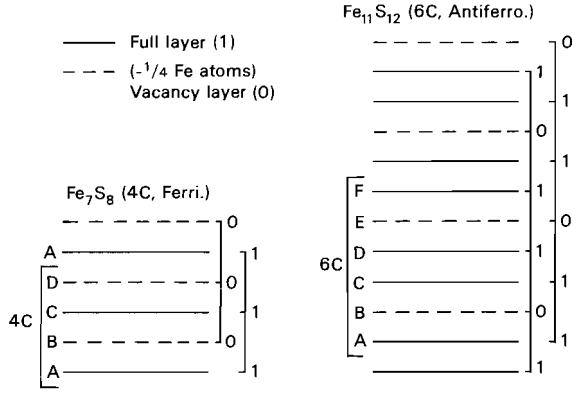

Fig. 3. Schematic representation of the 4C and 6C superstructures. In 4C pyrrhotite each other Fe-layer contains vacancies at one quarter of the Fe-positions. 6C pyrrhotite contains two Fe- layers without vacancies followed by one layer with vacancies. The vacancies are distributed spirally along the c-axis to attain maximum distances. This results in different positions for the vacancies in subsequent vacancy-bearing Fe-layers. The other superstructures, referred to as NC or intermediate pyrrhotite, are partially disordered. Non-integral superstructures occur, they are usually intergrown with 4C pyrrhotite.

The superstructures can be made visible by high resolution electron microscope observations (e.g. Morimoto et al., 1974; Pierce and Buseck, 1974) or determined by precession X-ray techniques (e.g. Koto et al., 1975; Morimoto et al., 1975A, 1975B, Kissin and Scott, 1982). Pyrrhotite compositions which do not match a specific superstructure composition can be intimate intergrowths of more superstructure types. Superstructures with non-integral repetition intervals are reported to occur predominantly at high temperatures (Nakazawa and Morimoto, 1970, 1971).

3.3 Bonding

The pyrrhotite electrical properties and the presence of various superstructures are related to the complicated bonding type which exists between the iron and sulphur ions mutually as well as between them.

Transition elements in the periodical system are characterized by partially filled d-orbitals. Iron (Fe^{o}) has a $[1s^2 2s^2 2p^6 3s^2 3p^6 4s^2]3d^8$ electron structure; Fe^{2+} a $[]3d^6$ and Fe^{3+} a $[]3d^5$ structure. When an iron ion would be "free" without interaction with neighbouring ions, the 3d-orbitals would be at the same energy level. However, this situation is never met. In crystals, iron ions are surrounded by negative ions (ligands) in a fourfold (tetrahedral) or sixfold (octahedral) coordination. Because iron in pyrrhotite is in sixfold coordination, we shall concentrate on the octahedral case.

In octahedral coordination, there is a splitting of the five d-orbitals of equal energy into a set of three and one of two orbitals, due to different overlap with the ligand orbitals. The situation is depicted in Fig. 4. The difference between the two energy levels is termed $_{\Delta}E$. The first 3d electron gains energy (the crystal field stabilization energy, CFSE), compared to the degenerate orbital situation, in occupying the lowest energy level. The second and third 3d electrons are placed in the low energy level with parallel spins (alpha-spin) for quantum mechanical grounds (gain of exchange energy). Whether the fourth electron is placed with a parallel spin in the high energy level (gain of exchange energy but loss of CFSE) or with an opposite spin direction (beta-spin) in the low energy level (gain of CFSE but no exchange energy gain), depends on the $_{\Delta}E$ and the exchange energy parameter. The same applies for the 5^{th}, 6^{th} and 7^{th} electron. The configuration with occupied high energy levels without completely filled low energy levels is called high-spin configuration; the other low-spin configuration. In pyrrhotite Fe^{2+} has the high-spin configuration; in pyrite Fe^{2+} is low spin. Therefore pyrite is diamagnetic.

When there is overlap between the metal and ligand orbitals, bonding occurs between the metal and ligands. Their atomic orbitals (AO) combine to molecular orbitals (MO). The number of MO's corresponds to the AO number. Atomic Orbitals with overlap form bonding and antibonding MO; non-overlapping AO's remain as non-bonding MO's. Schematized energy levels for σ- and for σ- and Π-bonding are in Fig. 5. Π-bonding generally occurs in sulphides by using ligand d-orbitals.

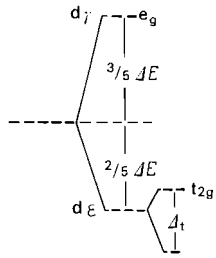

Number of d electrons	*Electron configuration* t_{2g}	e_g	*CFSE* ΔE	*Exchange energy* K
1	↑		−2/5	0
2	↑ ↑		−4/5	1
3	↑ ↑ ↑		−6/5	3
4 high-spin	↑ ↑ ↑	↑	−6/5+3/5	6
4 low-spin	↑↓ ↑ ↑		−8/5	3
5 high-spin	↑ ↑ ↑	↑ ↑	−6/5+6/5	10
5 low-spin	↑↓ ↑↓ ↑		−10/5	3+1
6 high-spin	↑↓ ↑ ↑	↑ ↑	−8/5+6/5	10
6 low-spin	↑↓ ↑↓ ↑↓		−12/5	3+3
7 high-spin	↑↓ ↑↓ ↑	↑ ↑	−10/5+6/5	10+1
7 low-spin	↑↓ ↑↓ ↑↓	↑	−12/5+3/5	6+3
8	↑↓ ↑↓ ↑↓	↑ ↑	−12/5+6/5	10+3
9	↑↓ ↑↓ ↑↓	↑↓ ↑	−12/5+9/5	10+6
10	↑↓ ↑↓ ↑↓	↑↓ ↑↓	−12/5+12/5	10+10

Exchange energies shown separately for the parallel and antiparallel sets.

Number of d electrons	*Gain in CFSE of low-spin relative to high-spin configuration*	*Loss in exchange energy of low-spin relative to high-spin configuration*
4	ΔE	$3K$
5	$2\Delta E$	$6K$
6	$2\Delta E$	$4K$
7	ΔE	$2K$

Fig. 4. Splitting of the atomic orbitals in octahedral coordination. Trigonal symmetry leads to a splitting of the lowest energy level. High-spin or low-spin electron configuration occurs depending on the magnitude of ΔE and the exchange parameter.

Only interaction between the metal ion and the neighbour ligands are taken into account in the simplified MO description above. The electrons are localized; i.e. they are related to one specific octahedral complex. In the pyrrhotite structure, there is a considerable overlap between the iron $3d^6$ and sulphur $3p^6$ orbitals. The actual situation in a pyrrhotite crystal is more complex for two reasons:

1) Neighbouring Fe-Fe and S-S interactions. These interactions become significant, when the iron/sulphur distance decreases below a certain value. This may give rise to delocalized electrons, which should possess metallic conductivity. At a certain Fe-Fe distance the Fe alpha-spin electrons are localized and the beta-spin electrons (with

no exchange energy) may be delocalized (Goodenough, 1978). An Fe-Fe distance of approximately 3.0 Å is suggested for the delocalization of beta-spin electrons in sulphides (Goodenough, op. cit). The Fe-Fe distance in pyrrhotite has figures of approximately this value, placing pyrrhotites on the border between semiconducting and metallic behaviour.

2) The presence of non-stoichiometry. Mössbauer data indicate that iron is all Fe^{2+} in pyrrhotite. Sulphur has thus an average negative valence of less than two in order to maintain electric neutrality. The Fe d-orbital has a lower energy than the top of the valence band, so the d-orbitals will be completely filled and the valence band will contain all the holes (Ward, 1970). The holes (positive charges) are in orbitals which are centered on sulphur. This leads to localized holes (forming of S_2^{2-} ions as in pyrite) when the sulphide concentration exceeds a certain value. A p-type metallic sulphide sublattice is observed when the sulphide concentration is below that specific value (as in pyrrhotite; cf. Ward, 1970).

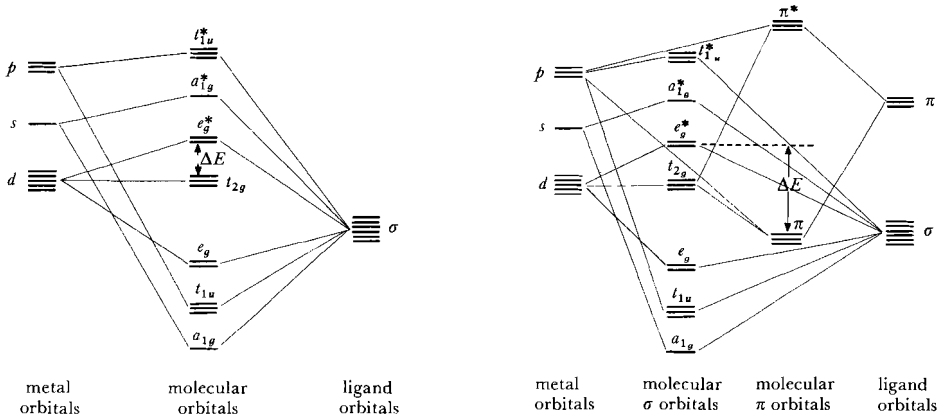

Fig. 5. Schematic energy level diagram for molecular orbitals with σ and σ plus Π-ligand orbitals. In sulphides, Π-bonding occurs using ligand d-orbitals.

The vacancies show, in principle, some preference for alternate layers when being distributed throughout the pyrrhotite lattice, because of the reduced electrostatic repulsion between shared octahedral site faces (Goodenough, 1978). Change of superstructure type can occur isochemically by changing the amount of vacancies per layer (Marusek and Mulay (1980) describe an isochemical 5C to 4C transition). The value of the superstructure parameter N (both integral and non-integral) decreases with increasing temperature (Nakazawa and Morimoto, 1971).

The existence of many superstructures, both integral and non-integral, occasionally intimately intergrown, indicates that their energy levels will be close to each other. Therefore, one expects a complex composition/temperature-dependent phase diagram for pyrrhotite compositions.

4 THERMODYNAMIC STABILITY

Phase relations in the troilite-pyrrhotite-pyrite area of the Fe-S system have often been studied in the past. A complete understanding of

the phase relations in the pyrrhotite region is not yet reached, despite much experimental effort. A recently published phase diagram (Kissin and Scott, 1982) is presented in Fig. 6. Their phase diagram is based on experiments with synthetic pyrrhotites and incorporates many previous results (Toulmin and Barton, 1964; Nakazawa and Morimoto, 1970, 1971; Sugaki and Shima, 1977; Scott and Kissin, 1973; Craig and Scott, 1974; Taylor and Williams, 1972; Bennett et al., 1972).

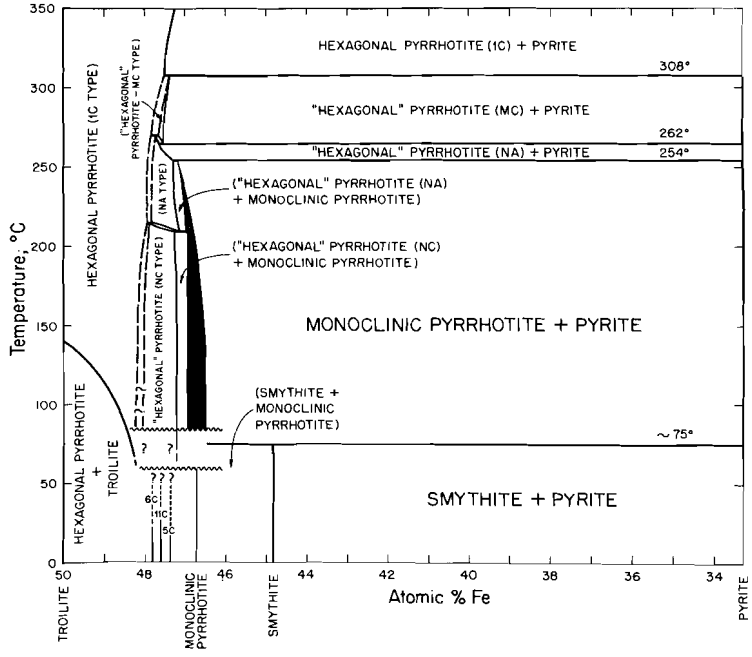

Fig. 6. Pyrrhotite phase diagram (after Kissin and Scott, 1982). The superstructure nomenclature of Nakazawa and Morimoto (1971) is used. NC and MC pyrrhotite are very similar. In X-ray single crystal images of the latter subsidiary reflections near the main reflections are not present. The NA type has also a 3C superstructure; it is named NA to indicate the non-integral character of the a-axis.

Troilite coexists with hexagonal pyrrhotite (of undefined superstructure type) at low temperatures. Troilite inverts to hexagonal pyrrhotite of 1C superstructure type at the so called alpha-transition (e.g. Goodenough, 1978). The temperature at which the alpha-transition occurs, lowers with increasing vacancy content to approximately 48 atomic percent Fe. Its continuation to lower Fe-percentages is unknown. The low-temperature integral superstructures (6C, 11C and 5C) evolve into a "hexagonal pyrrhotite" field of NC type with increasing temperature. However, the precise temperature(s?) of the superstructure change(s) is unknown. At temperatures slightly above 200 °C, the NC alters to the NA type (the so called λ-transition; change of an antiferro- to a ferrimagnetic pyrrhotite structure, cf. section 6.5). The high-temperature 1C type is separated by a two-phase field from the hexagonal NC type and the NA type at higher temperatures. Because of experimental difficulties, the position of the two-phase fields is somewhat hypothetical. The hexagonal NC and NA types are separated at their

sulphur-rich border by well-established two-phase fields from the monoclinic pyrrhotite. At temperatures above 254 °C all pyrrhotites invert to hexagonal NA type pyrrhotite, which inverts to hexagonal MC pyrrhotite and ultimately to hexagonal 1C pyrrhotite. Pyrite coexists with monoclinic pyrrhotite at low temperatures (below 254 °C) and with hexagonal pyrrhotite at high temperatures.

The phase relations in Fig. 6 refer to stable phases. Most of experimental problems in determining these stable phase-relations can be traced back to the widespread occurrence of metastable phases in the pyrrhotite region, especially at relatively low temperatures. Some of the high-temperature phases can be quenched, whereas others (partially) revert to low-temperature phases (Kissin and Scott, 1982 and references therein), making the determination of stable phases difficult. Also the nucleation of pyrite is kinetically inhibited during experimental time-spans in "dry" systems: when monoclinic pyrrhotite is heated to temperatures above 300 °C it converts to hexagonal pyrrhotite without the nucleation of pyrite. X-ray methods for the determination of pyrrhotite Fe-contents are based on this property.

The occurrence of marcasite as an initial replacement product of monoclinic pyrrhotite in a mineral specimen is reported by Fleet (1978). The structural re-arrangements of the pyrrhotite lattice for transformation to marcasite are far less than those for pyrite nucleation. This accounts for the marcasite occurrence as initial pyrrhotite replacement product. When oxygen is available, thermomagnetic data indicate that pyrrhotite reacts to magnetite at temperatures from 350 to over 500 °C depending on the pyrrhotite type (e.g. Schwarz, 1975; Bennett and Graham, 1980). When heated in argon, sulphur-loss occurs at elevated temperatures. At temperatures up to some 300 °C the loss is confined to the surface of pyrrhotite grains, at temperatures above 400 °C sulphur-loss occurs throughout the whole grain volume (Schwarz and Harris, 1970). Minute amounts of magnetite can be produced at temperatures over 500 °C when heating pyrrhotite in an argon atmosphere (Schwarz, 1965).

5 MAGNETIC PROPERTIES

The atoms in each-Fe layer are ferromagnetically coupled in pyrrhotite. Antiferromagnetic coupling exists between neighbour Fe-layers. This gives rise to the existence of two magnetic sublattices in the pyrrhotite crystal structure. An overall magnetic moment arises when the two sublattices do not cancel each other and ferrimagnetism results. The maximum magnetic moment occurs in monoclinic (4C) pyrrhotite: all vacancies are in one sublattice. In ideal cases, hexagonal pyrrhotites (5C, 11C and 6C) have vacancy distributions with an equal amount of vacancies in each of the two sublattices. Hexagonal pyrrhotites should therefore be antiferromagnetic with no overall magnetic moment. However, also hexagonal pyrrhotite appears to have not fully compensated sublattices resulting in a (much weaker) overall magnetic moment.

The Curie point of monoclinic pyrrhotite is reported between 315 and 325 °C and of hexagonal pyrrhotite between 265 and 275 °C (e.g. Schwarz, 1968; Schwarz and Vaughan, 1972; Schwarz, 1975). Isomorphous substitution lowers the Curie point (Vaughan et al., 1971). The incorporation of slight amounts of oxygen in the pyrrhotite lattice may lead to disorientation of the antiferromagnetic coupling between neighbouring Fe layers and to a Curie point of 570-575 °C without the actual nucleation of magnetite (Onufrienok and Zvegintsev, 1981).

The thermomagnetic features of natural and synthetic pyrrhotite are well known (e.g. Hayase et al., 1963; Schwarz, 1967, 1968, 1969; Schwarz and Harris, 1970; Vaughan et al., 1971; Schwarz and Vaughan, 1972). Pyrrhotite of known composition is heated in the presence of magnetic field and the magnetization as function of temperature is recorded. Two basic types of thermomagnetic curves are distinguished (Fig. 7):

1) The "normal type" with continuously decreasing magnetization until the Curie temperature is reached (Weiss type).
2) The "λ-type" with an increasing magnetization above 210 °C up to approximately 240 °C with a Curie temperature of 265-275 °C.

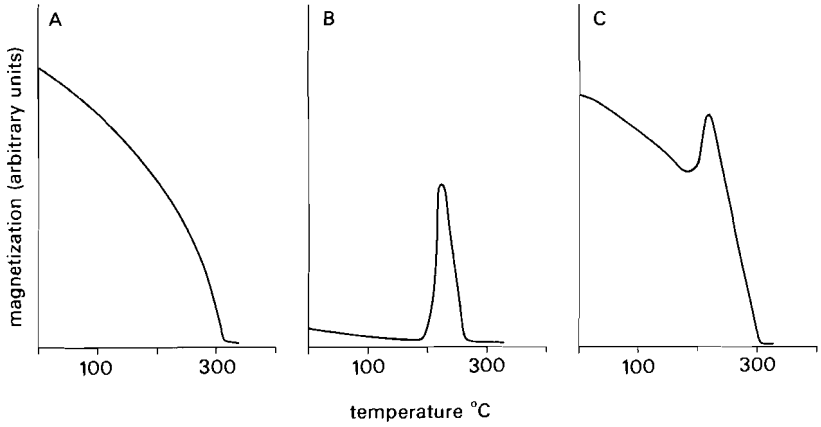

Fig. 7. Schematic thermomagnetic curves of Normal, Lambda and Mixed type pyrrhotite

The normal type is typical for monoclinic pyrrhotite and the λ-type for hexagonal pyrrhotite. Due to a change in superstructure the antiferromagnetic 5C, 11C and 6C structures alter to a ferrimagnetic NA structure with a corresponding increase in magnetization at the so-called "λ-transition". "Mixed type" thermomagnetic curves occur frequently in natural samples because of the intergrowths of monoclinic and hexagonal pyrrhotites. Schwarz (1975) shows how the relative contents of monoclinic and hexagonal pyrrhotite can be derived from "mixed type" thermomagnetic curves. A magnetic phase diagram compiling the thermomagnetic behaviour is shown in Fig. 8 (after Schwarz and Vaughan, 1972). Bennett and Graham (1980) show that hexagonal pyrrhotite can be magnetized at will after a heating cycle by changing the cooling rate. Dependent on the cooling rate, the high-temperature ferrimagnetic λ-phase is quenched to different extents. The λ-transition is a vacancy reordering process. The activation energy for the λ-transition is determined by Marusek and Mulay (1980). Its reaction rate (compatible with rates for other vacancy reordering processes) is strongly temperature dependent. Bennett and Graham (1981) showed that the maximum reaction rate is at temperatures slightly below the λ-transition itself. Hence, by rapid cooling the ferrimagnetic λ-phase can be metastably preserved at low temperatures. The formation of thermodynamically stable low-temperature phases is kinetically inhibited.

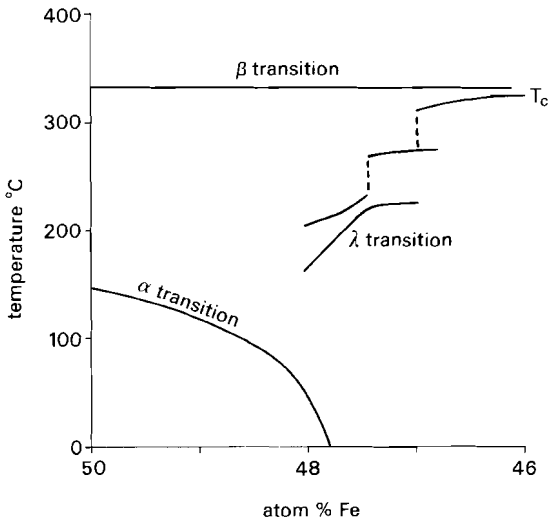

Fig. 8. Simplified magnetic phase diagram (after Schwarz and Vaughan, 1972). The Curie temperature of the λ-pyrrhotite phase seems to vary discontinuously with composition.

The pyrrhotite domain structure has been the subject of considerable study, because of its relatively large magnetic domains and the fact that no ionic polishing is required to obtain suitable polished surfaces needed for domain observation with Bitter techniques. The domain structure in small pyrrhotite grains is relatively simple: 180 ° domain walls prevail and closure domains are rare except in the vicinity of inclusions (Soffel, 1977, 1981; Halgedahl and Fuller, 1983). Large grains are characterized by wavy domain walls (Halgedahl and Fuller, 1981). Grains above some 100 micrometer are true multidomain (MD). Grains between 10 and 40 micrometer show pseudo-single-domain (PSD) behaviour. The NRM in grains smaller than 10 micrometer is characterized by four or less domains with decreasing grain size. After saturation a considerable amount of such grains, however, remain in a metastable SD state, because they cannot nucleate domain walls (Halgedahl and Fuller, 1983). The SD threshold size is estimated between 1.5 and 2 micrometer (Soffel, 1977; Halgedahl and Fuller, 1983). Clark (1984) estimated a slightly larger SD threshold size of approximately 3 micrometer. Halgedahl and Fuller (1981) showed that large AF-treated pyrrhotite grains have linear domain walls and that such grains have wavy domain walls when thermally treated. The linear domain walls required fields of a few thousand Am^{-1} (several mTesla) before their motion could be detected under a microscope, whereas the wavy walls could be moved much easier.

Schwarz (1975) advised against the application of AF techniques for the demagnetization of specimens with relatively high pyrrhotite contents (> 1 percent), because the screening of pyrrhotite leads to imhomogeneous demagnetization fields due to its relatively high electrical conductivity. AF demagnetization of samples containing few small isolated pyrrhotite grains would yield good results.

The low-field susceptibility of pyrrhotite has a magnetite-like figure in basal plane directions. It has paramagnet-like figures parallel to the c-axis (e.g. Schwarz, 1975). The magnetocrystalline anisotropy greatly dominates shape anisotropy in pyrrhotite. The high-field susceptibility along the hard axis is $70*10^{-8}$ m^3kg^{-1} (Schwarz and Vaughan, 1972). The pyrrhotite magnetostriction constant is smaller than $7*10^{-6}$, an order of magnitude smaller than magnetite (Soffel, 1977). Halgedahl and Fuller (1981) reported for single phase Fe_7S_8 a coercive force (H_c) of 9.04 kAm^{-1} (113 Oe) a spontaneous magnetization of 20.4 Am^2kg^{-1} and a ratio of the saturation remanence (J_{rs}) to the saturation magnetization (J_s) of 0.14. Soffel (1981) determined for PSD grains a H_c of 14.4 kAm^{-1} (180 Oe) and showed that the grains saturated in approximately 80 kAm^{-1} (1 kOe) fields. Saturation of SD grains needs larger magnetic fields. Clark (1984) reported grain-size dependence of hysteresis parameters of dispersed sized natural monoclinic pyrrhotite in a grain-size range from some 80 micrometer down to <3 micrometer. His study is the only one reporting actual grain-size dependence of pyrrhotite rockmagnetic parameters. H_c (10.8 to 73.6 kAm^{-1}), H_{cr} (14.8 to 99.6 kAm^{-1}) and $H_{cr'}$ (21.6 to 107.2 kAm^{-1}) (the last two parameters denote the remanent coercive force and remanent acquisition coercive force respectively) all show smooth increasing trends with decreasing grain size in accordance with a gradual transition from MD to SD structures. The low field susceptibility decreases with grain size from $31*10^{-6}$ to $13*10^{-6}$ m^3kg^{-1}. J_{rs} increases with decreasing grain size; in the smallest grain-size fractions a decrease was observed. The J_{rs}/J_s ratio increases with decreasing grain size from 0.23 to 0.58, only the smallest grain-size fraction showed an anomalous low figure for this ratio (attributed by Clark to the presence of superparamagnetic grains in this fraction). The theoretical single domain J_{rs}/J_s ratio, assuming a unique hard axis and triaxial symmetry in the basal plane is calculated to be 0.75 (Dunlop, 1971).

6 IMPLICATIONS FOR THE PRESENT STUDY

The pyrrhotite rockmagnetic characteristics, in a grain-size dependent framework, are rather poorly documented up till now. Clark's (1984) study, the single one reporting pyrrhotite grain-size dependence, refers to pure monoclinic pyrrhotite. For mixed pyrrhotite no grain-size dependent data exist at all. The present research intends to contribute to the knowledge of the grain-size dependence of some important rockmagnetic parameters (J_s, J_{rs}, H_c, H_{cr} and X_{in}) of natural pyrrhotite. Also the low- and high-temperature behaviour of a room temperature induced saturation remanence will be compared with TRM (induced in the geomagnetic field) behaviour.

7 REFERENCES

Arnold R.G., Reichen L.E., 1962, Measurement of the metal content of naturally occurring metal deficient hexagonal pyrrhotite by an X-ray spacing method, Am. Min. 47, 105-11.

Bennett C.E.G., Graham J., 1980, New observations on natural pyrrhotites. Part III. Thermomagnetic experiments, Am. Min. 65, 800-7.

Bennett C.E.G., Graham J., 1981, New observations on natural pyrrhotites: magnetic transition in hexagonal pyrrhotite. Am. Min. 66, 1254-7.

Bennett C.E.G., Graham J., Thornber M.R., 1972, New observations on natural pyrrhotites. Part I: Mineragraphic techniques, Am. Min. 57, 445-61.

Bertaut E.F., 1953, Contribution à l'étude des structures lacunaires: la pyrrhotine, Acta Cryst. 6, 557-61.

Carpenter R.H., 1974, Pyrrhotite isograde in SE Tennessee and SW North Carolina, Geol. Soc. Amer. Bull. 85, 451-76.

Chikazumi S., 1964, Physics of magnetism, John Wiley and Sons, New York, 554pp.

Clark D.A., 1984, Hysteresis properties of sized dispersed monoclinic pyrrhotite grains, Geophys. Res. Letters 11, 173-6.

Craig J.R., Scott S.D., 1974, Sulphide phase equilibria, in Ribbe P.H. ed., Sulfide Mineralogy, Mineral. Soc. America short course notes Vol 1, CS1-CS110.

Dunlop D.J., 1971, Magnetic properties of fine grained hematite, Ann. Géophys. 27, 269-93.

Engel R.F., Peacor D.R., Kelly W.C., 1978, A new 5C pyrrhotite, Am. Min. 63, 1274-77.

Fleet M.E., 1978, The pyrrhotite-marcasite transformation, Can. Min. 16, 31-5.

Fleet M.E., MacRae N., 1969, Two phase hexagonal pyrrhotites, Can. Min. 9, 699-705.

Freeman R., 1986, Magnetic mineralogy of pelagic limestones, Geophys. J. R. astr. Soc. 85, 433-52.

Haigedahl S.L., Fuller M., 1981, The dependence of magnetic domain structure upon magnetization state in polycrystalline pyrrhotite, Phys. Earth Planet. Inter. 26, 93-7.

Helgedahl S.L., Fuller M., 1983, The dependence of magnetic domain structure upon magnetization state with emphasis upon nucleation as a mechanism for pseudo-single-domain behaviour, J. Geophys. Res. B 88, 6505-22.

Hayase K., Otsuka R., Mariko T., 1963, Magnetic properties of natural pyrrhotite, Mineral. J. (Tokyo) 4, 41-56.

Kissin S.A., Scott S.D., 1982, Phase relations involving pyrrhotite below 350 °C, Econ. Geol. 77, 1739-54.

Kligfield R., Channell J.E.T., 1981, Widespread remagnetization of Helvetic limestones, J. Geoph. Res. B 86, 1888-1900.

Koto K., Morimoto N., Gyobu A., 1975, The superstructure of the intermediate pyrrhotite. I. Partially disordered distribution of metal vacancies in the 6C type, $Fe_{11}S_{12}$, Acta Cryst. B 31, 2759-64.

Marusek L.A., Mulay L.N., 1980, Polytypism in the cation-deficient iron sulphide, Fe_9S_{10}, and the magnetokinetics of the diffusion process at temperatures about the antiferro- to ferrimagnetic (λ) phase transition, Phys. Rev. B 21, 238-44.

Morimoto N., Gyobu A., Tsukuma K., Koto K., 1975A, Superstructure and non-stoichiometry of intermediate pyrrhotite, Am. Min. 60, 240-8.

Morimoto N., Gyobu A., Mukaiyama H., Izawa E., 1975B, Crystallography and stability of pyrrhotites, Econ. Geol. 70, 824-33.

Morimoto N., Nakazawa H., Nishiguchi K., Tokonami M., 1970, Pyrrhotites: stoichiometric compounds with composition $Fe_{n-1}S_n$ (n GE 8), Science 168, 964-6.

Morimoto N., Nakazawa H., Watanabe E., 1974, Direct observation of metal vacancy in pyrrhotite $Fe_{1-x}S$, by means of an electron microscope, Proc. Japan Acad. 50, 756-9.

Nakazawa H., Morimoto N., 1970, Pyrrhotite phase relations below 320 °C, Proc. Japan Acad. 46, 678-83.

Nakazawa H., Morimoto N., 1971, Phase relations and superstructures of pyrrhotite $Fe_{1-x}S$, Mat. Res. Bull 6, 345-58.

Naldrett A.J., Kullerud G., 1967, A study of the Strathcona mine and its bearing on the origin of the nickel-copper ores of the Sudbury district, Ontario, J. Petrol. 8, 453-534.

Onufrienok V.V., Zvegintsev A.G., 1981, Magnetic ordering in hexagonal pyrrhotite at high temperature, Geomagn. Aeron. (USSR) 21, 666-8 (eng. ed.).

Pierce L., Buseck P.R., 1974, Electron imaging of pyrrhotite superstructures, Science 186, 2209-12.

Rochette P., 1987, Metamorphic control of the magnetic mineralogy of Black Shales in the Swiss Alps: toward the use of "magnetic isograde", Earth Plan. Sci. Letters 84, 446-56.

Schouten C., 1962, Determination tables for ore microscopy, Elsevier Sci. Publ. Comp. Amsterdam - New York, 242pp.

Schwarz E.J., 1965, Thermomagnetic properties of sulphide ore from the Noranda area, Canada, measured with a magnetic balance, Can. J. Phys. 43, 220-6.

Schwarz E.J., 1967, Dependence of the magnetic properties on the thermal history of natural polycrystalline pyrrhotites $Fe_{0.89}S$, J. Geomagn. Geoelectr. 19, 91-101.

Schwarz E.J., 1968, Magnetic phases in natural pyrrhotite $Fe_{0.91}S$ and $Fe_{0.89}S$, J. Geomagn. Geoelectr. 20, 67-74.

Schwarz E.J., 1969, Thermomagnetics of pyrrhotite, Geol. Surv. of Can. Paper 69-1B, 41-4.

Schwarz E.J., 1975, Magnetic properties of pyrrhotite and their use in applied geology and geophysics, Geol. Surv. Can. Paper 74-59, 24pp.

Schwarz E.J., Harris D.C., 1970, Phases in natural pyrrhotite and the effect of heating on their magnetic properties, J. Geomagn. Geoelectr. 22, 463-70.

Schwarz E.J., Vaughan D.J., 1972, Magnetic phase relations of pyrrhotite, J. Geomagn. Geoelectr. 24, 441-58.

Scott S.D., Kissin S.A., 1973, Sphalerite composition in the Zn-Fe-S system below 300 °C, Econ. Geol. 68, 475-79.

Soffel H.C., 1977, Pseudo-single domain effects and single-domain multidomain transition in natural pyrrhotite deduced from domain structure observations, J. Geophys. 42, 351-9.

Soffel H.C., 1981, Domain structure of natural fine-grained pyrrhotite in a rock matrix (diabase), Phys. Earth Plan. Inter. 26, 98-106.

Sugaki A., Shima H., 1977, Studies on pyrrhotite group minerals (3). On solvuses of solid solutions among troilite, hexagonal and monoclinic pyrrhotites below 300 °C, Tohoku Univ. Sci. Rept. ser 3 13, 165-82.

Taylor L.A., Williams K.L., 1972, Smythite, $(Fe,Ni)_{3.25}S_4$ - a redefinition, Am. Min. 57, 1571-77.

Thompson J.F.H., Nixon F., Sivertsen R., 1980, The geology of the Vakkerlien Nickel Prospect, Kvikne, Norway, Bull. Geol. Soc. Finland 52, 3-21.

Toulmin P. III, Barton P.B. jr., 1964, A thermodynamic study of pyrite and pyrrhotite, Geochim. Cosmochim. Acta 28, 641-71.

Vaughan D.J., Schwarz E.J., Owens D.R., 1971, Pyrrhotites from the Strathcona Mine, Sudbury, Canada: A thermomagnetic and mineralogical study, Econ. Geol. 66, 1131-44.

Yund R.A., Hall H.T., 1969, Hexagonal and monoclinic pyrrhotites, Econ. Geol. 64, 420-3.

CHAPTER 7

SAMPLE PREPARATION AND CHARACTERIZATION OF THE PYRRHOTITES

1 INTRODUCTION

Pyrrhotite abundances in rocks are generally extremely low, apart from pyrrhotite-bearing sulphidic ores. For the magnetic experiments pyrrhotite was therefore collected from those ores. Various ore types were sampled: An orthomagmatic disseminated Fe-Ni-Cu ore (Isola di Vocca, Sesia Valley, Ivrea Zone, Italy; abbreviation: DIS), re-heated volcano-sedimentary pyritic ores (Ortano and Ginevro, both from Elba, Italy; abbreviations respectively: EOR and EGI) and a pyrite-pyrrhotite-chalcopyrite-bearing pyrometasomatic ore (Temperino, Tuscany, Italy; abbreviation: TTE). A concise description of the samples is given in chapter eight; some background information concerning sample locations can be found in appendix 1.

2 SEPARATION PROCEDURE

Grain-size fractions of pyrrhotite were obtained from ore samples in a basically similar way as the goethite grain-size fractions (cf. chapter 2). Crushing of the raw samples and the first sieving step were done in air. Heavy liquid separation was not performed because the amount of light grains in the raw sample was negligible.

Pyrrhotite readily tarnishes in a moist oxygenated atmosphere. Sample treatment should therefore be carried out in a water-free environment, preferably under an inert atmosphere throughout the separation procedure. Therefore the pyrrhotite grain-size fractions were stored in an argon atmosphere during and after the separation procedure. No alteration of the pyrrhotite grains was observed during storage for periods up to 18 months, the time-interval in which the magnetic experiments were performed.

It appeared during the magnetic separation that the TTE, EOR and EGI pyrrhotites had a high magnetic susceptibility. The DIS pyrrhotite had a much lower susceptibility. Separation of the grains of the former three pyrrhotites in a Franz-isodynamic separator was greatly hindered by magnetic clustering of the grains leading to clogging of the separation tube. Therefore pyrrhotite was concentrated from the coarse grain-size fractions (> 37 micrometer) by moving a hand magnet quickly back- and forwards over the crushed rock sample at a distance of a few centimeters. A certain amount of non-pyrrhotite minerals was also attracted by the magnet. By repeating this procedure up to ten times, pyrrhotite concentrates of a high purity were obtained (>> 95 %, optical control, transmittent light). The DIS sample was separated with the Franz Isodynamic Separator according to the procedure described in chapter two. Each raw grain-size fraction was separated two times.

The fine grain-size fractions (< 37 micrometer) were separated with the equipment described in Dekkers et al. (in prep.); the separation tube was placed at a distance of one centimeter from the Franz Isodynamic Separator to avoid clogging of the grains, when separating the EGI, TTE and EOR samples. The DIS sample could be treated with the separation tube attached to the Franz magnet.

Ultrasonic microprecision sieving was carried out under a CO_2 atmosphere to prevent oxidation of the small grains (when microsieving in air, small pyrrhotite grains oxidize instantaneously) according to the procedure described in chapter two. To remove small, magnetically ad-

hered grains from large grains (> 75 micrometer) the grains were several times over a longer period exposed to ultrasonic waves (up to seven times up to 60 seconds); it turned out that no ultrasonic damage was done to the grains. The grain size of each fraction was checked optically (transmittent light); sieving was repeated until the amount of grains smaller than the lower limit of each fraction was less than one percent. The amount of intergrowths (ubiquitous in the coarse grain-size fractions of the DIS pyrrhotite) and the magnetite impurity contents (in the EGI fractions) were established by point counting (reflected light). Results are compiled in Table I.

Table I: Amount of intergrowths, pyrrhotite and magnetite contents of the pyrrhotite grain-size fractions.

	TTE			EOR			DIS			EGI		
fraction	po	mg	int.	po	mg	int.	po	mg	int.	po	mg	int.
250 - 150	>99	bd	bd	>99	bd	bd	31	bd	100	78	22	bd
150 - 100	>99	bd	bd	>99	bd	bd	48	bd	90	78	22	bd
100 - 75	>99	bd	bd	>99	bd	bd	72	bd	50	80	20	bd
75 - 55	>99	bd	bd	>99	bd	bd	63	bd	50	81	19	bd
55 - 40	>99	bd	bd	>99	bd	bd	70	bd	30	81	19	bd
40 - 30	>99	bd	bd	>99	bd	bd	88	bd	10	86	14	bd
30 - 25	>99	bd	bd	>99	bd	bd	94	bd	<5	86	14	bd
25 - 20	>99	bd	bd	>99	bd	bd	96	2	bd	84	16	bd
20 - 15	>99	bd	bd	92	bd	bd	97	1	bd	92	8	bd
15 - 10	95	bd	bd	80	bd	bd	90	2	bd	83	9	bd
10 - 5	65	bd	bd	70	bd	bd	59	1	bd	78	6	bd
< 5	60	bd	bd	60	bd	bd	57	bd	bd	54	3	bd

Volume percentages; grain sizes in micrometer; po = pyrrhotite; mg = magnetite; int. = intergrowths; bd = below limit of detection (< ±1%). The percentages refer to the total sample. The difference between the sum of the pyrrhotite and magnetite percentages and 100 percent is the percentage silicate minerals remaining in each fraction. The intergrowth percentage refers to the amount of pyrrhotite grains which are intergrown with silicate minerals.

3 CHARACTERIZATION OF THE PYRRHOTITES

The high susceptibility of the TTE, EOR and EGI pyrrhotites implies that they are monoclinic (or contain a dominating monoclinic phase in case of a composite pyrrhotite). The DIS pyrrhotite should contain hexagonal pyrrhotite (with possibly minor monoclinic pyrrhotite). Monoclinic pyrrhotite is the most iron-deficient pyrrhotite (Fe_7S_8); hexagonal pyrrhotite contains more iron (or equivalent atoms such as Ni and Cu). These differences are confirmed by microprobe and X-ray diffraction analyses.

3.1 Chemical composition

Microprobe (MP) analyses (compiled in Table II) reflect the differences outlined above. TTE and EOR pyrrhotite (respectively 46.97 and 46.86 atom % Fe_{eq} = equivalent Fe, i.e. Fe + Ni + Cu + Zn + Mn) approach the ideal monoclinic pyrrhotite composition (46.67 atom % Fe) best. EGI pyrrhotite contains slightly more Fe_{eq} (47.15 atom %) and DIS pyrrhotite has the highest Fe_{eq} content (47.75 atom %). Apart from Ni, contents of other non-Fe elements are insignificant in pyrrhotite samples. The Ni- content is most high in DIS pyrrhotite (0.39 atom % or 0.52 weight %), in TTE and EOR pyrrhotite Ni-amounts are close to the

limit of detection; EGI pyrrhotite has a slightly raised Ni content (0.27 atom % or 0.41 weight %). The low trace-element content is confirmed by the wet- chemical (WC) analyses (cf. Table III). DIS pyrrhotite has by far the highest Ni-, Cu-, Co- and Mn-contents. The relatively high Co-content reflects its orthomagmatic origin. The difference in Cu between the MP and the WC analyses can be due to traces chalcopyrite enclosed in the pyrrhotite. The differences also indicate that the number of spot analyses has to be fairly high to obtain reasonable contents below 0.3 weight percent, when performing microprobe measurements. Considering standard deviations TTE, EOR and EGI pyrrhotite have approximately similar compositions and DIS pyrrhotite is distinctly Fe-richer than the other three.

Table II: Average pyrrhotite composition determined by microprobe analyses

	TTE			EOR			DIS			EGI		
	aver.	st.d.	norm.	aver.	st.d.	norm.	aver.	st.d.	norm.	aver.	st.d.	norm.
S	53.03	0.19	39.27	53.14	0.35	39.39	52.25	0.30	38.47	52.85	0.23	39.04
Fe	46.76	0.18	60.32	46.70	0.36	60.30	47.41	0.29	60.80	46.95	0.34	60.41
Mn	0.02	0.03	0.02	0.01	0.02	0.01	0.01	0.02	0.01	0.02	0.03	0.02
Ni	0.17	0.14	0.23	0.14	0.10	0.19	0.39	0.11	0.52	0.27	0.08	0.41
Cu	0.06	0.09	0.09	0.03	0.05	0.04	0.05	0.06	0.07	0.04	0.06	0.06
Zn	0.04	0.08	0.06	0.04	0.08	0.06	0.08	0.13	0.12	0.04	0.08	0.06
total	100.08		99.99	100.06		99.99	100.19		99.99	100.18		100.00

Analyses were carried out with a TPD (Technisch Physische Dienst) microprobe fitted with a TRACOR Northern Energy Dispersive (ED) system. Operating conditions were 15 keV and 2 - 3 nA. ZAF matrix correction was applied. aver. = average atom percentage; st.d. = standard deviation; norm. = normalized weight percentage. Most spots contained no detectable Mn, Cu and Zn. Ni is enhanced in the DIS pyrrhotite and slightly raised in EGI pyrrhotite; in the others its amount is insignificant. TTE 32 spot analyses; EOR 21 analyses; DIS 16 analyses; EGI 16 analyses. Fe_7S_8 contains 53.33 atom % S (4C superstructure); Fe_8S_9 52.94 atom % S; Fe_9S_{10} 52.63 atom % S (5C); $Fe_{10}S_{11}$ 52.38 atom % S (11C) and $Fe_{11}S_{12}$ 52.17 atom % S (6C).

Table III: Trace element content (wet chemical) ppm

	TTE	EOR	DIS*	EGI
Co	215	320	755	440
Pb	<dl	<dl	<dl	<dl
Ba	<dl	<dl	<dl	<dl
Mn	430	85	815	285
V	<dl	<dl	528	<dl
Zn	795	<dl	325	<dl
Cu	<dl	715	3220	835
Ni	85	130	2430	205
Cr	< dl	<dl	<dl	<dl

* The DIS sample contains 37 percent non-pyrrhotite minerals (almost exclusively silicates, >99 percent). Analyses were carried out by the Service Laboratory, Institute of Earth Sciences, State University of Utrecht. All elements were analyzed with ICPES (Induction Coupled Plasma Emission Spectrometry); the limit of detection for each element is approximately 10 ppm.

Assuming stoichiometric compositions for the 4C, 5C and 6C pyrrhotites the relative abundance of ferrimagnetic (4C) and antiferromagnetic

(5C, 11C and 6C) pyrrhotite in the samples can be calculated from the MP analyses. Results are compiled in Table IV.

Table IV: estimate of the relative abundances of ferri- and antiferromagnetic pyrrhotite

	4C/(4C + 5C)	4C/(4C + 6C)	$4C^*/(4C^* + 5C)$	$4C^*/(4C^* + 6C)$
TTE	57	74	--	--
EOR	73	81	--	--
DIS	0	0	0	10
EGI	31	59	71	88

Contents are in percentages and refer to the abundance of the 4C phase. 4C is assumed to be Fe_7S_8; 5C: Fe_9S_{10}; 6C: $Fe_{11}S_{12}$. $4C^*$ is assumed to be Fe_8S_9. For TTE and EOR calculation with $4C^*$ would result in negative $4C^*$ abundances for both samples. The actual abundance of each superstructure type is in between the values listed in Table IV, depending on the actual composition of the coexisting pyrrhotite superstructures.

3.2 XRD-features

All pyrrhotites are well-crystalline; reflections used for the calculation of the unit cells are listed in Table V. The monoclinic reflection at d = approx. 2.04 Å (in the hexagonal structure the reflections at d = 2.058 and d = 2.04 Å coincide) is distinctly stronger in the TTE, EOR and EGI samples than in the DIS sample. This indicates that the ferrimagnetic 4C phase is more abundant in the former three pyrrhotites. The dimensions of the pyrrhotite unit cell and of the basic NiAs-cell are given for each sample in Table VI.

Table V: d-spacings pyrrhotite reflections used for unit cell calculation

indices	TTE 4C	EOR 4C	DIS 4C	DIS 5C	DIS 6C	EGI 4C
220, 400	2.9513	2.9461	2.9550	200	200	2.9528
±404, ±224	2.6209	2.6140	2.6209	205	206, 00<u>13</u>	2.6192
-408, -228	2.0585	2.0545	2.0565	10<u>13</u>, 20<u>10</u>	20<u>12</u>	2.0589
408, 228	2.0415	2.0379	2.0412	---	---	2.0438
040, 620	1.7130	1.7108	1.7139	220	30<u>10</u>, 220	1.7147

4C, 5C and 6C refer to the pyrrhotite superstructure.

D-spacings of the reflections agree with literature data (e.g. Vaughan et al., 1971; Desborough and Carpenter, 1965). β-angles concur with those reported in literature (β = 90.45; cf. Ward, 1970). The cell dimensions of the present pyrrhotites are slightly smaller than those reported by Ward (op. cit.). Cell dimensions of the basic NiAs- cells of the present pyrrhotites are in good agreement with reported ones (a-axis 3.45 Å and c-axis 5.75 Å; cf. Nakazawa and Morimoto, 1971; Engel et al., 1978; Deer et al., 1980).

Table VI: Unit cell dimensions of the pyrrhotite samples

	TTE 4C	EOR 4C	DIS 4C	DIS 5C	DIS 6C	EGI 4C
a-axis	11.840 ± 0.007	11.818 ± 0.007	11.847 ± 0.007	6.846 ± 0.003	6.852 ± 0.004	11.843 ± 0.007
b-axis	6.845 ± 0.004	6.835 ± 0.004	6.849 ± 0.004	6.846 ± 0.003	6.852 ± 0.004	6.850 ± 0.004
c-axis	22.706 ± 0.013	22.656 ± 0.013	22.669 ± 0.013	28.504 ± 0.014	34.131 ± 0.018	22.720 ± 0.013
volume	1840 ± 1	1830 ± 1	1839 ± 1	1156 ± 1	1387 ± 1	1843 ± 1
α	90.00 ± 0.015	90.00 ± 0.014	90.00 ± 0.015	90.00 ± 0.000	90.00 ± 0.000	90.00 ± 0.015
β	90.410 ± 0.000	90.409 ± 0.000	90.369 ± 0.000	90.00 ± 0.000	90.00 ± 0.000	90.369 ± 0.000
γ	90.00 ± 0.000	90.00 ± 0.000	90.00 ± 0.000	120.00 ± 0.013	120.00 ± 0.014	90.00 ± 0.000
NiAs-cell						
a-axis	3.42	3.42	3.42	3.42	3.43	3.42
c-axis	5.68	5.66	5.67	5.70	5.69	5.68

Cell dimensions are in Å; cell volumes in $Å^3$. 4C, 5C and 6C refer to the pyrrhotite superstructure.

The position of the hexagonal d_{102} reflection is composition-dependent (e.g. Arnold, 1967; Yund and Hall, 1969). Hence, it can be used for the determination of the pyrrhotite chemical composition. Before the X-ray run to determine the d_{102} reflection was performed, the pyrrhotites were converted to monophase hexagonal pyrrhotite of the same overall composition by heating in vacuo to 350 °C (the exsolution of monoclinic pyrrhotite to pyrite and a Fe-richer pyrrhotite is kinetically inhibited for the duration of the annealing) and subsequently quenched (Arnold, 1967). The single peak hexagonal d-spacings were fitted with the Yund and Hall (1969) calibration curve. Si was used as internal standard. Results are compiled in Table VII. This method yielded somewhat lower Fe-contents than those determined with the microprobe, although the differences for TTE, EOR and EGI pyrrhotite are relatively small. The largest difference is observed in the DIS pyrrhotite sample, in which hexagonal pyrrhotite should prevail because of its low magnetic susceptibility. A reason for this bias could be the fact that the Yund and Hall (1969) calibration curve was determined with extremely pure pyrrhotite compositions (analytical grade reagents were used for the pyrrhotite synthesis); lower Fe-contents in the present pyrrhotite could be due to the presence of non-Fe elements (esp. Ni) in the present natural pyrrhotites. The amount of non-Fe elements is most high in the DIS pyrrhotite. It is therefore believed that the Fe-contents determined with the XRD method, are too low.

Table VII: Atomic percentage iron calculated with the XRD method.

	d_{102}	Fe at.%
TTE	2.0583	46.65
EOR	2.0591	46.72
DIS	2.0588	46.69
EGI	2.0588	46.69

Debye-Scherrer camera; Fe K_α-rays.

4 PREPARATION OF THE ARTIFICIAL SAMPLES

Room and low temperature experiments were carried out with artificial samples of pyrrhotite dispersed in an epoxy resin matrix (araldit D, hardener HY 956; Cyba-Geigi). These samples were standard sized paleomagnetic samples and contain approximately 100 mg pyrrhotite (approximately 0.2 volume percent). The dimensions for the high field experiments were small cylinders of 5 mm height and 4.5 mm diameter (sizes of the sample holder). They contained 5 to 6 mg pyrrhotite (approximately 2 volume percent). These small samples were sized down on a lathe from larger specimens. Pyrrhotite saturation remanences per unit mass for both specimen types appeared to be similar, so particle-interaction will not dominate the derived rockmagnetic parameters.

For thermal experiments, pyrrhotite was first dispersed in a calciumcarbonate-waterglass mixture (with ascorbic acid added, a moderate reducing agent to maintain reducing conditions within the specimen). Hardening was done in a CO_2 atmosphere to accelerate its speed and to keep the oxygen concentration low. After being hardened, the specimens appeared to be extremely fragile and needed a re-enforcement to withstand routine sample handling. This was achieved by soaking the specimens in waterglass once more. However, the results of trial measurements were ambiguous. Microscopic investigation revealed alteration halo's around the pyrrhotite grains (reflected light). Consequently, it was obligatory to look for another non-magnetic medium for thermal experiments.

After having tested various non-magnetic materials, CM Löt soldering investment (dental cement) was selected for thermal experiments. This material is a mixture of bassanite ($CaSO_4.0.5H_2O$) and quartz (XRD determination). It can withstand temperatures up to 1700 °C. It is reasonably non-magnetic (J_{rs} is approximately $4 * 10^{-4}$ Am^2kg^{-1}, the lowest remanence of all materials tested). This matrix remanence does not contribute too much to the total remanence when dealing with the strongly magnetic pyrrhotite. However, the soldering investment is too magnetic for meaningful experiments with much weaker magnetic minerals such as hematite and goethite.

Hardening is achieved within ten minutes by adding small amounts of demineralized water while stirring. Hence, the reaction time for pyrrhotite alterations is short. Pyrrhotite saturation remanences and initial susceptibilities measured in epoxy resin specimens and soldering investment yielded equal results, so the pyrrhotite grains are not altered during the hardening of the latter matrix. Because of the fast hardening, pyrrhotite grains should be dispersed homogeneously in the matrix before adding demineralized water. Also for the thermal experiments each standard sized specimen contained some 100 mg pyrrhotite.

5 REFERENCES

Arnold R.G., 1967, Range in composition and structure of 82 natural terrestrial pyrrhotites, Can. Min. 9, 31-50.

Deer W.A., Howie R.A., Zussmann J., 1980, An introduction to the rock-forming minerals, Longman London, 528pp.

Dekkers M.J., Hartstra R.L., Mullender T.A.T., in prep., A device for the magnetic separation of fine-grained particles.

Desborough G.A. Carpenter R.H., 1965, Phase relations of pyrrhotite, Econ. Geol. 60, 1431-50.

Engel R.F., Peacor D.R., Kelly W.C., 1978, A new 5C pyrrhotite, Am. Min. 63, 1274-7.

Nakazawa H., Morimoto N., 1971, Phase relations and superstructures of pyrrhotite, $Fe_{1-x}S$, Mat. Res. Bull. 6, 345-58.

Vaughan D.J. Schwarz E.J., Owens D.R., 1971, Pyrrhotites from the Strathcona Mine, Sudbury, Canada: A thermomagnetic and mineralogical study, Econ. Geol. 66, 1131-44.

Ward J.C, 1970, The structure and properties of some iron sulphides, Rev. Pure Appl. Chem. 20, 175-206.

Yund R.A., Hall H.T, 1969, Hexagonal and monoclinic pyrrhotites, Econ. Geol. 64, 420-3.

CHAPTER 8

MAGNETIC PROPERTIES OF NATURAL PYRRHOTITE PART I: BEHAVIOUR OF INITIAL SUSCEPTIBILITY AND SATURATION-MAGNETIZATION RELATED ROCKMAGNETIC PARAMETERS IN A GRAIN-SIZE DEPENDENT FRAMEWORK.

Abstract

The grain-size dependence of the initial susceptibility (X_{in}), saturation magnetization (J_s), saturation remanence (J_{rs}), coercive force (H_c), remanent coercive (H_{cr}) and remanent acquisition coercive ($H_{cr'}$) is reported for four natural pyrrhotites in a grain size range from 250 micrometer down to <5 micrometer. X_{in} decreases with grain-size (range $7*10^{-5}$ - $1*10^{-5}$ m^3kg^{-1}); H_c, H_{cr} and $H_{cr'}$ all increase with decreasing grain size (ranges respectively 7 - 80, 8 - 85 and 14 - 80 kAm^{-1}). The magnitudes of J_s (8.9 to 16.7 Am^2kg^{-1}) and J_{rs} (2.0 - 6.0 Am^2kg^{-1}) correspond with the trend indicated by the microprobe analyses (47.8 down to 46.9 atom percent equivalent Fe). J_{rs} shows a maximum in the PSD region (range 2.0 - 6.0 Am^2kg^{-1}). J_s shows a marked decrease for the finest grain-size fractions. Typical for pyrrhotite are a large H_c/H_{cr} ratio and a J_{rs}/X_{in} ratio which is larger than H_{cr}. When the presence of pyrrhotite has been established in a sample, its grain size is preferably determined by the H_{cr} trend because pyrrhotite compositional differences hardly show up in this trend.

1 INTRODUCTION

The solid solution series of Fe-S compounds of composition $Fe_{1-x}S$, with x varying between zero and 0.13, is usually referred to as pyrrhotite. Nearly stoichiometric FeS is known as troilite (an Fe-deficiency between 0.003-0.006 formula units is reported, cf. Ward, 1970). Though the pyrrhotite potential of carrying a remanent magnetization is well-established for a long time (e.g. Bertaut, 1953), pyrrhotite was long-time regarded as a magnetic mineral of minor paleomagnetic importance, because it was believed to occur almost exclusively in relation with sulphidic ores. However, the existence of pyrrhotite without spatial relation with these ores is increasingly reported. It is nowadays known from various types of igneous rocks (e.g. Soffel, 1977), in metamorphic rocks (e.g. Carpenter, 1974; Rochette, 1987) and also in sediments (e.g. Kligfield and Channell, 1981; Freeman, 1986). This considerably increases the paleomagnetic significance of pyrrhotite.

The pyrrhotite crystal structure consists of alternating iron and sulphur layers, based on the NiAs crystal structure. The atoms in each Fe-layer are ferromagnetically coupled; antiferromagnetic coupling exists with each neighbour Fe-layer. The crystallographic c-axis is the hard axis of magnetization; the easy directions are confined to the basal plane which shows a (strong) trigonal anisotropy (Bin and Pauthenet, 1963). The initial susceptibility is extremely anisotropic with magnetite-like figures in the basal plane and paramagnet-like figures along the hard axis (Schwarz, 1975). All iron in pyrrhotite is ferrous iron and the valence of sulphur is less than two (Ward, 1970). Pyrrhotite contains a certain amount of vacancies depending on its chemical composition. The most Fe-deficient pyrrhotite (Fe_7S_8) has a monoclinic crystal structure; the more Fe-rich pyrrhotites are hexagonal.

Since the vacancies show some tendency to concentrate in alternate Fe-layers (Goodenough, 1978), the vacancy distribution has direct consequences for the pyrrhotite magnetic properties. The vacancy distribution

can be described by so-called superstructures. The more common integral superstructures are the 4C superstructure for the ferrimagnetic monoclinic Fe_7S_8 (Bertaut, 1953) and 5C, 11C and 6C superstructures for the antiferromagnetic hexagonal pyrrhotite (e.g. Fleet and MacRae, 1969; Morimoto et al., 1970, 1975A). Also non-integral superstructures, previously thought to occur only at elevated temperatures, are also reported at ambient temperatures (e.g. Morimoto et al., 1975A, 1975B).

Natural pyrrhotite usually consists of mixtures of superstructures of monoclinic and hexagonal pyrrhotite (e.g. Arnold, 1967), which results in an intermediate overall composition. Different superstructures can co-exist within a single pyrrhotite crystal. This can be detected with X-ray methods (e.g. Morimoto et al., op. cit.), with high resolution electron microscopy (e.g. Morimoto et al., 1974; Pierce and Buseck, 1974) or made visible microscopically by applying etching techniques (e.g. Naldrett and Kullerud, 1967).

The 4C pyrrhotite saturation magnetization is reported to be 20 Am^2kg^{-1} (e.g. Schwarz and Vaughan, 1972; Halgedahl and Fuller, 1981). Besnus and Meyer (1964) reported a saturation magnetization of 22.5 Am^2kg^{-1} for an unspecified natural pyrrhotite crystal. The saturation magnetization of mixed pyrrhotite depends on the content of 4C pyrrhotite present. Domain observations (Soffel, 1977, 1981; Halgedahl and Fuller, 1981) showed that 180 ° domain walls prevail in the pyrrhotite domain structure. Grains of approximately 100 micrometer size showed true multidomain (MD) behaviour; the range between 2-3 and 40 micrometer is regarded as pseudo-single domain (PSD) region. The SD/PSD border is found between 1.5 and 2 micrometer (Soffel, 1977). Clark (1984) calculated 3 micrometer for the SD/PSD transition. The coercive force for a large MD crystal is 9.0 kAm^{-1} (Halgedahl and Fuller, 1981) and for the PSD range 14.3 kAm^{-1} (Soffel, 1981). The ratio of the saturation remanence and saturation magnetization for the large MD crystal is reported to be 0.14 (Halgedahl and Fuller, 1981). Clark (1984) described hysteresis properties of sized monophase monoclinic 4C pyrrhotite fractions in a grain size range of 83 micrometer down to <3 micrometer. He found a steadily increasing coercive force (10.7-73.2 kAm^{-1}), remanent coercive force (14.7-113.4 kAm^{-1}) and remanent acquisition coercive force (21.5-106.6 kAm^{-1}) with decreasing grain size. The initial susceptibility decreases with grain size, whereas the saturation remanence increases with decreasing grain size down to 15 micrometer and subsequently decreases slightly with a further decrease in grain size.

Grain-size dependence of these and other rockmagnetic parameters for pyrrhotite is presently poorly documented: Clark's (1984) study is the only one which reports grain-size dependent trends in pyrrhotite. The present study reports the grain-size dependence of the saturation magnetization (J_s), saturation remanence (J_{rs}), the initial specific susceptibility (X_{in}) the coercive force (H_c) and remanent coercive force (H_{cr}) as well as the remanent acquisition coercive force ($H_{cr'}$) in a grain-size range from 250 micrometer down to smaller than 5 micrometer. Therefore a series of artificial samples using the methodology of Dankers (1978, 1981) and Hartstra (1982A) was prepared containing homogeneously dispersed natural pyrrhotite of a well-defined grain-size range.

1.1 Sample description and preparation of the artificial specimens

Pyrrhotite, belonging to various geologic associations, was selected for investigation from four locations. Pyrrhotite was sampled at Isola di Vocca (Ivrea Zone, Italy) from an orthomagmatic disseminated Fe-Ni-Cu ore in a noritic-gabbroic complex (cf. Rivalenti, 1979; Bigioggero et

al., 1979; Natale and Zuchetti, 1979; Ferrario et al., 1983); at Temperino (Tuscany, Italy) from a pyrometasomatic pyrrhotite-pyrite-chalcopyrite ore zone (cf. Bodechtel, 1965, 1968); and at Ortano and Ginevro (both on Elba, Italy) from re-heated, originally volcano-sedimentary, pyrite-hematite ores (cf. Bodechtel, 1965; Dimanche, 1971; Waldeck, 1977). All samples contained well-crystalline pyrrhotite. A concise description of each pyrrhotite sample is given below; for a more detailed overview the reader is referred to Dekkers (1988). Chemical and X-ray diffraction data of the pyrrhotites and the intergrowth amount are compiled for each final grain-size fraction in Tables I up to III.

1.1.1 Isola di Vocca (abbreviation DIS)

The DIS pyrrhotite belongs to a pyrrhotite-pentlandite-chalcopyrite ore assemblage with minor mackinawite, magnetite, ilmenite and sphalerite. The host rock mineralogy is dominated by olivine and pyroxenes. Magnetite occurs only accessory (<2%) in the pyrrhotite concentrate; pentlandite and chalcopyrite are hardly observed. The grains in the final fractions are approximately equidimensional. The larger grain-size fractions (> 30 micrometer) consist of pyrrhotite intergrown with silicates.

1.1.2 Temperino (abbreviation TTE)

The TTE pyrrhotite is concentrated from a pyrite/pyrrhotite skarn from a complex Cu-Zn bearing ore zone. Pyrrhotite and pyrite occur in a long prismatic habit in sheaf-like aggregates intergrown predominantly with ilvaite. The width of the sulfide parts is a few hundred micrometer. The pyrrhotite concentrates contain equidimensional grains. Intergrowths are rare, no magnetite is traced.

1.1.3 Ortano (abbreviation EOR)

Pyrrhotite, collected from the mine dumps at Ortano on the Eastern coast of Elba, is intergrown with epidote, ilvaite and minor hedenbergite. The pyrrhotite is well-developed in the skarn. The separated grain-size fractions consist of equidimensional pyrrhotite grains. The intergrowth amount is insubordinate; no magnetite is traced.

1.1.4 Ginevro (abbreviation EGI)

Pyrrhotite occurs as minor mineral in a magnetite/hedenbergite skarn at Ginevro on the South-Eastern coast of Elba. Pyrrhotite-rich parts of the skarn zone were sampled from the mine dumps. The final grain-size fractions consist of a mixture of equidimensional pyrrhotite and magnetite grains. They occur predominantly as separate monomineralic grains; the magnetite content decreases with grain size from 25 weight percent down to approximately 5 weight percent.

Table IA: Average pyrrhotite composition determined by microprobe analyses

	TTE			EOR			DIS			EGI		
	aver.	st.d.	norm.	aver.	st.d.	norm.	aver.	st.d.	norm.	aver.	st.d.	norm.
S	53.03	0.19	39.27	53.14	0.35	39.39	52.25	0.30	38.47	52.85	0.23	39.04
Fe	46.76	0.18	60.32	46.70	0.36	60.30	47.41	0.29	60.80	46.95	0.34	60.41
Mn	0.02	0.03	0.02	0.01	0.02	0.01	0.01	0.02	0.01	0.02	0.03	0.02
Ni	0.17	0.14	0.23	0.14	0.10	0.19	0.39	0.11	0.52	0.27	0.08	0.41
Cu	0.06	0.09	0.09	0.03	0.05	0.04	0.05	0.06	0.07	0.04	0.06	0.06
Zn	0.04	0.08	0.06	0.04	0.08	0.06	0.08	0.13	0.12	0.04	0.08	0.06
total	100.08		99.99	100.06		99.99	100.19		99.99	100.18		100.00

Analyses were carried out with a TPD (Technisch Physische Dienst) microprobe fitted with a TRACOR Northern Energy Dispersive (ED) system. Operating conditions were 15 keV and 2 - 3 nA. ZAF matrix correction was applied. aver. = average atom percentage; st.d. = standard deviation; norm. = normalized weight percentage. Most spots contained no detectable Mn, Cu and Zn. Ni is enhanced in the DIS pyrrhotite and slightly raised in EGI pyrrhotite; in the others its amount is insignificant. TTE 32 spot analyses; EOR 21 analyses; DIS 16 analyses; EGI 16 analyses. Fe_7S_8 contains 53.33 atom % S (4C superstructure); Fe_8S_9 52.94 atom % S; Fe_9S_{10} 52.63 atom % S (5C); $Fe_{10}S_{11}$ 52.38 atom % S (11C) and $Fe_{11}S_{12}$ 52.17 atom % S (6C).

Table IB: Pyrrhotite trace element content (wet chemical) ppm

	TTE	EOR	DIS*	EGI
Co	215	320	755	440
Pb	<dl	<dl	<dl	<dl
Ba	<dl	<dl	<dl	<dl
Mn	430	85	815	285
V	<dl	<dl	528	<dl
Zn	795	<dl	325	<dl
Cu	<dl	715	3220	835
Ni	85	130	2430	205
Cr	< dl	<dl	<dl	<dl

* The DIS sample contains 37 percent non-pyrrhotite minerals (almost exclusively silicates, >99 percent). Analyses were carried out by the Service Laboratory, Institute of Earth Sciences, State University of Utrecht. All elements were analyzed with ICPES (Induction Coupled Plasma Emission Spectrometry); the detection limit (dl) for each element is approximately 10 ppm. Comparison of Table IA and IB shows that the number of spots in the MP analyses is too low to obtain reasonable estimates for elements which are below 0.3 atom percent.

The pyrrhotite grain-size fractions were obtained by subsequent crushing, sieving, magnetic separation and ultrasonic micro-precision sieving. Crushing was performed in a copper mortar. The first sieving step was performed to optimize the magnetic separation step. The A.S.T.M. sieving set was used, wet-sieving was performed with acetone as flushing fluid. The coarse grain-size fractions (> 37 micrometer) of the TTE, EOR and EGI samples were separated by moving a hand magnet quickly back- and forwards over the sample at a few centimeters distance. The DIS fractions were separated magnetically with a Frantz-isodynamic separator adapted for separation in a liquid medium (ethanol was used). The fine grain-size fractions (<37 micrometer) were all separated with the aid of the modified Frantz-isodynamic separator; an input of the grains in suspended form was created (Dekkers et al., in prep.). Micro-precision sieving was carried out in an ultrasonic bath to remove fine,

magnetically adhered pyrrhotite particles from coarse ones. Each separation step was carried out as much as possible in an inert atmosphere, because pyrrhotite tarnishes easily in moist air. This applies especially for the micro-precision sieving step: when microsieving in contact with air pyrrhotite grains oxidize instantaneously. The grains disintegrate, colouring the acetone red brown. When sieving was performed in an inert atmosphere, no red-brown colouring of the acetone occurs and the pyrrhotite grains retain their typical brassy colour. After the separation procedure, the grain-size fractions were stored in an argon atmosphere.

Table II: Unit cell dimensions of the pyrrhotite samples

	TTE 4C	EOR 4C	DIS 4C	DIS 5C	DIS 6C	EGI 4C
a-axis	11.840 ± 0.007	11.818 ± 0.007	11.847 ± 0.007	6.846 ± 0.003	6.852 ± 0.004	11.843 ± 0.007
b-axis	6.845 ± 0.004	6.835 ± 0.004	6.849 ± 0.004	6.846 ± 0.003	6.852 ± 0.004	6.850 ± 0.004
c-axis	22.706 ± 0.013	22.656 ± 0.013	22.669 ± 0.013	28.504 ± 0.014	34.131 ± 0.018	22.720 ± 0.013
volume	1840 ± 1	1830 ± 1	1839 ± 1	1156 ± 1	1387 ± 1	1843 ± 1
α	90.00 ± 0.015	90.00 ± 0.014	90.00 ± 0.015	90.00 ± 0.000	90.00 ± 0.000	90.00 ± 0.015
β	90.410 ± 0.000	90.409 ± 0.000	90.369 ± 0.000	90.00 ± 0.000	90.00 ± 0.000	90.369 ± 0.000
γ	90.00 ± 0.000	90.00 ± 0.000	90.00 ± 0.000	120.00 ± 0.013	120.00 ± 0.014	90.00 ± 0.000
NiAs cell						
a-axis	3.42	3.42	3.42	3.42	3.43	3.42
c-axis	5.68	5.66	5.67	5.70	5.69	5.68

Cell dimensions are in Å; cell volumes in $Å^3$. The indicated errors are standard deviations. 4C, 5C and 6C refer to the pyrrhotite superstructure. In hexagonal pyrrhotite the 408 and -408 reflections coincide and have a d-value of approximately 2.06 Å, depending on the pyrrhotite chemistry. In monoclinic 4C pyrrhotite the 408 and -408 reflections show up as a doublet at approximately d = 2.06 and d = 2.04 Å. Both reflections of this doublet are of similar intensity in TTE, EOR and EGI pyrrhotite; the second (monoclinic) reflection is much weaker developed in the DIS pyrrhotite sample. This indicates that the ferrimagnetic 4C phase is less present in the latter sample than in the former three. A distinct lower susceptibility of the DIS pyrrhotite, observed during the magnetic separation step, is in agreement with the X-ray determination.

The results of the magnetic separation were checked optically (transmitted and reflected light) and with X-ray diffraction; the grain-size ranges were controlled optically (transmitted light). The grain-size fractions were homogeneously dispersed in an epoxy resin matrix (Araldit D-hardener HY 956, Cyba-Geigi) or in a quartz/bassanite matrix (CM Löt soldering investment for dental metal work). Susceptibility measurements were corrected for the diamagnetic matrix moment, no correction had to be made for the remanent magnetization of both matrixes. Approximately 100 mg pyrrhotite was put in standard-sized paleomagnetic specimens (0.2 percent by volume). Samples for high field susceptibility measurements were sized down on a lathe from epoxy resin cylinders initially both one centimeter diameter and height to cylinders of 4.5 mm diameter and 5 mm height. Each final cylinder contained some 5 mg pyrrhotite (2 percent by volume).

Table III: Amount of intergrowths, pyrrhotite and magnetite contents of the pyrrhotite grain-size fractions determined by point-counting (reflected light microscopy).

	TTE			EOR			DIS			EGI		
fraction	po	mg	int.	po	mg	int.	po	mg	int.	po	mg	int.
250 - 150	>99	bd	bd	>99	bd	bd	31	bd	100	78	22	bd
150 - 100	>99	bd	bd	>99	bd	bd	48	bd	90	78	22	bd
100 - 75	>99	bd	bd	>99	bd	bd	72	bd	50	80	20	bd
75 - 55	>99	bd	bd	>99	bd	bd	63	bd	50	81	19	bd
55 - 40	>99	bd	bd	>99	bd	bd	70	bd	30	81	19	bd
40 - 30	>99	bd	bd	>99	bd	bd	88	bd	10	86	14	bd
30 - 25	>99	bd	bd	>99	bd	bd	94	bd	<5	86	14	bd
25 - 20	>99	bd	bd	>99	bd	bd	96	2	bd	84	16	bd
20 - 15	>99	bd	bd	92	bd	bd	97	1	bd	92	8	bd
15 - 10	95	bd	bd	80	bd	bd	90	2	bd	83	9	bd
10 - 5	65	bd	bd	70	bd	bd	59	1	bd	78	6	bd
< 5	60	bd	bd	60	bd	bd	57	bd	bd	54	3	bd

Volume percentages; grain sizes in micrometer; po = pyrrhotite; mg = magnetite; int. = intergrowths; all in percentages; bd = below detection limit (< ±1%). The percentages refer to the total sample, in the fine grain size fractions silicate minerals remain present. The intergrowth percentage refers to the amount of pyrrhotite grains which are intergrown with silicate minerals.

1.2 Instrumentation for the magnetic measurements

Initial susceptibility was measured with a Jellinek KLY-1 susceptibility bridge. Acquisition curves of the isothermal remanent magnetization (RA curves) in fields up to 1600 kAm^{-1} (2 Tesla) were determined with a Förster fluxgate magnetometer type 1.107, which was calibrated with an astatic magnetometer. Hysteresis loops in a 240 kAm^{-1} field (0.3 Tesla) were determined by measuring the imbalance of a pair of coils, one of which contained the specimen. Measurements were carried out using an AC field. The determinations mentioned so far were carried out at the Paleomagnetic Laboratory "Fort Hoofddijk" (University of Utrecht, The Netherlands).

A field of only 240 kAm^{-1} is too small to obtain correct figures for the pyrrhotite saturation magnetization. Therefore magnetization curves were determined in fields up to 12000 kAm^{-1} (15 Tesla). Measurements in fields up to 1040 kAm^{-1} (1.3 Tesla) were done with a vibrating sample magnetometer (Foner type); in higher fields a ballistic magnetometer was employed. These high field measurements were carried out at the High Field Magnet Laboratory at the Department of Physics, University of Nijmegen (The Netherlands).

2 RESULTS

2.1 Susceptibility measurements

The susceptibility measurements were corrected for the diamagnetic moment of the matrix. Partial hysteresis loops in 240 kAm^{-1} fields (Fig. 1A) reveal that only the coarse grain size fractions (from the 75-55 micrometer fraction upwards) show a reversible magnetization behaviour in the highest fieldstrengths reached by this low field equipment. Finer grain-size fractions do not show such behaviour in fields up to 240 kAm^{-1}. The fieldstrength above which reversible behaviour is observed, increases with decreasing grain size. For the <5 micrometer

fractions this field is some 800 kAm^{-1} (Fig. 1B). Hence, such fields are required for a proper determination of the coercive force.

In extremely small applied fields the movement of the spontaneous magnetization from one easy direction to a more favourably positioned one is fairly difficult as is indicated by the onset of the magnetization curves (Fig. 1B) and the low initial susceptibility (Fig. 2, Table IV). Domain walls move relatively easy in pyrrhotite in somewhat larger applied fields as is indicated by the steep rise of the magnetization curves. In high applied fields the spontaneous magnetization is pulled out of the basal plane. This is opposed by a strong magnetocrystalline anisotropy. Large fields are required to saturate a set of randomly distributed pyrrhotite grains (Fig. 1C).

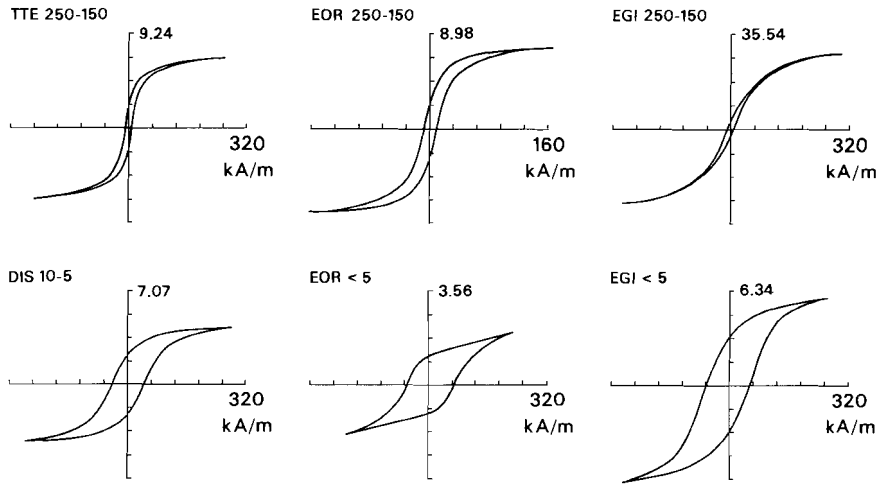

Fig. 1A. Partial hysteresis loops in 160 kAm^{-1} (0.2 Tesla) or 240 kAm^{-1} (0.3 Tesla) fields. The coarse grain-size fractions already behave reversibly in these small fields. The numbers on the ordinates refer to the magnetization in Am^2kg^{-1}.

Hysteresis loops of pyrrhotite are characterized by steep rising branches in small fields and much less steep continuations in higher fields leading to a more or less rectangular curve (Fig. 1A). Pyrrhotite hysteresis loops are much more rectangular than magnetite hysteresis loops: the branches of the hysteresis loop of the EGI 250-150 micrometer fraction containing 25 weight percent magnetite (as separate monomineralic grains) are much more gently increasing and decreasing with the external field than loops of samples without magnetite containing the same grain size range (e.g. TTE 250-150 micrometer and EOR 250-150 micrometer).

The initial susceptibility (X_{in}) is decreasing with grain size (Fig. 2 Table IV, cf. p. 154). Similar grain-size fractions of the different pyrrhotite samples have initial susceptibilities of the same order. The much larger X_{in} of the EGI samples is due to their magnetite content. The much more pronounced decreasing X_{in} trend with grain size in the EGI pyrrhotite fractions is also caused by a decreasing magnetite content with smaller grain size (cf. Table III). Figures for the pyrrhotite initial susceptibility are somewhat lower than Clark's (1984) figures

for pure ferrimagnetic 4C pyrrhotite. The more or less constant X_{in} in the DIS fractions for grain sizes larger than 30 micrometer is due to the presence of ubiquitous silicate intergrowths in these coarse fractions limiting the size of the pyrrhotite parts in these grains to approximately 30 micrometer.

The susceptibility of the hard axis, derived from the high field parts of the magnetization curves, is for EGI $34*10^{-8}$, for TTE $38*10^{-8}$, for EOR $38*10^{-8}$ and for DIS pyrrhotite $32*10^{-8}$ (all figures are in m^3*kg^{-1}). These figures are of the same order as those determined by Schwarz and Vaughan (1972).

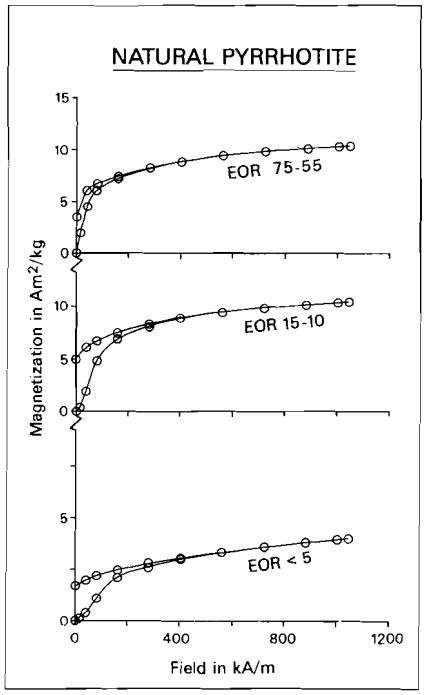

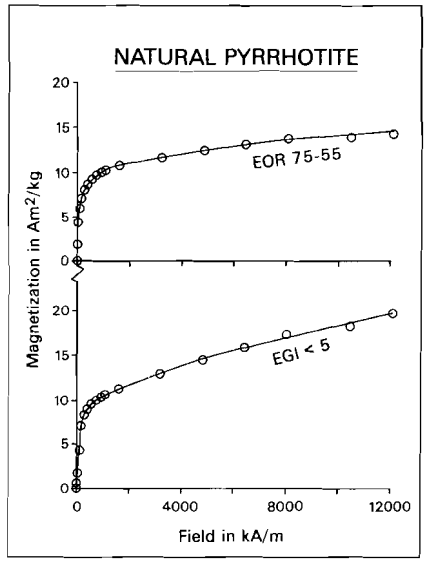

Fig. 1B. Magnetization curves in fields up to 1040 kAm^{-1} (1.3 Tesla). The fine grain-size fractions show reversible hysteresis behaviour in fields above some 800 kAm^{-1} (1 Tesla).

Fig. 1C. Magnetization curves in fields up to 12000 kAm^{-1} (15 Tesla). The coarse grain-size fractions tend to be saturated in this field, whereas the magnetization of the fine grain-size fractions still increases. The magnetizations are corrected for the diamagnetic matrix moment.

The saturation magnetization (J_s) is approximately grain-size independent (Fig. 3; Table IV) with a tendency to decrease with grain size. In the finest grain-size fractions a clear J_s decrease is observed. A slightly decreasing J_s with decreasing grain size is reported for magnetite by Mauritsch et al. (1987).

TTE pyrrhotite has the highest average J_s (approx. 16.7 Am^2kg^{-1}), followed by EOR and EGI pyrrhotite (respectively 11.5 and approximately 12.6 Am^2kg^{-1}) and DIS pyrrhotite (approx. 8.9 Am^2kg^{-1}). The EGI figures have to be regarded as somewhat approximate because of the large influence of the magnetite present in these fractions (cf. Table III) on

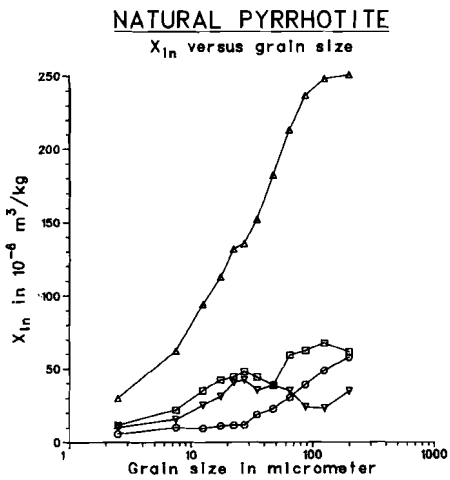

Fig. 2. X_{in} versus grain size. Squares denote TTE pyrrhotite, circles EOR pyrrhotite, triangles EGI pyrrhotite and inverted triangles DIS pyrrhotite. The higher X_{in} of the EGI fractions is caused by their magnetite content.

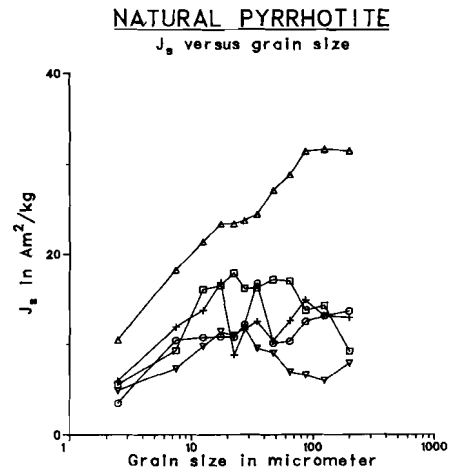

Fig. 3. J_s versus grain size. For symbol meanings see Fig 2. The magnetite correction in the EGI fractions is based on a saturation magnetization of 90 Am^2kg^{-1} for magnetite. The magnetite corrected EGI figures are indicated by plus symbols. The corrected figures have to be regarded as somewhat approximate because one percent error in magnetite weight percentage leads to a change in pyrrhotite saturation magnetization of about 1 Am^2kg^{-1}.

the pyrrhotite J_s determination (one percent difference in magnetite weight percentage leads to a change of about 1 Am^2kg^{-1} in the corresponding pyrrhotite J_s). Mark the impact of only 5.5 weight percent

magnetite on the corrected pyrrhotite J_s figure for the smallest EGI fraction (Table IV).

The J_s trend corresponds well with the compositions indicated by the microprobe analyses (Table IA). The most Fe-deficient pyrrhotite has the highest saturation magnetization. Fluctuation in J_s values of the same pyrrhotite could be caused, apart from errors inherent in the J_s determination procedure (estimation of the magnetite amount in the EGI fractions, estimation of the pyrrhotite amount occurring intimately intergrown with silicates in the coarse DIS fractions), by minute compositional changes between fractions of the same pyrrhotite sample. The J_s decrease in the coarsest TTE fractions could be explained in this way. It should be realized that small differences in pyrrhotite chemical composition result in considerable differences in saturation magnetization.

It was tested whether the J_s decrease in the fine grain-size fractions could be related to a change in pyrrhotite composition. This was done with the TTE fractions because the J_s decrease is largest in TTE pyrrhotite. The six finest fractions were heated in vacuo (10^{-6} mm Hg) at 350 °C and subsequently quenched to obtain monophase hexagonal (high-temperature) pyrrhotite. The exact position of the compositional dependent d_{102} reflection (single hexagonal reflection at 2.06 Å) was determined with Philips diffractometer system PW 1700 (Cu K_α-rays) at room temperature with silicon as internal standard (the d=1.9201 Å reflection was used). The position of the d_{102} reflection was fitted with the Yund and Hall (1969) calibration curve. The resulting Fe-atom percentages were 46.68, 46.54, 46.59, 46.65, 47.05 and 46.73 respectively for the 30-25, 25-20, 20-15, 15-10, 10-5 and <5 micrometer fractions (the standard deviation of the X-ray method is estimated at 0.06 atom percent Fe by Yund and Hall, op. cit). Slight compositional differences exist and the decrease in J_s in the 10-5 micrometer grain-size fraction may be related to its more Fe-rich composition. The <5 micrometer fraction with an even much lower J_s, however, has a composition approaching that determined in the coarser fractions with a much higher J_s. The low J_s of the <5 micrometer fraction can thus not be related to a change in chemical composition.

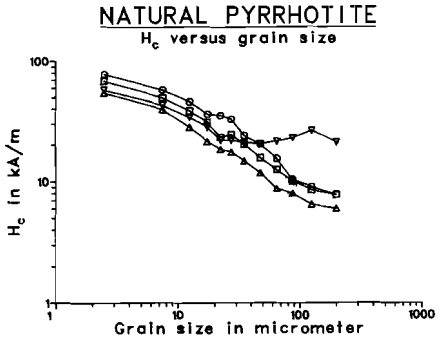

Fig. 4. H_c versus grain size. For symbol meanings see Fig. 2.

The coercive force (H_c) increases with decreasing grain size for all samples (Fig. 4; Table IV). No large differences are observed between the different pyrrhotites. H_c figures derived in the present study concur with Clark's (1984) determinations and for MD grains with the

determination of Halgedahl and Fuller (1981). The figures for the PSD range in the present study are somewhat higher than those for this range reported by Soffel (1981). H_c is roughly proportional to the logarithm of the grain size throughout the investigated grain-size range. $H_c \sim d^{-0.67}$ is obtained for the present pyrrhotites for grain-size fractions from five micrometer upwards, which is in reasonable agreement with Clark's (1984) determination of $d^{-0.79}$ for a similar grain-size range. The nearly constant H_c in the coarse fractions of DIS pyrrhotite is due to the silicate intergrowths in these fractions. The H_c trend for the magnetite-bearing EGI fractions is below the other curves, because the magnetite H_c is smaller than the pyrrhotite H_c (e.g. Dunlop, 1986; Heider et al., 1987; Worm and Markert, 1987; also for crushed grains e.g. Hartstra, 1982B; Day et al., 1977).

2.2 Remanence measurements

Acquisition curves of the isothermal remanent magnetization (RA curves) are similar for identical grain-size fractions in all samples except for the magnitude of their saturation remanence (J_{rs}). The fine grain-size fractions are saturated in larger fields than coarse fractions (Fig. 5).

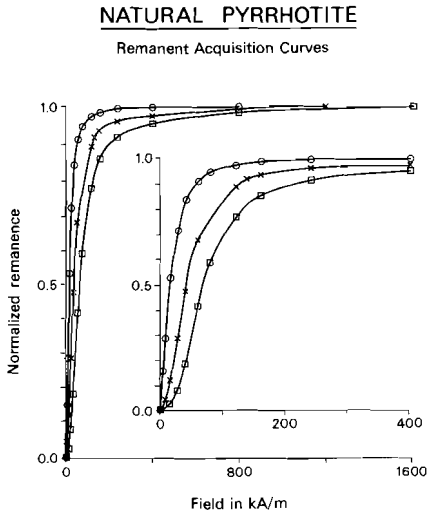

Fig. 5. Examples of acquisition curves of the isothermal remanent magnetization (RA curves) for pyrrhotite normalized to their saturation remanence. Identical grain-size fractions of different pyrrhotite samples revealed identical shapes for their normalized RA curves with coarse grain-size fractions saturating in smaller fields than fine grain-size fractions. Circles denote the TTE 150-100 micrometer, crosses the DIS 10-5 micrometer and squares the EOR 30-25 micrometer fraction respectively. The inset shows the same RA curves with a four times expanded abscissa to display more clearly the differences in grain size behaviour in small applied fields.

J_{rs} shows a maximum in the 10 to 30 micrometer range (Fig. 6; Table IV). Absolute figures are somewhat lower than in pure 4C pyrrhotite (Clarke, 1984), especially in the fine grain-size range. The trend in J_{rs} between the samples is the same as the J_s trend: TTE

pyrrhotite has the highest J_{rs}, followed in decreasing order by EGI and EOR and finally by DIS. Since J_{rs} of magnetite (e.g. Hartstra, 1982B) and pyrrhotite are of the same order, the magnetite contribution to the J_{rs} does not largely affect the pyrrhotite trend in the EGI fractions (cf. Fig. 6).

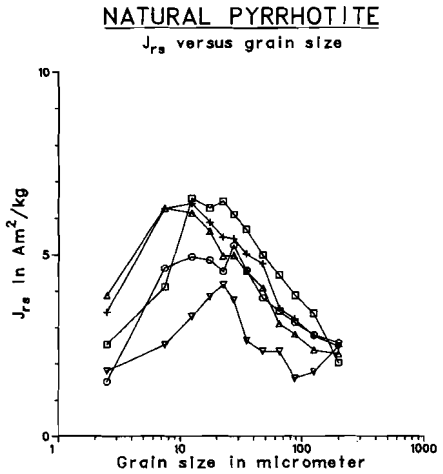

Fig. 6. J_{rs} versus grain size. For symbol meanings see Fig. 2. The magnetite-corrected J_{rs} figures for the EGI pyrrhotite fractions are indicated with plus symbols. Hartstra's (1982B) magnetite J_{rs} values were employed because the present magnetite grains underwent similar treatment during the sample preparation procedure. The most Fe-deficient pyrrhotite (TTE) with consequently the highest J_s (Fig. 3) has also the highest J_{rs}. The compositional J_s and J_{rs} trends are equal.

The reason for the J_{rs} decrease in the small grain-size fractions is not known (also observed by Clark (1984) in pure 4C pyrrhotite, albeit to a lesser extent). In the <5 micrometer fractions this could partially be due to the presence of superparamagnetic (SP) particles. However, if present, their amount will be insubordinate. In the other fractions SP particles will be (virtually) absent, so the reason for the J_{rs} decline has to be sought for elsewhere. It could be that the domain walls occupy a relatively large part of the grain volume, reducing the effective mass of the grains.

The remanent coercive force (H_{cr}) and remanent acquisition coercive force (H_{cr}') both increase with decreasing grain size (Figs. 7 and 8). H_{cr} obeys a $\sim d^{-0.66}$ relationship and H_{cr}' is proportional to $d^{-0.47}$ for grain size fractions upwards from the <5 micrometer fractions. The differences between the different pyrrhotite samples are much smaller than in the H_c plot (Fig. 4). The H_{cr} and H_{cr}' figures derived by Clark (1984) are somewhat larger than those determined in the present study. This could be due to the presence of harder fine-grained particles in Clark's grain-size fractions. The presence of magnetite hardly shows up in the H_{cr} and H_{cr}' trends of the EGI fractions. The constant H_{cr} and to a lesser extent H_{cr}' in the coarse fractions of the DIS sample can be attributed to the presence of silicate intergrowths. The true SD region is not yet reached in the <5 micrometer fractions, since H_c and H_{cr} both still increase with respect to the 10-5 micrometer fractions albeit slightly less than would follow from the $\sim d^{-n}$ relationships. This

concurs with the determinations of the pyrrhotite SD threshold size at 1.5-2.0 micrometer (Soffel, 1977) or at 3 micrometer (Clark, 1984).

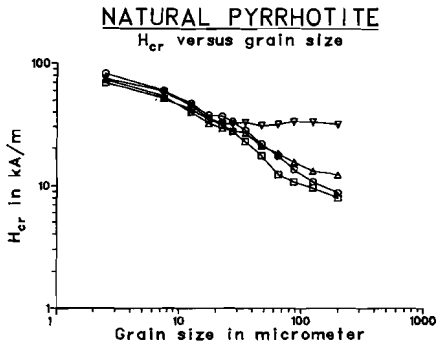

Fig. 7. H_{cr} versus grain size. For symbol meanings see Fig. 2. Mark that the differences between the pyrrhotite samples in H_{cr} are considerably less than in H_c (Fig. 4).

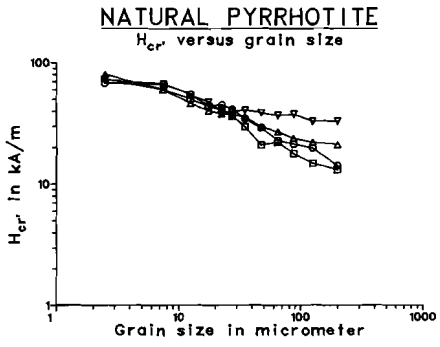

Fig. 8. $H_{cr'}$ versus grain size. For symbol meanings see Fig. 2. Chemical differences between the pyrrhotites also hardly show up in the $H_{cr'}$ values.

Table IV: Some rockmagnetic parameters for natural pyrrhotite

Grain size fraction	χ_{in} m^3kg^{-1} 10^{-5}	H_c kAm^{-1}	H_{cr} kAm^{-1}	$H_{cr'}$ kAm^{-1}	J_{rs} Am^2kg^{-1}		J_s Am^2kg^{-1}	
TTE 250 - 150	6.15	7.78	7.96	13.05	2.04		9.2	
TTE 150 - 100	6.75	8.49	9.55	14.80	3.40		14.2	
TTE 100 - 75	6.24	10.02	10.74	17.82	3.89		13.7	
TTE 75 - 55	5.93	12.41	12.34	21.96	4.46		17.0	
TTE 55 - 40	3.86	15.60	17.51	21.01	5.00		17.1	
TTE 40 - 30	4.43	20.21	22.68	29.92	5.70		16.2	
TTE 30 - 25	4.81	24.27	27.45	36.61	6.10		16.2	
TTE 25 - 20	4.45	23.08	31.04	40.58	6.47		17.9	
TTE 20 - 15	4.26	30.96	34.62	43.93	6.28		16.4	
TTE 15 - 10	3.49	38.68	41.78	50.45	6.54		16.0	
TTE 10 - 5	2.19	49.74	51.72	60.00	4.12		9.3	
TTE < 5	1.17	68.04	70.03	73.85	2.54		5.4	
EOR 250 - 150	5.76	7.77	8.75	14.08	2.58		13.6	
EOR 150 - 100	4.87	9.04	10.74	19.82	2.80		13.1	
EOR 100 - 75	3.92	10.28	13.53	21.41	3.15		12.5	
EOR 75 - 55	3.03	15.36	17.51	22.92	3.46		10.4	
EOR 55 - 40	2.25	20.13	21.88	29.28	3.81		10.1	
EOR 40 - 30	1.88	23.87	28.25	34.62	4.58		16.7	
EOR 30 - 25	1.17	32.71	33.02	41.38	5.25		12.1	
EOR 25 - 20	1.15	35.17	36.61	45.12	4.55		10.8	
EOR 20 - 15	1.11	36.05	37.40	44.17	4.86		10.8	
EOR 15 - 10	0.94	45.76	46.95	55.23	4.95		10.8	
EOR 10 - 5	0.99	57.69	60.08	66.53	4.64		10.4	
EOR < 5	0.57	77.35	83.16	67.88	1.51		3.5	
EGI 250 - 150	25.08	6.00	12.34	21.17	2.28	2.48	31.4	12.9
EGI 150 - 100	24.83	6.45	13.13	22.20	2.39	2.78	31.5	13.1
EGI 100 - 75	23.70	7.96	15.52	23.95	2.82	3.25	31.4	14.9
EGI 75 - 55	21.33	8.75	18.30	27.14	3.11	3.54	28.8	12.6
EGI 55 - 40	18.22	11.70	21.09	29.68	4.09	4.76	27.1	10.4
EGI 40 - 30	15.22	14.72	26.66	35.81	4.55	5.03	24.5	12.5
EGI 30 - 25	13.55	17.43	27.85	37.64	4.98	5.44	23.8	11.6
EGI 25 - 20	13.19	18.30	29.44	38.04	4.97	5.48	23.4	8.8
EGI 20 - 15	11.27	21.41	32.23	40.35	5.65	5.89	23.4	16.8
EGI 15 - 10	9.04	28.17	39.79	46.31	6.19	6.40	21.3	13.7
EGI 10 - 5	6.22	39.79	53.72	60.00	6.28	6.27	18.2	11.9
EGI < 5	3.10	54.27	74.01	80.77	3.89	3.43	10.5	5.9
DIS 250 - 150	3.45	21.04	31.43	33.26	2.49		7.9	
DIS 150 - 100	2.30	26.45	33.02	33.02	1.78		5.9	
DIS 100 - 75	2.40	23.00	33.02	37.64	1.60		6.6	
DIS 75 - 55	3.49	21.41	31.51	37.00	2.35		6.9	
DIS 55 - 40	3.85	20.37	30.80	38.83	2.36		9.0	
DIS 40 - 30	3.52	20.93	32.71	40.58	2.64		9.6	
DIS 30 - 25	4.25	21.88	31.83	39.63	3.76		11.8	
DIS 25 - 20	4.08	21.88	31.99	39.39	4.18		11.0	
DIS 20 - 15	3.09	28.17	35.41	47.75	3.86		11.4	
DIS 15 - 10	2.50	34.06	44.96	54.83	3.31		9.8	
DIS 10 - 5	1.54	43.13	58.89	67.32	2.53		7.3	
DIS < 5	1.04	57.46	75.60	72.42	1.81		4.9	

The second columns of J_{rs} and J_s of the EGI fractions refer to the *specific* parameters corrected for the magnetite content of each fraction (cf. Table III). Especially the J_s corrected figures are prone to a rather large error (the scatter in the individual values for each fraction is rather large) due to the fact that a one percent error in the magnetite weight percentage determination leads to an increase (or decrease) of approximately 1 Am^2kg^{-1} in the "magnetite corrected" pyrrhotite J_s figures. The magnetite impact on the correction of J_{rs} is considerably less, because the saturation remanence of magnetite and pyrrhotite per unit mass are of the same order.

Table V: Ratios of some pyrrhotite rockmagnetic perameters

	H_c/H_{cr}	H_{cr}/H_{cr}'	J_{rs}/J_s		J_{rs}/χ_{in} kAm^{-1}	$(J_{rs}/\chi_{in})/H_{cr}$
TTE 250 - 150	0.98	0.61	0.22		33.17	4.17
TTE 150 - 100	0.89	0.64	0.24		50.37	5.27
TTE 100 - 75	0.93	0.60	0.28		62.34	5.80
TTE 75 - 55	1.01	0.56	0.26		75.21	6.10
TTE 55 - 40	0.89	0.83	0.29		129.53	7.40
TTE 40 - 30	0.89	0.76	0.35		128.67	5.67
TTE 30 - 25	0.88	0.75	0.38		126.82	4.62
TTE 25 - 20	0.74	0.76	0.36		145.39	4.68
TTE 20 - 15	0.89	0.79	0.38		147.42	4.26
TTE 15 - 10	0.93	0.83	0.41		187.39	4.48
TTE 10 - 5	0.96	0.86	0.44		188.13	3.64
TTE < 5	0.97	0.95	0.47		217.09	3.10
EOR 250 - 150	0.89	0.62	0.19		44.79	5.12
EOR 150 - 100	0.84	0.54	0.21		57.50	5.35
EOR 100 - 75	0.76	0.63	0.25		80.36	5.94
EOR 75 - 55	0.88	0.76	0.33		114.19	6.52
EOR 55 - 40	0.92	0.75	0.38		169.33	7.74
EOR 40 - 30	0.84	0.82	0.27		243.62	8.62
EOR 30 - 25	0.99	0.80	0.43		448.72	13.59
EOR 25 - 20	0.96	0.81	0.42		395.65	10.81
EOR 20 - 15	0.96	0.85	0.45		437.84	11.71
EOR 15 - 10	0.98	0.85	0.46		526.60	11.22
EOR 10 - 5	0.96	0.90	0.44		468.69	7.80
EOR < 5	0.93	1.22	0.43		264.91	3.18
EGI 250 - 150	0.49	0.58	0.07	0.19	9.09	0.74
EGI 150 - 100	0.49	0.59	0.08	0.21	9.62	0.73
EGI 100 - 75	0.51	0.65	0.09	0.22	11.90	0.77
EGI 75 - 55	0.48	0.67	0.10	0.28	14.16	0.77
EGI 55 - 40	0.56	0.71	0.13	0.46	19.92	0.94
EGI 40 - 30	0.55	0.74	0.18	0.40	28.45	1.07
EGI 30 - 25	0.63	0.74	0.19	0.47	33.36	1.20
EGI 25 - 20	0.62	0.77	0.20	0.62	34.80	1.18
EGI 20 - 15	0.66	0.80	0.22	0.35	44.72	1.39
EGI 15 - 10	0.71	0.86	0.26	0.47	62.06	1.56
EGI 10 - 5	0.74	0.89	0.34	0.53	98.71	1.84
EGI < 5	0.73	0.92	0.33	0.58	111.94	1.51
DIS 250 - 150	0.67	0.94	0.32		72.17	2.30
DIS 150 - 100	0.80	1.00	0.30		77.39	2.34
DIS 100 - 75	0.70	0.88	0.24		66.67	2.02
DIS 75 - 55	0.68	0.85	0.34		67.34	2.14
DIS 55 - 40	0.66	0.79	0.26		61.30	1.99
DIS 40 - 30	0.64	0.81	0.28		75.00	2.29
DIS 30 - 25	0.69	0.80	0.32		88.47	2.78
DIS 25 - 20	0.68	0.81	0.38		102.45	3.20
DIS 20 - 15	0.80	0.74	0.34		124.92	3.53
DIS 15 - 10	0.76	0.82	0.34		132.40	2.94
DIS 10 - 5	0.73	0.88	0.35		164.29	2.79
DIS < 5	0.76	1.04	0.37		174.04	2.30

The second J_{rs}/J_s column for the EGI fractions refers to the magnetite corrected saturation magnetization/saturation remanence ratio. Due to uncertainties in the magnetite percentage leading to relatively large errors in especially the pyrrhotite J_s, the "magnetite corrected" J_{rs}/J_s ratios have to be regarded as somewhat approximate. The fluctuations in the ratio superposed upon a increasing trend with decreasing grain size are due to (small) errors in the magnetite weight percentage determination.

3 DISCUSSION

3.1 Ratios of some rockmagnetic parameters

The J_{rs}/J_s ratio is increasing with decreasing grain size from approximately 0.2 to close to 0.5 (Fig. 9; Table V). The magnetite influence in the EGI fractions shows up in their lower uncorrected J_{rs}/J_s ratio. The spreading in the ratios for the corrected EGI fractions is related to their J_s correction for magnetite which is very sensitive for small errors in the determination of the magnetite content. The nearly constant ratios for the coarse DIS fractions again are due to silicate intergrowths.

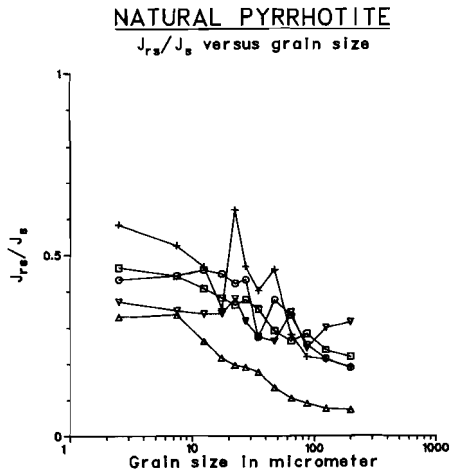

Fig. 9. J_{rs}/J_s versus grain size. For symbol meanings see Fig. 2.

The J_{rs}/J_s ratio of 0.14 determined by Halgedahl and Fuller (1981) for large polycrystalline pyrrhotite crystals concurs with the trend indicated by the present pyrrhotites. Clark's (1984) J_{rs}/J_s ratios for the coarse grain-size fractions are in good agreement with the present determinations; he obtained slightly larger figures for his fine grain-size fractions. The increase in J_{rs}/J_s ratio tends to slow down from some 25 micrometer downward for EOR and DIS pyrrhotite. The ratios obtained for the <5 micrometer fractions are distinctly lower than the model ratio of 0.75 for SD grains (Dunlop, 1971). This is also observed by Clark (1984). Apparently one of the easy axes is dominating, resulting in a uniaxial behaviour. The observation of Bin and Pauthenet (1963), who found six easy directions in the basal plane with one axis dominating, points also in this direction.

The H_c/H_{cr} ratio is remarkably close to unity for the TTE and EOR grain-size fractions; it displays no grain-size dependent trend (Fig. 10; Table V). For the DIS fractions the ratio is smaller (about 0.7). The magnetite-bearing EGI fractions have lower H_c/H_{cr} ratios.

The $H_{cr}/H_{cr'}$ ratio increases with decreasing grain size from approximately 0.6 up to 1.0 (Fig. 11; Table V), an indication that self-demagnetization of MD grains could play an important role. This $H_{cr}/H_{cr'}$

ratio is similar for all pyrrhotite samples, since the magnetite content does not emerge in the H_{cr} and $H_{cr'}$ trends.

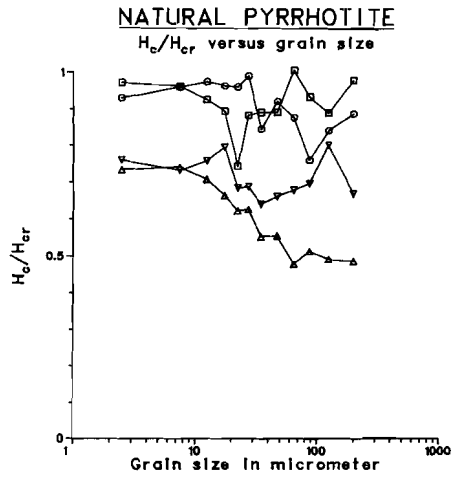

Fig. 10. H_c/H_{cr} versus grain size. For symbol meanings see Fig. 2. The large figures, which are uniform throughout the investigated grain-size range, make this ratio discriminatory between pyrrhotite and magnetite (the EGI ratios are smaller than the others).

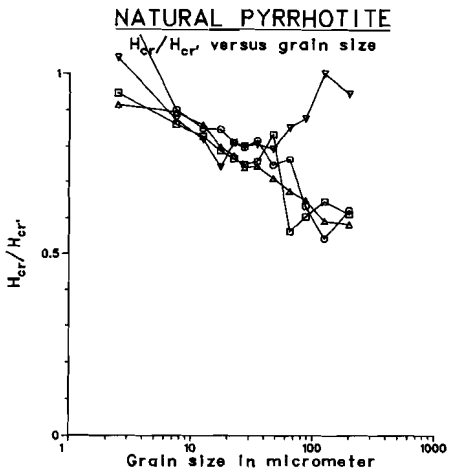

Fig. 11. $H_{cr'}/H_{cr}$ versus grain size. For symbol meanings see Fig. 2. Its increase with decreasing grain size might be related to self-demagnetization effects which are more pronounced in MD grains.

J_{rs}/X_{in} ratio increases with decreasing grain size (Fig. 12; Table V); only EOR fractions display high ratios in the intermediate grain-size range. The J_{rs}/X_{in} ratios are typically larger than H_{cr} figures for pyrrhotite. $(J_{rs}/X_{in})/H_{cr}$ figures are larger in 4C-rich pyrrhotite (TTE, EOR) than in more Fe-rich pyrrhotite (DIS, Table V).

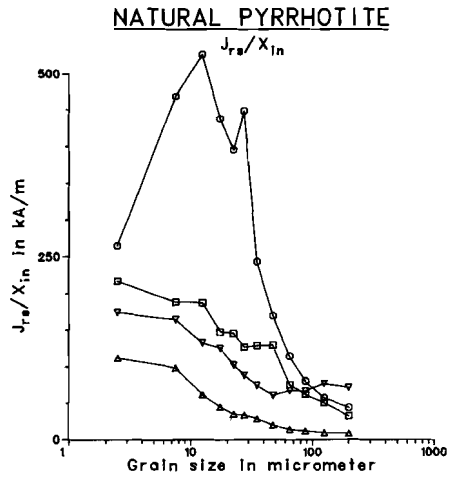

Fig. 12. J_{rs}/X_{in} versus grain size. For symbol meanings see Fig. 2. The ratio is larger than H_{cr} throughout the investigated grain-size interval.

3.2 Comparison of pyrrhotite room temperature hysteresis parameters with those of magnetite

The following comparison between pyrrhotite and magnetite rockmagnetic parameters is made using magnetite data of O'Reilly (1984), Dunlop (1986), Heider et al. (1987) and Worm and Markert (1987). The pyrrhotite saturation magnetization is smaller than that of magnetite whereas the saturation remanence is of the same order (except in the small grain- size fractions, where the magnetite saturation remanence is considerably larger). Pyrrhotite has thus typically higher J_{rs}/J_s ratios than magnetite as is demonstrated by the low uncorrected EGI figures (Table V). The pyrrhotite initial susceptibility is considerably smaller than that of magnetite in similar grain-size ranges. Its coercive force is larger than the magnetite coercive force.

For comparison of pyrrhotite remanent coercive force and remanent acquisition coercive force with the same parameters for magnetite only magnetite data referring to annealed crushed grains are available (e.g. Day et al., 1977; Hartstra, 1982B). The hysteresis properties of such magnetite are influenced by stress (e.g. Dunlop, 1986; Heider et al., 1987). No data on H_{cr} and $H_{cr'}$ for large non-crushed magnetite grains have yet been published. H_{cr} as well as $H_{cr'}$ for pyrrhotite are larger than the respective parameters for magnetite in the fine grain size fractions and smaller in the coarse grain-size fractions. H_{cr} and $H_{cr'}$ are more or less equal for both minerals in the 75 - 55 micrometer range. Since crushing enlarges the magnetite coercive forces, it is reasonable to expect that the magnetite parameters will be smaller than those for pyrrhotite for non-crushed magnetite grains throughout the whole investigated grain-size range. Pyrrhotite is thus magnetically "harder" than magnetite. Titanomagnetite shows, compared with pure magnetite, an increasing hardness with rising Fe^{2+} content due to the anisotropic character of the Fe^{2+} ion. The hardness of pyrrhotite could

possibly be explained similarly, because all iron in pyrrhotite is considered to be in the divalent state.

The H_{cr}/H_{cr} ratio is similar for pyrrhotite and magnetite in the coarse grain-size range, but this ratio increases with decreasing grain size in pyrrhotite whereas it is approximately grain-size independent in magnetite. Typical for pyrrhotite is its high H_c/H_{cr} ratio, which is approximately uniform throughout the investigated grain-size interval. Another discriminatory parameter between pyrrhotite and magnetite is the J_{rs}/X_{in} ratio which is considerably larger in pyrrhotite. This ratio is larger than H_{cr} for pyrrhotite and smaller than H_{cr} for magnetite.

The presence of pyrrhotite in a sample can thus be established by a high H_c/H_{cr} ratio or by a J_{rs}/X_{in} ratio which is larger than H_{cr}, when it is decided to leave heat treatment of the sample to avoid possible chemical alterations. The pyrrhotite grain-size interval can subsequently be determined by the observed coercive force or, preferably, by the remanent coercive force, because compositional differences in pyrrhotite appear to have only minor influence on its remanent coercive force.

3.3 Evaluation of the origin of anisotropy in pyrrhotite

The area between the ordinate, the descending branch of the hysteresis loop and the extrapolated line for the determination of the saturation magnetization minus the energy of the demagnetizing field ($0.5N*J_s^2$) represents the reversible magnetization work (e.g. Appel, 1987).

$$W_{rev} = HdJ - 0.5N*J_s^2$$

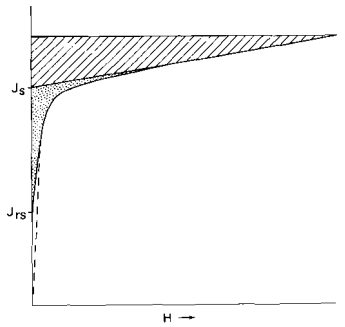

Fig. 13. The dotted area represents W_{rev}; the hatched area represents the minimum work done against the hard axis anisotropy.

HdJ can be planimetrically determined. For the present pyrrhotites it appeared that $0.5N*J_s^2$ (N was set at 0.33) constitutes at most a few percent of HdJ (due to a relatively low J_s). Therefore uncertainties regarding the actual value of the demagnetization factor lead to negligible error in the W_{rev} determination.

Anisotropy can have its cause in shape, stress or magnetocrystalline anisotropy. The observed anisotropy can be a mixture of these three contributions. Usually one type of anisotropy is dominating. Neglecting shape anisotropy, it is first assumed that stress anisotropy is domina-

ting. W_{rev} is then related to the average stress anisotropy energy (E_{sa}) by

$$W_{rev} = E_{sa} = 0.75 * \lambda * \sigma_i$$

where λ denotes the magnetostriction constant and σ_i the average internal stress. Soffel (1977) determined a maximum value for the magnetostriction constant of $7*10^{-6}$ for pyrrhotite (the high Fe^{2+} amount in pyrrhotite apparently does not lead to high magnetostriction constants as in titanomagnetite). Calculation of average internal stress from the present pyrrhotite data yields figures between 3500 and 7000 MPa, which are unreasonably large. This is demonstrated by the range of 27 to 63 MPa for average internal stress in titanomagnetites calculated by Appel (1987) and by a stress of some 200 MPa which is considered reasonable for ceramic materials (cf. O'Reilly, 1984). One may thus conclude that stress is not dominating.

The magnetocrystalline anisotropy for pyrrhotite is given by Bin and Pauthenet (1963) as

$$E_{an} = K_1*\sin^2(\Theta)*\sin^2(\Phi) + K_2*\sin^4(\Theta)*\sin^4(\Phi) + K_3*\cos^2(\Theta) + K_4*\cos^4(\Theta) + K_5*\sin^2(\Theta)*\cos^2(\Theta)*\sin^2(\Phi) + \ldots$$

Θ is the angle between the magnetization direction and the easy axis. Φ is the angle in the basal plane between an easy axis and the projection of direction of magnetization onto the basal plane. They neglect terms of K_5 and above. At room temperature K_1 is $0.35*10^5$ Jm^{-3}, K_2 approximately zero, K_3 $1.18*10^5$ Jm^{-3} and K_4 $32.2*10^5$ Jm^{-3}. The large K_3 and K_4 are related to the pyrrhotite hard axis of magnetization (measured with applied field parallel to c-axis) and K_1 and K_2 to basal plane anisotropy. Bin and Pauthenet (1963) note during their measurements six easy directions of magnetization in the basal plane with one axis dominating. They ascribed this to twinning in their pyrrhotite crystal.

Since the reversible work determined for the present pyrrhotites is referring to the energy necessary to overcome basal plane anisotropy (the hard axis behaviour is excluded by the extrapolation to J_s) and J_{rs}/J_s ratios of close to 0.5 were found in the smallest pyrrhotite fractions, we treat the anisotropy as uniaxial for approximation. W_{rev} is related to the anisotropy energy (E_k) as

$$W_{rev} = E_k = 0.66 * K_{an}$$

where K_{an} is the magnetocrystalline anisotropy constant. Calculation yields anisotropy constants in a range of 0.35 up to $0.70*10^5$ Jm^{-3} for all pyrrhotites, in fair agreement with the $0.35*10^5$ Jm^{-3} determination of K_1 by Bin and Pauthenet (1963). The minimum work done against the anisotropy of the hard axis is given by the hatched triangle in Fig. 13. Assuming uniaxial anisotropy for the hard axis like Besnus et al. (1968) calculation yields an anisotropy constant range of 5 to $8*10^5$ Jm^{-3} for the hard axis. The obtained range is similar to the anisotropy used by Besnus et al. (op. cit.).

3.4 Trends in coercive and remanent coercive force

The present pyrrhotites consist of various intergrown superstructures. Three of the samples (TTE, EOR and EGI) have compositions close "ideal 4C pyrrhotite" so that the 4C superstructure is dominating. The

fourth (DIS) is a more Fe-rich pyrrhotite which consists apart from the 4C superstructure of antiferromagnetic NC superstructures. All pyrrhotites show smooth grain-size dependent trends in H_c, H_{cr} and $H_{cr'}$ (Figs. 4, 7, 8), so apparently the presence of the antiferromagnetic parts do not show up in these trends. It could be that the "antiferromagnetic" parts carry a kind of defect magnetization (non-integral superstructures) and as such can not be regarded as non-magnetic intergrowths. Nakazawa and Morimoto (1971) mention that the 5C, 6C etc. superstructures are (slightly) ferrimagnetic and not perfectly antiferromagnetic. Soffel (1981) reported the presence of "pseudo-domain-walls" which were immobile under the application of an external magnetic field, contrary to normal domain walls which moved due to the same field. He related the presence of pseudo domain walls to minute differences in pyrrhotite superstructure (which he could not make visible by etching).

4 CONCLUSIONS

The pyrrhotite rockmagnetic parameters, determined in the present study, show smooth grain-size dependent trends. The initial susceptibility is considerably smaller than that of magnetite and decreases with grain size ($7*10^{-5}$ - $1*10^{-5}$ m^3kg^{-1}). The susceptibility of the hard axis is approximately $30-40*10^{-8}$ m^3kg^{-1} for all pyrrhotites. The coercive force, remanent coercive force and remanent acquisition coercive force all increase with decreasing grain size respectively from 7 - 80 for H_c, 8 - 85 for H_{cr} and 14 - 80 for $H_{cr'}$ (all in kAm^{-1}). The coercive forces all obey d^{-n} relationships with grain size above 5 micrometer with n = 0.67 for H_c, n = 0.66 for H_{cr} and n = 0.47 for $H_{cr'}$. The pyrrhotite coercive force is larger than the magnetite coercive force; the remanent coercive force and remanent acquisition coercive force are smaller for pyrrhotite than for magnetite in the coarse grain-size fractions whereas the reverse is true in the fine grain-size fractions. The saturation remanence increases with decreasing grain size down to some 30 micrometer and decreases with a further grain-size decrease (increase from 2.0 to 6.0 Am^2kg^{-1}; decrease down to some 2.0 Am^2kg^{-1}). Its decrease in the fine grain-size range might possibly be related to a relatively large grain volume of domain walls. The saturation magnetization is approximately grain-size independent with a marked decrease for the finest fractions. The reason for this decrease it not known. It varies from approximately 16.7 Am^2kg^{-1} for TTE via 12.6 for EGI and 11.5 for EOR down to 8.9 Am^2kg^{-1} for DIS pyrrhotite. The trends indicated by figures for the saturation magnetization and saturation remanence correspond with the equivalent-Fe trend indicated by the microprobe analyses.

Typical for pyrrhotite are its large J_{rs}/J_s ratio (0.20 to close to 0.50) and its large H_c/H_{cr} ratio, which is uniform throughout the investigated grain-size interval (approximately 0.9 for relatively Fe-poor pyrrhotite and 0.8 for Fe-richer pyrrhotite). The $H_{cr}/H_{cr'}$ ratio increases with decreasing grain size indicative for self demagnetization of MD grains. The J_{rs}/X_{in} ratio is larger than H_{cr} for pyrrhotite; it increases with decreasing grain size. Calculation of the average internal stress from the reversible work given by the reversible part of hysteresis curves yields unreasonably large figures in a range of 3500-7000 MPa, so the anisotropy is not dominated by stress anisotropy. Assuming a dominating uniaxial magnetocrystalline anisotropy yields a range of $0.35-0.70*10^5$ Jm^{-3} for the anisotropy constant in fair agreement with the determination of $0.35*10^5$ Jm^{-3} of Bin and Pauthenet (1963).

Pyrrhotite and magnetite can be discriminated by the large J_{rs}/J_s and H_c/H_{cr} ratios for pyrrhotite and a J_{rs}/X_{in} ratio which is larger than H_{cr} for pyrrhotite. The presence of pyrrhotite in a sample can be established by the H_c/H_{cr} or the J_{rs}/X_{in} ratio; the pyrrhotite grain size can subsequently be derived by the H_{cr} trend, because pyrrhotite compositional differences appear to have only minor influence on H_{cr} vs. grain size trend.

Acknowledgements

Prof. Dr. J.D.A. Zijderveld critically reviewed the manuscript. The high field measurements were carried out the High Field Magnet Laboratory of the University of Nijmegen (The Netherlands) in cooperation with Dr. J.A.A.J. Perenboom. C.D. Laman (Institute of Earth Sciences, University of Utrecht) made the X-ray films and diffractograms. Trace element determinations were performed by the Service Laboratory (Institute of Earth Sciences, University of Utrecht). J.J.J. Bergenhenegouwen made the drawings. The investigations were supported by the Netherlands Foundation for Earth Science Research (AWON) with financial aid from the Netherlands Organization for the advancement of Pure Research (Z.W.O., grant 751-354-006).

5 REFERENCES

Appel E., 1987, Stress anisotropy in Ti-rich titanomagnetites, Phys. Earth Plan. Inter. 46, 233-40.

Arnold R.G., 1967, Range in composition and structure of 82 natural terrestrial pyrrhotites, Can. Min. 9, 31-50.

Bertaut E.F., 1953, Contribution à l'étude des structures lacunaires: la pyrrhotine, Acta Cryst. 6, 557-61.

Besnus M.J., Meyer A.J.P., 1964, Nouvelles données experimentals sur le magnétisme de la pyrrhotine naturelle; Inst. Phys. & Phys. Soc., Proc. Int. Conf. Magnetism, Nottingham, 507-11.

Besnus M.J., Munschy G., Meyer A.J.P., 1968, Sublattice rotations in ferrimagnets: the case of pyrrhotite, J. Appl. Phys. 39, 903-4.

Bigioggero B., Brigo L., Ferrario A., Gergnanin A., Montrasio A., Zuffardi P., 1979, Strona Valley (Fe-Ni-Cu) and (Fe-Ba) ore deposits: excursion book, Memorie di Sci. Geol. 33, 33-9.

Bin M., Pauthenet R., 1963, Magnetic anisotropy in pyrrhotite, J. Appl. Phys. 34, 1161-2.

Bodechtel J., 1965, Zur Genese der Eisenerze der Toskana und der Insel Elba, Neues Jb. Mineral. Abh. 103, 147-62.

Bodechtel J., 1968, Die Paragenesen der Skarnlagerstätten in den Monti di Campiglia/Toskana, Freib. Forsch. H. C231, 7-20.

Carpenter R.H., 1974, Pyrrhotite isograde in SE Tenessee and SW North Carolina, Geol. Soc. Amer. Bull. 85, 451-6.

Clark D.A., 1984, Hysteresis properties of sized dispersed monoclinic pyrrhotite grains, Geophys. Res. Lett. 11, 173-6.

Dankers P.H.M., 1978, Magnetic properties of dispersed natural iron-oxides of known grain-size, Ph.D. thesis University of Utrecht, 142pp.

Dankers P.H.M., 1981, Relationship between median destructive field and remanent coercive forces for dispersed magnetite, titanomagnetite and hematite, Geophys. J. R. astr. Soc. 64, 447-61.

Day R., Fuller M., Schmidt V.A., 1977, Hysteresis properties of titanomagnetites: grain size and compositional dependence, Phys. Earth Plan. Inter. 13, 260-7.

Dekkers M.J., 1988, Some rockmagnetic parameters for natural goethite, pyrrhotite and fine-grained hematite, Ph.D. thesis University of Utrecht, appendix 1.

Dekkers M.J., Hartstra R.L., Mullender T.A.T., in prep., A device for the magnetite separation of fine particles

Dimanche F., 1971, Les minerais de magnétite et les skarns du Ginevro (ile d'Elbe, Italie), Mineral. Deposita 6, 356-79.

Dunlop D.J., 1971, Magnetic properties of fine particle hematite, Ann. Geophys. 27, 269-93.

Dunlop D.J., 1986, Hysteresis properties of magnetite and their dependence on particle size: a test of pseudo-single-domain remanence models, J. Geophys. Res. B 91, 9569-84.

Ferrario A., Garuti G., Rossi A., Sighinolfi G.P., 1983, Petrographic and metallogenetic outlines of the "La Balma - M. Capio" Ultramafic - Mafic body (Ivrea - Verbano Basic Complex, NW Italian Alps), in: Schneider H.J. (ed.), Mineral deposits of the Alps and of the Alpine Epoch in Europe, Proceedings of the IV ISMIDA 1981, 28-40.

Fleet M.E., MacRae N., 1969, Two phase hexagonal pyrrhotites, Can. Min. 9, 699-705.

Freeman R., 1986, Magnetic mineralogy of pelagic limestones, Geophys. J. R. astr. Soc. 85, 433-52.

Goodenough J.B., 1978, Structural chemistry of iron sulfides, Mater. Res. Bull. 13, 1305-14.

Halgedahl S.L., Fuller M., 1981, The dependence of magnetic domain structure upon magnetization state in polycrystalline pyrrhotite, Phys. Earth Planet. Inter. 26, 93-7.

Hartstra R.L., 1982A, Some rockmagnetic parameters for natural iron-titanium oxides, Ph.D. thesis University of Utrecht, 145pp.

Hartstra R.L., 1982B, Grain-size dependence of initial susceptibility and saturation magnetization-related parameters of four natural magnetites in the PSD-MD range, Geophys. J. R. astr. Soc. 71, 477-95.

Heider F., Dunlop D.J., Sugiura N., 1987, Magnetic properties of hydrothermally recrystallized magnetite crystals, Science 236, 1287-90.

Kligfield R., Channell J.E.T., 1981, Widespread remagnetization of Helvetic limestones, J. Geoph. Res. B 86, 1888-1900.

Mauritsch H., Becke M., Kropácek V., Zelinka T., Hejda P., 1987, Comparison of the hysteresis characteristics of synthetic samples with different magnetite and haematite contents, Phys. Earth Plan. Inter. 46, 93-9.

Morimoto N., Gyobu A., Tsukuma K., Koto K., 1975A, Superstructure and non-stoichiometry of intermediate pyrrhotite, Am. Min. 60, 240-8.

Morimoto N., Gyobu A., Mukaiyama H., Izawa E., 1975B, Crystallography and stability of pyrrhotites, Econ. Geol. 70, 824-33.

Morimoto N., Nakazawa H., Nishiguchi K., Tokonami M., 1970, Pyrrhotites: stoichiometric compounds with composition $Fe_{n-1}S_n$ (n GE 8), Science 168, 964-6.

Morimoto N., Nakazawa H., Watanabe E., 1974, Direct observation of metal vacancy in pyrrhotite $Fe_{1-x}S$, by means of an electron microscope, Proc. Japan Acad. 50, 756-9.

Nakazawa H., Morimoto N., 1971, Phase relations and superstructures of pyrrhotite, $Fe_{1-x}S$, Mat. Res. Bull. 6, 345-58.

Naldrett A.J., Kullerud G., 1967, A study of the Strathcona mine and its bearing on the origin of the nickel-copper ores of the Sudbury district, Ontario, J. Petrol. 8, 453-534.

Natale P., Zucchetti S., 1979, Remarks on the Fe-Ni-(Cu) deposit of Campello Monti, Memorie di Sci. Geol. 33, 213-4.

O'Reilly W., 1984, Rock and mineral magnetism, Blackie Glasgow and London, 220pp.

Pierce L., Buseck P.R., 1974, Electron imaging of pyrrhotite superstructures, Science 186, 2209-12.

Rivalenti G., 1979, Guide to the excursion in the Balmuccia zone, Sesia Valley, Ivrea - Verbano complex, Memorie di Sci. Geol. 33, 3-9.

Rochette P., 1987, Metamorphic control of the magnetic susceptibility of black shales in the Swiss Alps: toward the use of "Magnetic Isograde", Earth Plan. Sci. Letters 84, 446-56.

Schwarz E.J., 1975, Magnetic properties of pyrrhotite and their use in applied geology and geophysics, Geol. Surv. Can. Paper 74-59, 24pp.

Schwarz E.J., Vaughan D.J., 1972, Magnetic phase relations of pyrrhotite, J. Geomagn. Geoelec. 24, 441-58.

Soffel H.C., 1977, Pseudo-Single-Domain effects and Single-Domain Multidomain transition in natural pyrrhotite deduced from domain structure observations, J. Geophys. 42, 351-9.

Soffel H.C., 1981, Domain structure of natural fine-grained pyrrhotite in a rock matrix (diabase), Phys. Earth Plan. Inter. 26, 98-106.

Waldeck H., 1977, Die Insel Elba - Mineralogie, Geologie, Geographie, Kulturgeschichte, Sammlung geologischer Führer Band 64, Gebr. Borntraeger Berlin - Stuttgart, 169pp.

Ward J.C, 1970, The structure and properties of some iron sulphides, Rev. Pure Appl. Chem. 20, 175-206.

Worm H.-U., Markert H., 1987, Magnetic hysteresis properties of fine particle titanomagnetites precipitated in a silicate matrix, Phys. Earth Plan. Inter. 46, 84-92.
Yund R.A., Hall H.T., 1969, Hexagonal and monoclinic pyrrhotites, Econ. Geol. 64, 420-3.

CHAPTER 9

MAGNETIC PROPERTIES OF NATURAL PYRRHOTITE

PART II

HIGH- AND LOW-TEMPERATURE BEHAVIOUR OF THE ISOTHERMAL REMANENT SATURATION MAGNETIZATION AND THERMOREMANENCE AS FUNCTION OF GRAIN SIZE.

Abstract

The magnetic behaviour of pyrrhotite during thermal demagnetization and low-temperature cycling was investigated by studying four natural pyrrhotites. Twelve grain-size fractions ranging from 250 micrometer down to <5 micrometer were homogeneously dispersed in a non-magnetic matrix. Normalized decay curves of the isothermal saturation remanence of natural pyrrhotite have nearly identical shapes regardless the sample and its grain size, when thermally demagnetized with the continuous thermal demagnetization method. Only small grain-size fractions (10-5 micrometer) have a blocking temperature spectrum slightly shifted to lower temperatures. Continuous thermal demagnetization of saturation remanences induced in previously thermal demagnetized samples results in identical curves for all fractions. Due to the (partial) preservation of high-temperature pyrrhotite phases, the saturation remanence is different before and after thermal demagnetization. When thermally demagnetized with the stepwise method, between-sample differences are minor, but coarse and fine grain-size fractions of the same sample have different decay curves with the fine fraction considerably more decreasing at lower temperatures (210-245 °C) followed by a slight increase at 260-300 °C.

TRM is decreasing with grain size. This unusual trend is tentatively explained by the absence of closure domains in pyrrhotite. Continuous thermal demagnetization results in identical decay curves for all fractions. Stepwise thermal demagnetization indicates that coarse grain-size fractions have sharp blocking temperature spectra. The blocking temperature spectrum broadens slightly with decreasing grain size.

The low-temperature behaviour of pyrrhotite is related to the strong temperature dependence of the anisotropy constants K_3 and K_4. A gradually increasing reversibility of low-temperature behaviour is observed with decreasing grain-size for J_{rs}, in agreement with a gradual approach of the SD state in the smallest grain size fractions (<5 micrometer). TRM showed a reversible low-temperature behaviour throughout the investigated grain-size range.

1 INTRODUCTION

Pyrrhotite, the solid solution series $Fe_{1-x}S$ with x varying between zero and 0.13, shows a complex composition-dependent thermomagnetic behaviour, which has been the subject of considerable study in the past (e.g. Haraldsen, 1941A, 1941B; Bertaut, 1953; Lotgering, 1956; Hayase et al., 1963; Schwarz, 1967, 1968, 1969; Schwarz and Harris, 1970; Vaughan et al., 1971; Schwarz and Vaughan, 1972; Schwarz, 1975; Bennett and Graham, 1980, 1981; Marusek and Mulay, 1980). The pyrrhotite structure, generally described by superstructures (e.g. Bertaut, 1953; Fleet and MacRae, 1969; Morimoto et al., 1970, 1975A, 1975B; Nakazawa and Morimoto, 1970, 1971; Koto and Kitamura, 1981) and its phase relations are

still not understood in detail, despite much research effort (e.g. Toulmin and Barton, 1964; Sugaki and Shima, 1977; Kissin and Scott, 1982, Barker and Parks, 1986).

Pyrrhotite has a hexagonal structure (based upon the NiAs-structure). The hexagonal structure distorts to a monoclinic one with a high vacancy content (over 0.11 formula units). Monoclinic pyrrhotite (4C pyrrhotite) is thought to be Fe_7S_8 (46.67 atom percent Fe) at room temperature. A compositional range between 46.4 and 46.9 atom percent Fe exists at somewhat elevated temperatures, i.e. above some 100 °C (e.g. Kissin and Scott, 1982). Hexagonal pyrrhotite (NC pyrrhotite; nomenclature Nakazawa and Morimoto, 1970, 1971) has a chemical composition which contains at least 47.3 to 47.5 atom percent Fe (e.g. Arnold, 1967; Yund and Hall, 1969; Kissin and Scott, 1982). The highest possible iron content is presumably close to 48 atom percent (corresponding to $Fe_{11}S_{12}$). Monoclinic pyrrhotite is ferrimagnetic; hexagonal pyrrhotite is ideally antiferromagnetic but a small ferrimagnetic moment is supposed to exist (Nakazawa and Morimoto, 1971).

The pyrrhotite Curie temperature is reported between 310 and 325 °C, slightly dependent on its composition (Lotgering, 1956). The presence of isomorphous substitution (e.g. Ni) in minor amounts may noticeably lower the Curie temperature (Vaughan et al., 1971).

Thermomagnetic curves of pyrrhotite allow for a rapid and straightforward quantitative distinction between monoclinic and hexagonal pyrrhotite based on the occurrence of the so-called λ-transition (e.g. Schwarz, 1968, 1975). Monoclinic 4C pyrrhotite shows reversible thermomagnetic behaviour without a λ-transition (e.g. Hayase et al., 1963; Schwarz, 1968). Typical for hexagonal pyrrhotite is the λ-transition which represents a change in the vacancy ordering pattern at some 200-210 °C, slightly dependent on the pyrrhotite chemical composition (Schwarz and Vaughan, 1972). The antiferromagnetic hexagonal NC pyrrhotite changes into ferrimagnetic pyrrhotite (λ-pyrrhotite phase with the NA superstructure, nomenclature Nakazawa and Morimoto, 1970, 1971). This increase in magnetization results in λ-shaped thermomagnetic curves. The λ-transition is reversible upon slow cooling (rate 0.5 °C/min.) through its temperature range (Schwarz and Vaughan, 1972), upon faster cooling the high-temperature ferrimagnetic λ-phase is quenched to an extent depending on the actual cooling rate. The λ-pyrrhotite phase has a Curie temperature of some 265 °C (e.g. Schwarz and Vaughan, 1972).

The thermal behaviour of pyrrhotite remanences is generally somewhat underexposed in the aforementioned thermomagnetic studies. For paleomagnetic purposes this remanence behaviour is of prime importance, especially because pyrrhotite is meanwhile recognized in a wide variety of rock types.

A comparison of the thermal behaviour of the isothermal saturation remanence (J_{rs}) and thermoremanence (TRM) of pyrrhotite in a grain-size dependent framework will be made in the present study. The pyrrhotite fractions of which the room temperature field-dependent rockmagnetic parameters were reported in Dekkers (1988A), are subjected to high- and low-temperature treatment.

The pyrrhotite samples studied comprise an orthomagmatic disseminated pyrrhotite (DIS, from Isola di Vocca, Ivrea zone, Italy), two re-heated pyrrhotites from originally volcano-sedimentary pyrite-hematite ores (EOR and EGI, respectively from Ortano and Ginevro, both from Elba island, Italy) and a pyrometasomatic pyrrhotite (TTE, from Temperino, Tuscany, Italy). All pyrrhotites are well-crystalline; chemical data are compiled in Table I. Concise sample descriptions are in Dekkers (1988A).

Grain-size fractions from 250 micrometer down to <5 micrometer, prepared according to the method described in Dankers (1978, 1981) and Hartstra (1982A), were homogeneously dispersed in an epoxy resin (Araldit D, Hardener CY 956, Ciba Geigi) or in a quartz/bassanite matrix (CM Löt soldering investment for dental metal work). Details concerning the preparation procedure are in Dekkers (1988B).

Table IA: Average pyrrhotite composition determined by microprobe analyses

	TTE			EOR			DIS			EGI		
	aver.	st.d.	norm.	aver.	st.d.	norm.	aver.	st.d.	norm.	aver.	st.d.	norm.
S	53.03	0.19	39.27	53.14	0.35	39.39	52.25	0.30	38.47	52.85	0.23	39.04
Fe	46.76	0.18	60.32	46.70	0.36	60.30	47.41	0.29	60.80	46.95	0.34	60.41
Mn	0.02	0.03	0.02	0.01	0.02	0.01	0.01	0.02	0.01	0.02	0.03	0.02
Ni	0.17	0.14	0.23	0.14	0.10	0.19	0.39	0.11	0.52	0.27	0.08	0.41
Cu	0.06	0.09	0.09	0.03	0.05	0.04	0.05	0.06	0.07	0.04	0.06	0.06
Zn	0.04	0.08	0.06	0.04	0.08	0.06	0.08	0.13	0.12	0.04	0.08	0.06
total	100.08		99.99	100.06		99.99	100.19		99.99	100.18		100.00

Analyses were carried out with a TPD (Technisch Physische Dienst) microprobe fitted with a TRACOR Northern Energy Dispersive (ED) system. Operating conditions were 15 keV and 2 - 3 nA. ZAF matrix correction was applied. aver. = average atom percentage; st.d. = standard deviation; norm. = normalized weight percentage. Most spots contained no detectable Mn, Cu and Zn. Ni is enhanced in the DIS pyrrhotite and slightly raised in EGI pyrrhotite; in the others its amount is insignificant. TTE 32 spot analyses; EOR 21 analyses; DIS 16 analyses; EGI 16 analyses. Fe_7S_8 contains 53.33 atom % S (4C superstructure); Fe_8S_9 52.94 atom % S; Fe_9S_{10} 52.63 atom % S (5C); $Fe_{10}S_{11}$ 52.38 atom % S (11C) and $Fe_{11}S_{12}$ 52.17 atom % S (6C).

Table IB: Trace element content (wet-chemical) ppm

	TTE	EOR	DIS*	EGI
Co	215	320	755	440
Pb	<dl	<dl	<dl	<dl
Ba	<dl	<dl	<dl	<dl
Mn	430	85	815	285
V	<dl	<dl	528	<dl
Zn	795	<dl	325	<dl
Cu	<dl	715	3220	835
Ni	85	130	2430	205
Cr	< dl	<dl	<dl	<dl

* The DIS sample contains 37 percent non-pyrrhotite minerals (almost exclusively silicates, >99 percent). Analyses were carried out by the Service Laboratory, Institute of Earth Sciences, State University of Utrecht. All elements were analyzed with ICPES (Induction Coupled Plasma Emission Spectrometry); the limit of detection for each element is approximately 10 ppm.

1.1 Magnetic measurements

Continuous and stepwise thermal demagnetization of the isothermal saturation remanence (J_{rs}) and a thermoremanent magnetization (TRM) induced in a field of 67 Am^{-1} (84 microTesla) by cooling from 340 °C were performed in an argon atmosphere to prevent chemical alteration of the pyrrhotite grains. Below 400 °C pyrrhotite alterations (oxidation phenomena with sulphur-loss) are confined to its surface (e.g. Schwarz and Harris, 1970; Bennett et al., 1972). Above this temperature homo-

genization of whole grains with considerable sulphur-loss occurs (Schwarz and Harris, 1970). Therefore the specimens were not heated to temperatures above 360 °C. Cooling rates during the stepwise treatment were 0.5 - 1 °C per minute to prevent quenching of high-temperature pyrrhotite structures. Cooling rates during continuous thermal treatment were much faster. The cooling rate of the sample strongly depends on the actual sample temperature: the highest rates (some 16 °C per minute) are observed at the onset of cooling trajectory, i.e. at 360 °C. In the 200 °C region a estimated rate of 10 °C per minute prevailed. Continuous recordings of J_{rs} and TRM behaviour were performed in a temperature interval of -196 °C up to 360 °C using a fluxgate spinner magnetometer type made suitable for high- and low-temperature measurements (HALT spinner) by inserting the specimen holder in a water-cooled furnace or in a dewar vessel in which aliquots of liquid nitrogen could be sprayed. Periodic remanence measurement and temperature regulation were controlled by a microcomputer system (Dankers, 1978, 1981; Hartstra 1982B, 1982C). Initial susceptibilities before and after heating cycles were determined at room temperature with a Jellinek KLY-1 susceptibility bridge.

2 RESULTS AND DISCUSSION

2.1 Thermal demagnetization experiments

2.1.1 Behaviour of the isothermal saturation remanence

Continuous thermal demagnetization curves (Fig. 1) are (virtually) identical for all samples characterized by a monotonous decrease up to the Curie temperature. Normalized decay curves have a similar shape regardless of the grain size of the fraction. Only the 10-5 micrometer grain-size fractions have a blocking temperature spectrum shifted to slightly lower temperatures when demagnetized for the first time ("A" curves). The shape of all fractions is identical, when J_{rs} is demagnetized for the second time ("B" curves). These "B" curves have a steeper approach to the Curie temperature than corresponding "A" curves (Fig. 1).

J_{rs} shows an increase after one thermal cycle in the coarse grain-size fractions, whereas a decrease with respect to the virgin J_{rs} is observed in some fine grain-size fractions (Table II, Fig. 2).

Fig. 1. Continuous thermal decay curves of the isothermal saturation remanence for a selected set grain-size fractions. Sample abbreviations: EOR = Ortano, TTE = Temperino, EGI = Ginevro, DIS = Isola di Vocca; the numbers after the sample abbreviation refer to the grain-size range in micrometer. The "A" curves denote thermal demagnetization curves of unheated samples; the "B" curves denote a second thermal demagnetization of a saturation remanence induced at room temperature in the same specimens after the first thermal demagnetization. The bending point at some 130-150 °C in the "A" curves is due to a chemical reaction of the matrix, the estimated "true" pyrrhotite remanence behaviour is dashed. The temperature lag provoked by the endothermic matrix reaction is illustrated in Fig. 1C, which depicts the temperature recorded by the temperature sensor (Pt100 resistance) in the furnace of the HALT spinner versus the temperature recorded by a thermocouple (PtRo10) moulded in a specimen consisting solely of matrix material (CM Lôt soldering investment). No endothermic matrix reaction was detected during a second heating run; temperatures measured with the Pt100 sensor were calibrated according to this run. No bending point is observed in the thermal decay curve when demagnetizing J_{rs} induced in unheated pyrrhotite in a non-reactive matrix (epoxy resin). No demagnetization above 160 °C is possible because the epoxy resin decomposes at higher temperatures.

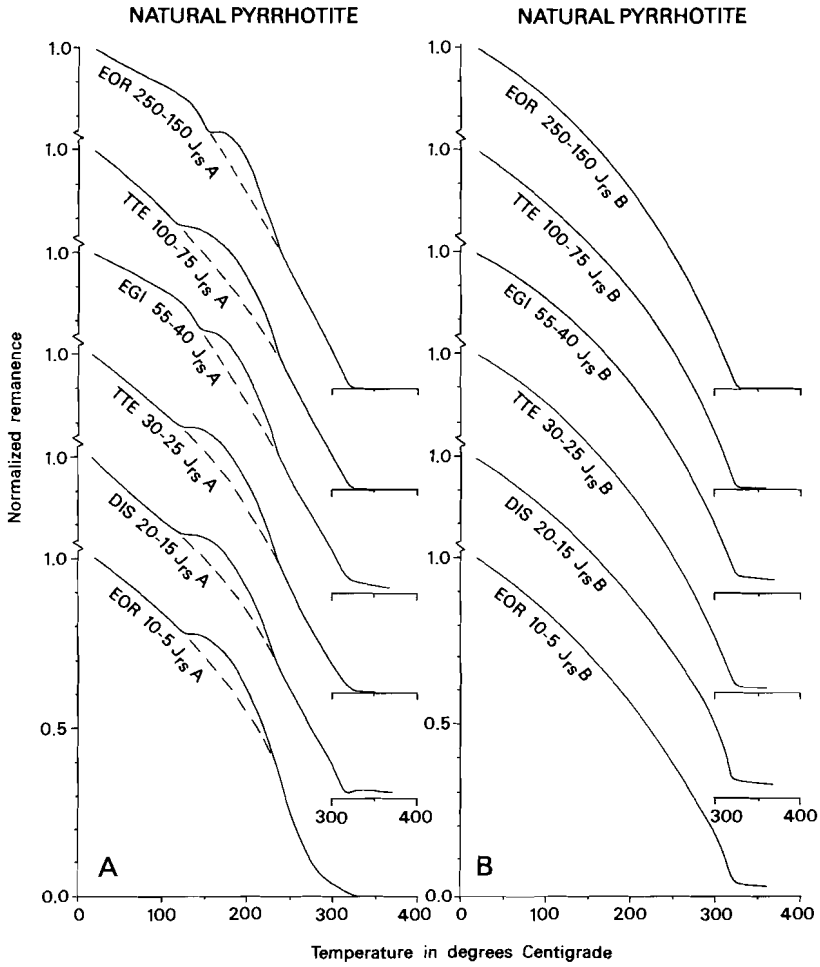
NATURAL PYRRHOTITE
NATURAL PYRRHOTITE
EOR 250-150 Jrs A
TTE 100-75 Jrs A
EGI 55-40 Jrs A
TTE 30-25 Jrs A
DIS 20-15 Jrs A
EOR 10-5 Jrs A
EOR 250-150 Jrs B
TTE 100-75 Jrs B
EGI 55-40 Jrs B
TTE 30-25 Jrs B
DIS 20-15 Jrs B
EOR 10-5 Jrs B
A
B
Normalized remanence
Temperature in degrees Centigrade
1.0
0.5
0.0
0
100
200
300
400

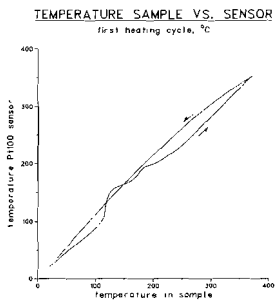
TEMPERATURE SAMPLE VS. SENSOR
first heating cycle, °C
temperature in sample

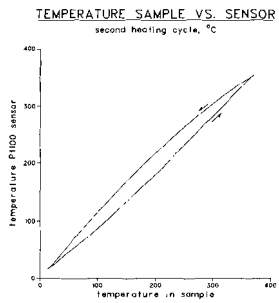
TEMPERATURE SAMPLE VS. SENSOR
second heating cycle, °C
temperature in sample

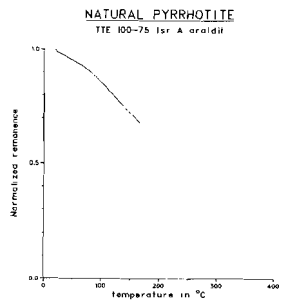
NATURAL PYRRHOTITE
TTE 100-75 Isr A araldit
Normalized remanence
temperature in °C

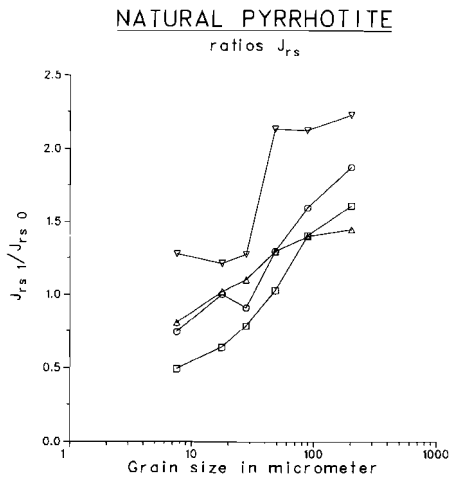

Fig. 2. Ratios of the saturation ramanence after (J_{rs1}) and prior to thermal treatment (J_{rs0}) versus grain size. TTE (Temperino) is denoted by squares, EOR (Ortano) by circles, EGI (Ginevro) by triangles and DIS (Isola) by inverted triangles.

The increase, which is the largest in the DIS fractions, is due to the metastable preservation of high-temperature pyrrhotite phases (characterized by MC and NA superstructures during cooling; cf. Nakazawa and Morimoto, 1971). DIS pyrrhotite contains the largest amount of hexagonal pyrrhotite so metastable preservation of NA pyrrhotite occurs to a higher extent than in the other pyrrhotite samples. J_{rs} after a second heating cycle is slightly smaller than after the first heating cycle (figures for EOR 30-25, 20-15, 10-5 respectively 4.35, 4.37 and 3.45 and for TTE 30-25, 20-15 and 10-5 respectively 4.14, 3.43 and 2.04; all in Am^2kg^{-1}). Most remanence is removed from the specimens at 320 °C, so the J_{rs} differences prior to annealing and after the first heating cycle reflect pyrrhotite properties. The remanence which remains after thermal demagnetization of the pyrrhotite, increases slightly. Pyrrhotite alteration during thermal treatment can not be totally suppressed, even in an inert atmosphere.

The fall of the J_{rs1}/J_{rs0} ratio (cf. Table II) with decreasing grain size might be related with the domain structure, which develops within the pyrrhotite grains during cooling: it is envisaged that the high-temperature pyrrhotite structure is partially preserved which leads to "domain" sizes smaller than the actual grain size. Mark that the differences of J_{rs1} between grain sizes of the same sample are much smaller than differences prior to thermal treatment (differences observed in the EGI fractions are partly due to their magnetite content). The pyrrhotite saturation remanence (at least J_{rs} of unheated pyrrhotites) first increases with decreasing grain size down to some 20 micrometer and shows a marked decrease with a further grain-size decrease (Dekkers, 1988A). This "domain-size reduction" may thus have an enlarging effect in the coarse grain-size fractions and a reducing effect on the J_{rs} in the fine grain-size fractions. The reducing effect is apparently larger than the increase due to the ferrimagnetic NA phase, when the original amount of hexagonal pyrrhotite is small as in the TTE and EOR samples.

Table II: J_{rs} in unheated pyrrhotite samples and the ratio between the saturation remanence after one heating cycle and unheated samples.

grain size	EOR			TTE			EGI			DIS		
	(1)	(2)	(3)	(1)	(2)	(3)	(1)	(2)	(3)	(1)	(2)	(3)
250 - 150	2.31	4.32	1.87	1.94	3.10	1.60	1.90	2.74	1.44	2.37	5.26	2.22
100 - 75	2.87	4.56	1.59	3.49	4.89	1.40	2.73	3.82	1.40	1.54	3.26	2.12
55 - 40	3.63	4.72	1.30	4.78	4.92	1.03	3.90	5.03	1.29	2.29	4.88	2.13
30 - 25	4.97	4.52	0.91	5.58	4.35	0.78	4.59	5.05	1.10	3.66	4.68	1.28
20 - 15	4.59	4.59	1.00	5.86	3.75	0.64	5.08	5.18	1.02	3.66	4.43	1.21
10 - 5	5.03	3.77	0.75	3.87	1.94	0.50	6.07	4.92	0.81	2.40	3.07	1.28

The first column (1) refers to J_{rs} (Am^2kg^{-1}) prior to thermal treatment (J_{rs0}), the second column (2) to J_{rs} after one heating cycle (J_{rs1}). The third column (3) denotes their ratio.

The initial susceptibility doubles after the first thermal treatment in the DIS 250-150 micrometer fraction (an increase from $0.27*10^{-6}$ to $0.57*10^{-6}$ m^3kg^{-1} was obtained; due to a slip in measuring procedure only the 250-150 micrometer fractions were measured for all samples so these fractions are only compared), presumably due to the presence of metastably preserved high-temperature pyrrhotite phases. The initial susceptibility does not change so much in the TTE, EOR and EGI fractions (respectively prior and after a heating cycle $0.48*10^{-6}$ and $0.46*10^{-6}$; $0.56*10^{-6}$ and $0.56*10^{-6}$; $2.54*10^{-6}$ and $2.38*10^{-6}$, all in m^3kg^{-1}). For the EGI fraction, this might be related to the presence of magnetite which dominates the initial susceptibility especially in this coarse fraction (Dekkers, 1988A). For TTE and EOR the initial susceptibility of metastably preserved high-temperature pyrrhotite phases is apparently similar to unheated pyrrhotite or the amount of metastably preserved phases is low. When fine grain-size fractions are annealed for thirty minutes at temperatures of 420 °C, their initial susceptibility showed an increase presumably due to the (partial) alteration of pyrrhotite to magnetite (demonstrated by the TTE <5 micrometer fraction: an increase from $0.092*10^{-6}$ via $0.23*10^{-6}$ after one time annealing to $0.44*10^{-6}$ m^3kg^{-1} after two times; for EOR <5 micrometer figures are respectively $0.042*10^{-6}$, $0.20*10^{-6}$ and $0.28*10^{-6}$ m^3kg^{-1}). The change in initial susceptibility was much less in coarse fractions.

Stepwise thermal demagnetization of J_{rs} reveals typical differences between coarse-grained (250-150 micrometer) and fine-grained (<5 micrometer) pyrrhotite fractions (Fig. 3). Coarse-grained fractions show slightly convex decay curves with a (virtually) monotonous decrease up to the Curie temperature (325 °C), whereas fine-grained fractions show a much larger decay up to 210-245 °C followed by a slight remanence increase, before the Curie temperature is reached. Tentatively this behaviour might be understood as follows. At approximately 210 °C the hexagonal pyrrhotite parts of the grains invert to NA pyrrhotite. Stable phase relations (e.g. Kissin and Scott, 1982) indicate that monoclinic pyrrhotite should also convert to (hexagonal) NA pyrrhotite + pyrite at some 250 °C and to (hexagonal) MC pyrrhotite + pyrite at some 260 °C. The nucleation of pyrite is kinetically inhibited. The inversion of monoclinic pyrrhotite to hexagonal pyrrhotite (in dry systems) is temperature dependent (Kullerud et al., 1963). It could be that in small grains suchlike inversion occurs at lower temperatures. Since it is happening in a field-free space, this would explain the extra remanence

decrease in the 210-245 °C range. The small increase at slightly higher temperatures might then possibly be related to the inversion to MC pyrrhotite (the Curie temperature of NA pyrrhotite is reported at 265 °C). Mark that the parts of the decay curve of the <5 micrometer fraction below 150 °C and above 300 °C can be thought connected by a smooth, slightly convex decay curve, like that of the 250-150 micrometer fraction. In this coarse fraction the extra decrease and increase as observed in the fine fraction would then be kinetically inhibited.

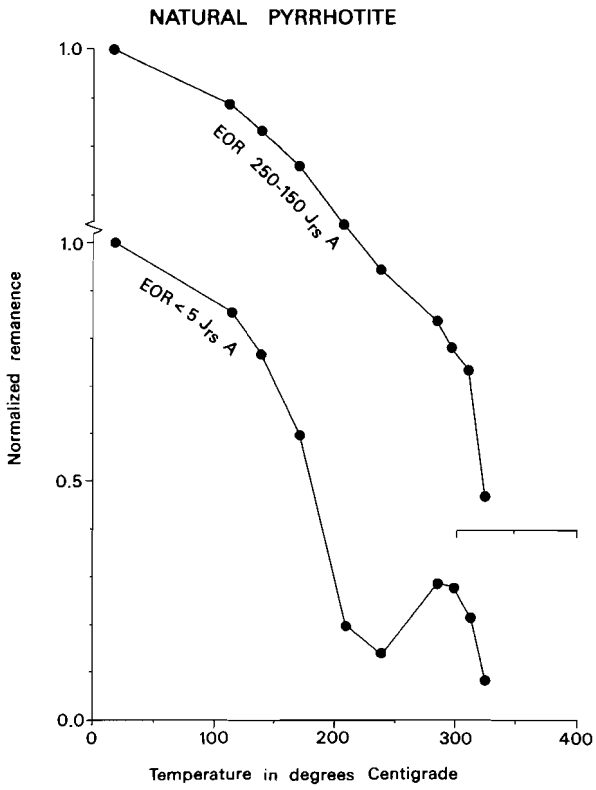

Fig. 3. Two examples of J_{rs} behaviour during stepwise thermal demagnetization. Mark the difference between the coarse and fine grain-size fraction of the same pyrrhotite.

It should be noted that the pyrrhotites which are stepwise treated have been relatively long at elevated temperatures. Another tentative explanation for the observed remanence behaviour could be seen in relation with the time available for pyrrhotite to take up oxygen from the specimen matrix (atmospheric oxygen is absent since the thermal demagnetization is carried out in an argon atmosphere). During superstructure changes (cf. the phase diagram presented by Kissin and Scott, 1982), which take some time because they require vacancy-rearrangements, pyrrhotite grains could be more prone to incorporation of oxygen from the specimen matrix. Pyrrhotite with oxygen incorporated without being

transformed to magnetite, is reported to have a Curie temperature of some 575 °C (Onufrienok and Zvegintsev, 1981). This might result in the observed remanence increase in the fine grains and could explain the relatively large remanence occasionally remaining after the 325 °C step. Again in coarse grains the uptake of matrix oxygen would be delayed to higher temperatures for kinetical reasons so that a remanence increase below the pyrrhotite Curie point is not observed. It should be emphasized once more at this stage, that both explanations given above should be regarded as tentative at present.

2.1.2 Behaviour of the thermoremanence

TRM shows generally a decreasing trend with grain size for all pyrrhotites (Fig. 4, Table III). This trend is opposite of the trend observed in magnetite grains below some 20 micrometer (e.g. Stacey and Banerjee, 1974; Hartstra, 1983), but is also observed in hematite grains (Hartstra, 1982A). Weak-field TRM of MD grains is thought to be a bulk effect, which is grain-size independent in true MD grains (e.g. Stacey and Banerjee, op. cit.). The increase in intensity observed in magnetite PSD grains is attributed to surface effects, in relation with closure domains and domain-wall moments (Stacey and Banerjee, op. cit.). The decrease with grain size observed in the pyrrhotite fractions, when approaching the PSD/SD transition region, might tentatively be related to the absence of closure domains in pyrrhotite in fine PSD grains (Soffel, 1981). The increase in TRM intensity observed in some pyrrhotites in the intermediate grain-size range, could be related to these phenomena. However, one should realize that these explanations are tentative and need more experimental data for their verification.

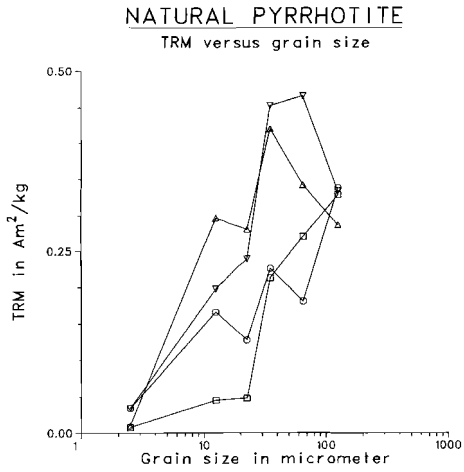

Fig. 4. TRM acquired by the pyrrhotite fractions in a field of 67 Am^{-1} (84 microTesla) as function of grain size. For symbol meanings cf. Fig. 2.

Table III: Pyrrhotite TRM as function of grain size.

grain size	EOR	TTE	EGI	DIS
150 - 100	0.339	0.329	0.287	0.334
75 - 55	0.182	0.271	0.343	0.467
40 - 30	0.227	0.214	0.421	0.454
25 - 20	0.128	0.048	0.281	0.240
15 - 10	0.166	0.045	0.297	0.198
< 5	0.034	0.008	0.010	0.034

TRM in Am^2kg^{-1}. In the calculation of the EGI fractions it was assumed that magnetite acquired a PTRM negligible compared to the pyrrhotite TRM.

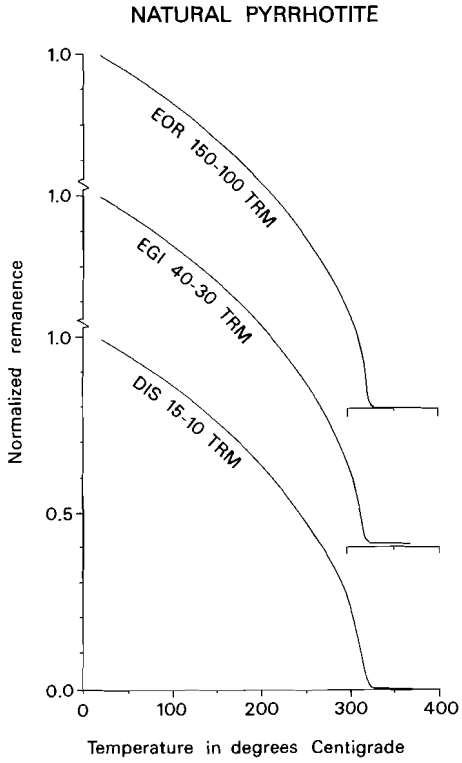

Fig. 5. Continuous thermal demagnetization curves of a TRM induced in a field of 67 Am^{-1} (84 micro-Tesla) normalized to their initial value. Sample abbreviations as in Fig. 2; the numbers refer to the grain size in micrometer.

All fractions, regardless of the pyrrhotite sample, display similar normalized TRM versus temperature curves, when treated with the continuous thermal demagnetization method. The demagnetization curves are steep, when approaching the Curie temperature (approx. 325 °C, Fig. 5). J_{rs} curves, also the "B" curves (Fig. 1), display less steep parts, when approaching the Curie temperature.

TRM decay curves obtained by stepwise thermal demagnetization (Fig. 6) reveal similar behaviour for fractions down to 40-30 micrometer

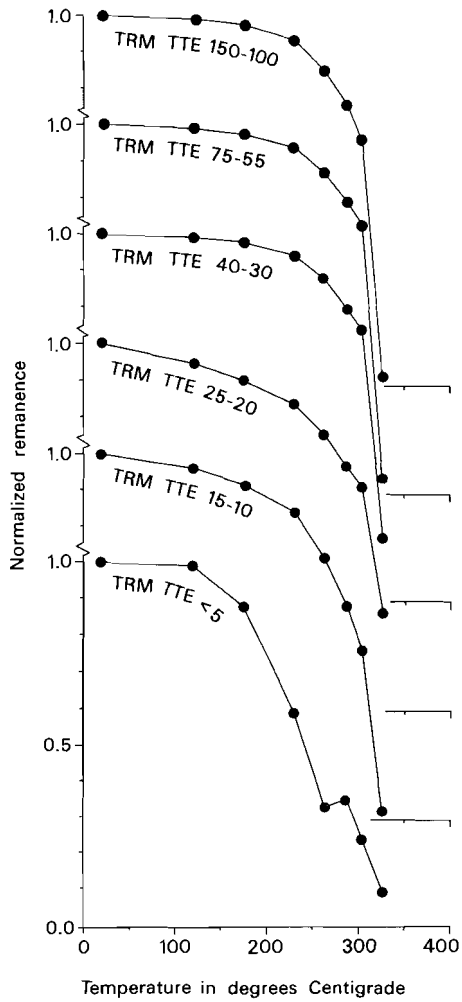

Fig. 6. Normalized stepwise decay curves of pyrrhotite TRM as function of grain size in the TTE sample. The curves of 40-30 micrometer and larger grain sizes are virtually identical with a steep blocking temperature spectrum indicated by the steep remanence fall above 300 °C. Fine grain-size fractions have an increasingly wider blocking temperature spectrum with decreasing grain size. The bending point in the TTE <5 micrometer fraction could possibly be related to the (complex) transition of monoclinic pyrrhotite into high-temperature hexagonal pyrrhotite which takes place at some 250-260 °C (Kissin and Scott, 1982). The reason why this effect is only detectable in remanence behaviour of almost SD particles and not in larger grain sizes, is unknown.

with virtually no decrease below some 225 °C. The steep blocking temperature spectrum is illustrated by the large remanence fall between 300 and 325 °C, in agreement with results of Halgedahl and Fuller (1981), who report that coarse-grained pyrrhotite acquires 90 percent of its total TRM between 300 and 325 °C. The blocking spectrum is increasingly less steep with falling grain size below 25 micrometer.

2.2 Low-temperature experiments

2.2.1 Behaviour of the isothermal saturation remanence

The pyrrhotite fractions behave similarly for all samples. As an example the behaviour of TTE pyrrhotite is shown (Fig. 7). When cooled down for the first time ("A" curves, cf. Fig. 7) a gradual remanence fall with decreasing temperature is observed in the coarsest grain-size fractions, which hardly returns when rewarming the specimen. The remanence decrease after a complete low-temperature cycle gradually diminishes with increasingly smaller grain-size fractions: the <5 micrometer fractions show an almost reversible low-temperature (LT) cycle (Fig. 7, Fig. 8, Table IV). The remanence slightly increases in this fraction upon cooling down to approximately -70 °C; in this temperature region a broad remanence maximum is observed. Upon further cooling the remanence is slightly decreasing. When cooling a second time ("B" curves in Fig. 7), a virtually reversible remanence temperature dependence is observed for all fractions, again with a broad maximum in the -70 °C temperature region.

The remanence decrease of the "A" curves in the coarse grain-size fractions might be related to a changing domain structure. Because the saturated state at room temperature represents certainly not the most favourable energy configuration and because the cooling is performed in a field-free space, a remanence decrease as observed can be expected since the accommodated domain energy configurations will represent a lower overall energy state than the saturated state. K_3 and K_4 of pyrrhotite show a strong temperature dependence (Bin and Pauthenet, 1963) with K_3 changing sign and K_4 showing a maximum at -68 °C. Apparently, in large grains, the energy minima are separated by relatively low barriers, which can be overcome by the changing anisotropy constant regime.

On the other hand, the SD grains as approached by the <5 micrometer fractions show already a reversible LT behaviour when cooled down for the first time. Their remanence behaviour during LT cycling will solely depend on the (reversible) temperature dependence of the anisotropy constants, if the saturated state represents an energy minimum surrounded by steep barriers. The gradual increasing reversibility of the "A" curves with decreasing grain size concurs with a gradual change from MD to SD pyrrhotite as inferred from domain observations (Soffel, 1977, 1981; Halgedahl and Fuller, 1983). The presence of intergrowths in the coarse DIS fractions (above some 30 micrometer; microscope observation; Dekkers, 1988A) is inferred from a smaller remanence loss than the other samples (cf. Table IV).

The "B" curves display also remanence trends which will be strongly dependent on the temperature dependence of the anisotropy constants. During the rewarming trajectory of the "A" curves, the energy state of the grains corresponding to the liquid nitrogen temperature is apparently preserved. Then, a second LT cycling will reveal reversible curves with a remanence behaviour dependent on the temperature regime of the anisotropy constants. The virtually reversible "B" curves concur with

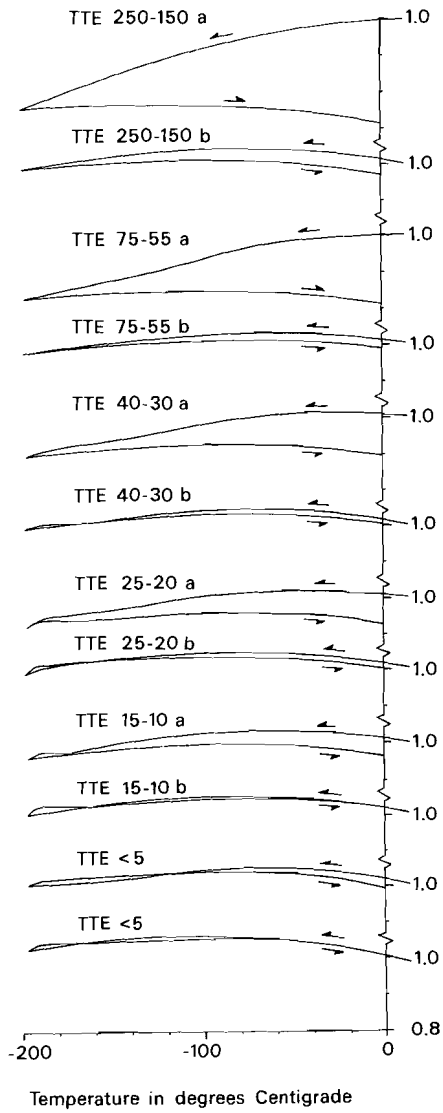

Fig. 7. Behaviour of pyrrhotite J_{rs} during low-temperature cycling down to the liquid nitrogen temperature normalized to their initial value as function of grain size. The behaviour of the TTE (Temperino) sample is shown; the other samples behaved similarly. The "A" curves refer to the first cooling cycle; the remanence remaining after this cycle, was subjected to a second cooling cycle, referred to as "B" curves. The "B" curves are normalized to their initial value, which is the endpoint value of the corresponding "A" curves at room temperature. Arrows indicate the cooling and rewarming curves. For further explanation see text.

the above sketched trend. The broad maximum observed in the -70 °C region agrees well with the maximum in K_4 and the sign change of K_3 determined at -68 °C (Bin and Pauthenet, 1963).

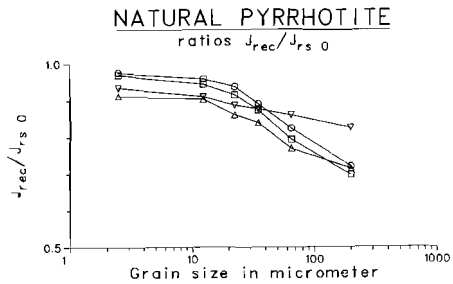

Fig. 8. Ratios of the remanence after the first cooling cycle ($J_{r\ rec.}$) and the saturation remanence before low-temperature treatment ($J_{rs\ 0}$) versus grain size. The ratio increases with decreasing grain size, indicating the increasing reversibility of the low-temperature curves with decreasing grain size. For symbol meanings cf. Fig. 2.

Table IV: Saturation remanence with the remanence part which remains after the first cooling cycle.

grain size	EOR		TTE		EGI		OIS	
250 - 150	2.45	0.72	2.02	0.70	2.00	0.72	2.45	0.83
75 - 55	3.48	0.82	4.30	0.80	3.04	0.77	2.35	0.86
40 - 30	4.60	0.89	5.61	0.88	4.67	0.84	2.57	0.88
25 - 20	4.48	0.94	6.42	0.92	4.96	0.86	3.90	0.89
15 - 10	5.00	0.96	6.61	0.94	5.83	0.90	3.19	0.91
< 5	1.30	0.98	2.46	0.97	3.62	0.91	1.78	0.93

J_{rs} (Am^2kg^{-1}) is listed in the first column; the ratio of the remanence remaining after one cooling cycle and the initial remanence in the second column.

2.2.2 Behaviour of the thermoremanence

TRM shows initially a small remanence increase followed by a small decrease in the coarse grain-size fractions, when cooled for the first time to -196 °C (Fig. 9). The onset of the decrease is situated at approximately -70 °C. The smallest grain-size fractions exhibit the largest remanence decrease; its magnitude may vary considerably. A second cooling cycle reveals reversible remanence behaviour.

A low-field MD pyrrhotite TRM domain structure hardly deviates from a thermally demagnetized one which represents a minimum energy configuration (Halgedahl and Fuller, 1981). So, contrary to the J_{rs} domain state, one might suppose that a MD TRM remanence will show already a more or less reversible behaviour during the first cooling cycle. The variable TRM decrease in small grain-size fractions during LT cycling might tentatively be explained by supposing that the relative positions of energy minima apparently enable a remanence accommodation to the changing anisotropy constants upon temperature in the TRM case, which results in a (varying) remanence decrease.

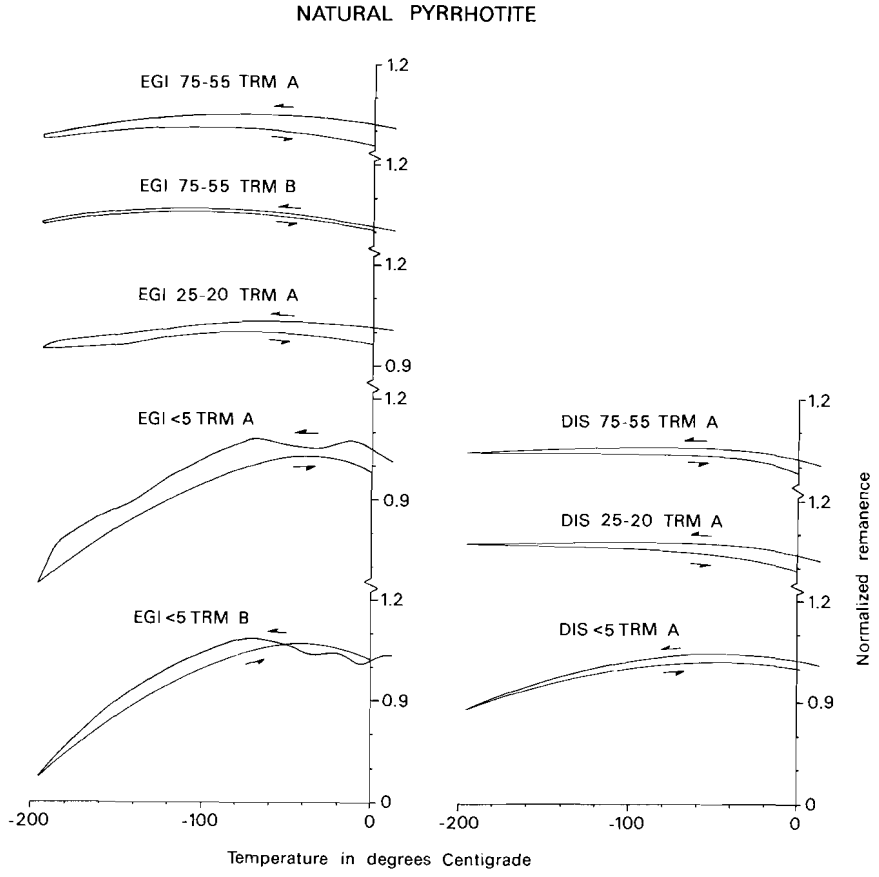

Fig. 9. Behaviour of TRM acquired in a 67 Am^{-1} (84 microTesla) field during low-temperature treatment for some pyrrhotite fractions. DIS and EGI denote the Isola di Vocca and Ginevro pyrrhotites respectively. The numbers after the sample label refer to the grain size in micrometer. An "A" curve refers to the first cooling cycle; a "B" curve to the second cooling cycle; both normalized to their initial value. Cooling and rewarming paths are indicated by arrows. The curves of the finest fractions have been smoothed because their TRM was close to the limit of detection of the HALT spinner.

3 CONCLUSIONS

It is known that many of the pyrrhotite high-temperature superstructures can be quenched (e.g. Kissin and Scott, 1982). The cooling rate determines to which extent the high-temperature superstructures are preserved. The impact of fast cooling on the pyrrhotite structure is demonstrated by a different J_{rs} before and after thermal treatment in the continuous thermal demagnetization equipment. The high-temperature superstructures are specially common in socalled intermediate pyrrhotites (mixtures of hexagonal and monoclinic pyrrhotites), which are supposed to represent the majority by far of natural pyrrhotites (Arnold, 1967). Haphazard quenching of high-temperature pyrrhotite phases

may influence thermal decay curves obtained by stepwise thermal demagnetization.

Stepwise thermal demagnetization revealed different pyrrhotite TRM and J_{rm} thermal decay curves. Cooling rates during the stepwise thermal demagnetization procedure were slow, so quenching of high-temperature phases will be avoided, at least to a large extent.

TRM thermal decay curves were typically block-shaped without grain-size dependence above grain size fractions of some 30 micrometer. In finer grain-size fractions thermal decay curves were increasingly less block-shaped with decreasing grain size.

J_{rm} thermal decay curves showed marked differences between coarse and fine grain-size fractions. Coarse fractions decreased more or less monotonously with a slightly convex decay curve. Fine fractions decreased much faster at low temperatures (up to 210-245 °C) and showed a remanence increase in the 260-300 °C temperature trajectory. When the part of the thermal decay curve in the fine grain-size fractions above some 280-300 °C is thought to be connected with its part below some 150 °C, a monotonous slightly convex decay curve like that of the coarse grain-size fractions is obtained. The difference in thermal decay curves is tentatively attributed to sluggishness of superstructure changes in coarse grain-size fractions. If it is allowed to extend this J_{rm} behaviour to other low-temperature remanences, this may lead to erroneous interpretations of thermal demagnetization curves. The remanence increase in the 260-280 °C temperature range could be interpreted as a separate remanence component, whereas it is inherent to the remanence behaviour of a single component remanence of fine-grained pyrrhotite. Data on the thermal behaviour of other low-temperature remanences are greatly needed to investigate whether such extension is allowed.

Continuous thermal demagnetization has the advantage above stepwise thermal demagnetization that it infers no cooling. In this way the haphazard partial quenching of high-temperature pyrrhotite phases is avoided. Normalized decay curves of continuous thermally demagnetized pyrrhotites show a great similarity for all pyrrhotite samples regardless of their grain size. J_{rm} decay curves are slightly convex and decrease monotonously with increasing temperature. Small grain-size fractions have a blocking temperature spectrum slightly shifted to lower temperatures. Normalized TRM decay curves show the same features with a steeper approach to the Curie temperature; they are (virtually) identical for all pyrrhotites regardless the grain size.

Besides showing complex superstructure changes at elevated temperatures, pyrrhotite is a highly reactive phase at already moderately elevated temperatures in the presence of a (water-rich) vapour phase. It converts to hematite- or magnetite-like phases depending on the redox conditions in the furnace and in the specimen itself. Though pyrrhotite alteration is not specifically studied in the present contribution, it could not completely be avoided in fine grains despite heating in an inert atmosphere. In natural samples, pyrrhotite alteration may occur to a much larger extent. The alteration products may acquire spurious remanences. Even if they do not show such behaviour, they have impact on the thermal decay curve of the sample, because they form at the expense of pyrrhotite. A decay curve can be, as such, a combination of "true" thermal demagnetization and chemical break-down of pyrrhotite.

Low-temperature (LT) cycling of J_{rm} revealed a gradually decreasing remanence with decreasing temperature in coarse grain-size fractions. The remanence which disappeared during cooling is not recovered during rewarming. During cooling, the energy level corresponding to the room temperature J_{rm} domain state has irreversibly changed due to accommo-

dation to changing temperature. For MD grains levels of local minimum energy are apparently not separated by high energy barriers. The remanence decrease during the cooling path gradually diminishes with decreasing grain size. This results in a gradually increasing reversibility of the first cooling cycle with decreasing grain size, corresponding to a gradual approach to the SD state. This state is apparently characterized by an energy level surrounded by large energy barriers. The remanence at -196 °C in the <5 micrometer fractions (small PSD grains) is virtually the same as the original room temperature remanence. The LT curve shows a broad remanence maximum during a temperature interval at approximately -70 °C corresponding to the maximum of K_3 and the sign-change of K_4.

When the recovered remanence is subjected a second time to LT treatment, all grain-size fractions showed reversible cooling and rewarming paths with a remanence maximum in the same temperature range.

TRM, representing an energy state close to the minimum energy state of thermally demagnetized pyrrhotite (Halgedahl and Fuller, 1981), shows more or less reversible remanence behaviour already during the first cooling cycle. When cooling TRM-carrying pyrrhotite samples, coarse grain-size fractions show a slight remanence increase down to approximately -70 °C with hardly any decrease during further cooling. Fine grain-size fractions show a similar remanence increase during cooling to the same temperature. Upon further cooling to the liquid nitrogen temperature the remanence is gradually decreasing. This remanence decrease shows between-sample differences, unlike the behaviour of J_{rs} during cooling.

Acknowledgements

Prof. Dr. J.D.A. Zijderveld critically reviewed the manuscript. It would have been hardly possible to keep the HALT spinner in top running condition without the assistance of T.A.T. Mullender. Drs. M.I. Pieters assisted during the sampling campaign for this research. J.J.J. Bergenhenegouwen made the drawings. These investigations were supported by the Netherlands Foundation for Earth Science Research (AWON) with financial aid from the Netherlands Organization for the Advancement of Pure Research (Z.W.O., grant 751-354-006).

4 REFERENCES

Arnold R.G., 1967, Range in composition and structure of 82 natural terrestrial pyrrhotites, Can. Min. 9, 31-50.

Barker W.W., Parks T.C., 1986, The thermodynamic properties of pyrrhotite and pyrite: a re-evaluation, Geochim. Cosmochim. Acta 50, 2185-94.

Bennett C.E.G., Graham J., 1980, New observations on natural pyrrhotites. Part III. Thermomagnetic experiments, Am. Min. 65, 800-7.

Bennett C.E.G., Graham J., 1981, New observations on natural pyrrhotites: magnetic transition in hexagonal pyrrhotite. Am. Min. 66, 1254-7.

Bennett C.E.G., Graham J., Thornber M.R., 1972, New observations on natural pyrrhotites. Part I: Mineragraphic techniques, Am. Min. 57, 445-61.

Bertaut E.F., 1953, Contribution à l'étude des structures lacunaires: la pyrrhotine, Acta Cryst. 6, 557-61.

Bin M., Pauthenet R., 1963, Magnetic anisotropy in pyrrhotite, J. Appl. Phys. 34, 1161-2.

Dankers P.H.M., 1978, Magnetic properties of dispersed natural iron-oxides of known grain-size, Ph.D. thesis University of Utrecht, 142pp.

Dankers P.H.M., 1981, Relationship between median destructive field and remanent coercive forces for dispersed magnetite, titanomagnetite and hematite, Geophys. J. R. astr. Soc. 64, 447-61.

Dekkers M.J., 1988A, Magnetic properties of natural pyrrhotite part I: Behaviour of initial susceptibility and saturation-magnetization related rockmagnetic parameters in a grain-size dependent framework, In: Some rockmagnetic parameters for natural goethite, pyrrhotite and fine-grained hematite, Ph.D. thesis University of Utrecht, chapter 8 (Phys. Earth Plan. Inter., in press).

Dekkers M.J., 1988B, Sample preparation and characterization of the pyrrhotites, In: Some rockmagnetic parameters for natural goethite, pyrrhotite and fine-grained hematite, Ph.D. thesis University of Utrecht, chapter 7.

Fleet M.E., MacRae N., 1969, Two-phase hexagonal pyrrhotites, Can. Min. 9, 699-705.

Halgedahl S.L., Fuller M., 1981, The dependence of magnetic domain structure upon magnetization state in polycrystalline pyrrhotite, Phys. Earth Planet. Inter. 26, 93-7.

Halgedahl S.L., Fuller M., 1983, The dependence of magnetic domain structure upon magnetization state with emphasis upon nucleation as a mechanism for pseudo-single-domain behavior, J. Geophys. Res. B 88, 6505-22.

Haraldsen H., 1941A, Uber die Eisen(II)-Sulphidmischkristalle, Zeitschr. Anorg. Allgem. Chemie 246, 169-94.

Haraldsen H., 1941B, Uber die Hochtemperaturumwandlungen der Eisen-Sulphid Mischkristalle, Zeitschr. Anorg. Allgem. Chemie 246, 195-226.

Hartstra R.L., 1982A, Some rockmagnetic parameters for natural iron-titanium oxides, Ph.D. thesis University of Utrecht, 145pp.

Hartstra R.L., 1982B, High-temperature characteristics of a natural titanomagnetite, Geophys. J. R. astr. Soc. 71, 455-76.

Hartstra R.L., 1982C, A comparative study of the ARM and I_{sr} of some natural magnetites of MD and PSD grain size, Geophys. J. R. astr. Soc. 71, 497-518.

Hartstra R.L., 1983, TRM, ARM, and Isr of two natural magnetites of MD and PSD grain size, Geophys. J. R. astr. Soc. 73, 719-37.

Hayase K., Otsuka R., Mariko T., 1963, Magnetic properties of natural pyrrhotite, Mineral. J. (Tokyo) 4, 41-56.

Kissin S.A., Scott S.D., 1982, Phase relations involving pyrrhotite below 350 °C, Econ. Geol. 77, 1739-54.

Koto K., Kitamura M., 1981, The superstructure of the intermediate pyrrhotite. II. One-dimensional Out-of-step vector of Fe vacancies in the incommensurate structure with compositional range from Fe_9S_{10} to $Fe_{11}S_{12}$, Acta Cryst. A37, 301-8.

Kullerud G., Doe B., Buseck P.R., Troften P.F., 1963, Heating experiments on monoclinic pyrrhotites, Carnegie Inst. Washington Year Book 62, 210-3.

Lotgering F.K., 1956, On the ferrimagnetism of some sulphides and oxides, Philips Res. Rep. 11, 190-249.

Marusek L.A., Mulay L.N., 1980, Polytypism in the cation-deficient iron sulphide, Fe_9S_{10}, and the magnetokinetics of the diffusion process at temperatures about the antiferro- to ferrimagnetic (λ) phase transition, Phys. Rev. B 21, 238-44.

Morimoto N., Gyobu A., Tsukuma K., Koto K., 1975A, Superstructure and non-stoichiometry of intermediate pyrrhotite, Am. Min. 60, 240-8.

Morimoto N., Gyobu A., Mukaiyama H., Izewa E., 1975B, Crystallography and stability of pyrrhotites, Econ. Geol. 70, 824-33.

Morimoto N., Nakazawa H., Nishiguchi K., Tokonami M., 1970, Pyrrhotites: stoichiometric compounds with composition $Fe_{n-1}S_n$ (n GE 8), Science 168, 964-6.

Nakazawa H., Morimoto N., 1970, Pyrrhotite phase relations below 320 °C, Proc. Japan Acad. 46, 678-83.

Nakazawa H., Morimoto N., 1971, Phase relations and superstructures of pyrrhotite $Fe_{1-x}S$, Mat. Res. Bull. 6, 345-58.

Onufrienok V.V., Zvegintsev A.G., 1981, Magnetic ordering in hexagonal pyrrhotite at high temperature, Geomagn. Aeron. (USSR) 21, 666-8 (eng. ed.).

Schwarz E.J., 1967, Dependence of the magnetic properties on the thermal history of natural polycrystalline pyrrhotites $Fe_{0.89}S$, J. Geomagn. Geoelectr. 19, 91-101.

Schwarz E.J., 1968, Magnetic phases in natural pyrrhotite $Fe_{0.91}S$ and $Fe_{0.89}S$, J. Geomagn. Geoelectr. 20, 67-74.

Schwarz E.J., 1969, Thermomagnetics of pyrrhotite, Geol. Surv. of Can. Paper 69-1B, 41-4.

Schwarz E.J., 1975, Magnetic properties of pyrrhotite and their use in applied geology and geophysics, Geol. Surv. Can. Paper 74-59, 24pp.

Schwarz E.J., Harris D.C., 1970, Phases in natural pyrrhotite and the effect of heating on their magnetic properties, J. Geomagn. Geoelectr. 22, 463-70.

Schwarz E.J., Vaughan D.J., 1972, Magnetic phase relations of pyrrhotita, J. Geomagn. Geoelectr. 24, 441-58.

Stacey F.D., Banerjee S.K., 1974, The physical principles of rock magnetism, Elsevier Scientific Publ. Comp., Amsterdam-London-New York, 195pp.

Soffel H.C., 1977, Pseudo-Single-Domain effects and Single-Domain Multidomain transition in natural pyrrhotite deduced from domain structure observations, J. Geophys. 42, 351-9.

Soffel H.C., 1981, Domain structure of natural fine-grained pyrrhotite in a rock matrix (diabase), Phys. Earth Plan. Inter. 26, 98-106.

Sugaki A., Shima H., 1977, Studies on pyrrhotite group minerels (3). On solvuses of solid solutions among troilite, hexagonal and monoclinic pyrrhotites below 300 °C, Tohoku Univ. Sci. Rept. ser 3 13, 165-82.

Toulmin P. III, Barton P.B. jr., 1964, A thermodynamic study of pyrite and pyrrhotite, Geochim. Cosmochim. Acta 28, 641-71.

Vaughan D.J. Schwarz E.J., Owens D.R., 1971, Pyrrhotites from the Strathcona Mine, Sudbury, Canada: A thermomagnetic and mineralogical study, Econ. Geol. 66, 1131-44.

Yund R.A., Hall H.T, 1969, Hexagonal and monoclinic pyrrhotites, Econ. Geol. 64, 420-3.

CHAPTER 10

SOME REMANENT MAGNETIC PROPERTIES OF FINE-GRAINED NATURAL LOW-TEMPERATURE HEMATITE

Abstract

The grain-size dependence of some remanent magnetic properties of a natural low-temperature hematite is reported. Because of the provenance of extremely fine-grained hematite in sediments, seven grain- size fractions were prepared in the sub-10 micrometer range. The finest fraction comprised the <0.25 micrometer grain size range. Hematite from a gossan in Montarnu (France) was upgraded by magnetic separation. Separation results were checked with X-ray diffraction analysis. The 10-5 micrometer fraction was obtained by micro-precision sieving; finer grain-size fractions by centrifuging. The grain-size ranges for each fraction were checked with an electron microscope. Microprobe analyses revealed a hematite without much substitution (minor Si and Al were detected) with an excess water. The water content was confirmed wet-chemically. TGA indicated that water-loss during thermal treatment occurred throughout the whole temperature range of routine thermal demagnetization. Unit cell dimensions of the present hematite are very close to those of ideal hematite. The average crystallite size of the hematite (derived from X-ray line broadening) is approximately 600 Å.

The magnetic properties of the hematite appear to be strongly dependent on its thermal treatment. Prior to annealing the saturation remanence (J_{rs}) decreases with grain size (0.19-0.04 Am^2kg^{-1}). The remanent coercive force (H_{cr}; range 215 to 425 kAm^{-1}), remanent acquisition coercive force ($H_{cr'}$; range 205 to 360 kAm^{-1}) and median destructive field of the saturation remanence ($H_{1/2r}$; range 170 to 270 kAm^{-1}) all show a maximum in the 1.0-0.5 micrometer fraction. Combined with the absolute figure for H_{cr} the $J_{rs}/(H_{cr}*X_{in})$ parameter can be used as grain-size indicator. Low-temperature cycling of J_{rs} shows a gradually, slightly decreasing remanence without a Morin transition. Identical curves are observed for all grain-size fractions. The Morin transition is suppressed due to microcrystalline character of the present hematite.

After annealing at 700 °C J_{rs} shows considerably lower values (range 0.05-0.003 Am^2kg^{-1}). Both H_{cr} and $H_{cr'}$ have increased (ranges respectively 415 to 650 kAm^{-1} and 340 to 610 kAm^{-1}). A maximum for both parameters is observed in the 2.1-1.0 micrometer fraction. After annealing the fractions show a Morin transition during low-temperature cycling of the saturation remanence. Annealing has resulted in enlargement of the crystallites making up the grains. TRM, induced in a 67 Am^{-1} field, decreases with grain size. The specific volume TRM decreases from 0.47 to 0.05.

The large differences in behaviour before and after annealing indicate that synthetic hematite prepared at relatively high temperatures by dehydrating goethite or oxidizing magnetite are not representative for natural low-temperature hematite.

The different rockmagnetic properties before and after annealing principally might provide a basis for the discrimination in sediments between a hematite DRM with a high-temperature origin and a hematite CRM which has a low-temperature origin. Two natural red beds, one with a CRM and one with a DRM associated with high-temperature hematite, broadly show the expected differences in coercivity and in annealing behaviour, although a full account of all aspects of the observed behaviour can not yet be given.

1 INTRODUCTION

1.1 Hematite in sediments

The remanence carried by hematite in red beds and other sediment types resides for a large part in extremely fine grains. Most research is confined to red beds because of their paleomagnetic importance. Hematite grains in red beds can be divided into several types. Formerly, such division was based largely upon the size of the grains: specularite (black-coloured hematite with grain sizes larger than some 1 micrometer) and pigment (red-coloured hematite with grain sizes smaller than some 1 micrometer) were recognized. The specularite was thought to carry a depositional remanent magnetization (DRM) and the pigment a chemical remanent magnetization (CRM) (e.g. Collinson, 1974). However, this rather straightforward division has been refined considerably. Walker et al. (1981), in an elaborate SEM study on the Moenkopi Formation (Arizona, Colorado, USA), recognized hematite in six modifications: microcrystalline hematite, specular hematite, polycrystalline and monocrystalline hematite grains, (partly) hematized ilmenite grains, grains consisting of primary hematite-ilmenite intergrowths and ultra-fine pigment. They argue that microcrystalline hematite, specular hematite (specularite), polycrystalline and monocrystalline hematite and also ultra-fine hematite pigment are all authigenic and, hence, carry a CRM. Authigenic hematite growth (i.e. CRM acquisition) is not necessarily of recent origin, i.e. related to weathering (e.g. Walker et al., 1981; Channell et al., 1982; Özdemir and Deutsch, 1984).

The remanence acquisition in red beds is still a controversial subject despite much research effort. Often CRM is put forward as the remanence type for red beds (e.g. Walker et al., 1981 and references therein). The authigenic hematite growth (i.e. CRM acquisition) is considered to be a long-time process (e.g. Roy and Park, 1972; Walker et al., 1981). This raises serious doubt on the value of red beds for magnetostratigraphic and geomagnetic research. However, DRM has also been proposed as the remanence type in red beds, e.g. Elmore and Van der Voo (1982), investigating the Copper Harbor Conglomerate (USA), recognized a remanence component of which the direction showed a bedding error. Therefore it was concluded that this component was of DRM origin. Also the results of van den Ende (1977), who studied paleosecular variation in the Permian red beds of Dôme de Barrot (France), indicate that in these red beds the remanence has a DRM origin. Any mechanism of CRM acquisition cannot explain the observed remanence behaviour, which shows loops similar to present day secular variation. It may thus well be possible that both mechanisms for remanence acquisition exist in red beds. Recognition of and discrimination between hematite from DRM and CRM origin by other means than analysis of paleomagnetic directions, obviously contributes to the interpretation of paleomagnetic red bed data. A warranted rockmagnetic analysis of red beds requires more data on the rockmagnetic properties of fine-grained hematite with a low-temperature origin.

1.2 Short outline of the hematite rockmagnetic properties

1.2.1 Magnetocrystalline and defect moment

Basically two types of magnetic moment are distinguished in hematite:
1) The magnetocrystalline moment related to spin canting (also referred to as canted, fundamental, intrinsic or anisotropic moment). This

moment disappears when cooling through the Morin transition (at −15 °C; cf. Morin, 1950; Néel and Pauthenet, 1952), because the spin direction changes from perpendicular to parallel to the c-axis.

2) The defect magnetic moment (also referred to as isotropic or magneto-elastic moment), which is not influenced by cooling.

The temperature of the Morin transition as well as its extent is shown to be dependent on the amount of substitution in the hematite. Haigh (1957A) shows that substitution of minor amounts Ti (up to one percent) lowers the temperature at which the transition occurs; substitution of Al (up to ten percent) hardly influences the transition temperature. Flanders and Remeikema (1965) report on the influence of minor amounts substituted Ti, Si, Mn, Sn, Cu, Al and Gd on the Morin transition. The transition is virtually suppressed by two percent Ti and one percent Sn. Its temperature range becomes considerably broader by substitution of two weight percent Cu. Si "tails off" the low-temperature part of the transition, i.e. it is extended to lower temperatures resulting in a "tail" of the transition. The impact of the other substituted elements is much less: the transition temperature is slightly lowered; the accompanying magnetization change is less, both compared to pure hematite.

The Morin transition is suppressed in extremely small hematite grains of a high purity (below some 0.03 micrometer; e.g. Bando et al., 1965; Schroeer and Nininger, 1967). The influence of substitution on this grain size is not known.

1.2.2 Grain-size dependent trends

The magnetic properties of hematite grains show grain-size dependent trends. Dankers (1978, 1981) and Hartstra (1982A) report the isothermal saturation remanent magnetization (J_{rs}) for various natural hematites in the order of 0.2 Am^2kg^{-1} with only minor variation. J_{rs} is grain-size independent in a range from 250 micrometer down to 5 micrometer. However, in grain sizes smaller than 5 micrometer J_{rs} (isothermal remanent magnetization (IRM) acquired in a 1520 kAm^{-1} (1.9 Tesla) field) is shown to decrease with decreasing grain size for synthetic hematite (Dunlop, 1971). Also the saturation magnetization (J_s) decreases with grain size. The J_{rs}/J_s ratio, however, increases.

The coercive force (H_c) of crushed natural hematite grains shows a maximum at a grain-size diameter of 10-15 micrometer (Chevallier and Mathieu, 1943). The remanent coercive force (H_{cr}) and remanent acquisition coercive force ($H_{cr'}$) for natural hematite increase with decreasing grain size in a range of 250 micrometer down to 5 micrometer. H_{cr} and $H_{cr'}$ figures for individual hematites show a distinct variation (H_{cr} and $H_{cr'}$ range varies approximately from 24 kAm^{-1} to 240 kAm^{-1} for 250-150 micrometer grain size and from 280 kAm^{-1} to 480 kAm^{-1} for <5 micrometer grain size; cf. Dankers, 1978, 1981; Hartstra, 1982A). In synthetic hematites with grain sizes smaller than 5 micrometer Dunlop (1971) reports increasing and decreasing $H_{cr'}$ trends with decreasing grain size for individual hematites, depending on their preparation method.

1.2.3 Relative hardness of the magnetocrystalline and defect moment

Conflicting results have been reported on the relative hardness of the magnetocrystalline and defect remanence type. Smith and Fuller (1967) studying natural samples containing single-crystal hematite,

conclude that the magnetocrystalline moment is softer than the defect moment. Haigh (1957B) and Dunlop (1971) on the contrary, show that the magnetocrystalline moment - with an H_{cr} in the order of 100 to 200 kAm^{-1} - is harder than the defect moment. Dunlop (1970) shows this also for fine-grained natural pigment. It should be mentioned at this stage that the hematites studied by Dankers and Hartstra (op. cit.) all exhibit a Morin transition during low-temperature cycling. The magnetocrystalline moment may thus show a widely varying hardness.

1.2.4 Superparamagnetic and single domain threshold sizes

Extremely fine grains are superparamagnetic. Various determinations are reported for the hematite superparamagnetic (SP) threshold size, i.e. the grain size at which the transition from unstable SP behaviour to the extremely stable single domain (SD) state occurs. Chevallier (1951) notes that hematite grains formed by the dehydration of goethite showed SP behaviour in grain sizes <0.1 micrometer. Also Strangway et al. (1968) placed the SP threshold size at approximately 0.1 micrometer. Hedley (1968) suggests the onset of SP behaviour at some 0.3 micrometer, but a small part (0.1% of the SD remanence) would persist at 0.02 micrometer.

Kündig et al. (1966) report a smaller SP threshold size of 0.012 micrometer grain diameter based on Mössbauer data. Banerjee (1971) determines the SP threshold size at 0.025 micrometer. It can be concluded that for relaxation times of geological interest the hematite SP threshold size will be in the order of 0.03 micrometer.

The SD threshold size is only vaguely defined for hematite. Dunlop (1971) concluded from the H_c maximum in the 10-15 micrometer grain-size range observed by Chevallier and Mathieu (1943), that the SP threshold size is located between 10 and 100 micrometer. Domain studies on well-crystalline hematite crystals reveal wall spacings of up to even 500 micrometer (e.g. Eaton and Morrish, 1969).

1.2.5 Change in magnetic properties due to annealing

The hematite magnetic properties may change upon heating. Especially the defect magnetic moment is thought to be sensitive to heat treatment (e.g. Smith and Fuller, 1967; Dunlop, 1971, 1972; Bucur, 1978). The hematite hardness increases with annealing due to annealing out of the defect moment. This is reported for natural samples as well as synthetic hematite (e.g. Dunlop, 1971, 1972). Most experimental data on annealing behaviour of fine-grained hematite are based on synthetic hematites. Usual preparation methods, however, involve heating to a few hundreds degrees Centigrade (e.g. Dunlop, 1971) and as such their behaviour might not be representative for low-temperature natural hematite. The investigations based on natural samples have the drawback that the grain size of the hematite is relatively poorly defined spectrum, which hinders a proper interpretation of grain-size aspects.

1.3 Implications for the present study

To arrive at more representative data on the behaviour of natural low-temperature hematite during annealing and to evaluate grain-size aspects, a set of artificial samples containing such hematite with a well-defined grain size was prepared. Raw sample material was collected from a hematite-rich gossan at Montarnu, France (Wilhelm and Kosake-

witch, 1978). Fine grain-size fractions of this hematite were homogeneously dispersed in a non-magnetic matrix.

2 SAMPLE PREPARATION AND HEMATITE CHARACTERIZATION

2.1 Sample preparation

The raw sample material (labelled FMW) constituted for the major part of hematite, but minor goethite and quartz (X-ray determination) appeared to be present. To concentrate the hematite, the raw sample material was crushed and magnetically separated. Crushing (gently) was done in a copper mortar to prevent magnetic contamination. To concentrate the hematite the crushed material was sieved in fractions down to <37 micrometer (A.S.T.M. sieve set; wet-sieving, acetone as flushing fluid). Thereafter the hematite was obtained by magnetic separation. Because of the interest in extreme fine grains, only the <37 micrometer fraction was magnetically separated, using a Frantz isodynamic separator adapted for separation in a liquid medium (Dekkers et al., in prep.). Results of the separation procedure were checked with X-ray diffraction (Debye-Scherrer Camera, Fe K_α-rays). Traces of goethite and quartz remained present.

The <37 micrometer fraction was divided into grain-size fractions with 5 micrometer intervals by ultrasonic micro-precision sieving down to 5 micrometer. A further division of the <5 micrometer fraction into six grain-size fractions was carried out by centrifuging, using a so-called pipette centrifuge. A pipette centrifuge (Fritsch analysette 21) is a centrifuge developed for grain size analysis in a grain-size range between 5 and 0.05 micrometer. A horizontally rotating disk contains the suspension to be analyzed. Six horizontally radiating capillaries debouching into a central capillary, are mounted in its centre. Desired aliquots (in the standard procedure 10 ml aliquots are extracted each time from the initial suspension, containing a volume of 180 ml) of the rotating suspension can be sucked through the capillaries at desired time intervals while the centrifuge is rotating. The maximum grain-size diameter in each aliquot can be calculated with Stokes' law written for angular velocity and correcting for a changing suspension level after each 10 ml aliquot extraction.

Grain-size separation of workable quantities can be obtained by sucking after a specific centrifuging time the total suspension volume within reach of the capillaries at once instead of several aliquots at distinct time intervals. The extracted suspension contains no grains with a larger diameter than a certain maximum diameter D corresponding to the rotation time of the centrifuge. The suspension which remains in the centrifuge after extraction, thus outside the reach of the capillaries, is enriched in grains with diameters larger than D. However, it contains also unwanted grains with diameters smaller than D, i.e. those grains smaller than D which were situated outside the reach of the capillaries in the initially homogeneous suspension. They are referred to as the tailing. By repeated centrifuging this tailing can be minimized.

Stokes' law is only obeyed when there is no interaction between the grains in suspension. For this reason, usually a peptisator is added, giving the suspended particles an electric charge leading to electrostatic particle repulsion. However, besides being of limited value in reducing the magnetic particle attraction, the peptisator adheres onto the hematite grains without being easily removed after the centrifuging procedure. It may cause alteration of the hematite during thermal expe-

riments (partial reduction to magnetite at high temperatures may be accelerated by the decomposition of the peptisator - organic chemical materials are usually applied). Experience indicates that the magnetic particle attraction in a half percent (by volume) hematite suspension in a liquid medium is that low that the conditions for the application of Stokes' law are not seriously violated. Consequently, hematite suspensions of a half percent by volume in ethanol without peptisator were centrifuged after being homogenized by ultrasonic waves for 15-20 minutes.

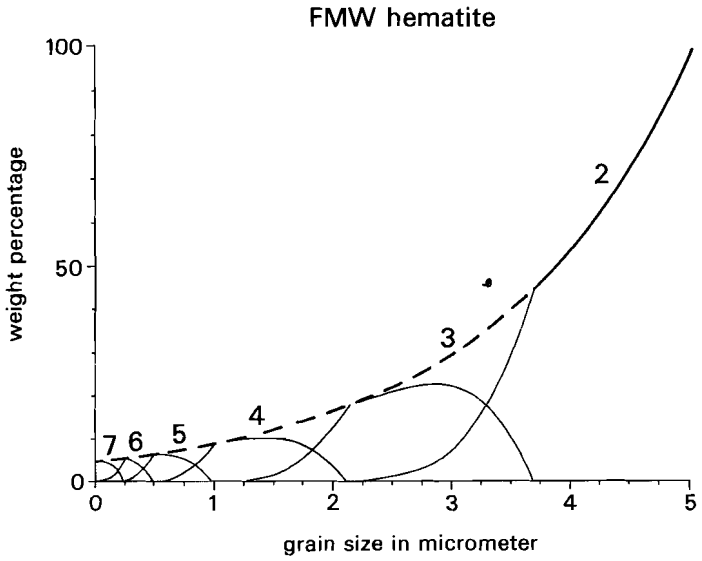

Fig. 1. Calculated grain size distribution in each grain size fraction in the <5 micrometer fractions, separated with the pipette centrifuge. The original unseparated grain size distribution (estimated from the mass of each separated fraction) is indicated with the dashed line. The 5-3.7 micrometer fraction is denoted with 2, the 3.7-2.1 micrometer fraction with 3, the 2.1-1.0 micrometer fraction with 4, the 1.0-0.5 micrometer fraction with 5, the 0.5-0.25 micrometer fraction with 6 and the smaller than 0.25 micrometer fraction with 7. The distribution within each fraction can be calculated by starting with a homogeneous distribution at the beginning of each centrifuge run and applying Stokes' law for separate infinite small grain size intervals making up the total fraction. The extracted suspension batch contains no grains larger than a certain diameter D. The batch, which remains in the centrifuge (remaining batch) after extraction is enriched in grains larger than D, but contains also a certain amount of grains smaller than D (tailing). The tailing constitutes of 1) those grains smaller than D which were already outside the reach of capillaries in the original homogeneous suspension and of 2) grains smaller than D which pass the reach of the capillaries during the spinning and extraction time. By repeated centrifuging of the remaining batch (which is homogenized between centrifuge runs) the tailing can be minimized. The distribution within each fraction is iteratively calculated using Stokes' law and starting with a homogeneous suspension with a grain size distribution obtained by the previous calculation. The upper limit of the largest fraction (i.e. fraction 2 with a grain-size range 5-3.7 micrometer) is the pore size of the sieve with the smallest pores in the set microprecisior sievas. This fraction was centrifuged eight times to remove the tailing as much as possible. Smaller fractions were centrifuged six times. It is obligatory to centrifuge fraction 2 a larger number of times, because the tailing of this coarsest fraction determines the yield of all finer fractions. Although it is impossible to remove the tailing completely, by repeated centrifuging a good grain-size separation with minor overlap between neighbouring fractions can be obtained.

Results of the grain size separation by means of the pipette centrifuge are depicted in Fig. 1; details of the separation procedure are described in Dekkers and Linssen (1987). Seven hematite fractions with the following ranges were obtained: 10-5 (microprecision sieved), 5-3.7, 3.7-2.1, 2.1-1.0, 1.0-0.5, 0.5-0.25 and <0.25 micrometer. Control of these calculated grain size ranges by electron microscopy (SEM and TEM techniques were used, the latter for the finest two fractions) yielded good agreement between the calculated ranges and those actually observed. The grains are approximately equidimensional. For rockmagnetic investigation the fractions were homogeneously dispersed in a non-magnetic matrix. Epoxy resin (Araldit D, Hardener CY 956; Ciba Geigi) was used as matrix for room and low-temperature investigation; a mixture of fine-grained calcined Al_2O_3 and waterglass for thermal experiments. The magnetic noise level of both types of matrixes was up to a few percent of the total signal.

2.2 Hematite characteristics determined with non-magnetic methods

The hematite unit cell and the average chemical composition, determined with microprobe analyses are compiled in Table I. The only major constituent is Fe_2O_3. Minor amounts Si, Al and S are present (calculated respectively as SiO_2, Al_2O_3 and SO_3). Other elements are detected in insignificant amounts (Ca, Mg, Mn) or their content is below the limit of detection (Ti). The hematite contains some 4 weight percent H_2O as the oxide sum does not equal one hundred percent. Wet-chemical analysis of the water content (Penfield method) of the hematite concentrate yields water percentages of 4.8 weight percent, in good agreement with weight percentage missing in the microprobe analysis. Thermographic analysis (Fig. 2) indicate that water-loss from this hematite during heating takes place over a broad temperature range. Water driven out off the hematite grains during hematite recrystallization will thus be available within the hematite grains throughout a complete thermal demagnetization run (up to 700 °C).

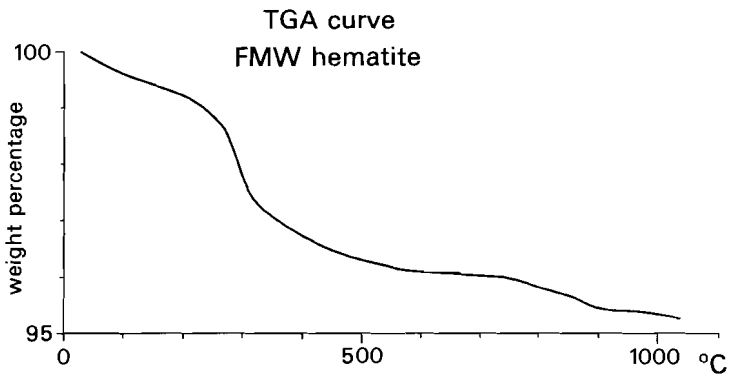

Fig. 2. TGA curve of the FMW hematite showing the loss of 4.8 weight percent water during annealing.

Calculation of the dimensions of the (hexagonal) unit cell (Table I) reveals dimensions close those of ideal hematite (*a*-axis 5.034; c-axis 13.77; both in Å). It may thus well be that a (major?) part of the Si is

not substituted in the hematite lattice but adsorbed onto or dispersed between small crystallites.

A backscattered electron image (Fig. 3) shows that minute compositional differences exist within the hematite on a microscale. Colloidal structures are clearly recognized indicating that the hematite had an amorphous precursor phase. These structures with corresponding compositional differences could not be observed with the normal image mode. The extremely small dimensions of the compositional differences (note the scale bar in Fig. 3) indicate that spot analyses with the microprobe analysis already represent averages (spot-size of 5 micrometer). The fine crystalline nature of the hematite is also demonstrated by an average hematite crystallite size of some 600 Å determined from X-ray line broadening. The crystallite size is smaller than the grain size. It can be presumed that this will be often the case when dealing with natural low-temperature hematite. Dunlop (1971) also notes that his synthetic hematites had crystallite sizes smaller than the grain size. Nevertheless his results and the results reported in the present contribution show evident grain-size trends.

Table I: Chemical composition and unit cell dimensions of the natural FMW hematite

	Oxide weight percentages		
	aver.	stdev.	stdev. aver.
SiO_2	2.29	0.60	0.103
Al_2O_3	1.04	0.49	0.084
TiO_2	0.00	0.00	0.000
Fe_2O_3	92.39	1.73	0.297
MnO	0.05	0.08	0.014
MgO	0.12	0.10	0.017
CaO	0.15	0.10	0.017
SO_3	0.62	0.27	0.046
total	96.69	1.45	0.249

Microprobe analyses were performed with a JEOL 8600 Superprobe fitted with a TN-5502 EDS analyzer. Operating conditions were 15keV and 2-3 nA. ZAF matrix correction was applied. Analyses are based on 34 spots, within-grain variation appeared to be not too large. aver. = average; stdev. = standard deviation; stdev. aver. = standard deviation of the average.

Hematite unit cell dimensions	
a-axis	5.024 ± 0.009
c-axis	13.77 ± 0.03

Cell dimensions are given in Å. Reflection positions were taken from a Debye-Scherrer film (Fe K_α-rays). Unit cell calculation is performed with the program UNITCELLD (Strom, 1976). Seven unweighted reflections are entered.

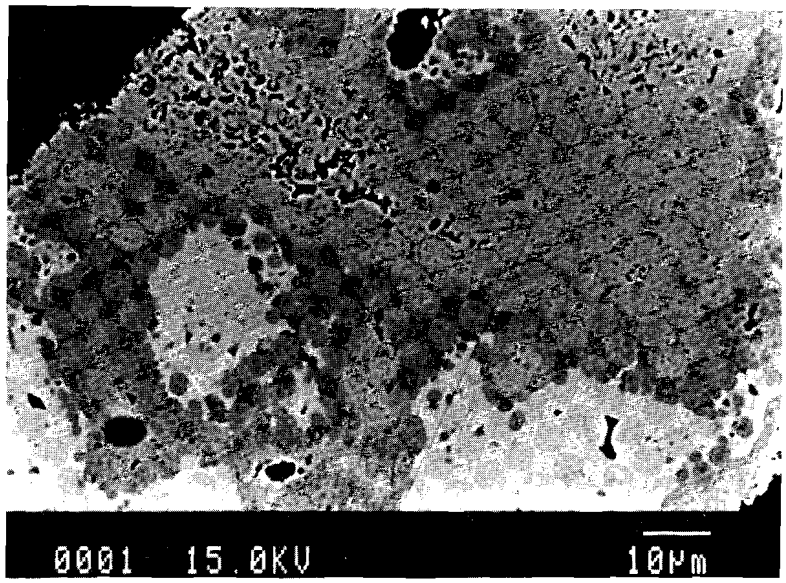

Fig. 3A. Backscattered electron image of the FMW hematite showing colloform textures. With normal image mode these textures are not detected and the grains seem homogeneous. This indicates their extremely small compositional difference.

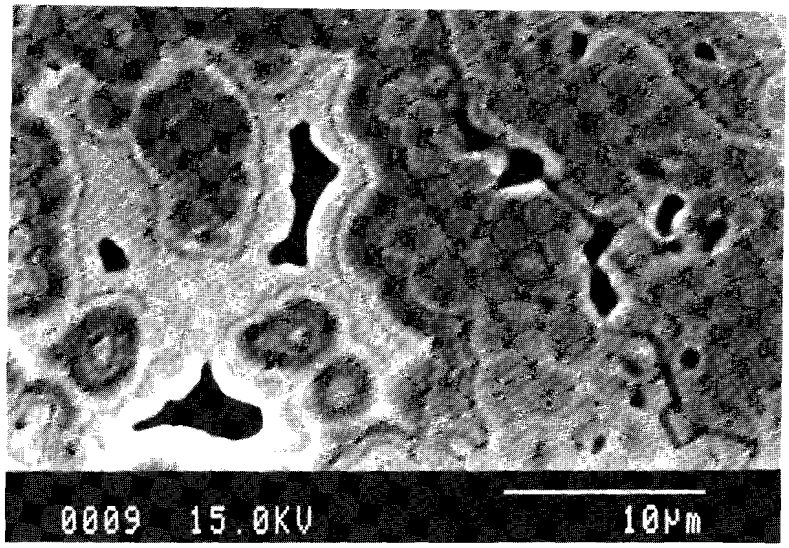

Fig. 3B. Close-up of a grain showing the fine crystalline nature of the colloform textures and small voids within the grain.

2.3 Instrumentation for the magnetic measurements

Initial susceptibilities were measured with a Jellinek KLY-1 susceptibility bridge. Remanence intensities were measured with a digital spinner magnetometer based on the Jellinek JR3 drive unit. This spinner is developed in the Utrecht Paleomagnetic Laboratory and has a sensitivity of 10^{-10} Am^2 and a reproducibility better than one degree for intensities exceeding 10^{-9} Am^2. During a later stage of the investigation measurements were done on a 2G-Enterprises cryogenic magnetometer with a sensitivity of 10^{-11} Am^2 and a slightly better angular reproducibility. Acquisition curves and hysteresis curves of the isothermal remanent magnetization (RA curves and RH curves respectively) were determined with a Förster fluxgate magnetometer type 1.107, calibrated with an astatic magnetometer. Continuous recordings of the saturation remanence (J_{rs}) and a TRM acquired in a 67 Am^{-1} field (84 microTesla) during low-temperature cycling were made with a fluxgate spinner magnetometer made suitable for measurements at high and low temperatures by placing the sample in a furnace or a dewar vessel respectively. Temperature regulation and periodic remanence measurements were controlled with a microcomputer system (Dankers, 1978, 1981; Hartstra, 1982B, 1982C). For stepwise thermal demagnetization of J_{rs} and TRM a thermal demagnetizer (rest-field less than 30-40 γ) designed in the Utrecht Paleomagnetic Laboratory, based on the Schönsted furnace was used. Heating to temperatures up to 700 °C was done in air.

3 RESULTS

The hematite material was processed in two separate series. The first series of seven grain-size fractions (hereafter referred to as Batch 1) was dispersed in epoxy resin and used for room and low-temperature measurements. The second series of five grain-size fractions (referred to as Batch 2) was dispersed in a matrix of fine-grained calcined Al_2O_3 and waterglass suitable for high-temperature measurements. The hematite content of the fractions in each batch decreased with grain size from some 250 mg for the coarse fractions down to 40 mg for the finest fractions. No magnetite-like minerals were traced in Batch 1; Batch 2 appeared to be contaminated with minute amounts magnetite- maghemite which were only traceable with the help of RA and RH curves (Fig. 4). During thermal treatment the creation of minute amounts magnetite-like minerals can hardly be avoided. Hence, usually traces of suchlike minerals will anyhow be present in thermally treated specimens. The magnetite/maghemite remanence is corrected for (so called "magnetite correction"); the magnetite/maghemite weight content is negligible compared to that of hematite.

The saturation remanence (J_{rs}) refers to the remanence acquired at room temperature in a field of 1670 kAm^{-1} (2.1 Tesla). The shape of the RA curves indicated that absolute saturation of the remanence is almost achieved in that field. The remanent coercive force (H_{cr}), remanent acquisition coercive force ($H_{cr'}$) and median destructive field ($H_{1/2r}$) are defined with respect to the 1670 kAm^{-1} J_{rs}.

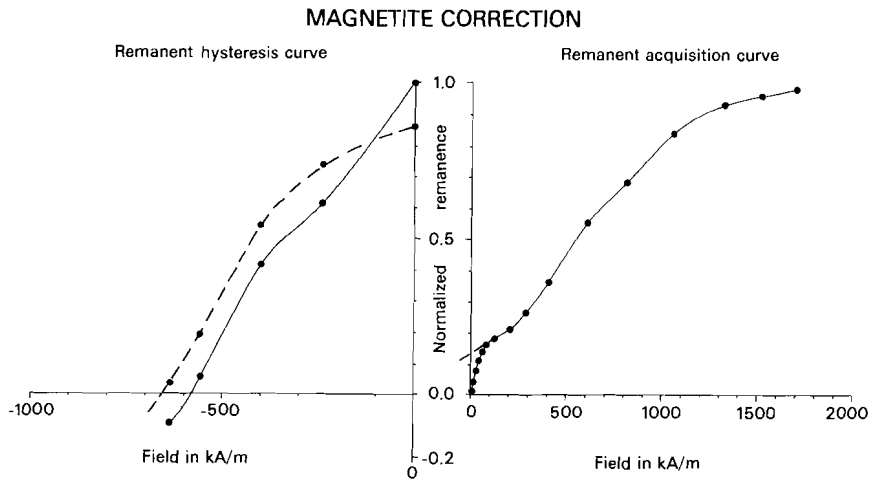

Fig. 4. The hematite remanent coercive force and remanent acquisition coercive force were determined by subtraction of the magnetite/maghemite contribution from the total sample remanent hysteresis (RH) and remanent acquisition (RA) curves respectively. The RA and RH curves are composites of two contributions one of which is saturating in below 160 kAm^{-1} (the magnetite-like impurity). This results in an inflection point in the RA curve and a distinct extra decrease in the RH curve in small applied fields. The slope of the RA curve in stronger fields than those corresponding to the inflection point is not influenced by the magnetic impurity. The magnetic content of this impurity is estimated by extrapolating the slope of that part of the RA curve to the ordinate. The shape of the RH curve is not influenced by the magnetic impurity in fields above some 16 kAm^{-1} because it is saturated in such low applied fields. This correction procedure is referred to in the text as "magnetite correction". The magnetic behaviour of hematite is indicated with dashed lines. Remanent coercive forces referring to hematite throughout the text have been "magnetite corrected".

3.1 Unheated samples

3.1.1 Room temperature measurements

3.1.1.1 Initial susceptibility and saturation remanence

Because of prime interest in fine grain sizes the 10-5 micrometer fraction of Batch 2 was not processed. The yield of the finest fraction (<0.25 micrometer) of Batch 2 was too low for meaningful experiments.

X_{in} is approximately 10^{-6} m^3kg^{-1} 10^{-6} without any evident grain-size dependence (cf. Table II). The slight increase in the finest fraction could be due to the approach of the superparamagnetic threshold size. The variety in the fractions of Batch 2 is due to slightly varying amounts of the magnetite-maghemite impurity. Dankers (1978) attributed the absence of a grain-size dependence in the initial susceptibility to a hematite type with a magnetic structure characterized by a large defect moment.

J_{rs} is decreasing with grain size (Table II; Fig. 5). The J_{rs} decrease is believed to reflect a "real" hematite feature (the amount non-magnetic minerals may be slightly higher in the fine fractions than in the coarse fractions; however, to explain the large J_{rs} differences observed, this would require unreasonably large amounts non- magnetic

minerals). A decreasing J_r or J_{rs} with grain size has also been reported for various hematites by e.g. Chevallier and Mathieu (1943) and Dunlop (1971).

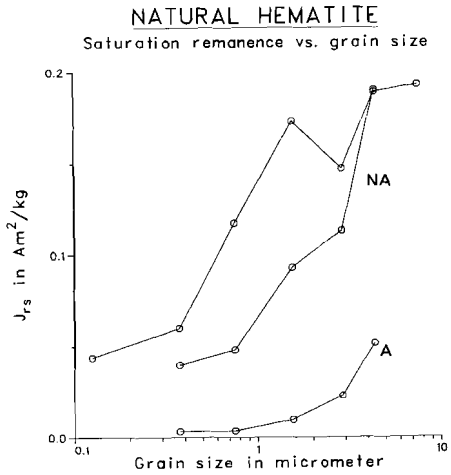

Fig. 5. Saturation remanence (J_{rs}) versus grain size for the FMW hematite. The upper two curves refer to non-annealed fractions (Batch 1 and Batch 2); they are indicated with "NA" in the figure. The lower curve refers to the annealed fractions of Batch 2; it is indicated with an "A" in the figure.

Relatively large differences between the two batches of the present hematite are related to the 'magnetite correction' (a precise determination of the magnetite contribution to the total J_{rs} is prone to a rather large error, when this contribution mounts up to over some 50 percent). J_{rs} figures for the 10-5 and 5-3.7 micrometer fractions correspond well with figures determined by Dankers (1978) and Hartstra (1982A) for hematite grains with diameters of 10-5 and <5 micrometer respectively.

Table II: X_{in} and J_{rs} as function of grain size for the FMW hematite

	X_{in}		J_{rs}	
	Batch 1	Batch 2	Batch 1	Batch 2
10.0 - 5.0	0.94	----	0.193	---
5.0 - 3.7	0.94	2.47	0.189	0.190
3.7 - 2.1	0.70	1.43	0.147	0.113
2.1 - 1.0	0.78	1.20	0.173	0.093
1.0 - 0.5	1.10	3.83	0.117	0.048
0.5 - 0.25	1.10	2.40	0.060	0.040
< 0.25	1.23	----	0.044	---

X_{in} in 10^{-6} m^3kg^{-1}; J_{rs} in Am^2kg^{-1}.

3.1.1.2 Remanent (acquisition) coercive force and median destructive field

H_{cr} (215 - 425 kAm^{-1}) is slightly larger than H_{cr}· (205 - 360 kAm^{-1}), which is larger than $H_{1/2r}$ (170 - 270 kAm^{-1}) (cf. Table III; Fig. 7; Fig. 8). AF decay curves of J_{rs} are shown in Fig. 6. Their shape gra-

dually changes from slightly convex for the coarse to concave for the fine grain-size fractions. Figures for H_{cr}, H_{cr}' and $H_{1/2I}$ as determined in the present study are smaller than figures for these parameters reported by Dankers (1978, 1981) and Hartstra (1982A) for comparable grain-size fractions. This applies specially for $H_{1/2I}$. The largest differences in H_{cr} respectively H_{cr}' are found with Dankers and Hartstra (op. cit.) hematites from high-temperature origin. H_{cr}/H_{cr}' ratios close to unity determined in the present study agree with their determinations. Dankers and Hartstra also report usually a larger H_{cr} than H_{cr}'.

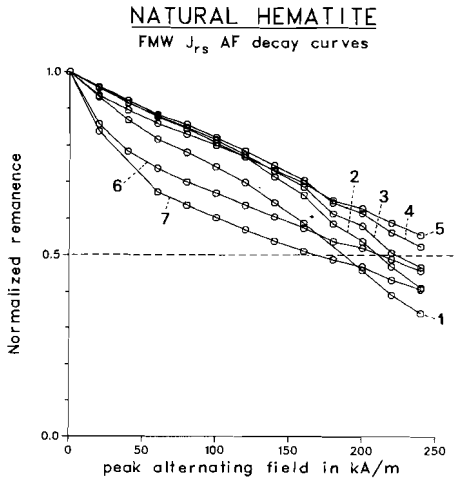

Fig. 6. AF decay curves of the saturation remanence of natural FMW hematite (non-annealed, Batch 1). The number refer to the grain size of each fraction: 1 denotes the 10-5 micrometer fraction; the others correspond to those of Fig. 1. $H_{1/2I}$ was derived by linear extrapolation in cases it could not be determined in the maximum alternating field available (240 kAm^{-1}).

H_{cr}, H_{cr}' and $H_{1/2I}$ determined in the present study all show a maximum in the 1.0-0.5 micrometer fraction. Hence, the coercivity-related parameters individually are not suitable as grain-size indicator. The $J_{rs}/(H_{cr}*X_{in})$ ratio, which is a quantity without dimension and as such independent of the hematite content in a specimen, is continuously decreasing with grain size (Table IV, Fig. 9). The absolute figures for each fraction, however, show a rather large variation due to variations in X_{in}. X_{in} is sensitive for minute magnetite/maghemite impurities (cf. Table II). Without the presence of such impurities, combination of H_{cr} and the $J_{rs}/(H_{cr}*X_{in})$ can discriminate between similar H_{cr} figures below and above the maximum observed in the 1.0-0.5 micrometer fraction.

The reason why the coercivity parameters show smooth grain-size dependent trends, despite the fact that the average crystallite size is smaller than the actual grain size of the fractions, is unknown. Apparently, the crystallites interact magnetically so that overall grain-size dependent trends result for the hysteresis parameters. The crystallite interfaces are important "defects" in the microstructure of the grains. A kind of analog between crystallites and domains may be possible. The crystallites would then be the equivalent of the "domains" and their interfaces that of the "walls", which, unlike "real" domain walls, cannot move. Decrease of the grain size will lead to a kind of

equivalent of the single domain state with a maximum in the hysteresis parameters. In the FMW hematite this state is apparently reached in the 1.0-0.5 micrometer fraction. The decrease in hysteresis parameters observed with a further grain-size decrease would then be related to the approach of the superparamagnetic threshold size.

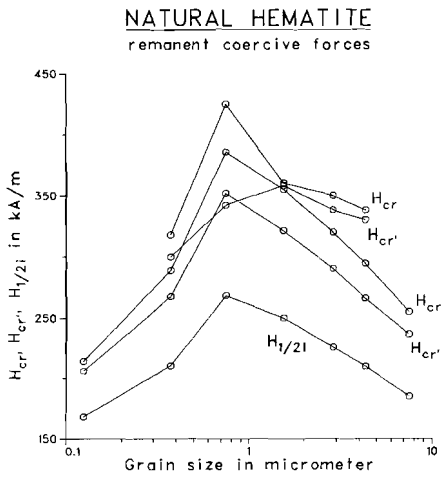

Fig. 7. Remanent coerciva force (H_{cr}), ramanent acquisition coercive force ($H_{cr'}$) and median destructive field of the saturation remanence ($H_{1/2I}$) versus grain size for the non-annealed FMW fractions.

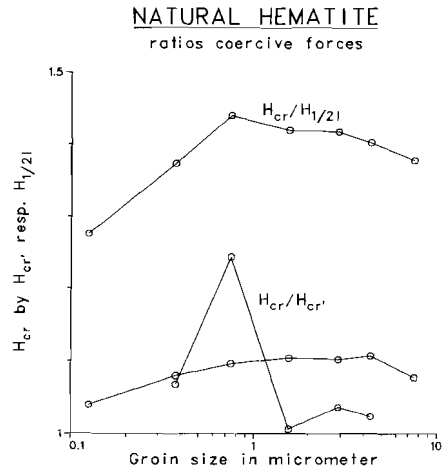

Fig. 8. Ratios of the remanent coercive force and the remanent acquisition coercive force ($H_{cr}/H_{cr'}$) and of the remanent coercive force and the median destructive field of the saturation remanence ($H_{cr}/H_{1/2I}$) versus grain size for the non-annealed FMW fractions.

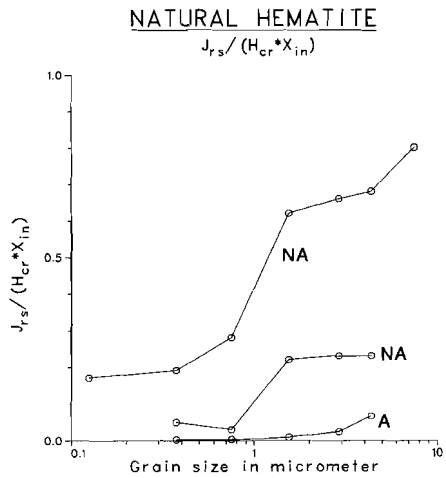

Fig. 9. $J_{rs}/(H_{cr}*X_{in})$ versus grain size for the FMW fractions. The ratio for the non-annealed fractions (Batch 1 and Batch 2) is indicated with "NA"; the ratio for the annealed fractions (Batch 2) is indicated with an "A" in the figure.

Table III: Remanent coercive force, remanent acquisition coercive force, medium destructive field and their ratios for fine-grained natural hematite.

	H_{cr} kAm^{-1}		$H_{cr'}$ kAm^{-1}		$H_{1/2\|}$ kAm^{-1}	$H_{cr}/H_{cr'}$		$H_{cr}/H_{1/2\|}$
	Batch 1	Batch 2	Batch 1	Batch 2	Batch 1	Batch 1	Batch 2	Batch 1
10.0 - 5.0	255	---	237	---	185	1.078	---	1.377
5.0 - 3.7	294	338	266	330	210	1.107	1.024	1.402
3.7 - 2.1	320	350	290	338	226	1.102	1.036	1.417
2.1 - 1.0	355	360	322	358	*250	1.104	1.006	1.419
1.0 - 0.5	386	425	352	342	*268	1.096	1.243	1.439
0.5 - 0.25	289	318	267	300	210	1.080	1.060	1.373
< 0.25	214	---	206	---	168	1.040	---	1.275

$H_{1/2|}$ figures marked with "*" are extrapolated ones. The linear shape of the AF decay curves allowed an extrapolation without serious error in $H_{1/2|}$ slightly beyond 240 kAm^{-1} (3000 Oe).

Table IV: Grain-size dependence of $J_{rs}/(H_{cr}*X_{in})$

	$J_{rs}/(H_{cr}*X_{in})$	
	Batch 1	Batch 2
grain size		
10.0 - 5.0	0.80	---
5.0 - 3.7	0.68	0.23
3.7 - 2.1	0.66	0.23
2.1 - 1.0	0.62	0.22
1.0 - 0.5	0.28	0.03
0.5 - 0.25	0.19	0.05
< 0.25	0.17	---

$J_{rs}/(H_{cr}*X_{in})$ in SI units.

3.1.2 Low-temperature behaviour of the saturation remanence

All fractions display identical behaviour during low-temperature (LT) cycling (Fig. 10). A monotonously slightly decreasing remanence is observed during cooling with the remarkable absence of a Morin transition. At -196 °C some 15 percent percent of the original room temperature remanence has disappeared. The remanence is partly recovering during rewarming; after a complete LT cycle approximately 10 percent of the original remanence is lost (Fig. 10A). The FMW hematite has thus a magnetic structure, characterized by a large defect magnetic moment. When cycling the recovered remanence a second time, (nearly) reversible behaviour during cooling and rewarming is observed (Fig. 10B; at -196 °C 10 percent of the initial remanence has disappeared).

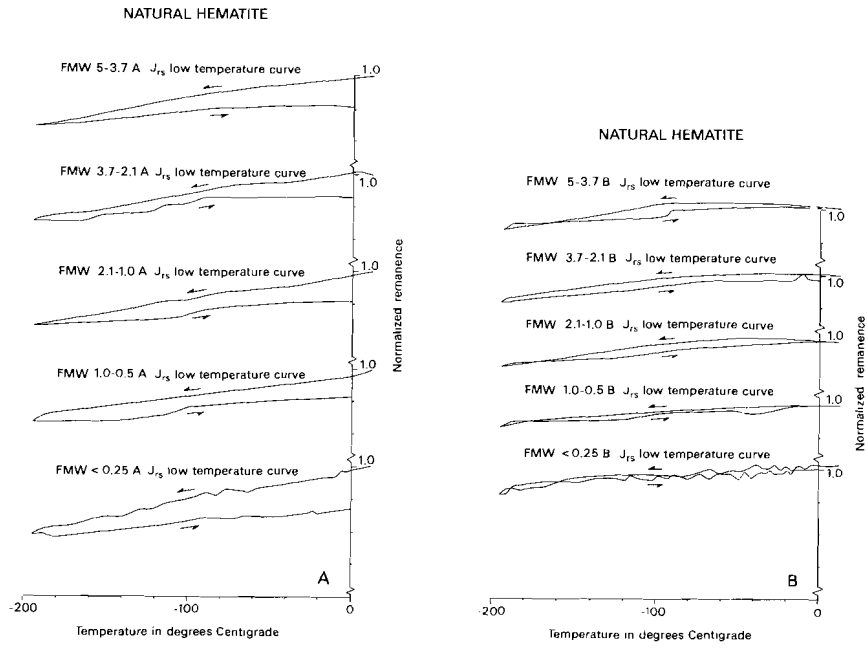

Fig. 10A. Low-temperature cycling of the saturation remanence for some fractions of the non- annealed FMW hematite. The numbers refer to the grain size in micrometer for each fraction. "a" denotes the first cooling cycle; arrows indicate the cooling and rewarming parts. Each curve shows a gradual remanence dacrease with decreasing temperature without a Morin transition. Mark the great similarity of the curves despite a rather large difference in grain size. The magnetocrystalline (canted) moment would show a Morin transition, so the remanence is carried by the defect moment in hematite.

Fig. 10B. Low-temperature cycling of the remanence remaining in the fractions after the first complete cooling cycle, denoted by "b" after the grain size indication. Each fraction shows reversible behaviour with hardly any remanence decrease.

The chemical composition of the hematite can not be the cause for the absence of a Morin transition. The minor amount of Al substituted in the hematite lattice has no influence on its low-temperature behaviour, since Al-doped hematite shows identical low-temperature behaviour as pure hematite (Haigh, 1957A; Flanders and Remeika, 1965). A cause for

the suppression of a Morin transition has to be sought for elsewhere. Surface effects are regarded as the cause for the suppression of the Morin transition in extremely fine (<0.03 micrometer) pure hematite grains (cf. Bando et al., 1965; Schroeer and Nininger, 1967). The present hematite grains have to be considered as composites of crystallites (average size 600 Å) with water and silica adsorbed predominantly to their interfaces. This results in a large increase of crystallite surface area within the grains and pins the spin structure to the hematite basal plane. The magnetic moment of the present hematite is thus a defect magnetic moment related to the presence of silica which limits the hematite crystallite size. The crystallite size of the present hematite is slightly larger than that below which no Morin transition occurs in pure hematite. No data exist regarding the influence of adsorbed and dispersed silica on the absence of a Morin transition in fine hematite crystallites. It could well be that such adsorbed silica enlarges the crystallite size below which no Morin transition occurs. The absence of the Morin transition is an intrinsic property of the hematite, i.e. related to the crystallites themselves which pin the spin structure to the basal plane. No grain-size dependence should occur. The hysteresis parameters would also be explained by magnetic interaction between the crystallites, so that grain-size trends are possible.

3.1.3 Stepwise thermal demagnetization of the saturation remanence

J_{rs} thermal decay curves of FMW hematite (Fig. 11) show blocking temperature spectra without a distinct maximum like that of TRM in hematite. The approach to the Néel temperature is increasingly less steep with decreasing grain size (Fig. 11). Dankers (1978) described a different behaviour of the hematite J_{rs} during stepwise thermal demagnetization. More than half of the initial J_{rs} remanence remained in his <5 micrometer fractions even after 620 °C. The J_{rs} blocking temperature spectrum of more crystalline (high-temperature) hematite appears to be considerably shifted to temperatures above 600 °C.

X_{in}, measured at room temperature after each thermal demagnetization step, starts increasing above 350 °C and shows a maximum in the 550 °C region (Fig. 12). The initial variation in X_{in} correlates with the magnetite-like impurity content of each fraction. The increasing susceptibility above 350 °C is probably due to the creation of a magnetite-like mineral. The production of minute amounts of such material is not unusual in this temperature region. It is observed in fine crystalline hematite produced by the conversion of goethite (Dekkers, 1988A). The produced magnetite is oxidized again at temperatures above 550 °C, since X_{in} is decreasing at higher temperatures. After the 700 °C step no traces of a magnetite-like mineral are detected in the RA and RH curves of the 5-3.7 micrometer fraction. In smaller grain-size fractions (with a slightly higher X_{in}, cf. Fig. 12) traces of such mineral are detected. The trend in X_{in} after the 700 °C heating step (cf. also Table V) correlates with the magnetite content determined with the RA curves. The decrease in magnetite amount during thermal demagnetization steps at temperatures above 550 °C might be related to the Al_2O_3-rich matrix. This matrix is rather porous and, as such, enables a better contact with the surrounding oxygen-rich atmosphere (air) than a $CaCO_3$-rich matrix. Chemical reactions occur in the latter, enclosing the specimen from a surrounding atmosphere.

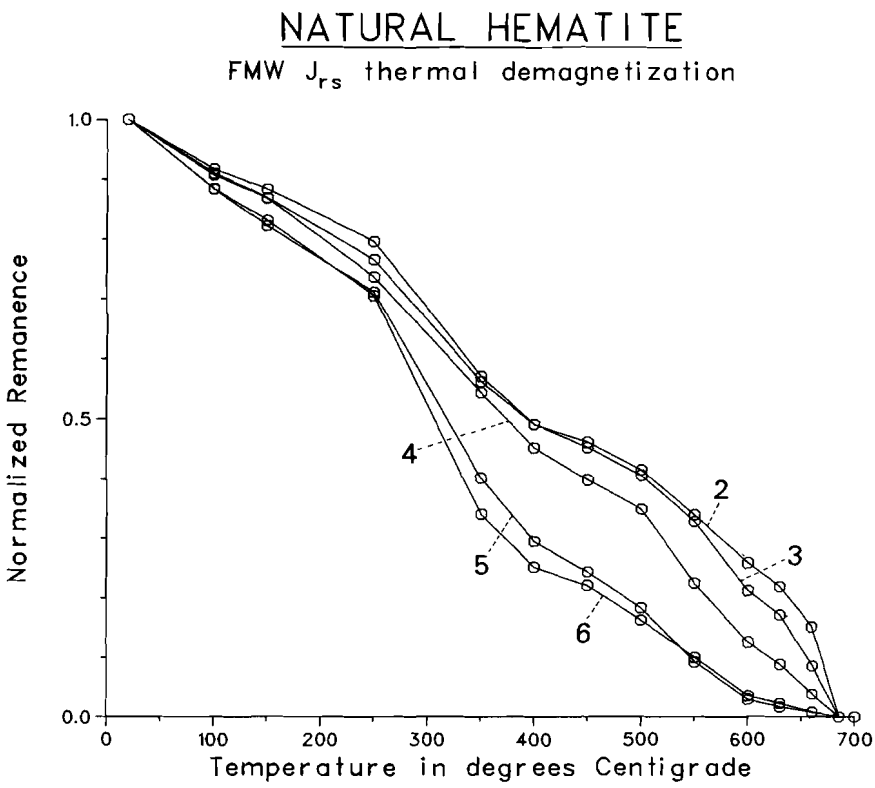

Fig. 11. Normalized decay curves of J_{rs} during stepwise thermal demagnetization of the non-annealed fractions of Batch 2. Fraction numbers, referring to their grain size ranges, correspond with those in Fig. 1. The hematite J_{rs} blocking temperature spectrum becomes broader with falling grain size as is shown by the increasingly less steep approach to the Curie point with decreasing grain size. The inflection point at approximately 300 °C could be due to recrystallization of hematite.

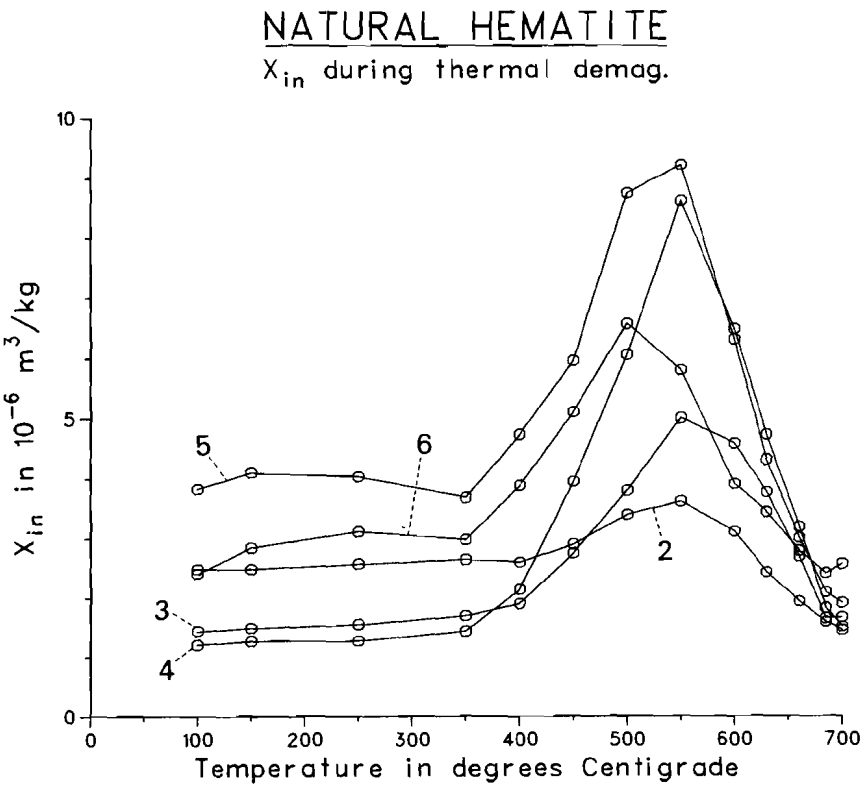

Fig. 12. The initial susceptibility (X_{in}) measured at room temperature after each demagnetization step of the thermal demagnetization of the saturation remanence of which the decay curves are shown in Fig. 11. The numbers correspond with those in Fig. 1. The maximum in the initial susceptibility is due to the production and subsequent break-down of magnetite.

3.2 Annealed samples

3.2.1 Saturation remanence and remanent coercive forces after the 700 °C thermal demagnetization step.

The saturation remanence after annealing ($J_{rs\ 700}$) is lower than before annealing ($J_{rs\ 25}$) and decreases with grain size (cf. Table V; Fig. 5). By annealing the hematite grains recrystallize; defects are diffused out off the lattice, resulting in larger crystallites. The more perfect hematite has a lower saturation remanence, because the defect moment has been considerably diminished. A decrease of J_{rs} with increasing annealing temperature (700, 800, 880 and 950 °C) was also found by Dunlop (1971) for hematite synthesized at temperatures of 500-600 °C.

The remanent coercive force after annealing ($H_{cr\ 700}$) and the remanent acquisition coercive force after annealing ($H_{cr\cdot\ 700}$) both are larger than those parameters prior to annealing (cf. Table VI and Table III). Such increasing hardness is also observed by Dunlop (1971) and

Bucur (1978) in fine-grained synthetic hematite and by Dunlop (1972) in fine-grained natural hematite. They attributed this to annealing out of the relatively soft defect moment. As will be shown in section 4.2, this is also the case for the present hematite. The $H_{cr\ 700}/H_{cr'\ 700}$ ratio is similar to the $H_{cr\ 25}/H_{cr'\ 25}$ ratio. (cf. Table VI and Table III). Figures for $H_{cr\ 700}$ and $H_{cr'\ 700}$ in the 5-3.7 micrometer fraction in the present study are in good agreement with those determined by Dankers (1978, 1981) and Hartstra (1982A) for their <5 micrometer fractions of hematites with a high-temperature origin.

Table V: J_{rs}, X_{in}, the ratio of J_{rs} before and after annealing and the ratio of J_{rs} and X_{in} times H_{cr} after annealing versus grain size

Batch 2	$J_{rs\ 700}$	$J_{rs\ 25}/J_{rs\ 700}$	$X_{in\ 700}$	$J_{rs\ 700}/(X_{in\ 700}{*}H_{cr\ 700})$
5.0 - 3.7	0.0514	3.7	1.45	0.066
3.7 - 2.1	0.0228	5.0	1.66	0.024
2.1 - 1.0	0.0097	9.6	1.51	0.009
1.0 - 0.5	0.0034	14.1	1.90	0.003
0.5 - 0.25	0.0032	12.5	2.56	0.003

$J_{rs\ 700}$ in Am^2kg^{-1}; $X_{in\ 700}$ in $10^{-6}\ m^3kg^{-1}$; $J_{rs\ 700}/(X_{in\ 700}{*}H_{cr\ 700})$ in SI units.

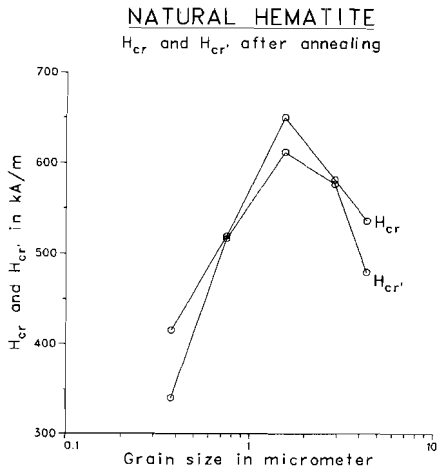

Fig. 13. Hematite remenent coercive force (H_{cr}) and remanent acquisition coercive force ($H_{cr'}$) versus grain size for the annealed fractions of Batch 2.

Table VI: Remanent coercive force and remanent acquisition coercive force after three times annealing at 700 °C and their ratios with non-annealed fractions.

	After three times annealing			Ratios with non-annealed fractions	
Batch 2	$H_{cr\ 700}$ kAm^{-1}	$H_{cr'\ 700}$ kAm^{-1}	$H_{cr\ 700}/H_{cr'\ 700}$	$H_{cr\ 700}/H_{cr\ 25}$	$H_{cr'\ 700}/H_{cr'\ 25}$
5.0 - 3.7	537	480	1.119	1.59	1.45
3.7 - 2.1	582	577	1.009	1.66	1.71
2.1 - 1.0	650	612	1.062	1.80	1.71
1.0 - 0.5	520	517	1.005	1.22	1.51
0.5 - 0.25	415	341	1.217	1.30	1.14

$H_{cr\ 700}$ and $H_{cr'\ 700}$ both show a maximum in the 2.1-1.0 micrometer fraction (Fig. 13; Table VI). The maximum figures are shifted one grain-size fraction upwards by the annealing process. The ratios of $H_{cr\ 700}/H_{cr\ 25}$ and $H_{cr'\ 700}/H_{cr'\ 25}$ (Fig. 14) show also a maximum in the 2.1-1.0 micrometer fraction, presumably due to the shift of the $H_{cr\ 700}$ and $H_{cr'\ 700}$ maxima to this fraction.

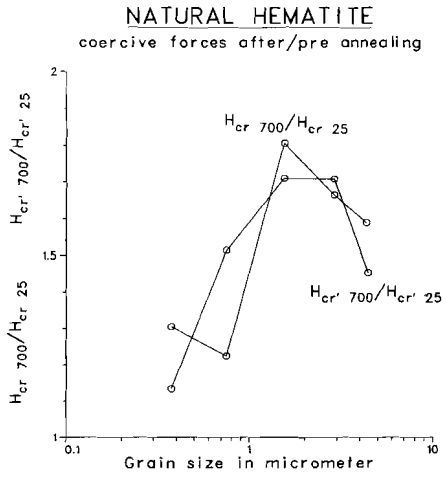

Fig. 14. Ratios of the remanent coercive force after and before annealing ($H_{cr\ 700}/H_{cr\ 25}$) and the remanent acquisition coercive force after and before annealing ($H_{cr'\ 700}/H_{cr'\ 25}$) versus grain size.

3.2.2 Low-temperature behaviour of the saturation remanence after thermal treatment

LT-cycling of J_{rs} after annealing (Fig. 15) reveals a Morin transition in all fractions indicative for development of the canted antiferromagnetic structure with the corresponding magnetocrystalline moment. The Morin transition takes place over a broad temperature interval. This points to a rather large crystallite size spectrum in the annealed FMW hematite grains. The relatively high Si-content possibly also contributes to the rather broad Morin transition interval since Si is known to "tail off" the magnetic moment below the Morin transition (Flanders and Remeika, 1965). Whether this is an intrinsic Si-feature or related to the fact that silica tends to reduce crystallite growth (Schwertmann and Taylor, 1972), is not known.

The defect moment is not completely removed by the thermal demagnetization. The defect moment could possibly be further diminished by annealing at higher temperatures down to figures of 5-10 percent of the original room temperature remanence, which are usually reported for hematite with a well-developed magnetocrystalline moment. This was not tested for the present research. The ratios of the initial J_{rs} and the remanence at -196 °C and the recovered remanence are compiled in Table VII. With decreasing grain size the moment which remains below the Morin transition tends to increase. This may be related to the fact the Morin transition is totally suppressed in extremely fine grains.

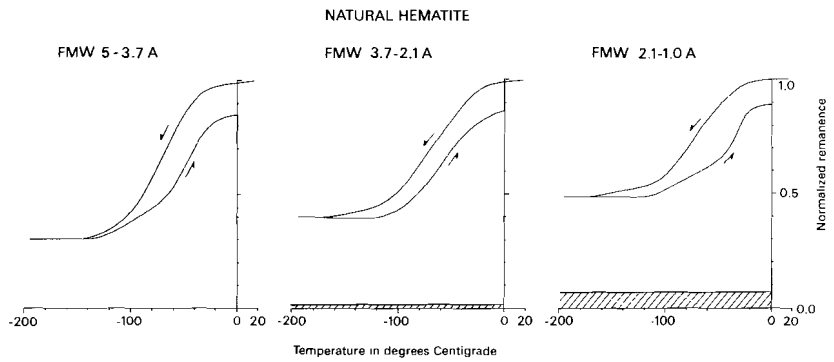

Fig. 15. Low-temperature cycling of the saturation remanence after annealing ($J_{rs\ 700}$) for some FMW fractions. The numbers refer to the grain size in micrometer; "A" indicates annealed. The cooling and rewarming parts are indicated by arrows. The curves have been slightly smoothed for the noise in the remanence measurements because the fractions had remanences close to the detection limit of the HALT spinner. The non-hematite contribution to the total remanence is indicated with the hatched area. After annealing, the FMW hematite fractions do show a Morin transition contrary to the fractions prior to annealing.

Table VII: Ratios of the remanence at -196 °C (J_{-196}) to the initial saturation remanence (after annealing, $J_{rs\ 700}$) and the recovered remanence (J_{rec}) to $J_{rs\ 700}$.

Fraction	$J_{-196}/J_{rs\ 700}$	$J_{rec}/J_{rs\ 700}$
5.0 - 3.7	0.31	0.85
3.7 - 2.1	0.38	0.87
2.1 - 1.0	0.45	0.88
1.0 - 0.5	0.4 - 0.5*	0.65 - 0.75*
0.5 - 0.25	0.5 - 0.6*	0.65 - 0.75*

* The low saturation remanence of these two fractions permits only a very approximate estimate of the ratios (the error in the measurements is large owing to the low sensitivity of the HALT spinner equipment).

3.2.3 Grain-size dependence of the thermoremanence

The intensity of the TRM for hematite decreases with grain size (Table VIII; Fig. 16). The specific volume TRM of the coarsest fractions fairly agrees with the value of approximately 0.4 determined by Dunlop (1971) for his fine grained hematite of similar grain size. A decreasing TRM-trend with grain size was also found for natural hematite by Hartstra (1982A) in a grain-size range from 250 micrometer downward. His figures for the smaller than 5 micrometer fraction correspond closely to the 5-3.7 micrometer fraction in the present study. The present FMW hematite lost its excess water during annealing (TGA, cf. Fig. 2). The resulting hematite is anhydrous. Therefore the parameters after annealing can be compared with Hartstra's (1982A) hematites which underwent similar annealing.

Table VIII: TRM of natural hematite versus grain size

grain size	TRM	sp. vol. TRM
Batch 2		
5.0 - 3.7	6.07	0.47
3.7 - 2.1	2.54	0.20
2.1 - 1.0	1.20	0.09
1.0 - 0.5	0.51	0.04
0.5 - 0.25	0.61	0.05

TRM in 10^{-3} Am^2kg^{-1}. sp. vol. TRM = specific volume TRM in SI units, calculated assuming a density of 5200 $kg*m^{-3}$ for hematite. Figures for the two smallest fraction are somewhat too large because of the presence of traces magnetite (cf. Fig. 17).

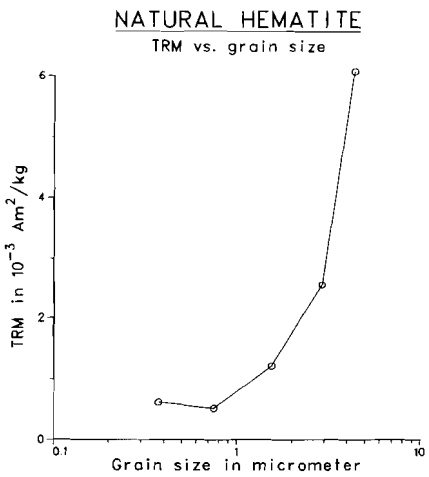

Fig. 16. TRM versus grain size for the annealed natural hematite. TRM was induced by cooling from 700 °C in a direct field of 67 Am^{-1}.

The grain-size trend observed in Hartstra's study (1982A) and in the present study is opposite to trends determined in magnetite (e.g. Hartstra, 1983; O'Reilly, 1984 and references therein) and in Ti-rich ilmeno-hematite (Westcott-Lewis, 1971). The hematite-ilmenite solid solution series ($Fe_{2-y}Ti_yO_3$ with y between 0 and 1) is ferrimagnetic in the compositional range from y=0.5 to 0.8 (investigated by Westcott-Lewis, op. cit.). Fe-richer hematite has a canted antiferromagnetic structure (e.g. Nagata, 1961; Westcott-Lewis and Parry, 1971; O'Reilly, 1984 and references therein) with, above the Morin transition, easy magnetization directions in the basal plane and a hard magnetization axis perpendicular to the basal plane. In this way the hematite structure resembles that of pyrrhotite, which indeed shows also a decreasing TRM-trend with grain size (Dekkers, 1988B). Closure domains are thought responsible for the increasing TRM with decreasing grain size in the PSD grain-size range of magnetite (Stacey and Banerjee, 1974). Closure domains are rarely observed in pyrrhotite (Soffel, 1981). It could be that the absence of closure domains in pyrrhotite is favoured by its hard axis of magnetization. When this tentative hypothesis is correct, the opposite TRM versus grain size trends in magnetite and Ti-rich hematite on one

side and Fe-rich hematite and pyrrhotite on the other side are related to whether the magnetic mineral is characterized by an easy axis or by an easy plane (hard axis). More data are needed, however, to ascertain the above hypothesis.

3.2.4 Stepwise thermal demagnetization of the TRM

Normalized decay curves of the TRM during stepwise thermal demagnetization (Fig. 17) show that a major part of the hematite TRM was acquired above 600 °C. Smaller grain-size fractions tend to have increasingly broader blocking temperature spectra.

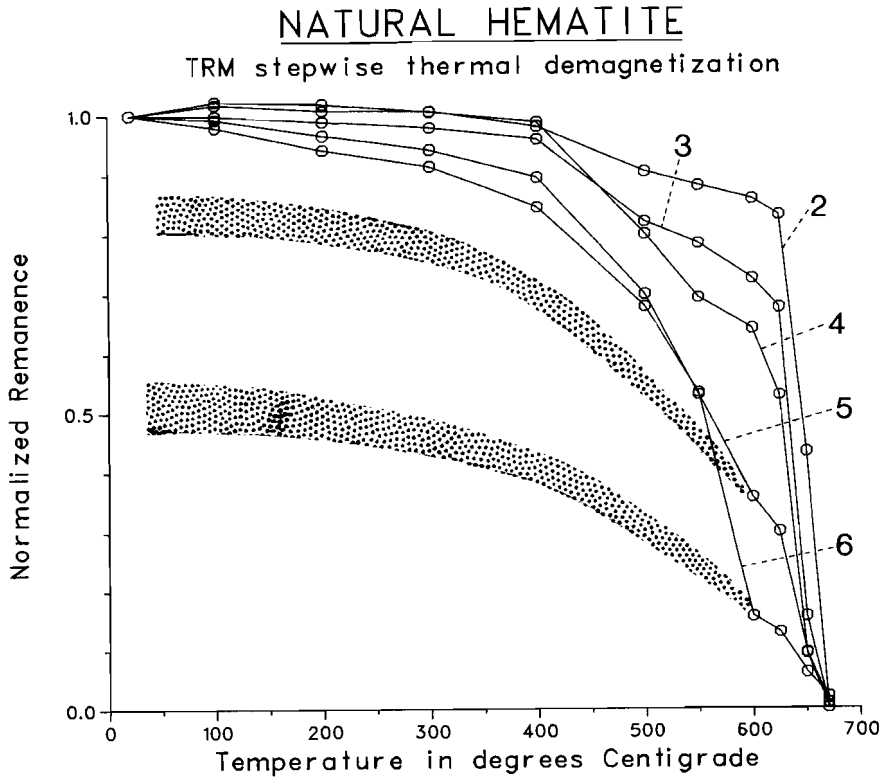

Fig. 17. Normalized TRM decay curves during stepwise thermal demagnetization. The fraction numbering corresponds to that in Fig. 1. The magnetite influence in fractions 4 and 5, but especially in fraction 6, emerges from the different shape of the decay curves of these fractions compared to those of fraction 2 and 3. In fraction 4 the relative magnetic amount of magnetite is small. In fraction 5 and 6 this will be larger. However, a reliable estimate is difficult to assess for these small grain size fractions, because the hematite TRM blocking temperature spectrum is not precisely known. For fraction 6 a crude and only approximate estimate of the magnetic magnetite content is made by extrapolating the decay between 600 and 625 °C (above the magnetite Curie point; hence decay solely due to hematite) down to some 300-400 °C (indicated by the dotted area). The decay of the sample TRM below this temperature is ascribed to magnetite. It is thus assumed that a hematite TRM is stable to heating up to some 300-400 °C also in this extremely small grains.

When annealing hematite to introduce for instance a TRM, a variable - but usually very small - amount of a magnetite-like mineral may be created within the specimen or a small amount may persist during annealing. This trace amount of the magnetite-like mineral may acquire a rather large part of the specimen TRM due to the high magnetite TRM per unit mass (cf. Fig. 17). The TRM decay curves of the smallest two fractions are distinctly influenced by trace amounts magnetite present in the fraction. Because the TRM behaviour of extremely fine-grained magnetite is difficult to assess, only the inferred approximate hematite TRM decay curves are sketched. No magnetite is detected in the 5-3.7 micrometer fraction (RA and RH curve after thermal demagnetization at 700 °C; by far the most alteration in the specimens will have occurred during the first thermal demagnetization, i.e. that of the J_{rs} of the FMW hematite in its initial low-temperature state), so its TRM decay curve represents true hematite behaviour. Its decay curve resembles the block-shaped TRM decay curves shown by e.g. van den Ende (1977) or Dankers (1978).

4 DISCUSSION

4.1 Grain-size dependence of rockmagnetic parameters in hematite

Unlike the rockmagnetic parameters of (titano-)magnetite which are amply studied, few studies describe grain-size dependence of rockmagnetic parameters of hematite, especially natural hematite. The rather fragmentary literature data indicate nonetheless that the hematite rockmagnetic parameters show a considerable variety. Hartstra (1982A), combining his results with those of Dankers (1978, 1981), tried to arrive at a classification for natural hematite based on its rockmagnetic properties in order to use hematite rockmagnetic parameters for granulometric purposes. He concluded that a consistent and practically useful classification was not yet within reach and that more data were needed.

The finest grain-size fraction in the hematites studied by Dankers and Hartstra was <5 micrometer. The remanent coercivities were most high in these fractions, indicating that a "SD state" would not yet be reached. However, domain studies on hematite single crystals by Eaton and Morrish (1969) reveal domain-wall spacings of up to several hundreds of micrometer. Data of Chevallier and Mathieu (1943) on presumably relatively well-crystalline hematite (no data on crystallite sizes are reported; their Elba hematite is known to be well-crystalline) indicate varying maxima in the coercive force from some 10-15 micrometer for the Elba hematite down to 3-5 micrometer for two hematites from the Vosges (France). Such maxima led Dunlop (1971) to place the hematite SD threshold size tentatively at some 10 micrometer. Dunlops (1971) synthetic hematite grains show H_{cr} maxima at some 5 micrometer and at approximately 1.5 micrometer.

The large discrepancies between these studies show that the hematite hysteresis parameters are extremely sensitive to whether the hematite grains are single crystals or polycrystalline aggregates. In single crystals the SD threshold size is reached only in very large grains; in polycrystalline grains an equivalent of the "SD threshold size" can be reached in grain sizes down to 1 micrometer. The crystallinity of the hematite may thus be crucial for the grain size in which the maximum in the hysteresis parameters is reached. Contrasting trends in hysteresis parameters between fine-grained hematites of similar grain sizes may possibly be related to different crystallite sizes. The impact of

substitution in hematite is at present difficult to evaluate because almost all data for fine-grained hematite refer to relatively pure hematite.

The presence of a "soft" defect moment and a "hard" magnetocrystalline moment in widely varying extents in hematite complicates further its hysteresis characteristics. The present low-temperature FMW hematite does not show any Morin transition prior to thermal treatment. The remanence constitutes thus (almost) completely of the defect moment. The remanent coercive forces are relatively low indeed. Their maxima are reached in the 1.0-0.5 micrometer fraction. The cause for grain-size dependent trends is not known. Possibly it may be sought for in a kind of magnetic interaction between the extremely closely spaced crystallites making up grains. The maxima in hysteresis parameters are then the result of a balance of magnetostatic energy, dominating in single crystals, and the impact of polycrystallinity.

4.2 Change in magnetic properties due to annealing

The magnetic properties of natural low-temperature hematite and that of the same hematite after thermal demagnetization up to 700 °C are distinctly different as is illustrated in the foregoing. The most striking difference is the absence of Morin transition prior to annealing (Fig. 10) and the appearance of a relatively well-developed one after thermal treatment (Fig. 15). This was attributed to the removal of excess water from the hematite resulting in larger crystallites. Also non-Fe elements are (partly?) removed from the hematite.

Regarding the chemical composition of a low-temperature hematite the following may be stated. A low-temperature hematite will generally contain hardly any isomorphous substitution of Al and Ti because of the extremely low mobility of these elements in the transport medium water (at least at low temperatures and prevailing Eh/pH conditions). On the other hand, Si can well be present in such hematite because many groundwaters are close to saturation with respect to amorphous silica. Excess water in the hematite structure is also well imaginable. Silica retards crystallite enlargement (Schwertmann and Taylor, 1972) and can be as such responsible for the absence of a Morin transition also in relatively large grains. With annealing, excess water and Si (to an unknown extent) are driven out of the crystallite aggregates resulting in a relatively pure and more crystalline hematite which shows a Morin transition. This behaviour is exhibited by the water-rich FMW hematite.

Annealing at temperatures up to 700 °C leads to a lower saturation remanence and higher remanent (acquisition) coercive force. Similar observations were made by Dunlop (1971) and Bucur (1978) on synthetic hematites. Dunlop (1971) argues that the trends in his annealing experiments can be explained by the gradual annealing out of the 'soft' defect moment. The behaviour of the natural FMW hematite also points to a harder magnetocrystalline moment than defect moment, in agreement with Haigh's (1957B) and Dunlop's (1971) observations. Annealing - in this case accompanied by loss of water - leads to a coarsening of the crystallites and the removal of defects from the lattice. Recrystallization is promoted by the water present in the original hematite grains. The increase in coercivity parameters is thus due to the harder magnetocrystalline moment; the shift in their maxima from the 1.0-0.5 micrometer to the 2.1-1.0 micrometer fraction may be a consequence of coarser crystallites.

The extra decrease in J_{rs} with decreasing grain size may possibly be seen in relation with the approach to perfect antiferromagnetic beha-

viour in extremely fine grains for well-crystalline hematite (Elba hematite) noted by Chevallier and Mathieu (1943). When defect hematite would show such behaviour to a lesser extent, an extra decrease in remanence with decreasing grain size may be expected by annealing, which promotes the development of the magnetocrystalline moment.

From the large differences in behaviour of the FMW hematite prior and after thermal treatment it may be concluded that synthetic hematites, prepared by decomposing goethite or oxidizing magnetite at some 500 °C and for which the magnetic properties are claimed to be independent of annealing at temperatures up to over 700 °C, are not representative for natural low-temperature hematite.

4.3 Discrimination between TRM and CRM in hematite

The foregoing illustrates that differences in hematite remanent coercive forces and differences in low-temperature behaviour may be related to the thermal history of the hematite. These differences might possibly be used for the discrimination between TRM and CRM in hematite. TRM has a high-temperature origin, whereas CRM has a low-temperature origin. Hematite with high-temperature characteristics in sediments can then be assigned with a DRM origin, whereas hematite with low-temperature characteristics is most probably carrying a CRM (a DRM, residing in grains which had originally a CRM, cannot be discriminated from a CRM which has grown in situ in the rocks of interest). In the following, hematite with a CRM is referred to as low-temperature hematite and hematite with a TRM is referred to as high-temperature hematite.

The remanent coercive force of a low-temperature hematite is lower than that of a high-temperature hematite of similar grain size. Low-temperature hematite shows no Morin transition at least in grains up to 10 micrometer diameter, whereas high-temperature hematite does show such transition. A complicating factor is that the Morin transition can be suppressed by Ti-substitution in the hematite lattice. It also disappears in extremely fine grains of pure hematite.

A redbed sample with a hematite TRM and one with a hematite CRM were subjected to annealing experiments. The TRM/DRM sample (ENR 77C) is from the Permian Dôme de Barrot redbeds with NRM directions consistent with Permian directions for stable Europe (van den Ende, 1977). The hematite in these red beds is of volcanic origin (Bordet, 1950). The CRM sample is a Triassic (Buntsandstein) red bed collected in a quarry in the region of Bieber (Western Germany) with an NRM direction corresponding to the present day geomagnetic field. Both samples were saturated in a field of 1670 kAm^{-1}, and subsequently H_{cr} was determined. Hereafter, the sample was saturated again in the original direction and subjected to LT-cycling. This procedure was performed on non-annealed samples, after 400 °C annealing and after 700 °C annealing. Results are compiled in Table IX and Fig. 18.

H_{cr} of ZBI 100B is lower than H_{cr} of ENR 77C at corresponding annealing temperatures (Table IX; Fig. 18). H_{cr} indicates an average grain size of the ZBI 100B sample of approximately 1 micrometer, if the FMW H_{cr} curves are applied. The $H_{cr\ 700}/H_{cr\ 25}$ ratio of ZBI 100B is similar to the ratio observed in the FMW fractions. The saturation remanence decreases with increasing annealing temperature. Also during LT-cycling the remanence is decreasing over a broad temperature range (since there are fine-grained magnetite-like minerals produced in the specimen representing thirty percent of the total remanence, the hematite remanence decrease is more than the decrease of the total sample

decrease). These data are in favour of a low-temperature origin of the hematite in the ZBI 100B sample. Its remanence, therefore, has to be a CRM.

Table IX: Saturation remanence (J_{rs}) and remanent coercive force (H_{cr}) at room temperature, after 400 °C annealing and after 700 °C annealing.

annealing	ENR 77C			ZBI 100B		
temp.	H_{cr}	$H_{cr\ 700}/H_{cr\ at}$	J_{rs}	H_{cr}	$H_{cr\ 700}/H_{cr\ at}$	J_{rs}
25	558	1.46	28.6	358	1.91	2.10
400	670	1.22	27.5	515	1.32	1.92
700	815	1.00	28.4	682	1.00	1.57

ENR 77C refers to the Dôme de Barrot redbed sample (TRM/DRM); ZBI 100B to the Bieber Buntsandstein redbed sample (CRM). H_{cr} in kAm^{-1}; J_{rs} in arbitrary units. $H_{cr\ at}$ is the remanent coercive force after the annealing temperature in the first column. $H_{cr\ 700}$ is the remanent coercive after the maximum annealing temperature.

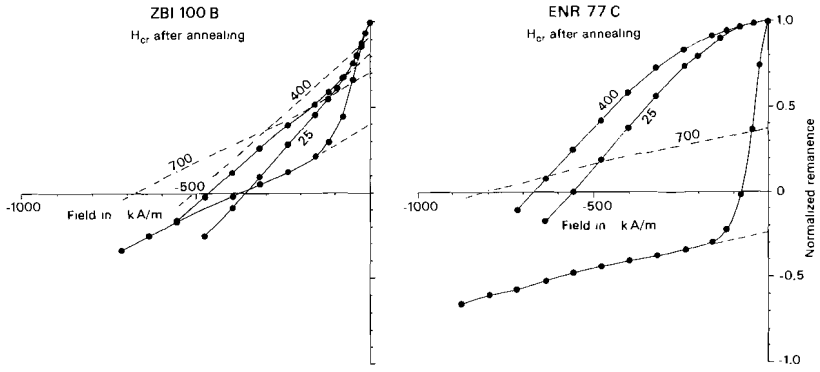

Fig. 18A. Remanent hysteresis curves of ENR 77C and ZBI 100B after annealing at different temperatures. The numbers refer to the annealing temperature. The magnetite which is produced in the specimen is extremely fine grained, because a high relaxation rate was detected during the measurements. The "magnetite corrected" hematite behaviour is indicated with dashed lines. The remanent coercive force (H_{cr}) increases with increasing annealing temperature.

The H_{cr} of ENR 77C is much higher than that of ZBI 100B (Table IX). This high H_{cr} points to a high-temperature origin for the hematite because the much lower H_{cr} of ZBI 100B is already close to the maximum H_{cr} in for low-temperature hematite. The H_{cr} in the ENR 77C sample also increases (to very high values) with annealing, but the saturation remanence does not change. The $H_{cr\ 700}/H_{cr\ 25}$ ratio of ENR 77C is distinctly lower than that of ZBI 100B. LT-cycling after 700 °C annealing results in nearly identical behaviour as for the non-annealed sample and after 400 °C annealing, however, without the appearance of a Morin transition. The suppression of the Morin transition can be due to extremely fine grain sizes or to Ti incorporated in the lattice. Resuming, the high absolute H_{cr} figure, the much lower $H_{cr\ 700}/H_{cr\ 25}$ ratio, the annealing-independent J_{rs} and identical low-temperature behaviour despite a wide range of annealing temperatures are in favour of a high-temperature origin of the hematite. The remanence in ENR 77C, therefore, has to be a DRM.

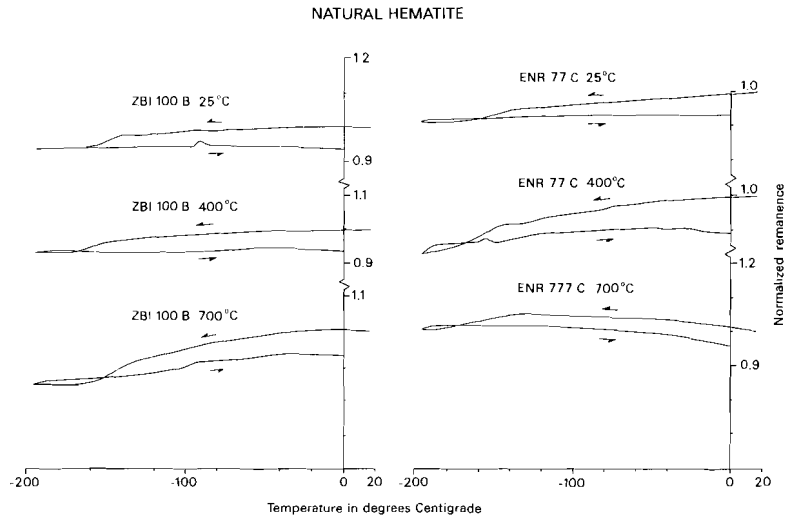

Fig. 18B. Low-temperature cycling of ENR 77C and ZBI 100B after different annealing temperatures. The cooling and rewarming parts are indicated by arrows. The remanence increase in ENR 77C after 700 °C is due to extreme fine magnetite grains produced in the specimen. The spontaneous magnetization increases with decreasing temperature for these extreme small grains. The hematite behaviour does not change by annealing in ENR 77C; the smaller relative decrease is due to the magnetite present in the sample after annealing, making up a large part of the total remanence (cf. Fig. 18A). The ZBI 100B specimen shows different low-temperature behaviour with increasing annealing temperature. After 700 °C a broad Morin transition is observed. The decrease in hematite remanence is 22 percent when correcting for the magnetite contribution to the total remanence.

The ENR 77C and ZBI 100B samples reflect differences between high- and low-temperature hematite in fair agreement with those outlined for the FMW hematite, but certainly not in all its aspects. For the ZBI 100B sample this may be related to the extent of hematite recrystallization during annealing. Kinetics of such recrystallization depend strongly on the availability of water. It may be that the hematite in ZBI 100B contains less, or hardly any, water. When this is the case, recrystallization will occur to a lesser extent. The resulting magnetic properties of the annealed hematite will be less extreme. The aspects of the ENR 77C sample during annealing are presently not completely understood and warrant further rockmagnetic investigation. The discrimination made above has a preliminary character. In general, there is a great need for more data regarding grain-size dependent trends of rockmagnetic parameters for natural hematite and their annealing behaviour, especially in the very fine grain-size range. Such trends may allow for a more complete determination of the hematite type present in rock samples and, as such, may contribute to the understanding of the remanence type (CRM vs. DRM) carried by the hematite in the samples of interest.

5 CONCLUSIONS

Prior to annealing, H_{cr} (215 - 425 kAm^{-1}), H_{cr}' (205 - 360 kAm^{-1}) and $H_{1/2I}$ (170 - 270 kAm^{-1}) of the FMW hematite all show a maximum in the 1.0-0.5 micrometer fraction. J_{rs} (0.19 - 0.04 Am^2kg^{-1}) decreases with

grain size throughout the investigated grain-size range (<10 micrometer). X_{in} shows no detectable grain-size dependence with figures around $1*10^{-6}$ m^3kg^{-1} with a tendency to rise in the smallest fraction. The figures for H_{cr} and $H_{cr'}$ correspond with those derived by Dankers (1978, 1981) and Hartstra (1982) for comparable grain-size fractions of hematite with a low-temperature origin. Because of the observed maxima H_{cr}, $H_{cr'}$ etc. cannot be straightforwardly used for granulometric purposes. The $J_{rs}/(H_{cr}*X_{in})$ parameter, which is without dimension and thus independent of the hematite amount, decreases continuously with grain size and therefore can be used as grain-size indicator when dealing with hematite samples without traces magnetite-like minerals.

The precise cause for the observed maxima in the hysteresis parameters is not known. Sparse literature data indicate that hematite hysteresis parameters seem to be sensitive to the degree of polycrystallinity of the grains. The maxima in a specific grain size may then possibly be understood as a subtle balance of the grain magnetostatic energy and its polycrystallinity. The decrease in hysteresis parameters in the extremely fine grain-size fractions (i.e. below the grain-size fraction in which the maximum coercivity parameters are observed) could then be related to the approach of the superparamagnetic threshold size in hematite.

Low-temperature cycling of the saturation remanence revealed curves with a gradually slightly decreasing remanence with falling temperature without the occurrence of a Morin transition, regardless of the grain size of the fractions. The hematite remanence is carried by the so-called defect moment. Chemically, the FMW hematite is rather pure so the chemical composition cannot be the cause for the absence of a Morin transition. The grains of the FMW hematite are polycrystalline aggregates (average crystallite size approx. 600 Å), so the suppression of the Morin transition is related to the crystallite size rather than with the grain size of the hematite.

After thermal demagnetization up to 700 °C the hematite magnetic properties change drastically. H_{cr} (415 - 650 kAm^{-1}) and $H_{cr'}$ (340 - 610 kAm^{-1}) increase and J_{rs} (0.05 - 0.003 Am^2kg^{-1}) decreases. Figures for H_{cr} and $H_{cr'}$ are in fair agreement with those for comparable fractions derived by Dankers and Hartstra (op. cit.) for hematite with a high-temperature origin. The maxima in H_{cr} and $H_{cr'}$ of the FMW hematite are in the 2.1-1.0 micrometer fraction; they shift towards larger grain sizes, presumably due to a decreasing polycrystallinity of the grains. J_{rs} decreases monotonously with grain size. The largest relative decrease is observed in the smallest grain-size fraction.

Low-temperature cycling of the saturation remanence of the FMW fractions after annealing revealed curves with a Morin transition. Defects are (partly?) removed from the grains by annealing and crystallites will be enlarged by the recrystallization process. The present hematite contains 4.8 weight percent water which escapes from the grains during annealing (TGA). This promotes recrystallization of the grains. The chemical composition indicates no major amounts of other elements than Fe. After annealing its behaviour is expected to be more like that of "model" hematite characterized by a Morin transition. Indeed after thermal treatment a (broad) Morin transition is observed. The increasing H_{cr} and $H_{cr'}$ indicate that the magnetocrystalline moment, associated with the occurrence of a Morin transition, is harder than the defect moment in agreement with the results of Haigh (1957B) and Dunlop (1971, 1972).

TRM was found to decrease with grain size. The TRM-trend of Hartstra (1982A) could be extended to smaller grain sizes. The specific volume

TRM (0.3-0.47) is in good agreement with the value of 0.4 determined by Dunlop (1971) for his fine-grained hematite.

The large differences in magnetic properties of the present FMW low-temperature hematite before and after thermal treatment indicate that synthetic hematites synthesized at high temperatures by e.g. decomposing goethite or oxidizing magnetite are not representative for natural low-temperature hematite.

The differences in remanent coercive force and in low-temperature behaviour observed in the FMW hematite before and after thermal treatment might provide a framework for the discrimination in red beds between TRM (in casu DRM with a high-temperature origin) and CRM which has a low-temperature origin. This is illustrated with two examples from natural samples. Preliminary interpretation of the results indicates that the observed properties before and after annealing are in broad agreement with those they should exhibit regarding the origin of their remanences. However, the complexity of the hematite magnetic properties and the scarcity of data on hematite annealing behaviour at relatively low annealing temperatures hinder a full account of all aspects of the observed behaviour in the natural samples.

Acknowledgements

E. Wilhelm (Bureaux des Recherches Géologiques et Minières, BRGM) provided valuable additional information concerning the Montarnu location and permission to collect samples. Drs. M.I. Pieters assisted during the sampling campaign. The members of the Centraal Laboratorium of the Ceramic Industry Sphinx (Maastricht, The Netherlands) are gratefully acknowledged for permitting us to use their pipette centrifuge equipment and supporting laboratory facilities. C. Laman (department of crystallography) made the X-ray determinations, P. van Krieken (department of sedimentology) carried out the TGA analysis and T. van Zessen (service Laboratory, IVA, University of Utrecht) the wet chemical water determination. Microprobe analyses and backscattered electron images were made under supervision of Dr. M.J. van Bergen with a JEOL 8600 Superprobe, equipped with a TN-5502 EDS analyzer, at the Vening-Meinesz Laboratory of Geochemistry, IVA Rijksuniversiteit Utrecht. These facilities are supported by the Netherlands Organization for the Advancement of Pure Research (Z.W.O.). Grain sizes were controlled with electron microscopical techniques at the electron microscope centre of the State University of Utrecht under supervision of Dr. H. van Roermund. Prof. Dr. J.D.A. Zijderveld critically reviewed the manuscript. J.J.J. Bergenhenegouwen made most drawings. The investigations were supported by the Netherlands Foundation for Earth Science Research (AWON) with financial aid from the Netherlands Organization for the Advancement of Pure Research (Z.W.O., MJD is acknowledging grant 751-354-006 and JHL grant 751-354-012).

6 REFERENCES

Bando Y., Kiyama M., Yamamoto N., Takada T., Shinjo T., Takaki H., 1965, The magnetic properties of α-Fe_2O_3 fine particles, J. Phys. Soc. Japan 20, 2086.

Banerjee, S.K., 1971, New grain size limits for paleomagnetic stability in haematite, Nature Phys. Sci. 232, 15-6.

Bordet P., 1950, Le dôme permien de Barrot (A.-M.) et son auréole de terrains secondaires, Bull. Serv. Carte géol. Fr. 48, 51-90.

Bucur I., 1978, Experimental study of the origin and properties of the defect moment in single domain haematite, Geophys. J. R. astr. Soc. 55, 589-604.

Channell J.E.T., Freeman R., Heller F., Lowrie W., 1982, Timing of diagenetic haematite growth in red pelagic limestones from Gubbio (Italy), Earth Plan. Sci. Letters 58, 189-201.

Chevallier R., 1951, Propriétés magnétiques de l'oxyde ferrique rhomboédrique (Fe_2O_3-α), J. Phys. Radium 12, 178-88.

Chevallier R., Mathieu S., 1943, Propiétés magnétiques des poudres d'héamites; influence des dimensions des grains, Ann. Physique 18, 258-88.

Collinson D.W., 1974, The role of pigment and specularite in the remanent magnetism of red sandstones, Geophys. J. R. astr. Soc. 38, 253-64.

Dankers P.H.M., 1978, Magnetic properties of dispersed natural iron-oxides of known grain-size, Ph.D. thesis University of Utrecht, 142pp.

Dankers P.H.M., 1981, Relationship between the median destructive field and remanent coercive forces for dispersed magnetite, titanomagnetite and hematite, Geophys. J. R. astr. Soc. 64, 447-61.

Dekkers M.J., in prep. A, Magnetic properties of natural goethite part three: investigation of the magnetic behaviour of minerals originating from goethite during thermal demagnetization.

Dekkers M.J., in prep. B, Magnetic properties of natural pyrrhotites part two: high- and low-temperature behaviour of the isothermal remanent magnetization and thermoremanence as function of grain size.

Dekkers M.J., Hartstra R.L., Mullender T.A.T., in prep., A device for the magnetic separation of fine-grained particles.

Dekkers M.J., Linssen J.H., 1987, Grain size separation with the pipette centrifuge, report Paleomagnetisch Laboratorium Fort Hoofddijk, 15pp.

Dunlop D.J., 1970, Hematite: intrinsic and defect ferromagnetism, Science 169, 858-60.

Dunlop D.J., 1971, Magnetic properties of fine particle hematite, Ann. Géophys. 27, 269-93.

Dunlop D.J., 1972, Magnetic mineralogy of unheated and heated red sediments by coercivity spectrum analysis, Geophys. J. R. astr. Soc. 27, 37-55.

Eaton J.A., Morrish A.H., 1969, Magnetic domains in hematite at and above the Morin transition, J. Appl. Phys. 40, 3180-5.

Elmore R.D., Van der Voo R., 1982, Origin of hematite and its associated remanence in the Copper Harbor conglomerate (Keweenawan), Upper Michigan, J. Geophys. Res. B 87, 10918-28.

Flanders P.J., Remeika J.P., 1965, Magnetic properties of hematite single crystals, Phil. Mag. 11, 1271-88.

Haigh G., 1957A, The effect of added titanium and aluminum on the magnetic behaviour of α-ferric oxide, Phil. Mag. 2, 505-20.

Haigh G., 1957B, Observations on the magnetic transition in hematite at -15 °C, Phil. Mag. 2, 877-90.

Hartstra R.L., 1982A, Some rockmagnetic parameters for natural iron-titanium oxides, Ph.D. thesis University of Utrecht, 145pp.

Hartstra R.L., 1982B, High-temperature characteristics of a natural titanomagnetite, Geophys. J. R. astr. Soc. 71, 455-76.

Hartstra R.L., 1982C, A comparative study of the ARM and I_{sr} of some natural magnetites of MD and PSD grain size, Geophys. J. R. astr. Soc. 71, 497-518.

Hartstra R.L., 1983, TRM, ARM and Isr of two natural magnetites of MD and PSD grain size, Geophys. J. R. astr. Soc. 73, 719-37.

Hedley I.G., 1968, Chemical remanent magnetization of the FeOOH, Fe_2O_3 system, Phys. Earth Plan. Int. 1, 103-121.

Kündig W., Bommel H., Constabaris G., Lindquist R.H., 1966, Some properties of supported small α-Fe_2O_3 particles determined with the Mössbauer effect, Phys. Rev. 142, 327-33.

Morin J., 1950, Magnetic susceptibility of α-Fe_2O_3 and Fe_2O_3 with added titanium, Phys. Rev. 78, 819-20.

Nagata T., 1961, Rock Magnetism, Maruzen Company Ltd. Tokyo, 2nd edition 350pp.

Néel L., Pauthenet R., 1952, Etude thermomagnétique d'un monocrystal de Fe_2O_3-α, C.R. Acad. Sci. (Paris) 234, 2172-4.

Özdemir Ö., Deutsch E.R., 1984, Magnetic properties of oolitic iron ore on Bell Island, Newfoundland, Earth Plan. Sci. Letters 69, 427-41.

O'Reilly W., 1984, Rock and mineral magnetism, Blackie Glasgow and London, 220pp.

Roy J.L., Park J.K., 1972, Red beds: DRM or CRM?, Earth Plan. Sci. Letters 17, 211-6.

Schroeer D., Nininger R.C. jr., 1967, Morin transition in α-Fe_2O_3 microcrystals, Phys. Rev. Lett. 19, 632-4.

Schwertmann U., Taylor R.M., 1972, The influence of silicate on the transformation of lepidocrocite to goethite, Clays Clay Minerals 20, 159-64.

Smith R.W., Fuller M., 1967, Alpha-hematite: stable remanence and memory, Science 156, 1130-3.

Soffel H.C., 1981, Domain structure of natural fine-grained pyrrhotite in a rock matrix (diabase), Phys. Earth Plan. Inter. 26, 98-106.

Stacey F.D., Banerjee S.K., 1974, The physical principles of rock magnetism, Elsevier Scien. Publ. Comp., Amsterdam-London-New York, 195pp.

Strangway D.W., Honea R.M., McMahon B.E., Larson E.E., 1968, The magnetic properties of naturally occurring goethite, Geophys. J. R. astron. Soc. 15, 345-59.

Van den Ende C., 1977, Palaeomagnetism of Permian red beds of the Dome de Barrot (S. France), PhD thesis University of Utrecht, 171pp.

Walker T.R., Larson E.E., Hoblitt R.P., 1981, Nature and origin of hematite in the Moenkopi Formation (Triassic), Colorado Plateau: a contribution to the origin of magnetism in red beds, J. Geophys. Res. B 86, 317-33.

Westcott-Lewis M.F., 1971, Grain size dependence of thermoremanence in ilmenite-haematites, Earth Plan. Sci. Letters 12, 124-8.

Westcott-Lewis M.F., 1971, Magnetism in rhombohedral iron-titanium oxides, Australian J. Phys. 24, 719-34.

Wilhelm E., Kosakevitch A., 1978, Chapeaux de fer; rapport de synthèse, unpublished report BRGM, 35pp.

APPENDIX 1

SOME BACKGROUND INFORMATION OF THE SAMPLING SITES

A concise outline of some literature concerning the geological context, mining history and inferred genesis of the ore deposits is listed below.

1 GOETHITES

1.1 Kahlenberg (MKB)

The abandoned quarry Kahlenberg (nowadays in use as waste disposal site) is located in the Rhinegraben 10 km North of the Kaiserstuhl (Western Germany). Mining took place in open pits and galleries from 1950 till 1967 (Sauer and Simon, 1975A). The lithology at the quarry site consists of an alternation of red to red-brown oolithic zones with sandy chalk, chalk and marly chalk. All zones are more or less oolithic. Various ore layers are present in the marine sedimentary sequence; the most important one is the Murchisonae-layer (Dogger-β) with a thickness of 10 to 11.5 m in the Kahlenberg area. The Fe-source to constitute the ore-layers is not definitely established. Two possible sources are: 1) input as trivalent Fe from brines or 2) as fine clastic material from the Rheno-Ardennic massif in the North. A third possibility is put forward by Eichler (1961). He proposed that the iron would be liberated on the sea floor by kaolinitization of illitic/montmorillonitic clays.

The goethite-rich ooids have sizes between 0.2 and 0.5 mm. They have an ellipsoidal to slightly rounded prismatic shape and are distinctly concentrically layered. The average chemical composition of the raw ore is presented in Table I (after various sources quoted in Sauer and Simon, 1975A).

Table I: Chemical composition of the Kahlenberg raw ore.

Fe	17 - 23	P	0.25 - 0.35
SiO_2	11 - 18	S	0.04 - 0.08
CaO	20 - 30	$Na_2O + K_2O$	0.4
MgO	0.8- 1.6	V	0.03
Al_2O_3	3.4- 5.0	TiO_2	0.15
$CO_2 + H_2O$(fixed)	18.5 - 25.2	Sr	traces
Mn	0.15 - 0.23	Zr	traces

Contents are in weight percentages referring to "dry" ore; "wet" ore contains 5.2 - 6.6 % H_2O.

Mineralogical constituents of the raw ore are goethite, (hydro-)hematite, chamosite, siderite, calcite, quartz, clay minerals (kaolinite, pyrophyllite, vermiculite), muscovite, sericitized feldspar and phosphorite (Eichler, 1961; Urban, 1966). The ooids themselves are goethite-rich; traces of clay minerals (kaolinite, pyrophyllite and vermiculite), hematite, siderite are present (op. cit.). Chamosite ooids (sometimes oxidized) occur rarely at specific levels of the ore layer. The chemical composition of the 0.12 - 0.25 mm ooid fraction is listed in Table II (cf. Urban, 1966).

Table II: Ooid chemical composition.

Fe_2O_3	FeO	SiO_2	Al_2O_3	MgO	CaO	H_2O
55.3	1.0	22.7	10.5	2.0	1.0	6.3

Contents in weight percentages

1.2 Zollhaus-Blumberg (MBL)

Zollhaus-Blumberg is located in the South of Western Germany at the Swiss border. Originally, mining was carried out in small open pits, probably already in the 17th century. Mining activity increased during the first decades of this century; from 1935 onwards till the closure of the mines in 1942, mining was performed in galleries (Sauer and Simon, 1975B). There are few outcrops of the ore-layers left; entrance in the old galleries is prohibited. Samples were collected from a small outcrop in an old quarry (nowadays in use as waste disposal site) north of the road from Zollhaus-Blumberg to Geisingen.

The Zollhaus-Blumberg oolithic sedimentary ore layer, known as Macrocephalenerz (Dogger-ϵ and Φ), is intercalated in Jurassic limestone. In the Blumberg area the ore-layer has a thickness of 3 - 4 m (see Sauer and Simon, 1975B p 108, for a detailed stratigraphic record). Ooids are in the range of 0.8 - 1.0 mm; in the upper and lower zones they are slightly larger: 1.2 - 1.4 mm. They are spherical to ellipsoidal and distinctly concentrically layered. Typical is the cloudy arrangement in the groundmass, sometimes enriched in thin layers. The following minerals are identified (cf. Gerbert, 1964):
Ooids: goethite with traces of clay minerals (illite, mixed-layered illite/montmorillonite, kaolinite), calcite, siderite, pyrite and quartz.
Groundmass: ankerite, clay minerals (illite, kaolinite, vermiculite, mixed-layered illite/montmorillonite), quartz, muscovite, phosphorite and traces organic material.

The chemical composition of the raw ore is presented in Table III (after Ziergiebel, 1942; Einecke, 1950).

Table III: Chemical composition of the Blumberg raw ore.

Fe	SiO_2	CaO	MgO	Al_2O_3	MnO	P	S	CO_2	V	TiO_2
22.55	22.4	12.6	2.02	10.77	0.17	0.44	0.19	10.0	0.07	0.40

Contents are in weight percentages and refer to "dry" ore. "Wet" ore contains 13% H_2O.

1.3 Menera (MEN)

The Menera mining district (East-Central Spain) is one of the oldest mining districts in the world (Zitzmann, 1978). There are Iberic galleries known; mining is documented from 350 years ago. Today only open pit mining is performed.

Many ore bodies are associated with a 60 km long lineament-like fault zone. Generally, the host rock is Ordovician (Ashgillian) limestone; however, some ore bodies are hosted by Upper Carboniferous carbonates. Ore bodies have sizes of 1.5 - 2 km length and 250 - 300 m wide; their thickness is up to 80 m.

Former genetic interpretation was based on their stratiform occurrence; a sedimentary formation was inferred. Nowadays the oxidic ores are thought to be the weathered "caprock" of hydrothermal-metasomatic siderite/ankerite deposits. Timing of carbonate mineralization is be-

tween Upper Carboniferous and the beginning of the Mesozoic era (Hartleb, 1968). Oxidation is considered to be of Alpine age. Cañada Guerrero (1972) proposed a different genetic history of the ores: he argues that acid Fe-bearing waters from weathering pyrite masses would have caused alteration of the Ordovician limestones and dolomites towards ankerite and siderite. The iron oxides would be enriched by dissolution.

Hematite and goethite are major constituents of the Menera ore paragenesis; siderite is a minor constituent. Occasionally, small barite cores are found in the oxidic masses. Argillic and calcareous intercalations are known in the ore-bodies (Cañada Guerrero, 1972). The chemical composition of the raw ore is given in Table IV (after Zitzmann and Neumann-Redling, 1977).

Table IV: Chemical composition of the Menere raw ore.

	Fe	Mn	SiO_2	Al_2O_3	S	P	CaO	MgO
lump ore	53.5	1.94	7.9	1.3	0.02	0.1	0.4	0.7
fine ore	53.3	2.32	7.5	1.3	0.02	0.1	0.2	0.3

Contents in weight percentages.

1.4 Sain Bel (FSB)

The FSB samples have been collected in a quarry in the former Sain Bel mining district, 25 km West of Lyon (France). Mining took place from 1860 till 1974, pyritic lenses were mined for sulphur. Shaft-mining was predominantly performed. Minor chalcopyritic zones were mined for copper; the copper tenor in the pyritic lenses is very low. The pyritic lenses are stratiform with a thickness varying between 1.5 and 25 m. Their lengths are in between 10 and 600 m. The host rock comprises a Devonian volcano-sedimentary series, regionally metamorphosed in the greenschist facies (extremely quartz-rich at the quarry site). A gossan is only developed in the quarry Saint-Antoine in the utmost south of the district.

In the absence of carbonates, pyrite oxidizes in an extremely acid environment. Iron migrates and precipitates as jarosite and goethite in the supergene zone. Further oxidation results in goethite with traces of hematite (Wilhelm and Kosakevitch, 1978). The chemical composition of the primary pyritic ore is listed in Table V (compiled from Bardin, 1971; Boudalon, 1966) and that of the Sain Bel gossan in Table VI (unpubl. report BRGM). Fe, Cu, Zn and to a minor extent P are leached in the supergene zone of the gossan; Pb seems to be slightly enriched. Compared to the original pyrite Fe, Co and Zn are leached in the gossan; tenors of Cu, Ni and Mo are similar.

Table V: Chemical composition of the primary Sain Bel pyrite.

Bardin (1971)			Boudalon (1966)	
	lowest value	highest value	Trace element content	
S	45.08	51.26	Ni	40
Fe	40.10	45.20	Co	60 - 120
Cu	0.08	2.10	Mo	60 - 700
Zn	0.06	0.74	Cu	100 - 800
Pb	0.01	0.021	Zn	140 - 1000
Mn	0.002	0.005	Pb	30 - 50
SiO_2	0.58	8.03	Ti	1300 - 6000
$BaSO_4$	0.09	5.23	Sc	50 - 60
Al_2O_3	0.31	1.12		
CaO	0.23	0.63		
MgO	0.10	0.13		
P	0.035	0.07		
As	0.006	0.06		

Contents in weight percentages; trace element contents in ppm.

Table VI: Chemical composition of the Sain Bel gossan.

SiO_2	68.10	Mn	20
Al_2O_3	2.89	P	274
Fe_2O_3	27.00	Ti	8990
MgO	0.54	Co	13
CaO	1.50	Cu	287
Na_2O	0.25	Zn	27
K_2O	1.63	Ni	32
		Mo	114

Constituents of the left column are in weight percentages; those of the right in ppm. The analytical data are means, based on eight samples.

1.5 Robe River (RR)

The Robe River mining district is located in the extremely Northern part of Western Australia. Its economic importance was discovered during the mid-fifties. Local prospection and exploration were carried out in the early sixties after the Government had removed the embargo on the export of iron ore. Goethite-rich ore was first produced in 1972 (Adair, 1975).

The ore consists of goethite-rich pisolites (Trendall, 1975). Typical for the Robe River deposits is that they are fillings in former stream valleys, which drained Proterozoic jaspilites (hematite-rich cherts). These rocks are seen as the source for the enormous quantity of iron needed for the pisolitic limonites. The age of the deposits is not precisely known: physiographic arguments (the resemblance of the old stream pattern to the present one) suggest a Tertiary age, whereas stratigraphic reasoning indicates a Mesozoic or younger age (Harms and Morgan, 1964). The limonitic crust is more resistant against erosion than the former channel-side walls, so that the ore bodies (numbered A to N upstream) appear as highs in the landscape (mesas). Thickness of the iron crust varies between several meters to several tens of meters. A detailed geologic history of the ore district is given by Harms and Morgan (1964).

The origin of the deposits is subject of some debate: Harms and Morgan (1964) favour a chemical sedimentary deposition of the iron (from the jaspilites) from solution or from reworked material nearby (penecontemporeneous). They see biologic activity (algae etc.) as the prime depositional factor. Abundant vegetation would have been present to stabilize the channel walls. MacLeod et al. (1963) favour a replacement of fluviatile sediments. Both mechanisms are alike: their difference is mainly to be found in the way the iron is transported to the depositional environment. Harms and Morgan (1964) foresee a stoping and swampy river system, whereas MacLeod et al. (1963) theory indicates that the bulk of the iron transport was in underground waters.

The pisolites are 1 to 3 mm long (sizes between 0.2 and 10 mm), have a subspherical to oval shape and are mostly close-packed, but not in immediate contact with each other. Abundant limonitized fossil wood is present in the deposits (5 to 25 %, locally the ore consists almost entirely of fossil wood). The wood was limonitized after deposition. The pisolites are coated with colloform bands of goethite; their cores consists of detrital quartz grains, brown limonitic silt fragments or fossil wood. Concentric layering is rarely observed. No deformation due to compaction is recognized.

The ore minerals are goethite, hematite and maghemite in varying proportions. The hematite content decreases (from some twenty to nil percent) with increasing distance to the jaspilitic iron source rock area. Maghemite is only present in subordinate amounts in the upper levels of the ore bodies (upper 3 m). Its precursor mineral is probably lepidocrocite although the latter is not identified in the ores. Common gangue minerals are clay minerals (kaolinite with minor montmorillonite and illite), calcite and quartz. The chemical composition of the bulk limonitic ore is presented in Table VII (after Harms and Morgan, 1964).

Table VII: Chemical composition of the Robe River raw ore.

	Lower Robe River	Middle Robe River
Fe	55.9	57.8
(Fe_2O_3)	80	82
SiO_2	4.9	5.0
Al_2O_3	3.6	2.4
S	0.04	0.03
P	0.02	0.03
TiO_2	0.15	0.19
Mn	0.05	0.04
Ign. loss 1000 °C	11.2	9.8
SiO_2/Al_2O_3	1.36	2.08

Contents in weight percentages. Main impurities are silica and alumina; trace element contents are below 20 ppm except for zinc (0.20 - 0.08 %).

2 PYRRHOTITES

2.1 Isola di Vocca (DIS)

Isola di Vocca is located on the Sesia stream in the Ivrea-Verbano zone in the vicinity of the Insubric line (Northern Italy). Numerous small pyrrhotite-pentlandite deposits are known in the Ivrea-Verbano Zone in the so called Basic Formation (BF). The BF is supposed to be a stratiform complex composed of a main noritic-gabbroic body and basal cyclic units of dunites, harzburgites, pyroxenites, norites and gabbros

of much smaller size (Rivalenti et al., 1975). The whole series intruded in the Kinzingitic series (high-grade metapelites with some metabasites and marbles intercalated). Slices of peridotite (tectonic contacts) are recognized at the base of the BF; they are interpreted as residual mantle material by Rivalenti et al. (op. cit.).

The sulphidic ore bodies are associated with ultramafic intercalations in the BF. Their ore-paragenesis usually consist of pyrrhotite, pentlandite and chalcopyrite with minor mackinawite, magnetite, ilmenite and sphalerite. The largest deposits were mined (usually in small galleries) for nickel in the 19th century and intermittently during the first half of this century. For detailed information the reader is referred to Bigioggero et al. (1979), Natale and Zucchetti (1979) and Ferrario et al. (1983) and to references cited in these papers.

Various locations were sampled in the Ivrea-Verbano Zone; the most promising location appeared to be that sampled North of Isola di Vocca in a cliff some 200 meters above river level. Samples were collected at the entrance of a small gallery where insignificant mining operation had been during the 19th century (Rivalenti, 1979). The ore-paragenesis consists of a relatively high pyrrhotite content with only trace amounts of magnetite. The mineralogy of the host rock is dominated by pyroxenes with minor olivine and plagioclase. A similar host rock mineralogy is found at Campello Monti (Strona Valley).

Polished section study of the DIS samples revealed that the amounts of penlandite and chalcopyrite are subordinate, while magnetite occurs only accessory (<1 %). Remobilization of ore minerals is observed, pyrrhotite (and pentlandite) are occasionally found in fractures. The grain sizes of the pyrrhotite crystals is usually small. Pyrrhotite-rich grains of larger sizes are thus composed of pyrrhotite and silicates irregularly intergrown.

2.2 Ginevro (EGI), Ortano (EOR), Temperino (TTE)

These sample locations all belong to the Tuscan metallogenetic province (Italy). The geologic history of the mineralizations is determined by and large by two events (Bodechtel, 1965):

1) Deposition of primary hematite/pyrite ore-lenses of submarine exhalative type associated with Rhaetian dolomitic limestones intercalated in Permo-Triassic schists.
2) Overprinting of the ore by Late Tertiary granitoid magmatism. On Elba island the primary ores were merely heated without transport of mineralizing hydrothermal fluids. This resulted in magnetite/pyrrhotite ore-deposits. On the mainland the heating was accompanied by mineralizing hydrothermal fluids from the granitoids. This led to skarn and vein-type mineralization characterized by a wide spectrum of associated metals (from high temperature related Sn-deposits to much lower temperature related Pb-Zn-deposits).

2.2.1 Ginevro (EGI)

Ginevro is one of the three abandoned iron mines in the Southeastern part of Elba on the peninsula Calamita (the other two mines are Sassi Neri and Calamita). Elba has an extensive mining history. Insignificant mining was performed intermittently from Etruscan times onward. From the Napoleonic time (1814-1815) mining for iron took place on a larger scale, especially from the beginning of this century. Iron and steel were produced on the island by blast furnaces in Porto Ferraio from 1902

till in the second world war, during which the plant was bombed. From 1947 onward raw ore was transported to the Tuscan mainland where it was processed (Waldeck, 1977). At present there is no active mining anymore on Elba. Ginevro was the last producing mine; Italsider Ltd. carried out mining until 1980. Open pit as well as shaft mining (below the Tyrenean Sea) was performed. The mine is currently hold stand-by.

The primary hematite/pyrite ore is associated with the Calcari Cavernosi. Heat from the Miocene East Elba granodiorite, which has intruded up to levels immediately below the deposits, transformed them into magnetite skarns with minor pyrrhotite (Bodechtel, 1965). The lens-shaped ores are up to some tens of meters thickness and some hundreds of meters length. Magnetite is by far the most important ore mineral; only traces of pyrrhotite occur. Skarns are well-developed in the silicate gangue in the vicinity of the ores. Silicate skarn minerals are hedenbergite, ferrotremolite, sodium-rich hornblende, grossularite, andradite and epidote (Dimanche, 1970, 1971). Dimanche (1971) argued that the skarn-mineral series is formed at temperatures of 400 to 500 °C. The ore-forming processes concentrated pyrrhotite in the silicate-rich parts of the skarn; this rock type was collected from the mine dumps after permission of the local mine authorities.

2.2.2 Ortano (EOR)

The abandoned Ortano mines are located in the centre of the East coast of Elba. A tourist centre is built on the former harbour facility of the mines. Mining took place in open pits (Waldeck, 1977). The quarries and dumps are by and large overgrown, only small outcrops are left.

The ore-paragenesis consists of hematite and pyrite, with increasing depth the pyrrhotite content and associated skarns increase. The East Elba granodiorite - which caused the trend observed - is at the Ortano site some 150 m below the quarries (Bodechtel, 1965). Silicate skarn minerals are epidote, ilvaite and hedenbergite (minor). Pyrrhotite-rich samples were collected from the mine dumps; magnetite contents appeared to be less than one percent.

2.2.3 Temperino (TTE)

The Temperino mine is situated in the Tuscan mainland 2 km North of Campiglia Maritimma. The mine is part of the famous Tuscan metallogenetic province, already known since Etruscan times (Bodechtel, 1968). The geologic history of the deposits is similar to that of the Elba deposits. The primary hematite/pyrite ore is also associated with the Calcari Cavernosi. In the Tuscan region, however, the thermo-metasomatic phenomena, associated with Late Tertiary granitic magmatism, are far better developed than on Elba. A small granitic outcrop is known a few kilometers West of the Temperino mine. Today, there is no active mining anymore for metals in the region. Massive chalk formations in the region are worked for the cement industry.

At Temperino shaft mining was performed. The ore body is associated with a quartz-porphyry. There are successively four different ore parageneses observed (Bodechtel, 1968):

1) Hedenbergite/ilvaite skarns with "Buntmetalsulphiden"
2) Chalcopyrite with pyrrhotite
3) Pyrite, pyrrhotite and ilvaite (occasionally)
4) Chalcopyrite with exsolution of sphalerite and traces of bismuth (the deepest zone in the mine).

Since it was impossible to enter the mine shafts to take samples in situ and no pyrrhotite-rich outcrops occur, pyrrhotite-rich skarns were collected from the mine dumps. The samples belong to the pyrite/pyrrhotite/ilvaite zone (zone 3).

Polished section study reveals pyrrhotite and pyrite as major ore-phases (some 75 and 20 percent of the ore minerals). Chalcopyrite is minor (5 %); magnetite is accessory (<1 %). Pyrrhotite and pyrite both have a long prismatic habit; sheaf-like aggregates with silicate intergrowths are ubiquitous. The thickness of the "lamellae" is in the order of some hundred micrometer, so monomineralic pyrrhotite can be concentrated for the grain-size range of interest (up to 250 micrometer).

3 HEMATITE

3.1 Montarnu (FMW)

The small hematite/goethite Montarnu gossan is loçated some twenty kilometers West of Autun in the Morvan (France). Insignificant mining was performed in the 19th century (Wilhelm and Kosakevitch, 1978). The quarry which is entirely surrounded by fir-wood, mounts some thirty meters length; it is a few meters deep. The dumps at the borders of the quarry are largely overgrown.

In a mylonitic part of the contact zone between a porphyritic granite and a fine-grained granite two veins occur: a pyrite/quartz vein and a chlorite vein. The gossan is developed in the weathering zone of the pyrite/quartz vein. Samples were taken in the hematite-rich zone constituting the quarry. Overgrowth-textures are recognized in hematite lumps. The hematite is chemically pure; only minor Al and Si are detected.

4 REFERENCES

Adair D.L., 1975, Middle Robe River iron deposits, in: Knight (ed.), Economic geology of Australia and Papua New Guinea Vol I: Metals, Austr. Inst. Min. Metall., 943-5.

Bardin D., 1971, Les amas pyriteux de Sain Bel (Rhône) liés au groupe spilites-kératophyres de la Brévenne, Bull. BRGM (2), 11.6.

Bigioggero B., Brigo L., Ferrario A., Gergnanin A., Montrasio A., Zuffardi P., 1979, Strona Valley (Fe-Ni-Cu) and (Fe-Ba) ore deposits: excursion book, Memorie di Sci. Geol. 33, 33-9.

Bodechtel J., 1965, Zur Genese der Eisenerze der Toskana und der Insel Elba, Neues Jb. Mineral. Abh. 103, 147-62.

Bodechtel J., 1968, Die Paragenesen der Skarnlagerstätten in den Monti di Campiglia/Toskana, Freib. Forsch. H. C231, 7-20.

Boudalon J., 1966, Fiche concernant le district de Chessy - Sain Bel (rédigée pour l'enquête sur le cuivre dans le monde).

Cañada Guerrero F., 1972, Yacimientos de mineral de hierro de Sierra Menera, edad de su formación y experimencias de laboratorio que se producen su génesis, Bol. geol. min. 83, 69-74.

Dimanche F., 1970, Les amphiboles et leurs associations dans les skarns à magnétite du Ginevro (île d'Elbe, Italie), Bull. Soc. fr. Minér. Cristallogr. 93, 89-100.

Dimanche F., 1971, Les minerais de magnétite et les skarns du Ginevro (île d'Elbe, Italie), Mineral. Deposita 6, 356-79.

Eichler J., 1961, Bericht über die Untersuchungsarbeiten an der Doggererz-Scholle von Kenzingen/Baden, unpubl. report Arch. Barbara Rohstoffbetr. GmbH, 37pp.

Einecke G., 1950, Die Eisenerzvorräte der Welt und der Anteil der Verbraücher und Lieferländer an deren Verwertung, Düsseldorf (Stahleisen).

Ferrario A., Garuti G., Rossi A., Sighinolfi G.P., 1983, Petrographic and metallogenic outlines of the "La Balma - M. Capio" Ultramafic - Mafic body (Ivrea - Verbano Basic Complex, NW Italian Alps), in:

Schneider H.J. (ed.), Mineral deposits of the Alps and of the Alpine Epoch in Europe, Proceedings of the IV ISMIDA 1981, 28-40.

Gerbert H., 1964, Mineralogische Untersuchen zur Genese oolitischer Eisenerze des Dogger-ε in Baden Württemberg, Arb. Geol. Pal. Inst. T.H. Stuttgart N.F. 41, 77pp.

Harms J.E., Morgan B.D., 1964, Pisolitic limonite deposits in north-west Australia, Proc. Australas. Inst. Min. Metall. 212, 91-124.

Hartleb J., 1968, Uber Vererzungen in den Keltiberischen Ketten (NE Spanien), Aufsluss 19, 313-5.

MacLeod W.N., Hunty L.E. de la, Jones W.R., Halligan R., 1963, A preliminary report on the Hammersley iron province, North West Division, Ann. Rept. Mines Dept. W.A. 1962, 90-100.

Natale P., Zucchetti S., 1979, Remarks on the Fe-Ni-(Cu) deposit of Campello Monti, Memorie di Sci. Geol. 33, 213-4.

Rivalenti G., 1979, Guide to the excursion in the Balmuccia zone, Sesia Valley, Ivrea - Verbano complex, Memorie di Sci. Geol. 33, 3-9.

Rivalenti G., Garuti G., Rossi A., 1975, The origin of the Ivrea - Verbano basic formation (Western Italian Alps) - Whole rock geochemistry, Boll. Soc. Geol. It. 94, 1149-86.

Sauer K., Simon P., 1975A, Die Eisenerze des Aalenium und Bajocium im Oberrheingraben (Grube Kahlenberg, Grube Schönberg und kleinere Vorkommen), in: Sammelwerk Deutschen Eisenerzlagerstätten Vol II Eisenerze im Deckgebirge (Postvaristikum) 3) Sedimentäre Eisenerze in Süddeutschland, Geol. Jahrb. D 10, 25-68.

Sauer K., Simon P., 1975B, Die Eisenerze im Callovium von Gutmadingen, Blumberg und Waldshut, in: Sammelwerk Deutschen Eisenerzlagerstätten Vol II Eisenerze im Deckgebirge (Postvaristikum) 3) Sedimentäre Eisenerze in Süddeutschland, Geol. Jahrb. D 10, 104-28.

Trendall A.F., 1975, Geology of Western Australian Iron ore, in: Knight (ed.), Economic geology of Australia and Papua New Guinea Vol I Metals, Austr. Inst. Min. Metall., 883-92.

Urban H., 1966, Bildungsbedingungen und Fazlesverhältnisse der marin-sedimentären Eisenerzlagerstätte am Kahlenberg bei Ringsheim/Baden, Jh. geol. Landesamt Baden-Württemberg 8, 125-267.

Waldeck H., 1977, Die Insel Elba - Mineralogie, Geologie, Geographie, Kulturgeschichte, Semmlung geologischer Führer Band 64, Gebr. Borntraeger Berlin - Stuttgart, 169pp.

Wilhelm E., Kosakevitch A., 1978, Chapeaux de Fer; rapport de synthèse, unpubl. report BRGM, Orleans, 35pp; as well as separate reports on the Sain Bel and Montarnu gossans.

Ziergiebel H., 1942, Die montangeologischen Verhältnisse der Brauneisenerz-Lagerstätten (Unter- und Mittelcallovium) in Blumberg und Umgebung (Baden), unpubl. report Arch. Geol. Landesambt Baden Württemberg, 68pp.

Zitzmann A. (ed.), 1978, Ojos Negros, Sierra Menera, in: The iron ore deposits in Europe and adjacent areas Vol II, Bundesanstalt für Geowissenschaften und Rohstoffe, 165-6.

Zitzmann A., Neumann-Redling Chr., 1977, The iron ore deposits of Spain, in: Zitzmann A. (ed.), The iron ore deposits of Europe and adjacent areas Vol I, Bundesanstalt für Geowissenschaften und Rohstoffe, 269-78.

APPENDIX 2

EXPLANATION OF SOME TECHNICAL TERMS

TRM Thermoremanent magnetization: The remanence acquired by cooling from above the Curie (or Neel) temperature to room temperature in a small magnetic field.

PTRM Partial thermoremanent magnetization: The remanence acquired by cooling through a certain temperature interval below the Curie temperature in a small magnetic field.

CRM Chemical remanent magnetization: The remanence acquired by magnetic minerals by growth through their superparamagnetic threshold size at a certain temperature below their Curie temperature.

IRM Isothermal remanent magnetization: The remanence acquired by application of a (high) direct magnetic field at room temperature.

J_{rs} Saturation IRM: Beyond a certain magnetic fieldstrength a specimen does not acquire a higher remanence anymore. The maximum remanence is referred to as J_{rs}, SIRM or Isr. Expressed in Am^2kg^{-1} (per unit mass) or in Am^{-1} (per unit volume).

J_s Saturation magnetization: Maximum magnetization which a specimen can acquire in a magnetic field. For weakly ferromagnetic materials, the magnetization is corrected for the high-field susceptibility by extrapolation to the ordinate. Expressed in Am^2kg^{-1} (per unit mass) or in Am^{-1} (per unit volume).

X_{in} Initial susceptibility: The ratio of the induced magnetization and the strength of the applied field. Expressed in m^3kg^{-1} (per unit mass) or dimensionless (per unit volume).

X_{hf} High-field susceptibility: The ratio of the induced magnetization acquired in high magnetic fields in the linear part of a magnetization curve and the field-interval of acquisition. Expressed in m^3kg^{-1} (per unit mass) or dimensionless (per unit volume).

H_c Coercive force: The back field required to reduce the remanence of a saturated specimen to zero. Expressed in Am^{-1}.

$H_{c\ ferr.}$ Ferromagnetic coercive force: The back field required to reduce the remanence of a saturated specimen to zero, corrected for the high-field susceptibility of the sample. Expressed in Am^{-1}.

H_{cr} Remanent coercive force: The back field required to reverse half of the remanence of a saturated specimen. Expressed in Am^{-1}.

$H_{cr'}$ Remanent acquisition coercive force: The magnetic field required to induce half of the saturation IRM in a non-magnetized specimen. Expressed in Am^{-1}.

$H_{1/2r}$ Median destructive field: The peak value of the strength of the alternating field to remove half of the original remanence

Alternating field demagnetization (AF demagnetization):

Progressive demagnetization technique in which a specimen is subjected to absolutely symmetrical alternating fields with stepwise increasing peak values. Between each step the remaining remanence of the specimen is determined.

Stepwise thermal demagnetization:

Demagnetization technique in which a specimen is heated to stepwise increasing temperatures (up to 700 °C) and cooled to room temperature in a field-free space. The remaining remanence is measured between each heating step.

Continuous thermal demagnetization:

Thermal demagnetization procedure in which the remanence of a specimen is continuously measured at increasing temperatures.

Low-temperature treatment or low-temperature cycling:

Procedure in which a specimen is cooled from room temperature down to liquid nitrogen temperature and vice versa under continuous measurement of its remanence.

CURRICULUM VITAE

Toegevoegd op verzoek van het College van Decanen van de Rijksuniversiteit Utrecht

Marinus Jacobus Dekkers werd geboren op 3 december 1956 te Willemstad (Curaçao). Hij behaalde in mei 1975 het diploma gymnasium β aan het Lorentz Lyceum in Eindhoven en begon in hetzelfde jaar met de studie Geologie aan de Rijksuniversiteit te Utrecht. In oktober 1978 werd het kandidaatsexamen G5 afgelegd en in mei 1982 het doktoraal examen met hoofdvak Geochemie en bijvakken Experimentele Petrologie en economische geologie (Cum Laude). Vanaf oktober 1977 tot mei 1982 werden diverse student-assistentschappen vervuld bij de afdelingen Geochemie, Kristallografie en Petrologie. Vanaf juni 1982 tot juli 1983 was hij als wetenschappelijk assistent werkzaam bij het Instituut voor Aardwetenschappen, afdeling Exogene Geochemie, in het kader van het EEG project "Geochemical controls of transport and deposition of uranium from solution". Hij was werkzaam als wetenschappelijk assistent bij het Paleomagnetisch Laboratorium "Fort Hoofddijk", vanaf augustus 1983 tot juli 1986 in dienst van de Nederlandse Organisatie voor Zuiver Wetenschappelijk Onderzoek en vanaf augustus 1986 tot juli 1987 verbonden aan de vakgroep Geofysica van het Instituut voor Aardwetenschappen.